PHD

Diagnostic and Therapeutic Approaches for the Control of Catheter-Associated Urinary Tract Infection

Milo, Scarlet

Award date:
2019

Awarding institution:
University of Bath

Diagnostic and Therapeutic Approaches for the Control of Catheter-Associated Urinary Tract Infection

Scarlet Milo

A thesis submitted for the degree Doctor of Philosophy

University of Bath

Department of Chemistry

February 2019

“An expert is a person who has made all the mistakes that can be made in a very narrow field.”

-Niels Bohr

Abstract

This research aims to investigate four novel approaches to the detection and prevention of catheter encrustation and blockage following infection by the Gram-negative, motile bacterium *Proteus mirabilis* (*P. mirabilis*). Expression of a potent bacterial urease elevates urinary pH, leading to the local supersaturation and precipitation of mineral deposits from the urine that occludes urine-flow through the catheter. Vesico-ureteric reflux following blockage by crystalline biofilms may result in serious symptomatic episodes such as pyelonephritis, endotoxic shock and septicaemia.

Three of the four described approaches for the management of catheter-associated urinary tract infection employ a dual-layered polymeric delivery system, in which a lower poly(vinyl alcohol) reservoir layer contains either a diagnostic (5(6)-carboxyfluorescein) or therapeutic (lytic bacteriophage) cargo. The hydrogel layer is capped and sealed by an upper layer of the pH-responsive polymer poly(methyl methacrylate-*co*-methacrylic acid) (Eudragit S100®). Alkalinisation of local urine media (pH >7) induces degradation of the Eudragit layer, thus releasing the contained cargo. Release of 5(6)-carboxyfluorescein results in a clear and unambiguous colour change to give advance warning (up to 14.5 hours) of impending catheter blockage, whilst bacteriophage release increased time to catheter blockage by 100% (13 hours to 26 hours).

The final approach describes the formulation and development of a novel small-molecule urease inhibitor, 2-mercaptoacetamide (2-MA), for the prevention of crystalline biofilm formation. Inhibition of bacterial urease without inducing bacterial cell death allows for the 'disarming' of *P. mirabilis* without directing population evolution via initiation of a selective pressure. Comparison of 2-MA with the approved drug acetohydroxamic acid (AHA) allows for direct evaluation against the current 'gold standard' in treatment of chronic urea-splitting infection.

All approaches were evaluated for clinical efficacy within a physiologically representative model of the catheterised tract. *In vitro* bladder models were formulated to emulate late-stage infection by uropathogenic clinical isolates (initial inoculum 10^8 CFU/mL), such that preventative strategies were evaluated under 'worst-case scenario' conditions. Performance within *in vitro* systems inoculated with *P. mirabilis* was directly compared to urease-negative *Escherichia coli* (*E. coli*), to assess uropathogenic specificity. Translation of these approaches into a clinical environment may allow a multifaceted approach to the detection and prevention of catheter blockage; a problem for which there is currently no effective control method.

Table of Contents

Acknowledgements

Firstly, I would like to thank my supervisor, Professor Toby Jenkins. Thank you for your constant support and patience. Even though some of your guidance has been questionable (namely "the wisdom of the free bar"), your positive outlook and confidence in my research has inspired me, and, despite our disagreements, has given me confidence in myself. In terms of travel and conferences, thank you for taking what constitutes a 'normal PhD' as an opening point for negotiation. The adventures you've allowed me to have throughout the last 4 years have given me memories I will cherish forever.

To all members of the Jenkins group who have helped me both in and outside the lab, it has been a pleasure sharing these years (and flow cabinet space) with you. I am grateful to Thet, Jess, Diana, George, Lauren and Laura for helping me endure years of relentless highs and lows. Particular thanks to Beth and Patricia, who have been there for me through thick and thin, and often seem to know me better than I know myself. Beth, thank you for putting up with me whilst writing this thesis (and accompanying me to Mordor. I promise to do the same for you).

To Hollie Hathaway, it's impossible to thank you in such a small space for everything you have done for me throughout my PhD. Despite everything I've achieved in the last 4 years, the friendship I have forged with you has been the most valuable of all. Thank you for being my unofficial second supervisor, lab assistant (until 3 am on bladder model day), proof-reader, travel partner and best friend. I will never forget jumping into a freezing waterfall with you, receiving third degree burns from NYC pizza, going on a hideously ill-equipped bear hunt, the luggage room, watching you fall out of a hammock, and not giving a rip snort about reviewer 2. Thank you, from the bottom of my heart, for everything.

Thank you to Tom for your infinite patience and encouragement. You never failed to give me perspective when everything seemed overwhelming, even if that perspective came in a wine glass. To Dad, Daisy, Irma, Will, Mabel, Zak, Minka, Benno, GMM, GPC, Nanna and Dick, I am hugely grateful to all of you for your never-ending supply of love and encouragement.

Mum, thank you for being there for me right from the beginning. I can never express how grateful I am to you for always being there to pick up the pieces no matter what. You have taught me how to deal with both success and failure, which, in the grand scheme of things, is the most important lesson of all. Thank you for always trying your best to understand the minutiae of catheter-based research, and feeding me roast potatoes when required.

Finally, to Mouse and Dude, thank you for always listening.

Dissemination of Research

Publications

- Milo, S.; Thet, N. T.; Liu, D.; Nzakizwanayo, J.; Jones, B. V.; Jenkins, A. T. A., An *in-situ* infection detection sensor coating for urinary catheters. *Biosensors and Bioelectronics* **81**, 166-172 (2016).
- Milo, S.; Hathaway, H.; Nzakizwanayo, J.; Alves, D. R.; Pérez-Esteban, P.; Jones, B. V.; Jenkins, A. T. A., Prevention of encrustation and blockage of urinary catheters by *Proteus mirabilis via* pH-triggered release of bacteriophage. *Journal of Materials Chemistry B* **5**, 5403-5411 (2017).
- Milo, S.; Acosta, F. B.; Hathaway, H. J.; Wallace, L. A.; Jenkins, A. T. A., Development of an Infection-Responsive Fluorescent Sensor for the Early Detection of Urinary Catheter Blockage. *ACS Sensors* **3**, 612-617 (2018).
- Milo, S.; Nzakizwanayo, J.; Hathaway, H. J.; Jones, B. V.; Jenkins, A. T. A., Emerging medical and engineering strategies for the prevention of long-term indwelling catheter blockage. *Proceedings of the Institution of Mechanical Engineers, Part H: Journal of Engineering in Medicine.* (E-pub ahead of print).
- Hathaway, H.; Milo, S.; Sutton, M. J.; Jenkins, A. T., Recent advances in therapeutic delivery systems of bacteriophage and bacteriophage-encoded endolysins. *Therapeutic Delivery* **8**, 543-556 (2017).
- Nzakizwanayo, J.; Pelling, H.; Milo, S.; Jones, B. V., *In vitro* Bladder Model for Studying Catheter-Associated Urinary Tract Infection and Associated Analysis of Biofilms. *Methods in Molecular Biology.* (Under Review).
- Pelling, H., Nzakizwanayo, J., Milo, S., Bock, L., Sutton, J. M., Jones, B. V., Bacterial Biofilm Formation on Indwelling Urinary Catheters. *Journal of Applied Microbiology*. (Submitted).

Patents

- UK Patent "Apparatus (Catheter Bag)". Milo, S., Jenkins, A. T. A., 2018. Patent number GB1801403.5.

Conference Participation

- **Invited Speaker** - Phages 2018, September 2018. University of Oxford, UK.
- **Invited Speaker** – Targeting Phage and Antibiotic Resistance (5th World Congress on Infectious Disease), May 2018. Florence, Italy.
- **Invited Speaker** – Albert Einstein College of Medicine, November 2016, New York, New York.
- **Oral Presentation** – Biosensors 2018, June 2018. Miami, Florida.
- **Oral Presentation** - BioNano Summer School, August 2014, 2015, 2016, 2017, 2018. Hirschegg, Austria.
- **Oral Presentation** – VBST Conference, September 2014 / May 2016. Bath, UK / Texel, Netherlands.
- **Poster Presentation** (Prize winner) – Innovating for Continence: The Engineering Challenge, April 2017. Chicago, Illinois.
- **Poster Presentation** – Phages 2016/2017, September 2016/2017. University of Oxford, UK.
- **Poster Presentation** – Incontinence: The Engineering Challenge, November 2015/2017. Institution of Mechanical Engineers, London, UK.
- **Delegate** – European Congress of Clinical Microbiology and Infectious Disease (ECCMID), April 2016. Amsterdam, Netherlands.

Acronyms and Abbreviations

[E]	Enzyme
[EI]	Enzyme-inhibitor complex
[ES]	Enzyme-substrate complex
[ESI]	Enzyme-substrate-inhibitor complex
[P]	Product
[S]	Substrate
2-MA	2-Mercaptoacetamide
AAS	Atomic absorption spectroscopy
AHA	Acetohydroxamic acid
AHL	*N*-Acyl homoserine lactones
AMPs	Antimicrobial peptides
AMR	Antimicrobial resistance
APTES	(3-aminopropyl)triethylsilane
B. bacteriovorus	*Bdellovibrio bacteriovorus*
C. ensiformis/ Jack Bean	*Canavalia ensiformis*
CAB	Catheter-associated bacteriuria
CAUTI	Catheter-associated urinary tract infection
CDC	Centres for Disease Prevention and Control
CE	Conformité Européene
CFU	Colony forming unit
CRISPR	Clustered regularly interspaced short palindromic repeats
CTR	Clinical Trial Regulation
DDD	Defined daily dose
DFP	Diisopropyl fluorophosphate
DMEM	Dulbecco's Modified Eagle Medium
DMF	N,N-Dimethylformamide
E. coli	*Escherichia coli*
ECDC	European Centre for Disease Prevention and Control
EDIC	Episcopic differential interference contrast
EPI	Efflux pump inhibitor
EPS	Extracellular polymeric substance
ESI	Electrospray ionisation
EU	European Union
FDA	Food and Drug Administration

GMP	Good manufacturing practice
H. pylori	*Helicobacter pylori*
HaCaT	Spotaneously transformed aneuploid immortal keratinocytes
HMDS	Hexamethyldisilazane
i4i	Invention for Innovation
IgA	Immunoglobulin A
IPATH	Center for Innovatve Phage Applications and Therapeutics
IVD	*In vitro* diagnostic
IVDR	*In Vitro* Diagnostic Regulation
K. pneumoniae	*Klebsiella pneumoniae*
LB	Luria-Bertani
LBDTA	LB-derivative soft top agar
LPI	Labile plasma iron
MDR	Medical Device Regulation
MIC	Minimum inhibitory concentration
MOI	Multiplicity of infection
MRSA	Methicillin-resistant *Staphylococcus aureus*
MS	Mass spectrometry
NHS	National Health Service
NIHR	National Institute for Health Research
NMR	Nuclear magnetic resonance
NSLB	Non-swarming LB
NTBI	Non-transferrin-bound iron
OD	Optical density
P. aeruginosa	*Pseudomonas aeruginosa*
P. mirabilis	*Proteus mirabilis*
PBS	Phosphate buffered saline
PDMS	Polydimethylsiloxane
PEG	Poly(ethylene glycol)
PNPG	*p*-Nitrophenylglycerol
POC	Point-of-care
Pta	*Proteus* toxic agglutinin
PVA	Poly(vinyl alcohol)
QSI	Quorum sensing inhibitor
RBC	Red blood cell
RBP	Receptor Binding Proteins

RLU	Relative light units
S. aureus	*Staphylococcus aureus*
SB	Stuart's Broth
SEM	Scanning electron microscopy
SEM	Standard error of the mean
TEM	Transmission electron microscopy
TSB	Tryptic soy broth
Urea	Urea aminohydrolase
VOC	Volatile organic compound
WHO	World Health Organisation
XTT	2,3-bis[2-methoxy-4-nitro-5-sulphophenyl]-2H-tetrazolium-5-carboxanilide

List of Figures

CHAPTER 1: THE CLINICAL PROBLEM: CATHETER-ASSOCIATED URINARY TRACT INFECTION

CHAPTER 2: DEVELOPMENT OF AN INFECTION-DETECTION SENSOR COATING FOR URINARY CATHETERS

CHAPTER 3: DEVELOPMENT OF AN EX-VIVO 'LOZENGE' SENSOR FOR THE EARLY DETECTION OF URINARY CATHETER BLOCKAGE

CHAPTER 4: PREVENTION OF ENCRUSTATION AND BLOCKAGE OF URINARY CATHETERS VIA PH-RESPONSIVE RELEASE OF BACTERIOPHAGE

CHAPTER 5: DEVELOPMENT OF A NOVEL SMALL-MOLECULE UREASE INHIBITOR FOR THE CONTROL OF URINARY CATHETER ENCRUSTATION

List of Tables

Introduction

Chapter 1: The Clinical Problem: Catheter-Associated Urinary Tract Infection

Since its initial inception into human medicine more than 3,500 years ago, the urinary catheter has become arguably the most venerable medical device used in modern medical practice, used on an intermittent or indwelling basis as a common management technique for urinary incontinence or retention.[1] The most commonly employed catheter design is the Foley catheter, whose design constitutes a flexible silicone or latex tube inserted into the bladder via the urethra, held in place by an intra-bladder balloon (Figure 1.1).

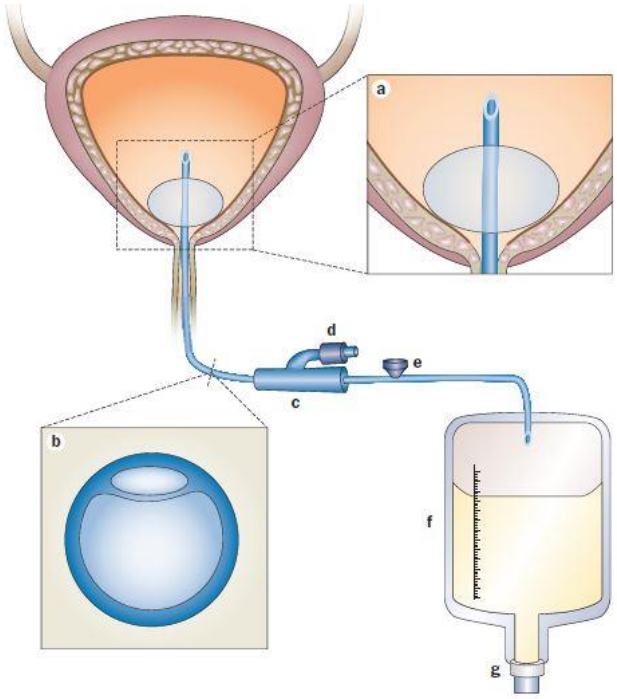

Figure 1.1: The catheterised bladder: A) The catheter is held in place by a reservoir balloon routinely inflated with sterile water/saline. Drainage is facilitated by an eyehole at the proximal end of the catheter. B) Cross-section of the Foley catheter double-lumen system. The large lumen facilitates urinary drainage; the small enables retention balloon inflation. C) The junction of catheter and sterile drainage system is preconnected and remains unbroken throughout the course of treatment. D) Valve for the inflation lumen. E) One-way sampling port, through which urine specimens for microbiological examination may be obtained. F) Accumulation of urine within the urinary drainage bag. G) Urine is emptied into the external environment via the outlet valve, such that the 'closed drainage system' remains intact and the sterility of the system is uncompromised. Reprinted with permission from Siddiq *et al.*[2] © Springer Nature 2012

It is estimated that approximately 100 million indwelling urinary catheters are sold worldwide annually.[3] Indeed, the Foley catheter is the most commonly deployed medical device, with numbers far outstripping other common devices such as central venous catheters or fracture fixation devices.[4] Consequently, catheter-associated urinary tract infection (CAUTI) constitutes 80% of all nosocomial infections worldwide.[5,6] In the UK, complications arising from the use of urinary catheters costs the National Health Service (NHS) between £1-2.5 billion, and accounts for ~2,100 deaths annually.[1] Approximately 15-25% of patients admitted to NHS hospitals each year will require urethral catheterisation, with the risk of developing bacteriuria increasing by roughly 5% each day.[7] Subsequent development of CAUTI is likely to prolong a patient's stay in hospital by 6 days and can be fatal, owing to the development of serious clinical sequelae such as pyelonephritis, endotoxic shock and septicaemia (13-30% mortality rate for CAUTI bacteraemia).[8,9]

1.1. Long-Term Indwelling Catheters

Catheter-associated bacteriuria (CAB) is defined as the presence of $\geq 10^5$ colony-forming units per millilitre (CFU/ml) of one or more bacterial species in a single catheter urine sample, and is universal in patients undergoing long-term indwelling catheterisation.[2] Indeed, more than 50% of catheters become colonised within 10-14 days of insertion. Fortunately, most cases of CAB are asymptomatic, and thus antibiotic prophylaxis is not recommended (owing to concerns about superinfection by multiresistant strains).[10] A recent survey of antimicrobial resistance by the European Centre for Disease Prevention and Control reported that the most commonly isolated uropathogens from CAB are resistant to at least one of the antimicrobial agents commonly used in clinical practice. Notably, 58.6% of *Escherichia coli (E. coli)* isolates were found to be at least one antimicrobial groups under regular surveillance (aminopenicillins, fluoroquinolones, third-generation cephalosporins, aminoglycosides and carbapenems).[11]

In contrast, the term CAUTI is used to refer to patients suffering from symptomatic infection. That is, significant bacteriuria as well as symptoms of clinical infection in the absence of any other identifiable sources. Although fewer than 3% of patients with asymptomatic infection develop complicate bacteraemia, given the ubiquitous and nature of these infections, CAUTI is one of the most frequent causes of secondary bloodstream infection found within the long-term care setting.[12]

1.2. History and Development of the Foley Catheter

Derived from the ancient Greek *kathiénai*, the word catheter can be literally translated as "to thrust into", or "to send down", and describes an instrument used to drain fluid from a body cavity. The chronology of the recorded development of the urinary catheter is decorated with a variety of different materials, including metals such as copper, tin and bronze in the 3rd century BCE, lead and papyrus utilised by the Egyptians, and organic materials such as lacquered palm leaves or hollow onion stems by the Chinese is 100 BCE.[1] However, the first example of a flexible catheter made from malleable gum-elastic did not emerge until the late 18th century, after its creation by Bernard (a French jeweller and goldsmith) following the development of natural rubber in 1735. Difficulties in achieving a compromise between rigidity and flexibility were not overcome until the vulcanisation of rubber was discovered by Charles Goodyear in 1839.[13] The modern-day Foley catheter was first introduced in the mid-1930s by Dr Frederick B. Foley[14] and, despite becoming the cornerstone for the management of the dysfunctional bladder within modern medicine, has revealed a plethora of medical complications, owing to its inherent design flaws and vulnerability to rapid-onset bacteriuria. Teflon-coated and silicone catheters were introduced in the 1960s and 1970s, respectively, with the goal of reducing patient discomfort and catheter encrustation. Attention was finally focused on reduction of bacterial biomass and subsequent infection in the 1980s and 1990s with the development of various antimicrobial catheter iterations, including chlorhexidine, silver oxide, colloidal silver and hydrogel, and nitrofurazone-impregnated catheters.[15]

1.3. Pathogenesis of CAUTI

Despite innate mechanical safeguards against microbial invasion of the urinary tract, long-term indwelling catheters are universally complicated by polymicrobial or dynamic bacteriuria.[6] Within the healthy, uncatheterised urinary tract, regular flushing of the urethra as a result of bladder emptying impedes ascending infection via mechanical means. Further intrinsic defences such as the lining of the bladder with glycosaminoglycan-coated urothelial cells also help to mitigate infection via the activation of microbial sensing proteins, thus triggering host defences with a cascade of cellular and molecular effectors.[1] Catheterisation of the urinary tract allows uropathogenic species opportunities to exploit the absence of such safeguards, resulting in successful colonisation and subsequent infection. Since catheterisation introduces a continuous drainage system, the resultant steady trickle of urine through the catheter is unable to impede the migration of bacterial cells. Furthermore, the retention balloon ensures that a reservoir of stagnant urine is maintained below the level of the eyeholes at the catheter tip. Consequently, a continuous culture system is initiated, whereby the urine is unceasingly

replenished form the kidneys, resulting in the rapid accumulation of staggeringly large bacterial populations, generally in the region of 10^8 cells per millilitre of urine.[16]

The majority of endemic CAUTI-causing microorganisms originate from the patient's own colonic and perineal flora. Bacterial entry into the catheterised bladder may occur via several routes. Organisms that colonise the periurethral skin may migrate into the bladder via the mucoid film that forms between the epithelial surface of the urethra and the catheter. Additionally, contamination of the junction between the catheter and drainage bag, or indeed of the urine within the drainage bag itself may allow transitory microflora access to the bladder via the intraluminal catheter surfaces during insertion or manipulation of the closed-collection system.[12]

1.4. Biofilms

Bacterial growth is generally characterised by two major phenotypes: single (planktonic) cells, and sessile aggregates, known as biofilms. The biofilm mode of growth enables single cells to assume a temporary multicellular lifestyle, within which cells may partake in "group behaviour", thus facilitating survival in adverse environments. The formation of a community of microorganisms attached to a surface has come to be recognised as a complex and multifaceted developmental process that is inherently dynamic and biologically responsive.[17,18] Biofilm formation on the surface of urinary catheters is particularly favoured as, upon insertion of the catheter, a host of urinary components (including proteins, electrolytes and other organic molecules) deposit on the surface, resulting in the formation of a conditioning film to which bacterial cells may adhere at an exacerbated rate.

A biofilm is a consortium of cells irreversibly attached to a surface via a self-excreted extracellular matrix, which accounts for approximately 90% of biofilm biomass.[19] The matrix is composed of extracellular polymeric substances (EPS), which, along with carbohydrate-binding proteins, pili, flagella, adhesive fibers and extracellular DNA, act as a stabilising scaffold for the three-dimensional biofilm structure.[20] Within the matrix, nutrients are trapped for metabolic use by the resident bacterial cells, and water is retained via hydrogen-bonding interactions with the hydrophilic polysaccharides.[19] Secreted enzymes may modify the composition of the EPS in response to changes in nutrient acquisition, thereby effectively tailoring the biofilm composition to the specific environmental niche.

Biofilms may form on biotic or abiotic surfaces and are prevalent in natural, industrial and hospital settings. Once a cell differentiates to the biofilm mode of growth, it undergoes a phenotypic shift in behaviour, in which large suites of genes are differentially regulated.[17]

1.4.1. Stages of Biofilm Development

Biofilm formation occurs via a series of five sequential steps, involving numerous conserved and/or species-specific factors (Figure 1.2).

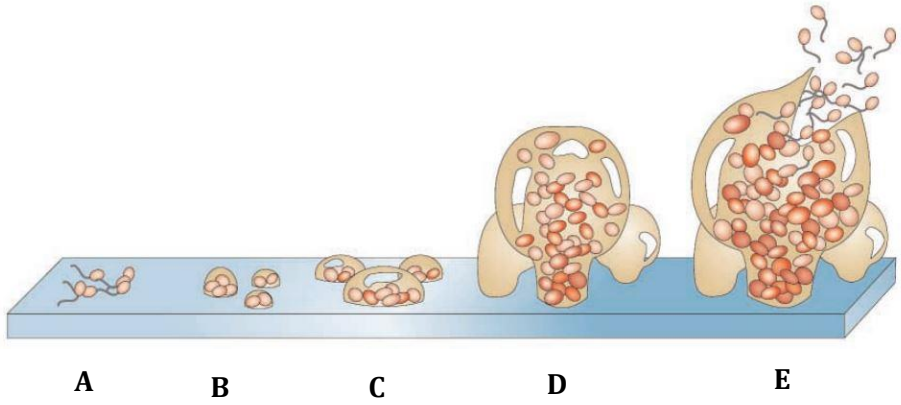

Figure 1.2: The five stages of biofilm development. A) Reversible attachment to a solid support. B) Irreversible attachment and aggregation. C) Biofilm maturation. Bacterial cells become layered and quorum sensing is initiated. D) Clusters reach maximum density. E) Matrix dispersion to facilitate colonisation of new environmental niches. Reprinted with permission from Davies *et al.*[21] © Springer Nature 2003

The first step involves the introduction of bacteria to a surface, a process which is largely stochastic, driven by Brownian motion and gravitational forces, and influenced by surrounding hydrodynamic forces. Velocity and direction toward or away from the contact surface are influenced greatly by nutrient properties, pH, ionic strength, temperature and bacterial cell-surface composition.[22] Upon intercepting the surface, adherence is mediated by extracellular adhesive appendages and secreted adhesins. However, this initial attachment is dynamic and reversible. Colonising bacteria may be perturbed by hydrodynamic or shear forces, as well as limitations on nutrient availability, thus leaving and re-joining the planktonic population according to external factors.[23]

Irreversible attachment is achieved by bacteria able to weather the shear forces and maintain contact with the surface. Multiplication of adherent cells form microbial aggregates of the same or different species. Subsequent secretion of the EPS forms a barrier between the bacterial community and the extracellular environment, the composition of which is largely species and condition-dependent.[24]

Maturation of the established community involves changes in gene expression and up-regulation of factors favouring sessility, such as those implicated in the formation of the EPS.

Proximity of cells within the biofilm community provides ideal conditions for the formation of nutrient gradients, gene transfer (Section 1.4.3) and quorum sensing (Section 1.4.2). Continuous replication and accumulation of EPS enables the formation of a three-dimensional structure which is able to resist mechanical stress and detachment of the community from the surface of the substrate.

Within the mature biofilm resides a bustling community of cells, actively exchanging products that play a pivotal role in maintaining a stable biofilm architecture and living environment for the resident cells. Once a critical concentration of cells is reached, biofilm dispersal may occur, as cells move back into the planktonic state in order to adsorb to previously uncontaminated surfaces, thus forming new biofilm micro-colonies in new environmental niches. Biofilm dispersal can be the result of several cues, such as alternations in nutrient availability, oxygen fluctuations and the accumulation of toxic products. This step is essential for the propagation and self-renewal of the community, avoiding overcrowded biofilms and thus the gradual decline of the community's health by size-limiting factors.[17,25]

1.4.2. Quorum Sensing

Quorum sensing in bacteria is a regulatory mechanism, which controls gene expression in a manner dependent on cell density. Bacteria within the biofilm engage in a coordinated 'decision-making' process via a chemical vocabulary. A single bacterium may perceive the bacterial cell density in the surrounding area, making it more likely to join and contribute towards biofilm formation. Bacterial colonies utilise quorum sensing to modulate a variety of chemical and cellular functions, including virulence, nutrient acquisition, conjugation, motility and secondary metabolite/toxin production.[26]

Both Gram-positive and Gram-negative bacteria utilise quorum sensing via the production, release and group detection of extracellular signalling molecules called autoinducers. Accumulation of autoinducers as cell density increases allows individual cells to monitor changes in population numbers and collectively alter global patterns of gene expression.[27] Gram-positive systems typically use secreted oligopeptides and two-component systems, consisting of membrane-bound sensor kinase receptors and cytoplasmic transcription factors that direct alterations in gene expression. The process and biological role of quorum sensing in Gram-positive bacteria have been extensively reviewed elsewhere.[28,29]

N-Acyl homoserine lactones (AHLs) are the most commonly used molecules used by Gram-negative bacteria as quorum sensing autoinducers. These molecules are comprised of an invariant homoserine lactone ring, attached to an acyl chain that may vary in length between

4-18 carbon atoms. Variation in length of the acyl chain may affect stability, thus having potential consequences for signalling dynamics.[27] Autoinducers are produced within the bacterial cell and freely diffuse across the inner and outer membranes. At levels of high cell density, when autoinducer concentration is sufficiently high, they bind to cytoplasmic receptors that operate as transcription factors. In many cases, autoinducers participate in forward feedback loops, whereby a low initial concentration of an autoinducer amplifies the production of a chemical signal involved in gene expression.

Quorum sensing has proved a promising therapeutic target in recent years, since the mechanistic understanding of quorum sensing systems and appreciation for their importance in bacterial pathogenesis has improved. As additional systems and signal molecules have been identified, so have examples of quorum sensing inhibition, by both signal-targeting enzymes[30,31] and small molecule inhibitors[32,33] of signal synthases and receptors. The possibility of targeting quorum sensing as a means to alleviate or prevent infection has been met with strong optimism in the wake of the antibiotic resistance crisis that currently impedes the treatment of many pathogenic infections.[29]

1.4.3. Gene Transfer and Antibiotic Resistance

Perhaps the most salient difference between biofilm-bound and free-living cells is their greater tolerance to antimicrobial agents and host defences. Owing to the dense and compact nature of a biofilm structure, the reduced rates of cellular growth and the diffusion limitations conferred by the EPS, bacteria within a biofilm are considerably protected from natural and chemical agents, rendering biofilm cells 10-1,000-fold less susceptible to antimicrobial therapy than their planktonic counterparts.[21] For instance, the antibiotic tobramycin requires a 1000-fold increase in concentration to kill biofilm cells of *Pseudomonas aeruginosa (P. aeruginosa)* growing on a urinary catheter, compared with planktonic cells of the same species.[34]

It is generally accepted that the basis for biofilm-specific antibiotic resistance is multifactorial, and depends on the agent, the bacterial strain and species, the developmental stage of the biofilm and the biofilm growth conditions.[35] Indeed, the biofilm EPS may act as an adsorbent or reactant, thereby reducing the concentration of agent able to interact with resident cells, which may themselves be physiologically different from planktonic cells (expressing protective factors such as multidrug efflux pumps and stress-response regulons).[36]

Even successful penetration of the biofilm by antimicrobial agents may be insufficient to completely eliminate the colony, owing to the presence of so called ‘persister cells’. These cells constitute approximately 1% of the biofilm population, and exist in a state of metabolic

dormancy. Persister cells survive antibiotic treatment without undergoing a phenotypic change, hence they are not referred to as resistant, but rather tolerant to antibiotic treatment. Metabolic quiescence appears to be responsible for the recalcitrance of chronic infection even after repeated antibiotic treatments, as these cells remain viable, thus repopulating biofilms when the concentration of antibiotic diminishes.[37]

Biofilms provide an ideal niche for the exchange of extrachromosomal DNA in the form of plasmids. Conjugation (the mechanism of plasmid transfer) has been found to occur at a greater rate between sessile cells.[38] Horizontal gene transfer has been proven to be of particular importance within multispecies biofilms, as resistance genes may be transferred between apathogenic and highly virulent strains both within and beyond species borders. The rate of genetic exchange occurring within the biofilm has the potential to allow significant spread of antibiotic resistance genes, allowing bacterial to rapidly adapt to changing environments.[39]

1.5. The CAUTI Microbiota

The microbiome of the colonized catheter is highly time dependent. Bacteriuria as a result of short-term intermittent catheterisation is generally resultant from a single species of uropathogen (the most common responsible organisms are *E. coli*, *Enterococcus faecalis and Staphylococcus aureus/ epidermidis*.[40] For long-term indwelling catheterisation, multispecies biofilms occur more frequently, consisting of organisms such as *P. aeruginosa*, *Providencia stuartii* and *Proteus mirabilis* (*P. mirabilis*) (Table 1.1).

Table 1.1: The incidence of uropathogens isolated from 106 catheter biofilms, from patients undergoing long-term indwelling catheterisation. Reproduced with permission from Macleod *et al.*[40] © Microbiology Society 2007

Species	% of catheters colonised by each species		
	All catheter biofilms	**Mixed-species biofilms (76 catheters)**	**Single species biofilms (30 catheters)**
*Pseudomonas aeruginosa**	36	41	23
Enterococcus faecalis	34	45	7
Escherichia coli	31	41	7
*Proteus mirabilis**	30	34	20
*Klebsiella pneumoniae**	18	24	3
*Morganella morganaii**	13	15	10
Providencia stuartii	10	12	7
*Staphylococcus aureus**	10	13	3
Enterobacter cloacae	9	9	7
*Klebsiella oxytoca**	9	11	3
*Providencia rettgeri**	5	5	3
Coagulase-negative staphylococci*	5	5	3
Citrobacter spp	4	5	3
*Proteus vulgaris**	3	3	3
* Indicates species capable of producing urease			

1.6. The Role of Proteus mirabilis

P. mirabilis is an organism of unique importance for patients undergoing long-term indwelling catheterisation. Since the CAUTI microbiome is highly time dependent, this species is seldom isolated following initial colonisation of the catheterised urinary tract. The longer the catheter is in place, the more likely it is to become colonised by *P. mirabilis*, hence this organism is isolated from approximately 40% of urine samples collected from patients with long-term indwelling catheters.[12]

P. mirabilis is a Gram-negative, dimorphic, motile member of the family Enterobacteriaceae, and readily colonises the lumen and external surfaces of all catheter types. It was observed by Roberts *et al.*[41] that *P. mirabilis* has the greatest ability to attach to catheters out of all Gram-negative organisms. This is achieved by the expression of 17 putative fimbrial operons, the most encoded by any sequenced bacterial species.[42]

1.6.1. The Swarming Motility

Merging mythology and morphology, *P. mirabilis* is named after the early sea god from Greek mythology, noted for being versatile and capable of assuming many forms.[43] Proteus appears in Homer's *Odyssey*, and is able to shift shape to avoid capture. Likewise, *P. mirabilis* is able to differentiate from short rods into elongated, multinucleate cells that express thousands of flagella. Ergo, *Proteus* species are distinguishable from almost any other genera by their ability to swarm across a solid surface.[44]

Microscopic examination of samples of infected urine reveals peritrichous planktonic *P. mirabilis* approximately 2 μm in length. The flagella of the vegetative bacteria are engaged in what is known as the swimming motility, where they may be likened to a rotating motor, coupled to allow the flow of protons across the membrane to provide rotational energy. In liquid planktonic culture, the swimming motility is the primary locomotive method employed by *P. mirabilis*, the direction of which is determined by the direction of flagella rotation, and is controlled by external sensory input linked to environmental influences.[45]

The presence of a solid or highly viscous surface provides the conditions required for the swarming motility to dominate. After adherence to the surface, cells undergo a rapid differentiation into multinucleate, 20-50-fold elongated swarmer cells with thousands of expressed flagella. Swarmer cells may then arrange themselves into parallel groups, entwined by the helical binding of their flagella around adjacent cells, forming raft-like structures that are capable of moving off rapidly in unison (Figure 1.3). By this mechanism, large populations

of *P. mirabilis* are able to effectively and efficiently colonise surfaces such as the luminal surfaces of the urinary catheter.[43]

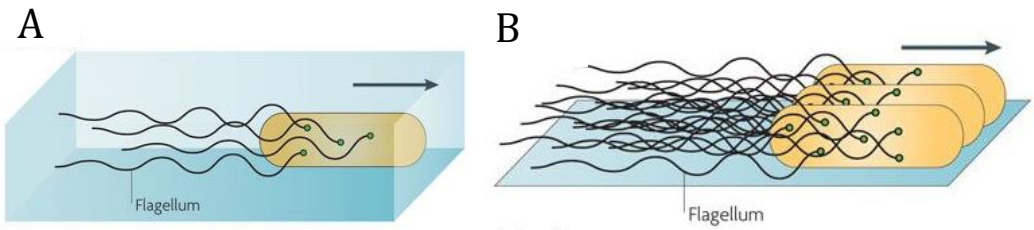

Figure 1.3: Locomotive mechanisms of *P. mirabilis*. A) The swimming motility, powered by rotating flagella in planktonic culture. B) The swarming motility, engaged on contact with a solid substrate, and powered by the multicellular movement of elongated cells with intertwined helical flagella. Adapted with permission from Kearns.[45] © Springer Nature 2010

P. mirabilis provides the most well-documented irregular swarming pattern of all motile bacteria. The characteristic bullseye pattern formed on the solid substrate occurs as a result of cyclic and synchronous waves of motility, followed by regular periods of swarming cessation. Each cycle of swarming produces one annulus of the pattern, and consists of a macroscopic 'zone of consolidation', or 'terrace'. The development of the concentric rings may be separated into three distinct phases: lag phase (the growth of the initial inoculum), swarming phase (independent movement of the swarming raft structures), and consolidation phase (uniform thickening of the newly formed terrace).[46]

Another fascinating aspect of the *P. mirabilis* swarming motility (and an example of the complexity of the interbacterial communications required to achieve it) is the Dienes phenomenon. Two swarming colonies of a single strain of *P. mirabilis* may merge with each other, whereas swarms of different strains form a distinct boundary where they meet, known as the Dienes line.[47] Formation of the Dienes line requires direct cell-cell contact and is thought to involve the killing of one strain at the boundary, for example by the production of the bacteriocin proticine.[48]

P. mirabilis' employment of the swarming motility facilitates colonisation of the urinary catheter by coordinating the rapid movement of bacteria from the site of contamination to the bladder via the luminal surface. Additionally, swarming cells of *P. mirabilis* have been shown to be capable of transporting other, non-motile organisms over the surface of the catheter, thus confirming the role that swarming plays in the initiation and pathogenesis of CAUTI.[49]

1.6.2. Toxin Production

P. mirabilis is capable of producing an arsenal of bacterial toxins. Haemolysin was originally proposed as a virulence factor, as cytotoxicity towards human renal epithelial cells is largely due to haemolysin, and strains with high haemolysin production are significantly more lethal than those with low production.[50,51] Haemolysin is also thought to facilitate bacterial spread within the kidney and pyelonephritis development during ascending CAUTI.[52] However, mutation of *hpmA*, the gene encoding this toxin, did not appear to affect kidney colonisation or tissue damage during colonisation. Hence, either haemolysin is not as active during infection as the *in vitro* data suggests, or the activity of other virulence factors masks its contribution.[43,53]

Proteus toxic agglutinin (Pta), encoded by the mosaic pathogenicity island ICE*Pm1*, is a bifunctional outer-membrane autotransporter that mediates cell-cell aggregation. It achieves bladder and kidney damage via damage to the structural integrity of the native cells.[54] In the proposed mechanism of action, Pta punctures the host cell membrane, inducing cytosol leakage, osmotic stress and depolymerisation of actin filaments.[9] Notably, simultaneous inactivation of Pta and *hpmA* facilitates a greater reduction in cytotoxicity than each mutation individually, indicating that the toxins act additively.[53] Indeed, Pta production by the *hpmA* mutant may explain why no difference in pathogenicity was observed between the haemolysin mutant and the parent strain.

1.6.3. Persistence and Immune Evasion

Infections by *P. mirabilis* in the catheterised urinary tract are notoriously difficult to treat, owing to the remarkable ability of this bacteria to persist despite antibiotic treatment and catheter change. Successful persistence within the host relies on the evasion of innate and adaptive immune responses. Once such mechanism of immune evasion employed by *P. mirabilis* is the variation in expression or composition of antigenic structures, such as outer-membrane proteins or fimbriae. The best-studied fimbrial type of *P. mirabilis*, MRP fimbriae, are known to be phase variable.[55] It is not yet known whether the other 16 types of fimbriae undergo phase variation, although any range of expression within such an extensive fimbriae library would contribute significantly to fitness.[43]

Furthermore, *P. mirabilis* encodes a metalloproteinase, ZapA, able to cleave serum and secretory immunoglobulins, thereby providing protection from the mucosal immune response.[56] ZapA may also be capable of cleaving cell matrix components such as collagen, fibronectin and laminin, as well as cytoskeletal proteins such as actin and tubulin.[57] The importance of ZapA in the bacteria's evasive procedures is emphasised by the finding that the

mutation of ZapA results in a significant decrease in bacterial cell recovery from the urine, bladder and kidneys.[58]

1.6.4. Horizontal Gene Transfer

The 94 kilobase mobile pathogenicity island, ICE*Pm1*, of *P. mirabilis* has been found to be present in several isolates of *Providencia stuartii and Morganella morganii*, suggestive of DNA transfer between bladder pathogens.[59] ICE*Pm1* is more prevalent in *P. mirabilis* clinical isolates taken from the urine of catheterised individuals than from other body sites, indicating that this mobile genetic element contributes to colonisation and pathogenicity within the catheterised urinary tract. As CAUTI is often initiated by the patient's own resident gut flora, the acquisition of ICEP*m1* may give some insight as to why these organisms (which are normally commensal) become pathogenic when they reach this site.[43] Additionally, it has been shown that ICE*Pm1* can excise from the *P. mirabilis* chromosome and integrate into ICE*Pm1*-deficient strains, provided that the integrase, chromosome-partitioning protein A, and the type IV secretion system remain intact.[60] These studies support the concept of horizontal gene transfer within the clinical setting, a phenomenon which may also allow for the transfer of antimicrobial resistance.

1.6.5. Cell-Cell Communication

Interbacterial communication and quorum sensing between cells of *P. mirabilis* is both elusive and complex. *P. mirabilis* lacks a clear AHL synthase homologue (LuxI), capable of producing *N*-acyl homoserine lactone signalling molecules typically used by Gram-negative species to sense population density and coordinate gene expression. However, *P. mirabilis* instead encodes a LuxR family transcriptional regulator, and seems to produce compounds with AHL-like activity.[44,61] However, AHLs secreted by other species present on the catheter may be able to modulate *P. mirabilis* swarming or virulence, since it has been found that the exogenous addition of AHL to a population of *P. mirabilis* has a strain-specific impact on virulence factor expression, swarming and biofilm formation.[62,63]

1.6.6. Urease and Catheter Encrustation

Arguably the most important aspect of *P. mirabilis* pathogenesis from a clinical perspective is the expression of bacterial urease and the subsequent catheter encrustation. Once colonised onto the catheter and uroepithelial surfaces, *P. mirabilis* must adapt and obtain nutrients from the urinary tract environment in which it thrives. The expression of a potent cytoplasmic nickel metalloenzyme, urease, allows *P. mirabilis* to exploit urea as a nitrogen source (Scheme 1.1). Nitrogen, in the form of ammonia, may then be assimilated into biomolecules via glutamine synthesis or glutamate dehydrogenase.[64]

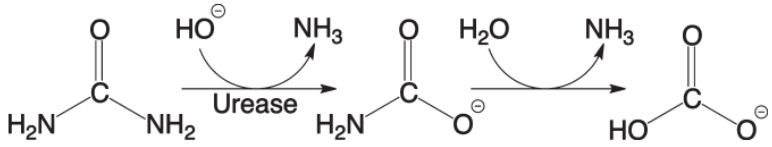

Scheme 1.1: Urease-catalysed hydrolysis of urea

A full discussion into the structure and mechanistic action of bacterial urease can be found in Chapter 5. Briefly, urea hydrolysis results in the production of carbonic acid and two molecules of ammonia. The physical manifestation of this enzymatic process within the catheterised bladder is the substantial and rapid rise in urinary pH, owing to the net production of ammonia which gradually accumulates within the urine reservoir. The alkalinised local environment may cause the urinary pH to rise to pH 7.5-9, compared to healthy, acidic urine pH of 5.5-6.5.[65] Consequently, local supersaturation and precipitation of polyvalent ions (primarily struvite, $MgNH_4PO_4.6H_2O$ and carbon apatite, $Ca_{10}(PO_4CO_3OH)_6(OH)_2$) into the catheter lumen may cause abrasive crystalline deposits to become incorporated into the catheter biofilms. Total occlusion of the catheter lumen may follow, in addition to severe bladder and urethral trauma upon removal.[44]

1.6.7. Structure and Formation of Crystalline Biofilms

For patients with long-term indwelling catheters, catheter changes are generally scheduled at approximately 10-12 week intervals, allowing contaminated urine to flow through an individual catheter for long periods of time. Consequently, thriving bacterial biofilm communities are formed, with the gentle flow of warm nutritious urine facilitating a continuous culture system, which prevents the community from becoming nutrient-limited.[66] All types of Foley catheter, including silver-coated and nitrofurazone-impregnated catheters, are susceptible to colonisation by crystalline biofilms. Motile bacteria such as *P. mirabilis* have

a competitive advantage when forming a biofilm, utilising flagella to overcome hydrodynamic and repulsive forces.[17]

In addition to biological factors, physical effects can prove powerful in the initiation of biofilm development. A study utilising episcopic differential interference contrast (EDIC) microscopy to compare the surface morphologies of different catheter types revealed that all catheter types display a rough, irregular surface, able to provide a nucleation site for the adhesion of bacterial cells in the early stages of biofilm formation.[67] The manufacturing techniques used to produce the eyeholes tear through the material, resulting in surfaces covered in microscale craters and crevices. All-silicone catheters have smoother surfaces than latex catheters, although irregularities are still commonplace around the eyeholes and in areas where extrusion manufacturing techniques produce striations on the luminal surfaces (Figure 1.4).[66,67]

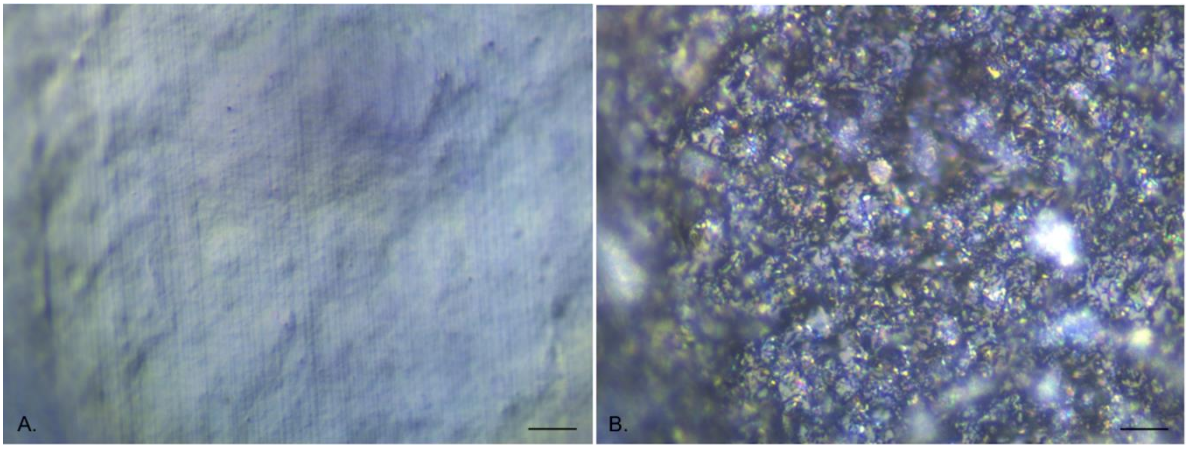

Figure 1.4: EDIC microscopy images of unused catheter surfaces, showing surface topography. A) All silicone catheter, showing luminal striations. B) Hydrogel latex catheter. (Magnification x1000, scale bar = 10 μm). © 2015 Wilks *et al.*[67]

1.6.8. Recurrent Crystalline Biofilms

Recurrent catheter blockage is a major issue within the healthcare setting, causing distress to both patients and caregivers, as well as proving costly to the health service. The usual management technique recommended for recurring blockage is simply the replacement of the blocked catheter with a new one.[68] Fresh catheters are thus placed directly into urine cultures of *P. mirabilis* at alkaline pHs, often containing microcrystals of calcium and magnesium phosphates. Examination of crystalline biofilm formation under these conditions in a laboratory model, revealed that catheter surfaces were covered in a microcrystalline layer

after just 1 hour. After 18 hours, the eyelets and luminal surfaces of all catheters were comprehensively covered by densely populated crystalline biofilms of *P. mirabilis*.[69]

Approximately 50% of patients who undergo long-term indwelling catheterisation will experience encrustation and blockage owing to *P. mirabilis* biofilms.[16] The consequences of blockage may vary greatly in terms of medical severity. Leakage around the outside of the catheter may cause patient incontinence, thus increasing need for nursing care. Complete blockage of the catheter lumen may cause retention of urine in the bladder and subsequent vesicoureteric reflux of urine to the kidneys. If the blockage is left untreated or unnoticed at this stage, patients are likely to suffer serious symptomatic episodes of pyelonephritis, bacteraemia and peri-urethral purulent infection, ultimately leading to chronic renal failure and death.[70]

1.7. Treatment and Prevention of CAUTI

Even with meticulous care, patients undergoing long-term catheterisation will experience bacteriuria owing to cross-contamination.[44] Since the majority of cases are asymptomatic in their early stages, treatment is not recommended, as a balance must be struck between the reduction in CAUTI morbidity and the forestalling of the emergence of antibiotic resistance. In long-term catheterisation, antibiotic therapy has little benefit, owing to the re-emergence of infection upon the changing of the catheter.[71] Indeed, bacteriuria is such a common occurrence, that treatment with prophylactic antibiotics inevitably leads to the emergence and selection of antibiotic-resistant strains of *P. mirabilis*, as well as the development of other multiresistant nosocomial strains. Consequently, patients are only treated in this manner if immunosuppressed (e.g. post-organ transplantation), at significant risk of bacterial endocarditis, about to undergo urinary tract instrumentation, or pregnant.[72]

Many efforts have been made to design catheters that are resistant to bacterial colonisation, with the overall aim or preventing CAUTI incidence and subsequent catheter blockage. Despite the large number of reported approaches appearing within the literature in recent years, few platforms have progressed to clinical studies, and even fewer to clinical practice. This lack of translational success can be attributed, in part, to the inherent complexity of the clinical problem, as well as the necessary interdisciplinary nature of the research required to overcome it.

1.7.1. Engineering Approaches

Despite its innate design flaws, the Foley catheter remains the fundamental linchpin in the management of the dysfunctional bladder. Variations on Foley's original design,[73,74] as well as additive devices[75] to be used with the current clinical setup have been explored. Recently, a novel catheter design has been described by Levering *et al*.[76] which aims to provide on-demand biofilm removal *in situ*. Active surface deformation via the utilisation of multi-inflation lumens facilitates the debridement of approximately 80% of a mixed community biofilm of *P. mirabilis* and *E. coli*. (Figure 1.5). Inflation of the four intra-wall inflation lumens simultaneously is able to supply sufficient strain around the intra-luminal perimeter to debond biofilms from the otherwise largely inaccessible main drainage lumen.

Other attempts to redesign aspects of the urinary catheter include the trefoil design described by Sun *et al.,*[77]whose profile proved successful in delaying the appearance of culturable organisms when tested in an *in vivo* rabbit model.

A 2018 commissioning brief by the National Institute for Health Research[78] outlines several modified catheter designs, including the Duette dual balloon urinary catheter (Poiesis Medical, Florida),[79] the CymActive™ bladder management system (Ingenion Medical Limited, London),[80] and the OPTION-*vf* and OPTION-*vm* gender specific valved catheters (Practica Medical Manufacturing Inc., Florida),[81] which allow urine storage within the bladder rather than in the collection bag. The valve design permits urine drainage in a manner similar to normal uncatheterised voiding, therefore avoiding the accumulation of stagnant urine beneath the eyehole level of a standard Foley catheter.

Such variation in catheter design may prove promising in the prevention of CAUTI. As well as the inherent advantages offered by the novel design of the catheter itself, catheters such as the trefoil and multi-inflation lumen design may also be coated with passive or stimuli-responsive coatings, thus providing a multifaceted approach to the prevention of encrustation and blockage.

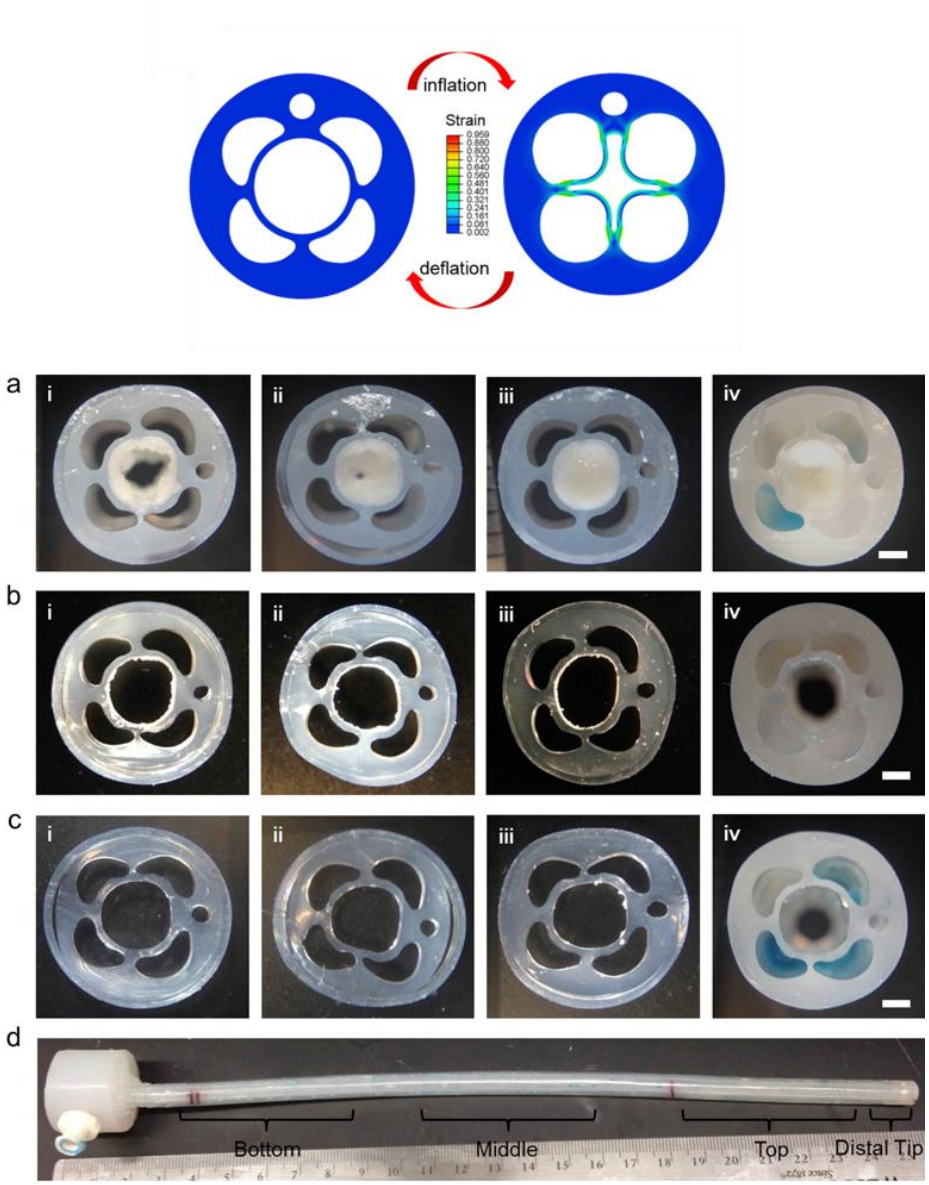

Figure 1.5: (Top) Cross-section of a silicone urinary catheter shaft with four inflation lumens. Strain contour plot shows model subjected to an inflation pressure of 80 kPa. (Bottom) Multi-inflation lumens capable of debridement of multispecies *P. mirabilis* and *E. coli* biofilms. Cross sectional images of A) control catheter (no inflation). B) First inflation after 30 hours of biofilm growth. C) Second inflation after 24 hours biofilm regrowth. D) Sections from which the cross-sections were obtained. i) bottom, ii) middle, iii) top, and iv) distal tip. Scale bars indicate 1 mm. Reprinted from Levering *et al*.[76] © 2016, with permission from Elsevier.

1.7.2. Medical Approaches

Over the past decade, imbibing or coating medical implants with antimicrobial solutions has been commonly used to control infection. A range of passive release-based systems have been investigated for the prevention or delay of catheter blockage, the most common of which is simple impregnation, where the agent is held within a reservoir and released via passive diffusion. In contrast to oral or systemic delivery of administration, release coatings provide the ability to deliver agents at a high local concentration, whilst limiting systemic exposure and potential toxicity. Though passive release coatings endeavour to achieve effective prophylaxis and/or treatment of established bacteriuria, the reservoirs of antimicrobial cargos are limited, thus their action is ultimately temporary. Passive release kinetic profiles generally follow first- or second-order kinetics (where an initial burst release is followed by a decreasing tail distribution).[82] The timeframe of release and subsequent decline in active concentration is highly application- and location-dependent, although generally lies within the region of hours or days. This provides a significant challenge in coating design, forcing a compromise between device function and reservoir capacity. As such, the design of coatings able to maintain antimicrobial concentrations throughout the therapeutic window sufficient to cause bacterial cell death, but without causing eukaryotic cytotoxicity, remains a significant challenge.[83]

1.7.2.1. **Antibiotics**

A number of antibiotics have been approved for used in medical impregnated catheters, for the prophylaxis of CAUTI. These include the nitrofurans nitrofurazone and nitrofurantoin, which are known to have a broad spectrum of activity against both Gram-negative and –positive pathogens, and are less prone to inducing antimicrobial resistance.[84] Nevertheless, these commercially-available antimicrobial catheters still lack strong evidence to support their routine use in CAUTI management.[85]

Though nitrofuran-coated catheters are well studied, a recent Cochrane review reported that whilst nitrofurazone-coated catheters did achieve a reduction in symptomatic CAUTI, the impact was of borderline statistical significance. Furthermore, patients treated with catheters of this type complained of greater pain compared with a standard unmedicated catheter, both while the catheter was *in situ*, and upon removal.[85] Owing to its poor clinical performance in large-scale trials, these catheters have been discontinued in the USA.

Whilst antibiotic-impregnated catheters may seem the obvious choice for CAUTI prevention, the inherent issue of antibiotic resistance can render these systems useless after the second or

third application. Antibiotic resistance within the catheterised urinary tract is particularly problematic, since biofilms required a high doses of antibiotics. A better understanding of resistance towards these agents is therefore required in order to develop coatings with a potent dose of antibiotics without promoting the development of resistant bacterial strains. An in-depth discussion of antibiotic resistance within the catheterised urinary tract, as well as potential alternatives, can be found in Chapter 4.

1.7.2.2. **Silver**

Silver has been used for centuries in the treatment of various maladies, or to prevent the transmission of infection. Since silver is one of the few antimicrobial agents for urinary catheter coatings that is approved by the Food and Drug Administration (FDA), commercially-available silver-coated catheters have been extensively studied clinically. For medical device coatings, silver ion release coatings can be designed in the form of silver alloy (often with gold or palladium), silver-containing polymers and silver nanoparticles. Silver is susceptible to oxidation in aqueous environments, releasing ions which are highly biocidal in nature. However, this influx of ions must be controlled and sustained, not least because fast and excessive release of ions may prove cytotoxic.[5]

In a major study conducted over a 40-month period (2007-10) on 7102 patients in the UK, silver alloy-coated latex catheters (Bardex IC, Bard Medical, Crawley, UK), were found to be less effective in reducing infection or cost of urethral catheterisation in comparison to antibiotic coatings. However, catheters of this type were not met with the same level of patient discomfort when compared to their antibiotic-impregnated counterparts.[86]

Further to its limited success in clinical trials, silver alloy has been combined with other materials to improve its antimicrobial efficacy. An epidemiological screening conducted by Rupp *et al.*[87] found that silver alloy hydrogel-coated catheters reduced the occurrence of CAUTI from 6.13/1000 catheters, to 2.62/1000 catheters in 2001-2002 (p = 0.002). In 2014, another study was conducted with silver alloy hydrogel catheters, with patients from 7 acute care hospitals.[88] According to the criteria of the National Healthcare Safety Network, a 58% relative reduction occurred in the incidence of CAUTI when silver alloy hydrogel catheters were employed, compared to standard catheters.

The exhaustive list of studies performed on silver coatings proves that research into finding the ideal antimicrobial coating for urinary catheters is both complex, and may require a combination of both novel and existing compounds. Despite the abundance of reports

suggesting silver to be a safe and effective antimicrobial agent, its efficacy in urinary catheters has proven limited. Thus, research on the use of silver for this application will likely continue through the advent of new combinations that endeavour to substantially increase its antimicrobial efficacy and decrease cytotoxicity.

1.7.3. Chemical Approaches

Many efforts have been made to design catheters that are resistant to bacterial colonisation. Approaches designed to prevent adhesion of bacteria generally aim to impede biofilm formation in its infancy by utilising unfavourable surface topography or surface chemistry. Since the host-derived conditioning film of urinary components begins at the point of catheter insertion, any existing surface properties of the material are often concealed, and pathogen attachment promoted. Thus, development of chemical modification approaches for prevention of CAUTI must not only target uropathogen attachment, but also urinary constituents.[83]

1.7.3.1. Anti-Adhesion/Antifouling Surfaces

Whilst the conceptual simplicity and potential biocompatibility of anti-adhesion coatings makes them an appealing approach, their antibacterial action requires extremely close proximity with bacterial cells. Catheter surfaces within such a complex biological matrix may become rapidly contaminated with non-specifically attached materials, thus compromising the defect-free surface. Nevertheless, the field of anti-fouling polymers is fast growing and showing significant promise. Poly(ethylene glycol) (PEG) is the most widely used polymer for antifouling in recent years,[89] although its efficacy largely depends on the surface grafting technique and the polymeric architecture.[90] Polymers such as PEG form a tightly-bound and structured hydration shell via hydrogen bonding, which creates a thermodynamically unfavourable surface for the adsorption of organic substances or particle adhesion. However, it has been demonstrated that PEG is susceptible to oxidative damage in the presence of oxygen and transition metal ions, thereby significantly worsening its antifouling properties. [91]

Zwitterionic materials, containing equal positive and negative charge functionalities are able to maintain electric neutrality and are well-known for their antifouling properties. Zwitterionic materials have recently been introduced on to polydimethylsiloxane (PDMS) (the material most commonly used for the production of Foley catheters).[91,92] much like PEG-based systems, the introduction of hydrophilic zwitterionic moieties leads to the formation of a bound water layer, thus rendering the surface thermodynamically unfavourable for the adhesion of fouling species.[92] Unlike PEG-based systems, however, formation of the hydration shell is via

electrostatic interactions which, as they are stronger than hydrogen bonding, result in denser and more tightly adsorbed water.[93]

1.7.3.2. **Nanostructured Materials**

The material and resulting surface topography from which a urinary catheter is formed can significantly impact the rate of biofilm formation. Recent studies have aimed to investigate and exploit the abilities of a material's surface topography in order to modulate cellular adhesion. Nature-inspired patterned surfaces, such as Sharklet™ have shown promise in the development of a benign surface treatment for the prevention of bacterial attachment.[94,95] The Sharklet micropatterned surface has been shown to inhibit colonisation and migration of uropathogenic *E. coli* under growth conditions *in vitro*.[96] The ability of the uropathogenic *E. coli* to colonise three variations of the Sharklet micropattern was assessed, all of which outperformed a standard PDMS control. An average of 47% reduction in CFU and bacterial area coverage was observed, in addition to 77% reduction in colony size, both in growth media and artificial urine.

Surface topographies such as Sharklet create mechanical stress on a settling bacterium, a phenomenon known as mechanotransduction. Nanoforce gradients caused by surface variations induce stress gradients within the lateral plane of the surface membrane of a settling microorganism during initial contact. The stress gradient disrupts normal cell function, forcing the cell to provide energy to adjust its contact area on each topographical feature in order to equalise the stresses. The expenditure of this energy is thermodynamically unfavourable, thus inducing its detachment and subsequent search for an alternative attachment site (Figure 1.6).[97]

The employment of inert nanostructured materials as anti-adhesive surfaces represents a paradigm shift in the current considerations of using chemical modifications to alter the surfaces of medical devices, by relying on a microscopic texture to provide an inhospitable surface for microorganism colonisation.

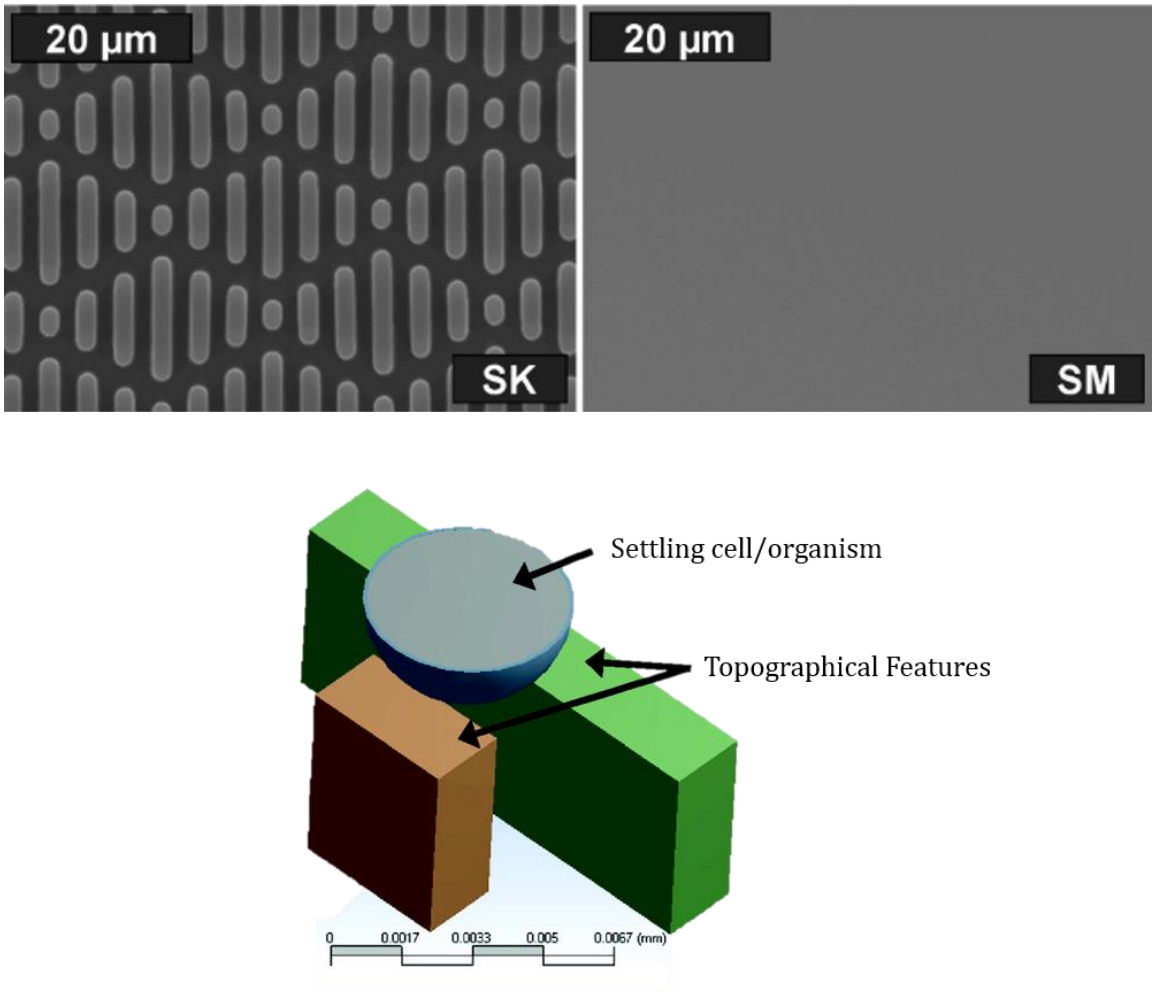

Figure 1.6: (Top) Scanning electron micrographs of force-gradient engineered topography Sharklet™ (SK) fabricated in PDMS, in comparison to a smooth PDMS surface (SM). (Bottom) Schematic of a settling cell/organism contacting two dissimilar topographical features, creating an effective stress gradient within the lateral plane. The separation distance between each feature induces strain on the cell membrane. Adapted with permission from Schumacher *et al*.[97] ©2008 American Chemical Society.

1.7.4. Stimuli-Responsive Approaches

Current research into stimuli-responsive systems has provided a potential solution to many of the issues encountered with standard passive-release strategies. Such systems rely on an external stimulus (either directly or indirectly associated with the onset of infection), in order to facilitate diagnosis or treatment. Direct stimuli caused by successful colonisation include specific biomarkers produced by pathogenic bacteria (e.g. enzymes and toxins), whilst a change in the physical conditions (e.g. pH or temperature) may provide indirect indication of infection. Crucially, stimuli-responsive materials are able to retain their diagnostic or

therapeutic capabilities until an endogenous factor initiates a burst response of the cargo contained within. This may manifest as a change in volume or structure of the cargo's reservoir material, or a bond cleavage of anchored moieties.[98]

The ability to control both the release kinetics and delivery location of a diagnostic or therapeutic cargo offers significant advantages over conventional passive release systems. Since the cargo is held within a reservoir until its release is initiated, sub-lethal exposure of antimicrobial agents to pathogenic bacteria, and subsequent development of resistance is circumvented. Furthermore, the cargo itself, which may be sensitive to external conditions with prolonged exposure, is protected. The concept of controlled release is particularly attractive for the treatment of CAUTI, owing to the time-dependent release of the cargo, since premature administration of a therapeutic agent will inevitably result in elution from the bladder, rendering the system ineffective before the progression of infection.

A recent study by Francesko *et al.*[99] utilises specific biomarkers to induce the release of antibacterial agents, via the disassembly of polycationic nanospheres. Catheter coatings were composed of intact, highly antibacterial polycationic nanospheres, processed from aminated cellulose (able to disrupt bacterial membranes) and bacteria-degrading hyaluronic acid. Coatings were found to be stable in the absence of bacteria, but disassembled gradually upon incubation with *P. aeruginosa*, thereby preventing biofilm formation under dynamic conditions using a model of the catheterised bladder. The outer, bacteria-responsive layer of hyaluronic acid was found to be degraded by pyocyanin (a redox-active virulence factor produced by *P. aeruginosa*), resulting in a 70% reduction in bacterial growth after 2 hours ($p < 0.001$).

The urease-catalysed hydrolysis of urea to ammonia by *P. mirabilis*, and the subsequent increase in urinary pH has been exploited in the development of pH-responsive systems for the prevention of CAUTI. These approaches will be discussed in Chapters 4 and 5. The urinary pH elevation provided by *P. mirabilis* infection is the obvious choice of stimulus to form the basis of a triggered-release system, since it is both rapid and significant within the catheterised urinary tract.

1.8. Conclusion and Project Aims

In summary, catheterisation of the urinary tract provides a significant risk to those undergoing long-term indwelling catheterisation, owing to the formation of crystalline biofilms following colonisation by *P. mirabilis*. Whilst many attempts have been made to render the current Foley catheter system less susceptible to infection, resistance to change of the current design by both care-givers and patients has rendered many of these approaches largely redundant. In particular, engineering-based approaches that encompass a completely redesigned catheter system have thus far proved unsuccessful in clinical translation. Furthermore, medicated catheters containing antibiotics (e.g. nitrofurans) and or silver derivatives have shown limited efficacy in clinical trials, owing to the masking of antimicrobial effects upon the initiation of a conditioning biofilm layer, or increased patient discomfort. Whilst it is widely acknowledged that the clinical, social, and economic burdens associated with the use of the Foley catheter have gained notoriety in recent years, it is also true to say that regulatory authorities, relevant industrial and commercial companies, as well as the scientific community have thus far failed to find a comprehensive solution. Thus, there exists a need for novel approaches to the prevention and detection of catheter encrustation and blockage that are sympathetic to the currently accepted Foley catheter design and closed drainage system, which has remained unchanged since its ubiquitary clinical introduction in the 1930s.

The aim of this thesis is to develop novel strategies for the detection and prevention of catheter encrustation and blockage. The research agenda for the following chapters will endeavour to design supplementary systems to the current Foley design, able to either detect *P. mirabilis* infection in advance of catheter blockage, or to delay blockage and extend the catheter lifetime. The diagnostic approaches (Chapters 2 and 3) will endeavour to facilitate advance warning of impending catheter blockage, in order to permit clinical intervention prior to the onset of serious symptomatic episodes. The therapeutic approaches (Chapters 4 and 5) will aim to utilise alternatives to antibiotics in order to delay biofilm formation and subsequent encrustation of the urinary catheter. The use of conventional antibiotics is deliberately avoided, since the overuse and exposure of sub-lethal concentrations of chemical antibiotics may rapidly induce the dawn of a post-antibiotic era.

Given the nature and complexity of the clinical problem, research which endeavours to extend catheter lifetime is inherently multidisciplinary. Hence, the strategies presented in this thesis aim to combine chemical, biological and engineering advances, whilst still maintaining aspects of the original design.

1.9. References

1. R. C. L. Feneley, I. B. Hopley and P. N. T. Wells, *Journal of Medical Engineering & Technology*, 2015, **39**, 459–470.
2. D. M. Siddiq and R. O. Darouiche, *Nature Reviews Urology*, 2012, **9**, 305–314.
3. S. Saint, J. Wiese and J. K. Amory, *American Journal of Medicine*, 2000, **109**, 476–480.
4. R. O. Darouiche, *Clinical Infectious Diseases*, 2001, **33**, 1567–1572.
5. P. Singha, J. Locklin and H. Handa, *Acta Biomaterialia*, 2017, **50**, 20–40.
6. J. Lo, D. Lange and B. H. Chew, *Antibiotics*, 2014, **3**, 87–97.
7. M. Kilonzo, *Policy Brief December 2015 Reducing hospital infections : which catheter ?*, 2015.
8. A. Cartwright, *British Journal of Nursing*, 2018, **27**, 7–12.
9. A. L. Flores-mireles, J. N. Walker, M. Caparon and S. J. Hultgren, *Nature Reviews Microbiology*, 2015, **13**, 269–284.
10. N. Høiby, T. Bjarnsholt, C. Moser, G. L. Bassi, T. Coenye, G. Donelli, L. Hall-Stoodley, V. Holá, C. Imbert, K. Kirketerp-Møller, D. Lebeaux, A. Oliver, A. J. Ullmann, C. Williams, ESCMID Study Group for Biofilms (ESGB) and Consulting External Expert Werner Zimmerli, *Clinical Microbiology and Infection*, 2015, **21**, S1–S25.
11. European Antimicrobial Resistance Surveillance Network (EARS-Net), *European Centre for Disease Prevention and Control*.
12. L. E. Nicolle, *Antimicrobial Resistance and Infection Control*, 2014, **3**, 1–8.
13. A. Lewis, *Drug Device Combination Products: Delivery Technologies and Applications*, Woodhead Publishing Ltd, Oxford, UK, 1st edn., 2010.
14. F. E. B. Foley, *The Journal of Urology*, 1937, **38**, 134–139.
15. K. Wagner, E. T. Bird and K. S. Scott Coffield, *Current Urology Reports*, 2016, **17**, 82.
16. D. J. Stickler, *Journal of Internal Medicine*, 2014, **276**, 120–129.
17. M. Kostakioti, M. Hadjifrangiskou and S. J. Hultgren, *Cold Spring Harbor perspectives in medicine*, 2013, **3**, 1–23.
18. M. RD and G. O'Toole, *Trends in Microbiology*, 2009, **17**, 73–87.
19. H.-C. Flemming and J. Wingender, *Nature Reviews Microbiology*, 2010, **8**, 623–633.
20. A. N. Norsworthy and M. M. Pearson, *Trends in Microbiology*, 2017, **25**, 304–315.
21. D. Davies, *Nature Reviews Drug Discovery*, 2003, **2**, 114–122.
22. R. M. Donlan, *Emerging Infectious Diseases*, 2002, **8**, 881–890.
23. Y. Wu and F. W. Outten, *Journal of Bacteriology*, 2009, **191**, 1248–1257.
24. K. G. Neoh, M. Li, E. T. Kang, E. Chiong and P. A. Tambyah, *Journal of Materials Chemistry B*, 2017, **5**, 2045–2067.
25. L. D. Renner and D. B. Weibel, *MRS bulletin / Materials Research Society*, 2011, **36**, 347–355.
26. M. Miller and B. Bassler, *Annual Review of Microbiology*, 2001, **55**, 165–199.
27. K. Papenfort and B. L. Bassler, *Nature Reviews Microbiology*, 2016, **14**, 576–588.

28. V. Monnet and R. Gardan, *Molecular Microbiology*, 2015, **97**, 181–184.
29. B. LaSarre and M. J. Federle, *Microbiology and Molecular Biology Reviews*, 2013, **77**, 73–111.
30. Y. Dong, J. Xu, X. Li and L. Zhang, *Proceedings of the National Academy of Sciences*, 2000, **97**, 3526–3531.
31. Y. Dong, L. Wang, L. Xu, H. Zhang, X. Zhang and L. Zhang, *Nature*, 2001, **411**, 813–817.
32. J. Rajkumari, S. Busi, S. Borkotoky, A. Murali, K. Suchiang and S. K. Mohanty, *Biotechnology Letters*, 2018, **40**, 1087–1100.
33. C. Lu, B. Kirsch, C. Zimmer, J. de Jong, C. Henn, C. Maurer, M. Musken, S. Haussler, A. Steinbach and R. Hartmann, *Chemistry & Biology*, 2012, **19**, 381–390.
34. J. C. Nickel, I. Ruseska, J. B. Wright and J. W. Costerton, *Antimicrobial Agents and Chemotherapy*, 1985, **27**, 619–624.
35. T. F. C. Mah and G. A. O'Toole, *Trends in Microbiology*, 2001, **9**, 34–39.
36. P. Gilbert, D. G. Allison and A. J. McBain, *Journal of Applied Microbiology*, 2002, **92**, 98–110.
37. T. K. Wood, S. J. Knabel and B. W. Kwan, *Applied and Environmental Microbiology*, 2013, **79**, 7116–7121.
38. A. P. Roberts, J. Pratten, M. Wilson and P. Mullany, 1999, **177**, 63–66.
39. J. L. Balcazar, J. Subirats and C. M. Borrego, *Frontiers in Microbiology*, 2015, **6**, 1–9.
40. S. M. Macleod and D. J. Stickler, *Journal of Medical Microbiology*, 2007, **56**, 1549–1557.
41. J. A. Roberts, N. Everett, M. Fussell and B. Kaack, *The Journal of Urology*, 1990, **144**, 264–269.
42. M. M. Pearson, M. Sebaihia, C. Churcher, M. A. Quail, A. S. Seshasayee, N. M. Luscombe, Z. Abdellah, C. Arrosmith, B. Atkin, T. Chillingworth, H. Hauser, K. Jagels, S. Moule, K. Mungall, H. Norbertczak, E. Rabbinowitsch, D. Walker, S. Whithead, N. R. Thomson, P. N. Rather, J. Parkhill and H. L. T. Mobley, *Journal of Bacteriology*, 2008, **190**, 4027–4037.
43. C. Armbruster and H. Mobley, *Nature Reviews Microbiology*, 2012, **10**, 743–754.
44. S. M. Jacobsen, D. J. Stickler, H. L. T. Mobley and M. E. Shirtliff, *Clinical Microbiology Reviews*, 2008, **21**, 26–59.
45. D. B. Kearns, *Nature reviews. Microbiology*, 2010, **8**, 634–44.
46. O. Rauprich, M. Matsushita, C. J. Weijer, F. Siegert, S. E. Esipov and J. A. Shapiro, *Journal of Bacteriology*, 1996, **178**, 6525–6538.
47. L. Dienes, *Journal of bacteriology*, 1946, **63**, 265–70.
48. A. E. Budding, C. J. Ingham, W. Bitter, C. M. Vandenbroucke-Grauls and P. M. Schneeberger, *Journal of Bacteriology*, 2009, **191**, 3892–3900.
49. N. Sabbuba, G. Hughes and D. J. Stickler, *BJU International*, 2002, **89**, 55–60.
50. H. L. Mobley, G. R. Chippendale, K. G. Swihart and R. A. Welch, *Infection and immunity*, 1991, **59**, 2036–2042.
51. G. R. Chippendale, J. W. Warren, A. L. Trifillis and H. L. Mobley, *Infection and immunity*, 1994, **62**, 3115–3121.
52. P. G. Peerbooms, A. M. Verweij and D. M. MacLaren, *Infect Immun*, 1984, **43**, 1068–1071.
53. P. Alamuri, K. A. Eaton, S. D. Himpsl, S. N. Smit and H. L. T. Mobley, *Infection and*

Immunity, 2009, **77**, 632–641.

54. P. Alamuri and H. L. T. Mobley, *Molecular Microbiology*, 2008, **68**, 997–1017.
55. F. K. Bahrani and H. L. T. Mobley, *Journal of Bacteriology*, 1994, **176**, 3412–3419.
56. B. W. Senior, L. M. Loomes and M. A. Kerr, *Journal of Medical Microbiology*, 1991, **35**, 203–207.
57. R. Belas, J. Manos and R. Suvanasuthi, *Infection and Immunity*, 2004, **72**, 5159–5167.
58. K. E. Walker, S. Moghaddame-Jafari, C. V. Lockatell, D. Johnson and R. Belas, *Molecular Microbiology*, 1999, **32**, 825–836.
59. E. L. Flannery, L. Mody and H. L. T. Mobley, *Infection and Immunity*, 2009, **77**, 4887–4894.
60. E. L. Flannery, S. M. Antczak and H. L. T. Mobley, *Journal of Bacteriology*, 2011, **193**, 4104–4112.
61. M. Boyer and F. Wisniewski-Dyé, *FEMS Microbiology Ecology*, 2009, **70**, 1–19.
62. D. Stankowska, M. Kwinkowski and W. Kaca, *J Microbiol Immunol Infect*, 2008, **41**, 243–253.
63. D. Stankowska, G. Czerwonka, S. Rozalska, M. Grosicka, J. Dziadek and W. Kaca, *Folia Microbiologica*, 2012, **57**, 53–60.
64. J. N. Schaffer and M. M. Pearson, *Microbiology spectrum*, 2015, **3**, 212–263.
65. J. A. Simerville, W. C. Maxted and J. J. Pahira, 2005, **71**, 1153–1162.
66. D. J. Stickler, *Nature Clinical Practice Urology*, 2008, **5**, 598–608.
67. S. a. Wilks, M. J. Fader and C. W. Keevil, *PLoS ONE*, 2015, **10**, 1–13.
68. K. Getliffe, *Journal of Wound, Ostomy and Continence Nursing*, 2003, **30**, 146–151.
69. D. J. Stickler and S. D. Morgan, *Journal of Hospital Infection*, 2008, **69**, 350–360.
70. J. W. Warren, D. Damron, J. H. Tenney, J. M. Hoopes, B. Deforge and H. L. Muncie, *Journal of Infectious Diseases*, 1987, **155**, 1151–1158.
71. J. W. Warren, *International Journal of Antimicrobial Agents*, 2001, **17**, 299–303.
72. J. Meddings, M. A. Rogers, S. L. Krein, M. G. Fakih, R. N. Olmsted and S. Saint, *BMJ quality & safety*, 2014, **23**, 277–289.
73. US6855126B2, 2005, 1–8.
74. US20130030415A1, 2011, 1–5.
75. US7829029B2, 2010, 1–21.
76. V. Levering, C. Cao, P. Shivapooja, H. Levinson, X. Zhao and G. P. López, *Biomaterials*, 2016, **77**, 77–86.
77. Y. Sun, Q. Zeng, Z. Zhang, C. Xu, Y. Wang and J. He, *Journal of Urology*, 2011, **186**, 1497–1501.
78. NHS and National Instituite for Health Research, Health Technology Assessment, https://www.nihr.ac.uk/funding-and-support/documents/current-funding-opportunities/hta/18 41 supp.pdf, (accessed 3 October 2018).
79. J. Beilan, T. Lund, K. Beane, R. Ordorica and D. Hernandez, *The Journal of Urology*, 2016, **195**, 227.
80. H. Homan, R. Dmochowski, J. Cochran, L. Karsh, N. Sherman and S. Yalla, *Neurology and*

Urodynamics, 2016, **35**, 630–635.

81. L. Stone, *Nature Reviews Urology*, 2015, **12**, 300.
82. E. P. Holowka and S. K. Bhatia, in *Drug Delivery*, Springer, New York, NY, 2014, pp. 7–62.
83. S. Milo, J. Nzakizwanayo, H. J. Hathaway, B. V. Jones and A. T. A. Jenkins, *Proceedings of the Institution of Mechanical Engineers, Part H: Journal of Engineering in Medicine*, 2018.
84. D. R. Guay, *Drugs*, 2001, **61**, 353–364.
85. T. Lam, O. Mi, E. Fisher, K. Gillies and S. Maclennan, *Cochrane Database of Systematic Reviews*, 2014, 1–92.
86. R. Pickard, T. Lam, G. Maclennan, K. Starr, M. Kilonzo, G. Mcpherson, K. Gillies, A. Mcdonald, K. Walton, B. Buckley, C. Glazener, C. Boachie, J. Burr, J. Norrie, L. Vale, A. Grant and J. N. Dow, *The Lancet*, 2012, **380**, 1927–1935.
87. M. E. Rupp, T. Fitzgerald, N. Marion, V. Helget, S. Puumala, J. R. Anderson and P. D. Fey, *American Journal of Infection Control*, 2004, **32**, 445–450.
88. J. W. Lederer, W. R. Jarvis, L. Thomas and J. Ritter, *Journal of Wound, Ostomy and Continence Nursing*, 2014, **41**, 473–480.
89. K. Knop, R. Hoogenboom, D. Fischer and U. S. Schubert, *Angewandte Chemie - International Edition*, 2010, **49**, 6288–6308.
90. R. Konradi, C. Acikgoz and M. Textor, *Macromolecular Rapid Communications*, 2012, **33**, 1663–1676.
91. A. Vaterrodt, B. Thallinger, K. Daumann, D. Koch, G. M. Guebitz and M. Ulbricht, *Langmuir*, 2016, **32**, 1347–1359.
92. A. Dundua, S. Franzka and M. Ulbricht, *Macromolecular Rapid Communications*, 2016, **37**, 2030–2036.
93. M. He, K. Gao, L. Zhou, Z. Jiao, M. Wu, J. Cao, X. You, Z. Cai, Y. Su and Z. Jiang, *Acta Biomaterialia*, 2016, **40**, 142–152.
94. R. Vasudevan, A. J. Kennedy, M. Merritt, F. H. Crocker and R. H. Baney, *Colloids and Surfaces B: Biointerfaces*, 2014, **117**, 225–232.
95. R. M. May, C. M. Magin, E. E. Mann, M. C. Drinker, J. C. Fraser, C. A. Siedlecki, A. B. Brennan and S. T. Reddy, *Clinical and Translational Medicine*, 2015, **4**, 9.
96. S. T. Reddy, K. K. Chung, C. J. McDaniel, R. O. Darouiche, J. Landman and A. Brennan, *Journal of Endourology*, 2011, **25**, 1547–1552.
97. J. F. Schumacher, C. J. Long, M. E. Callow, J. A. Finlay, J. A. Callow and A. B. Brennan, *Langmuir*, 2008, **24**, 4931–4937.
98. M. Cloutier, D. Mantovani and F. Rosei, *Trends in Biotechnology*, 2015, **33**, 637–652.
99. A. Francesko, M. M. Fernandes, K. Ivanova, S. Amorim, R. L. Reis, I. Pashkuleva, E. Mendoza, A. Pfeifer, T. Heinze and T. Tzanov, *Acta Biomaterialia*, 2016, **33**, 203–212.

Diagnostic Approaches

Chapter 2: Development of an Infection-Detection Sensor Coating for Urinary Catheters

2.1. Abstract

The research presented in this chapter describes the development and *in vitro* testing of an infection-responsive coating for urinary catheters, that provides a clear visual early warning of infection and subsequent catheter blockage. The system utilises pH as an indirect external marker of infection, thus rendering it sensitive to infections by *P. mirabilis*. The coating is comprised of a dual-layered system, in which the lower poly(vinyl alcohol) (PVA) reservoir layer contains the self-quenching dye 5(6)-carboxyfluorescein. This is capped by an upper layer of the pH-responsive polymer poly(methyl methacrylate-*co*-methacrylic acid) (Eudragit S100®). Elevation of the urinary pH (pH >7) as a consenquence of infection by *P. mirabilis* causes a significant morphological change in the Eudragit layer, thus releasing the dye to provide clear visual warning of impending blockage (Figure 2.1). Prototype coatings were evaluated in a clinically relevant *in vitro* bladder model, which provides a physiologically accurate representation of the catheterised urinary tract.

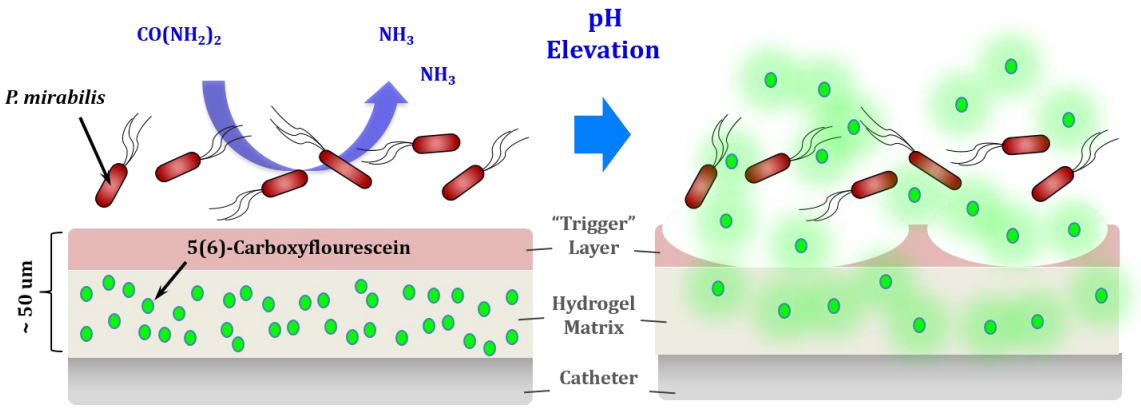

Figure 2.1: Schematic representation of the dual-layered polymeric architecture for the pH-responsive release of 5(6)-carboxyfluorescein from a urinary catheter coating.

This system aims to provide a proof-of-concept catheter coating, in order to investigate the delivery of small molecules directly into the bladder in response to infection. 5(6)-carboxyfluorescein acts as a 'model drug' for the release of therapeutic species into the bladder. The use of a diagnostic agent aims to reduce the administration of unnecessary antibiotics for infections of this nature, whilst reducing patient discomfort and clinical intervention.

2.2. Introduction

2.2.1. Point-of-Care Diagnostic Systems: The Clinical Need

In a medical sense, a diagnosis can be regarded as an attempt at classification of an individual's condition into separate and distinctive categories, to allow medical decisions regarding treatment and prognosis to be made. Recent technological advances have markedly improved the way in which infection and disease are clinically diagnosed, and are now beginning to make the transition from laboratory to clinic.

Point-of-care (POC) diagnosis is defined as medical diagnostic testing at or near the point of care. That is, at the time and place of patient care. This contrasts with the historical pattern, in which testing is wholly or mostly confined to the medical laboratory, and specimens from the POC are sent for analysis by trained personell. Results are generally obtained within hours or days, during which care must continue without the desired information. POC testing systems provide rapid results, facilitating actionable information that can lead to a change in patient management. Such results reduce the need for multiple patient visits, enable timely treatment, and aid the containment of infectious disease outbreaks. Crucially, POC disgnostics reduce reliance on presumptive treatment, thereby increasing antimicrobial stewardship.[1]

A 2015 interdisciplinary workshop organised by the Wellcome Trust examined the use of diagnostic tools to guide antibiotic usage in a range of common clinical scenarios. Rapid diagnostics were thought to play a vital role in the battle against drug-resistant infections by indentifying specific pathogens and allowing timely intervention. Increasing the availability of novel diagnostic technology allows for less indiscrimante use of antibiotics, a major driving factor in the emergence and spread of resistance. Specific goals outlined by the Wellcome Trust include the ability to identify high-risk patients; tools able to identify precise biomarkers indicative of location-specific infection may prove crucial for the prognosis of likely poor clinical outcomes.[2]

2.2.1.1. Prevention of Catheter Blockage: Current Strategies

The diagnostic challenge for CAUTI is inherently multifactorial. Uncomplicated cases of bacteriuria as a result of short-term, intermittent catheterisation do not generally lead to serious symptomatic episodes, and often self-resolve upon removal of the catheter. Patients suffering from CAUTI are likely to be elderly and residing in a care-home environment. Consequently, a range of undifferentiated symtoms (confusion, fever, incontinence) may be

indicative of unrelated conditions. Patients must hence be rapidly diagnosed as either requiring antibiotic intervention or not, often by unqualified personell, by determining whether or not they are progressing towards sepsis. In this scenario, overtreatment is common, thus there exists an urgent need for a diagnostic tool able to identify colonising bacteria. Further challenges lie in the ability to distinguish true infection from colonisaiton via an easily identifiable sensor system, which may alert even an untrained patient or caregiver to the type of intervention required.[2,3]

Current clinical guidelines for preventing catheter blockage as a result of CAUTI are simply to remove the catheter and avoid their use where possible.[4] There is currently no objective method of predicting catheter blockage. Where catheters must remain in place on a long-term indwelling basis, preventative measures for catheter encrustation and blockage include ensuring a consistent fluid intake, regular emptying of the drainage bag, maintaining good general hygiene, and performing regular catheter changes of 4-6 weeks post-insertion.[5]

In 2017, the Royal United Hospital (Bath, UK) introduced a novel 'catheter passport' for urology and community care outpatients, to improve catheter management and reduce recurrent blockage outside of the acute care setting.[6,7] One aspect of this newly implemented documentation is a 'catheter diary', whereby the catheterised patient may record the dates of catheter changes, as well as any adverse events such as blockage or bladder spasms. Despite being primitive and puerile, catheter diaries remain the primary method of predicting long-term indwelling catheter blockage. Indeed, guidelines recommended by the Centre for Disease Control are designed only for short-term urinary catheter use, thus often do not cover the frequency that indwelling catheters should be changed. Emphasis is therefore placed on evidence-based recommendations, driven by reimbursement and tradition.[8]

Given the sparce and nebulous nature of the clinical guidelines regarding the prevention of CAUTI in indwelling catheters, there exists a need for a rapid and accurate point-of-care diagnostic, able to identify the progression of CAB to CAUTI. Specifically, a diagnostic system able to give prior warning of explicit symptomatic epsiodes, namely catheter blockage, would be valuable to provide reliable and objective notification of blockage. Crucially, the diagnostic output must be easily interpretable, and not requiring specialist equipment or training, to render the technology accessible to patients outside the acute care setting.

2.2.2. Novel Diagnostic Systems for CAUTI

The design constraints of the current Foley catheter system are important considerations in the formulation of a novel sensor for infection by *P. mirabilis*, and subsequent catheter blockage. The concept of utilising urinary pH elevation to provide 'early warning' of blockage via creation of a sensor system compatible with the current design has been explored previously by Stickler *et al*.[9,10] The first iteration of these sensors involved the covalent linkage of the pH indicator bromothymol blue to cellulose acetate polymer. Despite successful *in vitro*[9] and clinical assessments[11] of this system, the sensor was deemed unsuitable for commercial development. Hence, the system was modified to improve commercial viability via the manufacture of a silicone-based formulation with the incoporated indicator and a hydrophilic filler. The sensor was housed within a small polyvinyl chloride connector, located in the junction between catheter and drainage bag. Despite its initial promise, the 'early warning' of catheter blockage in human trials was >18 days, thus calling into question whether this system can be considered an indicator of imminent blockage. Additionally, some participants in the trial reported leakage around the sensor, or expressed concerns over the additional length,[12] thereby highlighting the need for any novel sensor to be compatible with the existing closed-drainage system.

Other diagnostic urinary catheter accessories described in the literature include the development of a pH-sensitive, reversible colourimetric porous membrane as part of a multimodal system involving a nitrite sensor, embedded within a hydrogel matrix and coated onto the internal surface of the drainage tubing. Since nitrite (NO_2^-) is a metabolite of the biological nitrogen cycle,[13] but not a natural component of human urine, this system provides dual-aspect sensing technology to both alert to the presence of bacteriuria, and distinguish the presence of urease-producing species.[14]

Diagnostic accessories that do not rely on pH, but instead on electrochemical detection of urinary catheter biofilm formation, have also been described. Investigation into a sensor module employing electrical impedence utilising two or more substrate-integrated electrodes, allows for a rapid output signal for the presence of a bacterial biofilm as well as biofilm thickness and possible encrustation. This sensor may be combined with additional modules such as those detecting changes in pH/ body temperature to provide multifaceted feedback regarding the development of infection *in situ*.[15]

2.2.3. Carboxyfluorescein

Fluorescence spectroscopy is frequently used in aspects of biochemistry, cell biology, molecular biology and biophysics, owing to its sensitivity and rapid response times. Spectroscopic systems utilising fluorescent signals can be 100-fold more sensitive than absorption spectrophotometry, thus micromolar concentrations are sufficient to give a strong signal.[16] In particular, carboxy derivatives of fluorescein (Scheme 2.1) are widely used within bioconjugate chemistry, for example the synthesis of labelled oligonucleotides.[17,18] Carboxyfluorescein is a particulary valuable fluorescent agent in biochemical and medical diagnostic applications, owing to its combination of useful properties, including fluorescence, pH-sensitivity, biocompatibility and concentration-quenching.[19]

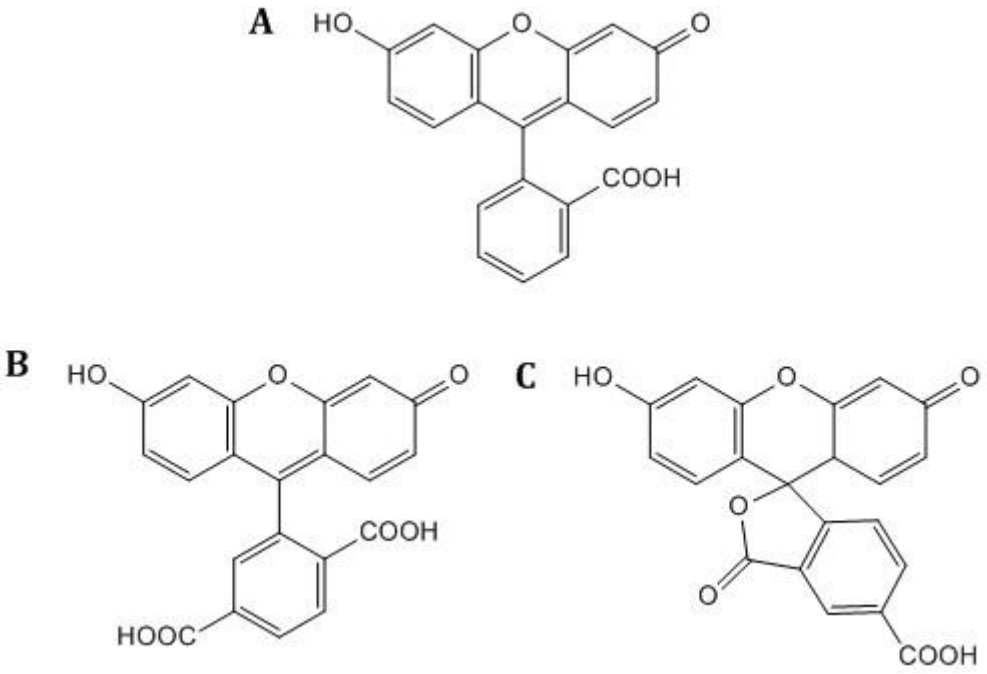

Scheme 2.1: Fluorescein (A) and its carboxy derivatives. (B) 6-carboxyfluorescein. (C) 5(6)-carboxyfluorescein.

Fluorecence quenching can be defined as a bimolecular process that reduces the fluorescence quantum yield, whilst leaving the fluorescence emission spectrum unchanged. Concentration-quenching, also known as self-quenching, refers to the quenching of a fluorophore by another of the same. Concentration quenching is a highly distance-depedent excited-state interaction between two fluorophores, via the formation of non-fluorescent dimers. It is widely accepted that concentration-quenching occurs as a result of internal conversion and intersystem crossing in the excited states of dimers in solution.[20] The fluorescence quantum yield can be strongly affected by dimerisation, since the intersystem crossing between the singlet and

triplet excited states may lead to a radiationless decay channel that cannot be realised in the monomeric species.[21] Concentration-quenching in carboxyfluorescein arises owing to the overlap of the absorption and emission spectrum, thus facilitating a reduction in fluorescence signal upon formation of non-fluorescent dimers.[22]

2.2.3.1. Carboxyfluorescein as a Model Drug

Carboxyfluorescein is frequently used as a hydrophilic model drug system in novel targeted drug delivery formulations. Such systems often include the encapsulation of a hydrophilic drug within the internal aqueous core of lipid vesicle systems (such as conventional liposomes,[23] transfersomes,[24] and ethosomes,[25] as well as biopolymer-based multilayers).[26] Release of carboxyfluorescein from the highly-concentrated aqueous core results in an increase in detectable fluorescence output.

A recent study by De Leo *et al.*[27] describes the formulation of a liposome-modified titanium surface as a strategy to locally deliver bioactive molecules from orthopaedic or dental implants. Titanium and its alloys are widely employed in medical implants owing to their mechanical properties, resistance to corrosion, and osseointegration capability. However, adverse reactions may occur at the tissue/implant interface, thereby limiting the success of biointegration. Carboxyfluorescein was used as a model biomolecule for delivery from liposome-based coatings for titanium implants, employing fluorescence microscopy for real-time imaging of cargo delivery to adherent cells, and subsequent cellular uptake. Carboxyfluorescein was detectable within MG63 human osteoblast-like cells after 1 hour incubation at 37 °C (Figure 2.2).

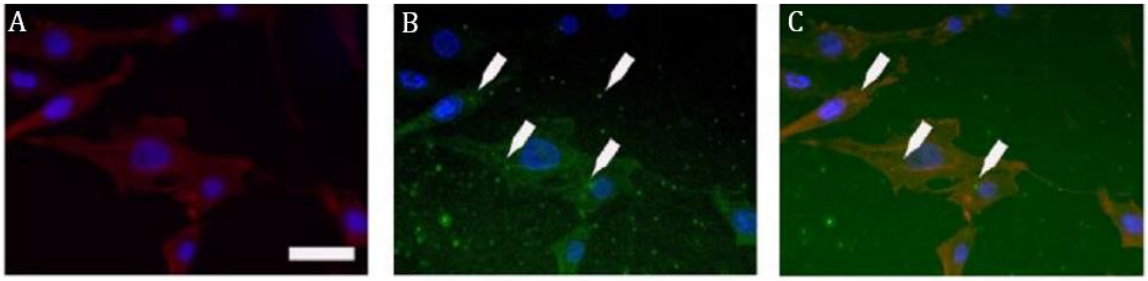

Figure 2.2: The use of carboxyfluorescein as a model drug. Fluorescence micrographs of MG63 human osteoblast cells cultured in the presence of carboxyfluorescein-loaded liposomes, anchored to titanium sheets. Fluorescence response detected in the cytoplasm after 15 minutes (A), 1 hour (B), and 2 hours (C) after incubation at 37 °C. Dotted green fluorescence (white arrows) shows cellular uptake of liposomes (scale bars 10 μm). Modified with permission from De Leo *et al.*[27] © 2017, with permission from Elsevier.

2.2.3.2. Carboxyfluorescein as a Diagnostic

The use of carboxyfluorescein as a diagnostic agent has proved promising in recent years, owing to its rapid and distinctive colour change upon dilution, ease of quantification and biocompatibility.[28] Encapsulation of carboxyfluorescein within a reservoir matrix may provide sufficiently high concentrations such that the fluorescence output is self-quenched. Upon release of the dye into the surrounding biological environment (in response to a physical or biological trigger), the fluorescence 'switch on' achieved by sudden dilution is visible to the naked eye, thus achieving a stimuli-responsive diagnostic system.

Such a system has recently been developed by Thet *et al*.[29], in which 5(6)-carboxyfluorescein is encapsulated within lipid vesicles and dispersed within a hydrogel matrix, to create a novel wound dressing prototype (Figure 2.3).

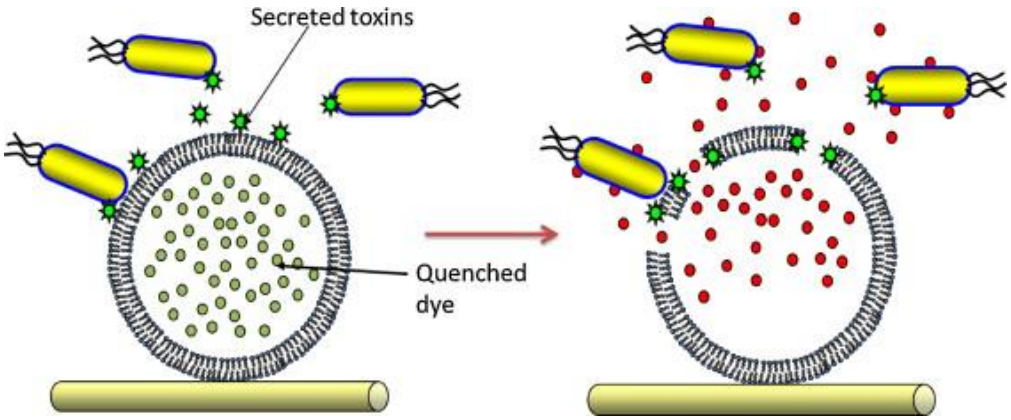

Figure 2.3: Schematic showing the diagnostic wound dressing concept. A lipid vesicle containing self-quenched dye 5(6)-carboxyfluorescein is lysed by secreted toxins from pathogenic bacteria. The resultant dye release manifests as a fluorescence 'switch on' following carboxyfluorescein dilution within the hydrogel matrix. Reproduced with permission from Zhou *et al*.[30] © 2011, with permission from Elsevier.

Since the composition of the vesicle loosely resembles a cellular membrane, cytotoxins released by pathogenic bacteria associated with skin wounds (e.g. *Staphylococcus aureus* (*S. aureus)*) are able to cause rapid lysis and subsequent fluorescent output as a result of carboxyfluorescein dilution within the hydrogel dressing (Figure 2.4).

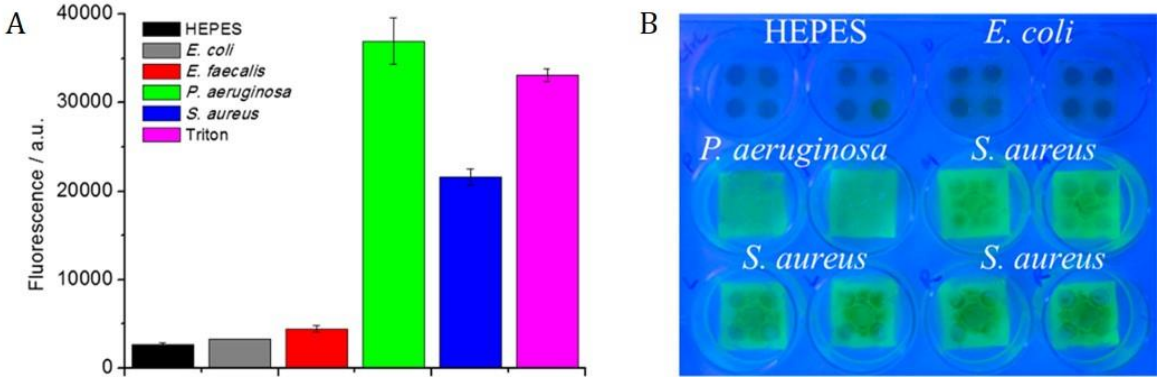

Figure 2.4: Response of prototype wound dressings to colony wound biofilm models of pathogenic bacteria (*Enterococcus Faecalis, P. aeruginosa* and *S. aureus*), and non-pathogenic bacteria (*E. coli).* HEPES buffer was used as a negative control, and the non-ionic surfactant Triton as a positive lysis control. (A) Quantitative fluorescence output. (B) Visual results (dressing fluorescence under UV light). Reproduced with permission from Thet *et al.*[29] © 2016 American Chemical Society.

The use of carboxyfluorescein's fluorescent properties in their own right as 'smart' diagnostic agents, provides an interesting development in the field of POC diagnostics. The identification of novel infection stimuli, alongside the advent of increasingly sensitive smart release technology reveals the potential to construct multiple new diagnostic systems, able to alert patients to bacterial colonisation via a clear and unambiguous colour change. Consequently, this may help to alleviate the pressure currently placed on chemical antibiotics by reducing or removing the need for prophylactic treatment.

2.2.4. pH-Responsive Polymeric Systems

All pH-sensitive polymers consist of either pendant acidic or basic groups, which may either accept or donate protons in response to changes in environmental pH. As basicity of the surrounding medium increases, pendant groups such as as methacrylic acid and acrylic acid undergo deprotonation and subsequent change in the net charge of the attached group, thus introducing repulsive forces within the polymer network. To offset such forces, counter ions from the surrounding medium enter the matrix, resulting in an alteration of the molecular structure of the gel to an expanded state. This phenomenon has been widely exploited within the field of pH-dependent drug release, particularly within the gastrointestinal system.[31]

pH-responsive systems have also shown significant promise in the fields of cancer therapy (since the extracellular space of cancer tissues has a slightly acidic pH, ranging from 6.5-7.2, compared to the healthy 7.4)[32,33], and chronic wound treatment (which exhibit alkaline pH

values ranging from 5.4-7.4,[34] compared to the healthy acidic value of 4.7-5.0)[35]. Futhermore, pH has provided a useful trigger in the field of drug release from urinary biomaterials. Irwin *et al*.[36] have investigated a novel drug delivery system for urinary catheters, which exploits the poor-solubility and pH-dependent physicochemical properties of the antimicrobial agent nalidixic acid within a hydrogel system. With a pKa of 6.0 ± 0.5,[37] nalidixic acid exists entirely in its ionised form at alkaline pH, thus displaying a higher affinity for aqueous media.[38] Release of nalidixic acid was almost instantaneous at pH 9,[36] effectively resulting in a pH-triggered 'burst' response from the hydrogel in response to infection by *P. mirabilis*.

2.2.4.1. Eudragit S100®

Eudragit S100® is a widely used functional copolymer poly(methyl methacrylate-*co*-methacrylic acid), containing a ratio of carboxyl groups to ester groups of 1:2. The polymeric structure of Eudragit is shown in Scheme 2.2.

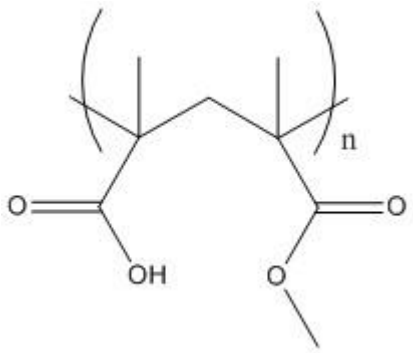

Scheme 2.2: Chemical structure of poly(methyl methacrylate-*co*-methacrylic acid) (Eudragit S100®).

Eudragit polymers are considered the 'gold standard' for functional coatings on oral solid dosage forms, and are widely used as enteric coating formulations for drug delivery. The use of Eudragit in early-stage research provides significant advantages in later scale-up, since all commercially available polymers have gained EXCiPACT™ certification, meaning that Good Manufacturing Practice (GMP) and Good Distribution Practice (GDP) standards are met.[39]

The pH-gradient existing in the bladder as a result of pathological conditions of *P. mirabilis* is sufficient to cause a change in the morphological structure of Eudragit. Such copolymers are of particular relevance to biomedical application as, beyond their biocompatibility, they remain neutral below pH 7, but become charged at alkaline pH. Thus, below pH 7, low permeability is displayed by the Eudragit polymer, owing to the uncharged hydroxyl groups, which may form hydrogen bonds with the carbonyl oxygen of the ester moiety. As the pH of the surrounding

medium rises above pH 7, the carboxylic acid groups become chaged and the polymer network begins to swell as a consequence of repulsion. This facilitates penetration of liquid media and subsequent liberation of any encapsulated species.[40,41]

The use of Eudragit polymers for pH-responsive delivery of biomolecules is ubiquitous throughout the literature. In addition to proving location-specific release within the colon,[42] Eudragit may also be used to protect sensitive biological cargos following oral delivery. A recent study by Vinner *et al*.[43] has utilised Eudragit S100 microspheres, formed using microfluidic glass capillary devices, to deliver *Clostridium difficile* bacteriophage to the colon via oral administration. In contrast to free bacteriophage, those encapsulated within the microparticles could withstand a 3 hour exposure to simulated gastric fluid (pH 2), before undergoing a pH-triggered burst response at within the colon (pH 7).

Eudragit S100 microspheres have also proved promising as an oral carrier for peptide drugs such as insulin.[44,45] Among all of the administratrative routes of human insulin, the oral route offers the maximum advantage in terms of patient compliance. Limitations of insulin delivered via this route however, include low oral bioavailability owing to degradation in the stomach, inactivation and digestion by proteolytic enzymes in the luminal cavity, and poor permeability across the intestinal epithelium. Entrapment of insulin within Eudragit microspheres facilitates its protection from gastric fluids, and subsequent release in the region of the gastrointestinal tract where the pH >7, that is, within the large intestine (where proteolytic enzyme concentration is lower). Early-stage *in vivo* studies using insulin-loaded Eudragit microspheres have demonstrated a prominent hypoglycaemic effect, suggesting that the polymer successfully protects the sensitive cargo from proteolytic degradation.[46]

2.3. Materials and Methods

2.3.1. Materials

Uropathogenic bacterial isolates *P. mirabilis* B4 and *E. coli* NSM59 were kindly contributed from a previously acquired collection (Dr Brian Jones, University of Bath).

Triethyl citrate, Luria-Bertani broth (LB), tryptic soy broth (TSB), yeast extract, tryptone, sodium chloride, magnesium sulphate, magnesium chloride hexahydrate, tri-sodium citrate, sodium oxalate, potassium di-hydrogen orthophosphate (potassium phosphate monobasic), potassium chloride, ammonium chloride, calcium chloride, urea, talc, 5(6)-carboxyfluorescein, PVA (14,600-18,600 $gmol^{-1}$), sodium phosphate monobasic, sodium phosphate dibasic, HEPES buffer and (3-aminopropyl)triethylsilane (APTES) were purchased from Sigma-Aldrich (Poole, Dorset, UK). Bacteriological agar was purchased from Oxoid (Basingstoke, Hampshire, UK).

Eudragit S100 was kindly donated by Evonik Industries (Darmstadt, Germany). Uncoated all-silicone foley catheters and drainage bags (2 L capacity) were obtained from Bard Medical Devision (Covington, GA).

2.3.2. Methods

2.3.2.1. Microbiological Methods

Strict aseptic technique was employed when handling bacterial cultures and sterilised culture media. Assays requiring sterility were undertaken in Grade II flow laminar flow hoods.

I. Principles of Bacterial Growth

For the study and quantification of bacterial growth, cells are first cultured in liquid medium, which provides optimum growth conditions and all nutrients required for cell proliferation. Aliquots of liquid growth culture are then plated onto solid agar medium, in order to quantify bacterial cell numbers. During cultivation in liquid media, bacteria exhibit four distinct phases of growth, which may be monitored according to the change in measurable cell density over time. The first is the initial lag phase, whereby the cells are preparing for replication (e.g. via DNA synthesis and production of various inducible enzymes). Cells then enter the log or exponential growth phase, within which cell division occurs at maximal rate, thereby increasing the total bacterial population exponentially. Following exponential growth, the cells

enter a stationary phase, as the population becomes nutrient limited or depleted by the accumulation of inhibitory metabolic products. During this period, the rate of cell division is equalled by that of cell death, thus there is no net population growth. Finally, upon the onset of conditions which are beyond the tolerance of the species, the cells enter the death phase, where the bacterial cell count begins to decline. Cell density may be assessed photometrically using optical density (OD) measurements (which correlate the degree of light scattering to the cell densitiy via quantification of solution turbidity). The generalised bacterial growth curve as a function of both viable cell count and OD is shown in Figure 2.5.

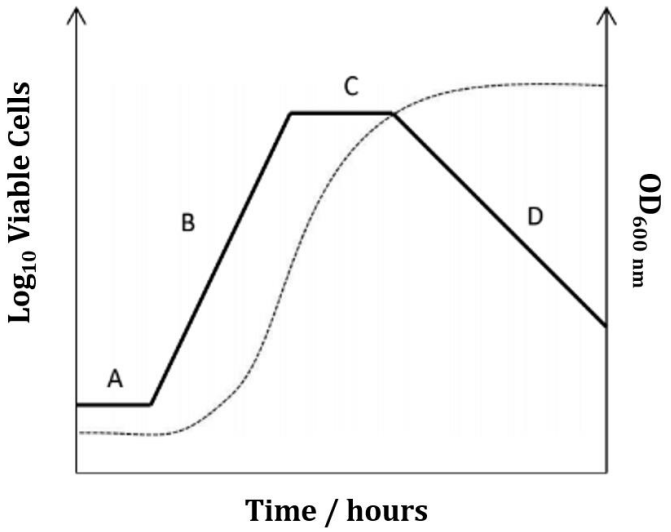

Figure 2.5: Bacterial growth curve showing changing viable cell count wih time in liquid media (solid line), and corresponding change in OD at 600 nm (dotted line). Bacterial growth occurs in four distinct phases. (A) lag phase. (B) Exponential growth phase. (C) Stationary phase. (E) Death phase. No significant reduction in OD is observed during the death phase, as dead cells still exhibit turbidity in liquid culture.

II. Bacterial Culture Conditions

LB media was prepared by dissolution of LB powder (20 g) in deionised water (1 L). LB agar was prepared by dissolution of LB agar powder (35 g) in deionised water (1 L). Non-swarming LB (NSLB) was used to allow the growth of single colonies of *P. mirabilis* on a solid agar surface. Tryptone (10 g), yeast extract (5 g) and bacteriological agar (15 g) were dissolved in deionised water (1 L). All media was autoclaved via subjection to high-pressure saturated steam at 121 °C for 20 minutes to ensure sterility.

Bacterial cultures were grown from freezer stocks via straking on an agar plate (LB/NSLB for *E. coli*/*P. mirabilis* respectively), followed by overnight static incubation at 37 °C. Liquid cultures were obtained via the addition of a single bacterial colony to LB broth (10 mL), followed by further overnight incubation with shaking (200 rpm).

III. Bacterial Quantification

Colony-forming units (CFU) are used to estimate the number of viable bacterial cells in a culture. Since one viable cell is able to give rise to one colony via replication by binary fission, CFU may be calculated by the plate counting method. Single colonies were obtained by plating onto nutrient agar, following serial dilution in liquid media. Briefly, test bacterial solution (100 µL) was added to sterile PBS (900 µL) and vortexed to mix. This solution was serial diluted 10-fold to a final dilution of 10^{-8}. Triplicate aliquots of each dilution (10 µL) were streaked on to LB/NSLB agar medium, and incubated statically overnight at 37 °C. Plates displaying 30-300 colonies were used to quantify CFU per unit volume (CFU/mL) according to Equation 1.

$$\mathrm{CFU/mL} = \frac{\text{Average number of colonies}}{\mathrm{d} \times \mathrm{V}} \qquad (1)$$

Where d is the dilution factor (from original culture), and V is the volume of inoculum (mL).

2.3.2.2. Analysis of 5(6)-Carboxyfluorescein Properties

I. pH-Dependency

The pH-dependent response of carboxyfluorescein was assessed via pH-adjustment of carboxyfluorescein solution (0.5 M in HEPES buffer) within the pH range of 2-10 in 0.5 increments. Fluorescence endpoints were measured using SPECTROstar Omega microplate reader (BMG Labtech, UK), using excitation and emission wavelengths of 485 ± 12 and 520 nm, respectively.

II. Concentration Quenching

Dilutions from carboxyfluorescein stock solution (50 mM) in HEPES buffer were undertaken to achieve a concentration range of 10 mM to 10 nM. Dilutions were adjusted to pH 6, 7 and 8 accordingly via the dropwise additions of NaOH/HCl (1 M). Fluorescence endpoint measurements were recorded on a microplate reader as above.

2.3.2.3. Materials Preparation

I. PVA Hydrogel Preparation

PVA (14,600-18,600 $gmol^{-1}$, 20% w/v) was added to deionised water and heated to 97 °C with constant stirring to facilitate dissolution. The cooled solution was stored at room temperature until required. Once cast, gels were stored overnight at -20 °C to promote cryogenic gelation. Prior to experimental use, gels were thawed at room temperature for 4 hours.

II. Swelling Ratios

Swelling behaviour of PVA hydrogels was investigated by comparing the mass of the dehydrated gels to that of the rehydrated form. PVA solutions (10% and 5% w/v, 500 µL) were cast into the wells of a 24-well microplate. After freeze thawing, gels were transferred to a 12-well microplate and coated with deionised water (1 mL). Plates were incubated at room temperature overnight to allow the gels to swell to their maximum mass, which was recorded. Gel specimens were then removed from the liquid media and incubated overnight at 37 °C to dehydrate. The dry mass was recorded, and the swelling ratio calculated according to Equation 2.

$$\text{Swelling ratio} = \frac{W_R - W_D}{W_D} \quad (2)$$

Where W_R is the mass of the rehydrated disk, and W_D is the mass of the dehydrated disk (g).

III. SEM of PVA Hydrogels

The internal porous structure of the PVA hydrogels was analysed by scanning electron microscopy (SEM) to assess the size and abundance of pores. Gels were freeze-dried (6 hours) and stored under vacuum overnight to ensure complete dehydration. Gels were sputter-coated with gold (Edwards S150B, 60 s) to reduce charging effects and thermal damage, and images obtained using a scanning electron microscope (JEOL SEM6480LV) operated at 10 kV.

IV. Preparation of Eudragit S100 Solution

The organic dip coating solution of Eudragit S100 was prepared according to the Eudragit technical information.[39] The formaulation was scaled for a 300 g suspension (Table 2.1).

Table 2.1: Componencts of Eudragit S100 organic dip coating solution

Compound	Mass (g)	Volume (mL)
Eudragit S100	15.6	-
Triethyl Citrate (plasticiser)	1.6	1.3
Talc (anti-tacking)	7.8	-
Acetone	-	108.5
Isopropanol	-	163.6
Deionised water	-	10.8

Eudragit powder was added gradually to half the diluent mixture, and stirred for 60 minutes until completely dissolved. To the remaining diluent mixture was added talc and triethyl citrate, and the resultant suspension stirred for 10 minutes with a high shear mixer. The excipient suspension was poured slowly into the Eudragit solution with constant stirring, before removing the talc via filtration under vaccum. The solution was stored at room temperature until required.

V. Dip Coating Optimisation

Sterile plastic rods were coated with PVA/carboxyfluorescein hydrogel according to Section 2.2.2.3.VIII, and dip coated with 10, 15 or 20 coats of Eudragit S100 solution to assess dye retention with different coating thicknesses. Release was assessed in phosphate buffer (10 mL) at pH 6, 7 and 8 to mimic healthy, and infected urine respectively. Sodium phosphate monobasic stock solution (0.1 M) and sodium phosphate dibasic stock solution (0.1 M) were mixed in the proportions indicated in Table 2.2. Final pH values were adjusted using a pH meter.

Table 2.2: Components of phosphate buffer (pH 6, 7 and 8)

pH	6	7	8
NaH_2PO_4 /mL	81.5	39.0	5.3
Na_2HPO_4 / mL	18.5	61.0	94.7

Observed fluorescence response was monitored using a microplate reader as above. Test solutions were returned to the bulk liquid after testing to maintain a constant volume.

VI. Silanisation of Urinary Catheters

The method for hydrophilisation of catheter surfaces via silanisation of the silicone surface was modified from Gencer *et al.*[47] Catheters were activated in 1:1 mixture of ammonia (33% v/v) and hydrogen peroxide (30% v/v) for 10 minutes with constant agitation, then rinsed with deionised water and dried under nitrogen. Catheters were then placed in APTES (1% v/v) dissolved in dry N,N-dimethylformamide (DMF) for 16 hours. The surface-modified catheters were subsequently washed with DMF and deionised water (x3), and dried under nitrogen. Water contact angle measurements were made to ensure the hydrophilic nature of the surface.

VII. Contact Angle Analysis of Modified Urinary Catheter Surfaces

Wettability of silanised and untreated PDMS catheter surfaces was assessed using water contact angle analysis. A sessile water droplet (5 μL) was placed onto the surface of a PDMS Foley catheter, and the contact angle measured immediately using a Dataphysics OCA20 goniometer. The results reported represent the average of five meaurements taken on different areas of the specimen. The contact angle was defined as the angle formed between the substrate surface and the tangent to the droplet surface.

VIII. Coating of Foley Catheters

To cooled PVA solution was added 5(6)-carboxyfluorescein solution (500 mM, adjusted to pH 6) at a 1:1 ratio. The resultant hydrogel solution (10 % w/v) containing carboxyfluorescein dye (250 mM) was stored in the dark at room temperature. Catheters were coated with the gel/dye solution (100 μL) between the retention balloon and the distal tip, and stored at -20 °C to promote cryogenic gelation. Catheters were thawed at room temperature (4 hours) before manually dip coating with the pH-responsive trigger layer. Catheters were coated 20 times in Eudragit S100 solution, with a 5 minutes solvent evaporation period at room temperature between each coating. Coated catheters were stored at 4 °C until required.

2.3.2.4. Physiological Representation

I. Artificial Urine Preparation

Streile artificial urine was prepared according to Stickler *et al.*,[48] and was used as a growth medium for *P. mirabilis* when clinically relevant conditions were required. Artifical urine stock solution at 5x concentration was composed according to Table 2.3.

Table 2.3: Components of 5x concentrated artificial urine stock solution

Compound	Mass (g)
Anhydrous sodium sulphate	11.50
Magnesium chloride hexahydrate	3.25
Sodium chloride	23.00
Tri-sodium citrate	3.25
Sodium oxalate	0.10
Potassium di-hydrogen orthophosphate	14.00
Potassium chloride	8.00
Ammonium chloride	5.00
Gelatine	25.00
TSB	5.00

Components of 5x artificial urine stock were dissolved in deionised water (850 mL). The pH of the resultant solution was adjusted to pH 5.7 via dropwise addition of sodium hydroxide solution (1 M). The solution was made up to 1 L with deionised water, and autoclaved to sterilise.

Calcium/urea stock solution at 5x concentration was prepared according to Table 2.4.

Table 2.4: Components of 5x concentrated calcium/urea solution

Compound	Mass (g)
Urea	125.00
Calcium chloride	3.25

Compounds were dissolved in sterile deionised water (350 mL) on a gently warming hotplate to counteract the endothermic solvation. The solution was made up to 400 mL, and filter sterilised through a 0.45 μm syringe filter (Sartorius, UK).

Final working concentration aritificial urine (5 L) was prepared according to Table 2.5.

Table 2.5: Components of working concentration artificial urine

Component	Volume (L)
5x Concentrated artificial urine stock	1.0
5x Concentration calcium/urea stock	0.4
Sterile deionised water	3.6

The final pH of working concentration artificial urine was adjusted to 6.1 before use.

II. *In Vitro* Bladder Models

Setup and operation of *in vitro* bladder models was followed according to Stickler *et al*.[48] The model consists of a double-chambered glass vessel maintained at 37 °C by an external water jacket. The model and associated tubing was first sterilised by autoclaving, and coated catheters inserted into the base via silicone tubing attached to a glass outlet at the base. The catheter retention balloon was inflated using sterile water (10 mL), achieving the sealing of the bladder outlet (Figure 2.6).

The catheter was attached to a sterile drainage bag to complete the full sterile closed drainage system. Sterile artificial urine was supplied to the bladder model via a peristaltic pump (Ismatec ISM1077A) at a flow rate of 0.75 mL/min. This allows a reservoir (~40 mL) of urine to collect in the bladder below the level of the catheter eyehole. As the volume of supplied urine increases, the overflow drains through the catheter to the collection bag.

For bladder models simulating infection, residual urine in the models was inoculated directly with *P. mirabilis* B4 or *E. coli* NSM59 bacteria (10^{10} CFU/mL). Clinical isolates were obtained from urinary tract infections from the Royal Sussex County Hospital or from University Hospitals Bristol for *P. mirabilis* and *E. coli*, respectively. Bacterial cultures were allowed to incubate within the bladder model for 1 hour to establish before flow was restored.

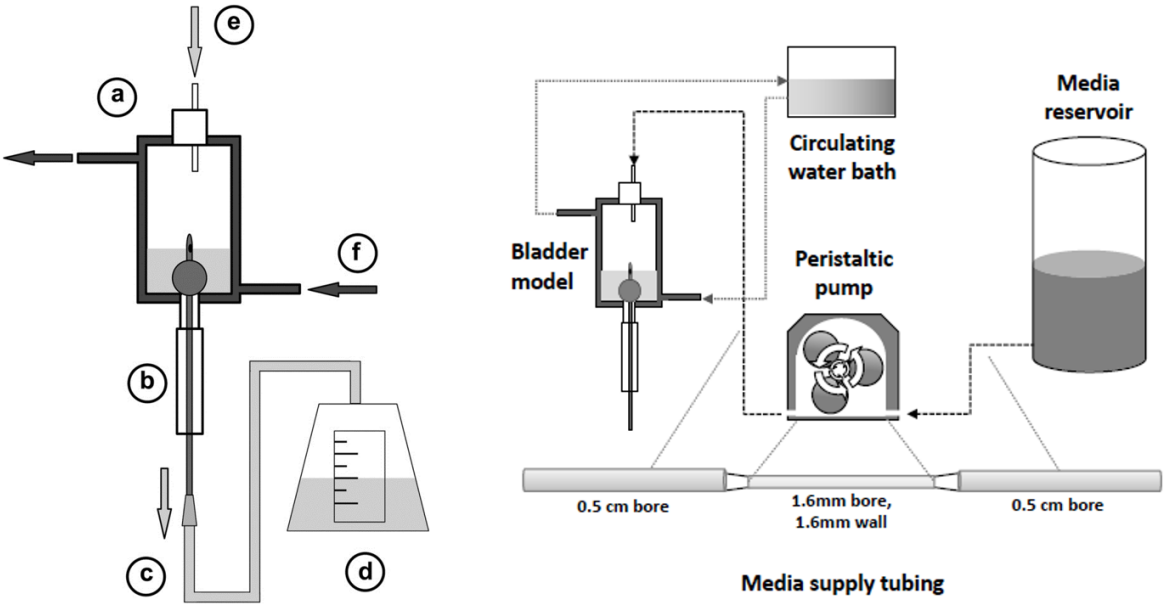

Figure 2.6: Schematic representation of the main components and connections in the *in vitro* bladder model system. (Left) Double-walled glass vessel representing the bladder (A). The Foley catheter is inserted through an outlet at the based of the vessel (B). Drainage tubing, mimicking the closed drainage system (C) is connected to a sterile drainage bag to collect urine outflow (D). Sterile artificial urine is supplied to the bladder via a peristaltic pump at a constant flow rate (E). Physiological temperature is maintained at 37 °C via a circulating water bath (F). (Right) Key features of media supply tubing, and flow of media/ water through the model. Media flow is governed by the peristaltic pump from the reservoir, whilst water flow through the bladder model's outer chamber is driven by a circulating water bath. Dimensions of media supply tubing show the short section of thick walled, small bore tubing that passes through the peristaltic pump, allowing the pump to efficiently supply media at a consistent flow rate of 0.75 mL/min.

2.4. Results and Discussion

2.4.1. Analysis of 5(6)-Carboxyfluorescein Properties

The suitability of carboxyfluorescein for the *in situ* sensing of CAUTI, and the mechanism by which the fluorescent signal propagates once released from the catheter tip, were important considerations when designing the infection-responsive prototype coatings.

The ability of carboxyfluorescein to self-quench (via the formation of non-fluorescent dimers) lends it well to this application, since the dye is released into a large volume of liquid media, thereby enhancing the fluorescent signal. Upon release of the dye into the urine diluent, the concentration is sufficiently lowered such that the self-quenching effect is inhibited and the fluorescence activated (Figure 2.7).

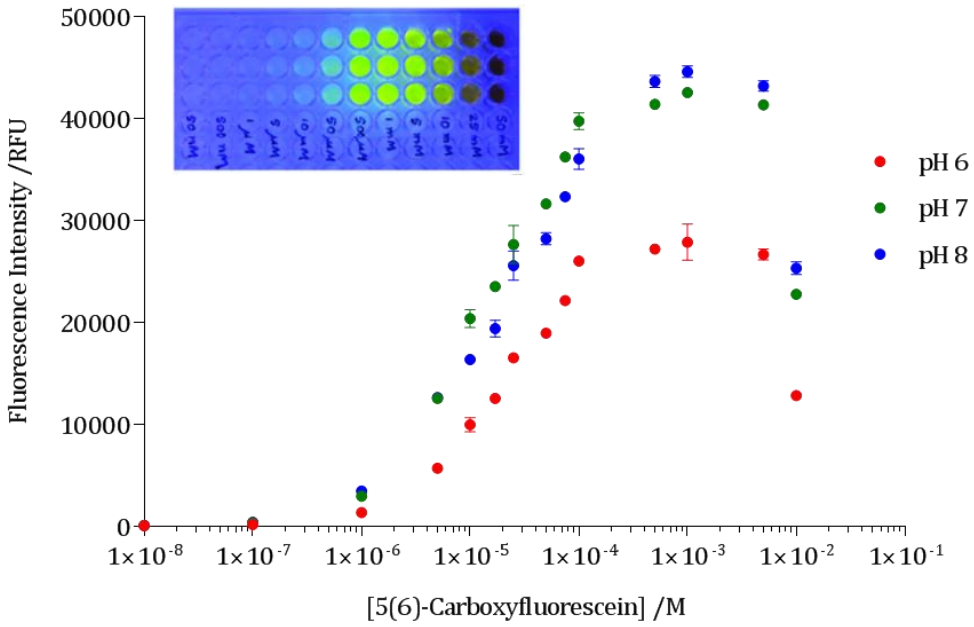

Figure 2.7: Analysis of 5(6)-carboxyfluorescein properties. Dependence of fluorescence emission on dye concentration at pH 6, 7 and 8. Self-quenching of the dye is observed at 10 mM. (Inset) Visual representation of carboxyfluorescein fluorescence at concentrations of 50 nM- 50 mM at pH 8.

Furthermore, higher pH of the diluent has been shown to improve the observed signal output (Figure 2.8). Since the pH of infected urine is highly alkaline (~pH 8), this may further enhance the visualisation of the resultant urinary colour change.

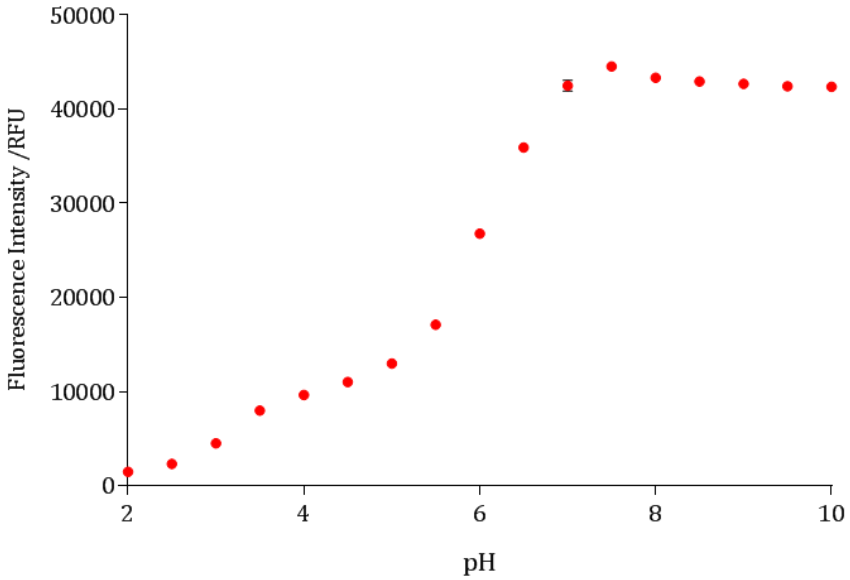

Figure 2.8: Dependenceof fluorescence emission on diluent pH. Measured signal is enhanced at alkaline pH.

The properties of self-quenching and pH-dependence render carboxyfluorescein a suitable dye for this application. Whilst the toxicological properties of 5(6)-carboxyfluorescein have not been thoroughly investigated, its parent compound, fluorescein, is approved by the FDA and widely used as a phthalic indicator dye for the diagnosis of corneal trauma. A broad range of fluorescein derivatives, including 5(6)-carboxyfluorescein, have been extensively used in the literature for the assessment of *in vitro* cell-mediated cytotoxicity, internalisation, transport, and cellular uptake, suggesting that the dyes themselves do not induce mammalian cell damage.[49,50]

2.4.2. Characterisation and Development of PVA Hydrogels

Properties of PVA at 5% and 10% w/v were investigated to assess both their physical characteristics and cargo encapsulation capability. The swelling behaviour and porosity were analysed in order to identify the concentration possessing the most suitable characteristics for the proposed catheter surface coating.

PVA hydrogels have proved promising in the field of biomedical engineering owing to their inherent biocompatibility.[51] The internal porous structure of the hydrogel also lends it to the encapsulation of a diagnostic or therapeutic cargo. PVA hydrogels were prepared via freeze thawing in order to promote inter-chain crosslinking, thus avoiding component leaching and subsequent toxicity issues associated with chemical crosslinking techniques.[52] The freezing of such gels, followed by thawing at room temperature initiates the crosslinking of structures

within the gel via the process of cryogenic gelation. The physical basis of this crosslinking technique lies in the freeze thawing-induced crystal formation, which facilitates a network structure of quasi-permanent crystallites. Liquid-liquid phase separation into regions of polymer-rich and polymer-poor phases, along with inter- and intra-molecular hydrogen bonding within the amorphous phase are thought to aid the gelation of PVA, owing to the nucleation of PVA crystallite 'cross-linking points'. Indeed, in-depth analysis of PVA cryogels in the literature[53] has proven the involvement of hydrogen bonding in this process (Scheme 2.3).

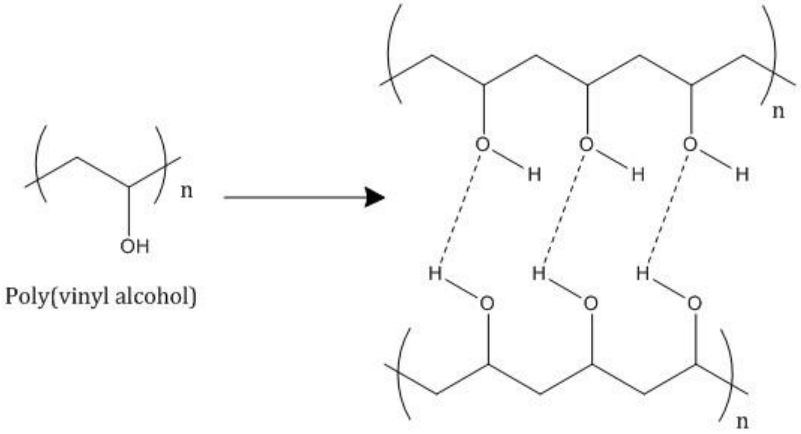

Scheme 2.3: Physical crosslinking of a PVA cryogel during freeze thawing

The formation of ice crystals during conventional freezing leads to an increased polymer concentration in the unfrozen phase. Hydrogen bonds may then form within the polymer rich phase, although crystal formation may in fact be hindered by the progression of gelation. Hence, mechanical properties such as gel rigidity may increase with the number of freeze thaw cycles undertaken. During the thawing process, the ice crystals melt, resulting in a porous polymeric cryogel, within which a diagnostic/therapeutic cargo may be encapsulated.

2.4.2.1. Swelling Ratios

Swelling ratios were calculated in order to assess the degree of porosity and ability to uptake aqueous solution within the gel structure. Calculations were undertaken using deionised water as swelling agent. Average swelling ratios of 5% and 10% PVA are shown in Table 2.6.

Table 2.6: Swelling ratios of 5% and 10% w/v PVA. (Data shown are average of triplicate values ± standard deviation)

PVA Concentration (% w/v)	Swelling Ratio
5	37.1 ± 1.1
10	13.0 ± 3.8

Both 5% and 10% w/v PVA hydrogels formed yielding, fexible structures after one freeze-thaw cycle. Structural rigidity of the 10% gel was significantly greater than the 5%, owing to the more densely packed polymer network. This was reflected in the measured swelling ratios; where the greatest values were observed for the lower polymer concentration. Crucially, the swollen state of the 10% hydrogel remained mechanically sound, whilst the 5% gel became loose and unstructured. These results suggest that the 10% w/v PVA hydrogel is more suitable for an intra-bladder catheter coating, since elastic chain networks with a high degree of porosity will allow effective encapsulation, and retention of a robust mechanical gel upon transformation to the swollen state will allow encapsulated material to move out from the structure, without degradation of the gel matrix itself.

2.4.2.2. SEM Images of PVA Hydrogels

SEM images of freeze-dried samples of 5% and 10% w/v PVA hydrogels, prepared by cryogenic crosslinking, were obtained to analyse the internal porous structure of each concentration. Owing to the inevitable collapse of the gels during sample preparation, the absolute pore sizes could not be accurately calculated from these images. However, the relative rigidity and thickness of the polymer 'walls', as well as the relative pore size could be estimated, thus giving some idea of potential encapsulation efficiency. Representative cross-sectional images of porous PVA hydrogels at 5% and 10% w/v are shown in Figure 2.9.

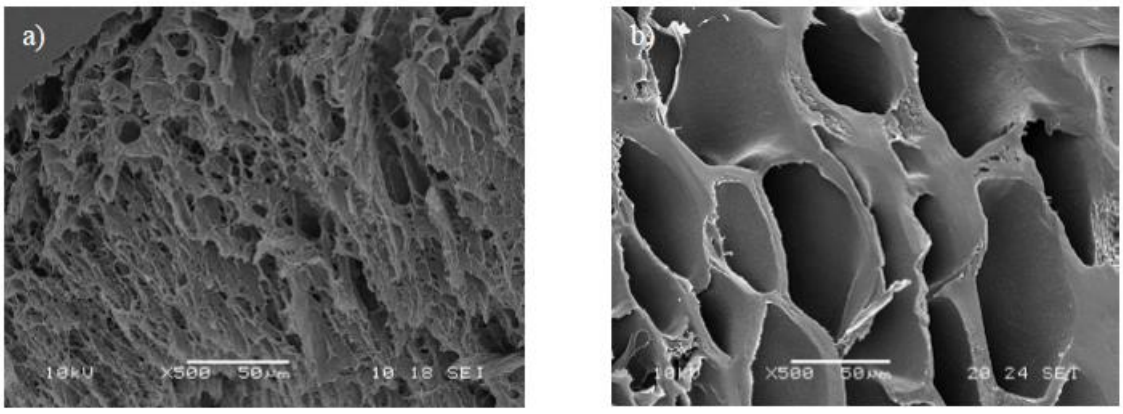

Figure 2.9: Comparison of cross-sectional SEM images of 5% w/v (A), and 10% w/v (B) PVA cryogels. (Magnification x 500, scale bar = 50 µm).

The fibrous nature of the 5% gel can be clearly observed using SEM, where polymer-rich regions are sparse and seemingly frangible. By contrast, the 10% gel appears more dense and

rigid. The stronger tensile strength and greater imperviousness to degradation upon incubation in liquid media , along with the greater density of polymer rich regions in the observed microstructure of the 10% gel, make this a more suitable candidate for the coating technology.

2.4.2.3. Silanisation of Urinary Catheters

In order to coat the hydrophobic surface of the silicone catheter with PVA hydrogel, it was necessary to modify the surface with a hydrophilic moiety. In this case, the silane APTES was used to introduce ethoxy groups onto the catheter surface. Although many attempts have thus far been made to improve the surface hydrophility of PDMS elastomer (for example via plasma treatment), these effects are often transient. Hydrophobic recovery is often observed on plasma-treated PDMS surfaces, and is sensitive to both time and temperature.[54] Modification of surface chemistry via silanisation promotes stable and long-term hydrophilisation, and renders the surface suitable for coating with a hydrogel material.[55] Silanisation of the PDMS surface with APTES enables the formation of self-assembled monolayers of molecules with reactive amino side chains, via the reaction of the APTES triethoxy group with the activated catheter surface.[47] Modification of catheter PDMS surfaces via APTES silanisation is shown in Figure 2.10.

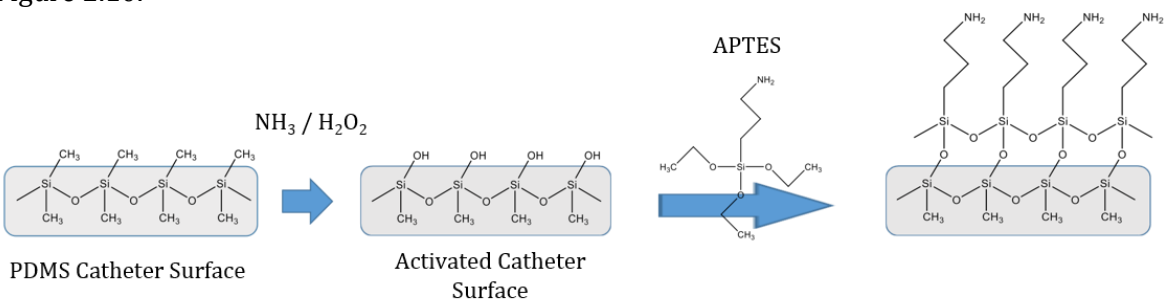

Figure 2.10: Schematic illustration of amino-silanisation using APTES on PDMS catheter surfaces, following surface activation with NH_3/H_2O_2.

Water contact angle measurements were made to ensure the hydrophilic nature of the surface. The surface wettability of the native PDMS exhibited a hydrophobic surface property (94.38 ° ± 0.86 °). Surface silanisation resulted in a significant reduction in the hydrophobicity of the surface (60.43 ° ± 2.0 °), as shown by the reduction of the observed contact angle to the

hydrophilic region (<90 °).[56] The increase in surface wettability of a standard all-silicone Foley catheter is show in Figure 2.11.

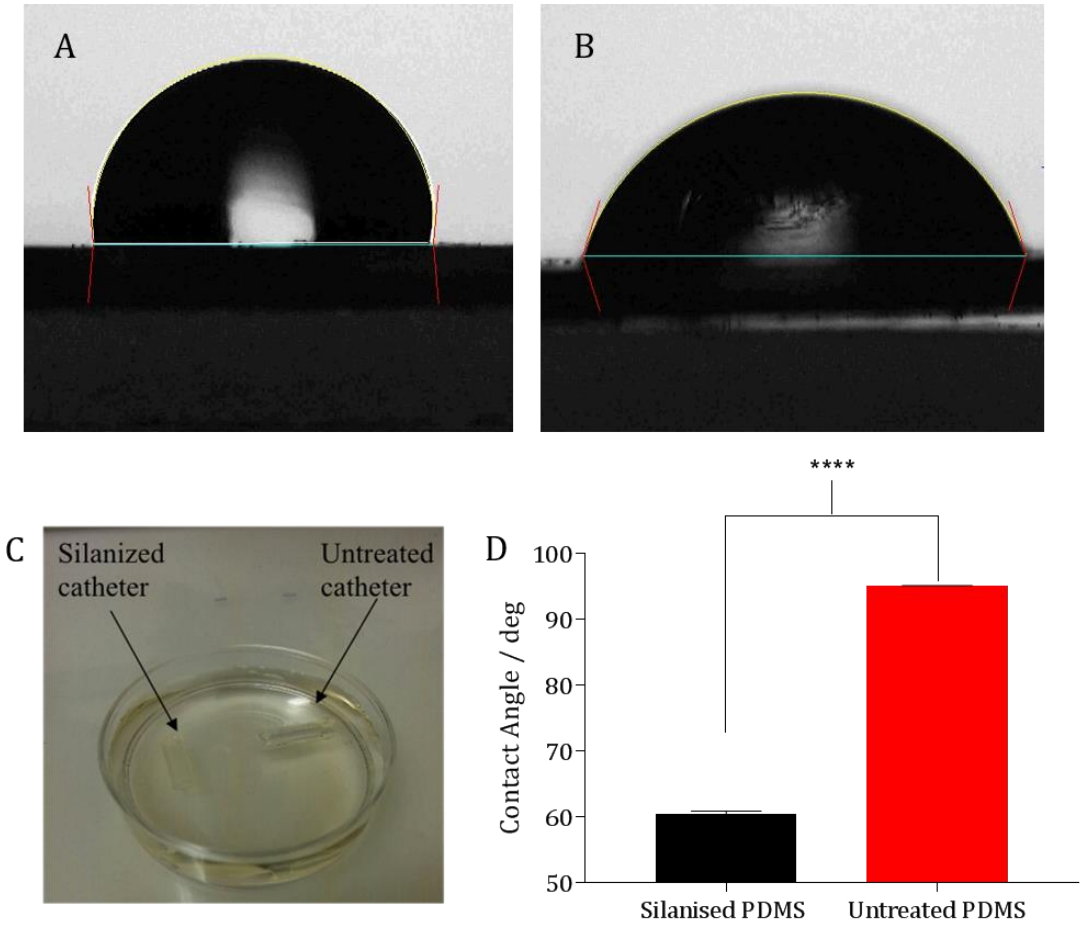

Figure 2.11: Surface modification of all-silicone Foley catheters via silanisation with APTES. Increase in surface hydrophilicity of PDMS elastomer was confimed via characterisation with water contact angle measurements. (A) Native PDMS surface, displaying a contact angle within the hydrophobic region (94.38 ° ± 0.86 °). (B) Modified PDMS surface, displaying a contact angle within the hydrophilic region (60.43 ° ± 2.0 °). (C) Catheter sections displaying increased surface wettability post-silanisation. The modified section becomes rapidly submerged on contact with water, whereas the untreated section remains at the gas/air interface. (D) Average contact angle measured on chemically modified vs. unmodified urinary catheters. Data shown are the average of 5 different points of contact ± standard error of the mean (SEM) ($p < 0.0001$).

2.4.3. Eudragit S100 Dip Coating Optimisation

The encapsulation efficiency of the Eudragit S100 trigger coating was investigated in solutions of phosphate buffer to simulate healthy (pH 6/7) and infected urine (pH 8). Sterile plastic rods imitating catheters were first coated with the 10% w/v PVA hydrogel reservoir layer (containing 250 mM 5(6)-carboxyfluorescein), before being manually dip coated in 10, 15 or 20 coats of the organic Eudragit S100 solution. Since the elevation of urinary pH to highly alkaline levels intitiates crystalline biofilm formation, the aim of this assay was to optimise the number of Eudragit coats that would result in dye release and subsequent fluorescence output at pH 8, but not at pH 6 or 7. The ability of the pH-responsive polymer at different film thicknesses to encapsulate dye within a PVA reservoir are shown in Figures 2.12, 2.13 and 2.14.

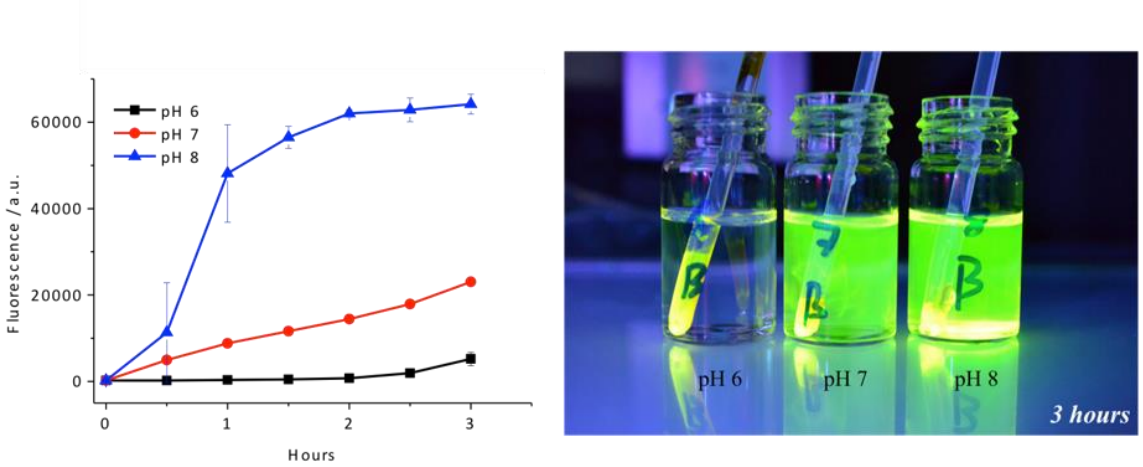

Figure 2.12: Encapsulation efficiency of 10 coats of Eudragit S100 at pH 6, 7 and 8. Leaching of the carboxyfluorescein fluorescent dye was observed after 3 hours incubation at room temperature.

Retention of the dye within the hydrogel reservoir was insufficient after 10 dips of Eudragit (Figure 2.12). Significant dye release was observed in the diluent at pH 7 after 3 hours incubation. When the film thickness was increased to 15 coats, the difference in observed fluorescence response between pH 7 and 8 became more conspicuous (Figure 2.13). Quantitative measurements of fluorescence output over 3 hours showed promising results, as visual dye release was observed only for buffer solution at pH 8. After 24 hours incubation, however, leaching of the dye was observed in solutions at both pH 6 and 7.

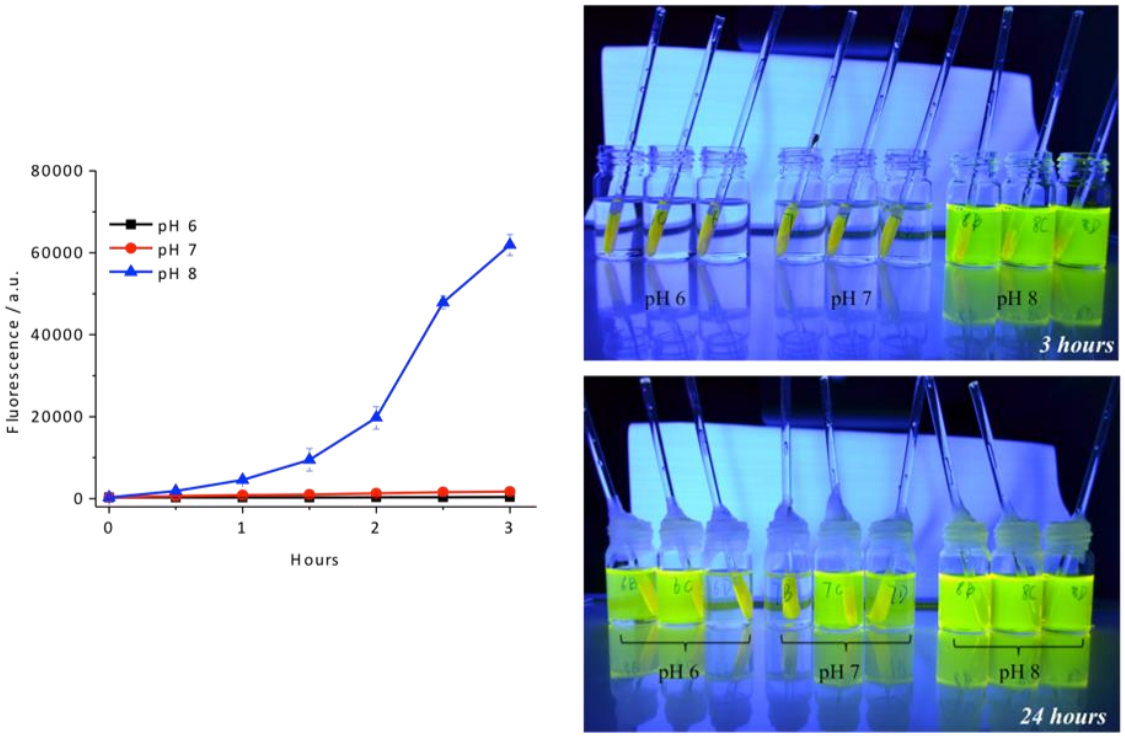

Figure 2.13: Encapsulation efficiency of 15 coats of Eudragit S100 at pH 6, 7 and 8. Coatings appeared stable after 3 hours incubation, although leaching of the carboxyfluorescein dye was observed after 24 hours incubation at room temperature.

Further increase of the Eudragit film thickness to 20 coats provided the complete encapsulation of dye after 24 hours incubation (Figure 2.14). Owing to increased coating thickness, the rate of observable dye release was slower at pH 8, although coatings appeared more stable to liquid penetration in buffer solutions imitating 'healthy' urine pHs.

Though uninfected urine typically displays pH ranging from ~6.1-6.5, in some cases, extremes of pH from a lower limit of 5.5 to an upper limit of 7.0 have been reported (although these extremes are typically associated with other underlying disorders).[57] Perhaps the more critical value to consider in terms of urinary catheter blockage is the pH at which crystal formation is initiated. This 'nucleation' pH is also variable between individuals, and has been reported to range from pH 6.75-8.95.[58] Considering the range of values observed for urinary pH and nucleation pH, the optimisation of a system to provide dye release at pH values greater than 7 appears to offer a good compromise between the requirement for sufficient accuracy and duration, and should be suitable for the majority of patients undergoing long-term indwelling catheterisation.

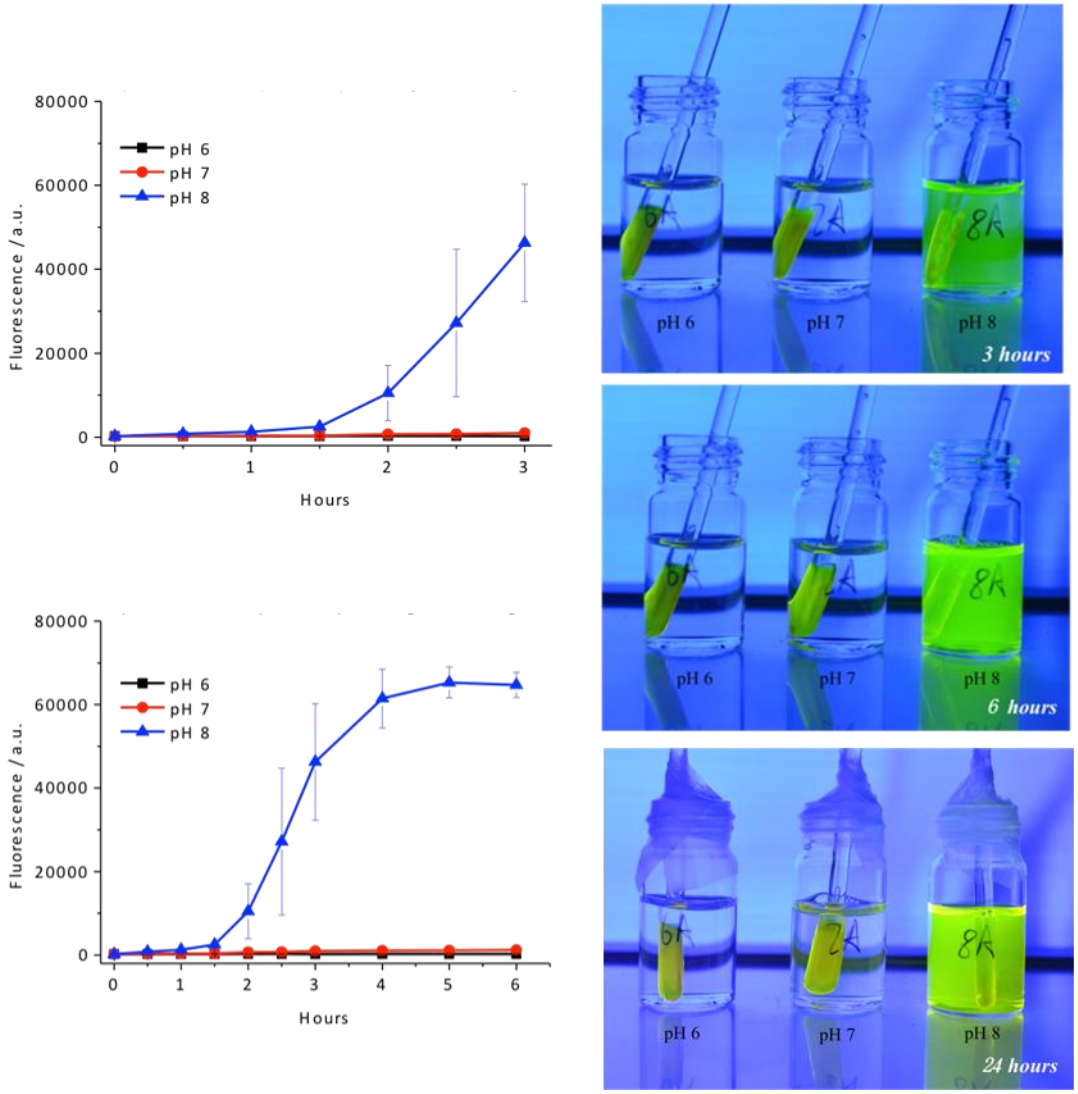

Figure 2.14: Encapsulation efficiency of 20 coats of Eudragit S100 at pH 6, 7 and 8. Coatings remained stable at pH 6 and 7 for 24 hours. No observable leaching of the dye was observed at simulated 'healthy' urine pHs. At pH 8, the rate of dye release was slower than for thinner film thicknesses, although maximum fluorescence output was observed after 6 hours incubation.

Overall, the carboxyfluorescein release assays showed that the encapsulation of the dye reservoir is dependent on Eudragit film thickenss. For further prototype production, 20 dip coats of Eudragit was employed, as it was concluded to provide an accurate fluorescence signal associated with infection by *P. mirabilis* and subsequent crystalline biofilm formation.

2.4.4. Sensor Coating Prototypes: *In Vitro* Evaluation

2.4.4.1. Bladder Infection Models

To evaluate the ability of the dual-layered diagnostic system to provide warning of impending catheter blockage following infection by *P. mirabilis*, the performance of coated catheters was assessed using the *in vitro* bladder model system, originally described by Stickler *et al*.[48] This model represents a full sterile closed-drainage system, as used in clinical practice, and provides a good representation of the *in vivo* catheterised urinary tract. Although studies on biofilms in models such as the modified Robbins device,[59] the constant film fermenter[60] and the flow cell,[48] have provided valuable fundamental information about the properties and developments on different types of materials in various conditions, the *in vitro* bladder model allows the study of biofilm formation under conditions in which the design features of the catheter, and the hydrodynamics of the catheterised bladder are considered.

Triggered release coatings containing carboxyfluorescein were applied directly to the top 1 cm of the distal tip of the catheter, above the retention balloon. Since the coating resides below the level of the catheter eyeholes, once the catheter is fitted the coated region sits within the pool of residual urine that forms within the bladder. Dye released from the sensor coatings may then travel to the collection bag, where its fluorescent signal may be detected by eye in advance of catheter blockage. Blockage can be readily identified in the bladder model system by monitoring the flow of urine. The flow of artificial urine supplied by the peristaltic pump is maintained at a constant flow rate of 0.75 mL/min, thus the running time of the model can be accurately determined by the volume of accumulated urine within the drainage bag. The mean natural filling rate of the bladder in a group of patients with an average age of 62.5 years, was found to be 0.76 mL/min.[61] Hence, this flow rate was used for all bladder model assays, in order to accurately mimic physiological conditions.

Since changes to the catheter surface may influence the rate of bacterial biofilm formation, it was first confimed that the coated catheters did not alter the ability of *P. mirabilis* to form crystalline biofilms and cause catheter blockage in this model system. In models containing coated catheters, *P. mirabilis* was able to rapidly infect and encrust catheters, causing complete catheter blockage in an average time of 16 hours. This is comparable to the time taken for the same bacterial strain to cause blockage in uncoated catheters under the same experimental conditions. In congruity with previous studies,[62,63] the encrustation and blockage of catheters was associated with an increase in urinary pH to an average value of 8.55. No significant

differences were observed in the ability of *P. mirabilis* to elevate urinary pH or grow and persist in the system in models fitted with coated catheters, in comparison to uncoated controls. (Figure 2.15)

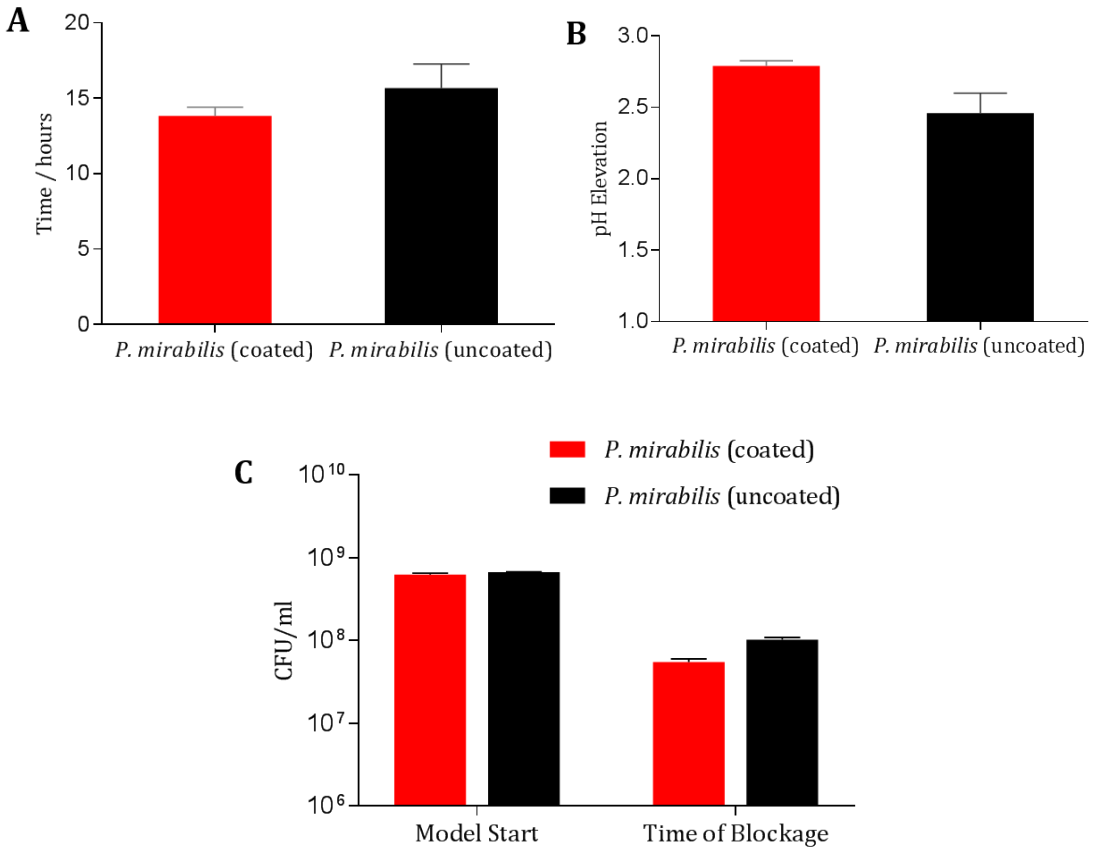

Figure 2.15: Assessment of coating impact on behaviour of *P. mirabilis* within the *in vitro* bladder model system. (A) Time taken for the catheter to block in models fitted with coated or uncoated Foley catheters. (B) Urinary pH elevation in models inoculated with *P. mirabilis* fitted with coated or uncoated catheters. The pH of uninoculated artitifical urine media was 6.10. Data shows the average number of pH units by which the pH rose between model activation and catheter blockage time. (C) Number of viable cells present in residual bladder model urine at model start, and at the time of catheter blockage. Data shown are the mean of triplicate repeats. Error bars represent SEM.

Artificial urine was deemed the most suitable medium for prototype testing, as the composition may be tightly controlled, meaning that batch-to-batch variation is eliminated. However, the model may also utilise pooled human urine, which suffers primarily from patient-dependent variability of composition (both inter- and intra-subject variability). Nevertheless, pooled human urine may provide certain advantages in later-stage prototype development since it is more representative of the *in vivo* conditions within the urinary tract.[64]

The limitations of this model are primarily related to the quantification of biofilm growth. Since the catheter is contained within the bladder, it is impossible to constitute a system in which fine differences in the abilities of different biomaterials to support bacterial growth can be quantitifed and resolved. Nevertheless, this model has proven instrumental in providing information regarding the formation, physiology and control of catheter biofilms. In this work in particular, these models have proven invaluable in assessing the variance in blockage times, as well as the degree of advanced warning achieved from the diagnostic coatings.

2.4.4.2. Activation of Catheter Coating and Advance Warning of Blockage

The duration of early warning provided by the triggered-release coatings was assessed using the *in vitro* bladder model system as described. Dye release and subsequent urine colour change was monitored throughout the course of the experiment, and the time between visual urinary colour change and catheter blockage was calculated. The blockage of catheters in models infected with *P. mirabilis* was deemed the experimental end-point.

Since the application of this technology will often be in alerting patients and/or carers in the ambulatory care environment, the visual signal is required to be easily visible without the use of specialist equipment. Therefore, the sensor coating deployment was based on direct, subjective assessment of colour change by eye, under ambient lighting. Visual observation of carboxyfluorescein release was used to prompt associated quantitative analysis of urinary fluorescence, viable cell count and pH of residual urine. The response of coatings to models infected with *E. coli* was also evaluated, as this species is unable to express urease, and thus unable to cause catheter encrustation and blockage. The ability of the coatings to discriminate between urease-producing *P. mirabilis* and non-urease producing *E. coli* was vital for preventing false positive results, therefore allowing for accurate warning of impending blockage.

In models devoid of of *P. mirabilis*, no visible colour change was observed in the collected urine. In uninoculated models, or those infected with *E. coli*, coatings remained intact, hence no dye release was noted at any point during the experiment (Figure 2.16). This demonstrates the stability of the coatings in the absence of urease. In models infected with *P. mirabilis*, a distinct colour change was observed within urine contained within the bladder models at an average of 4.2 hours after the model start. Despite being clearly visible within the residual bladder

urine, the signal was not visible with in the drainage bag until 6.2 hours after the start of the experiment (Figure 2.17).

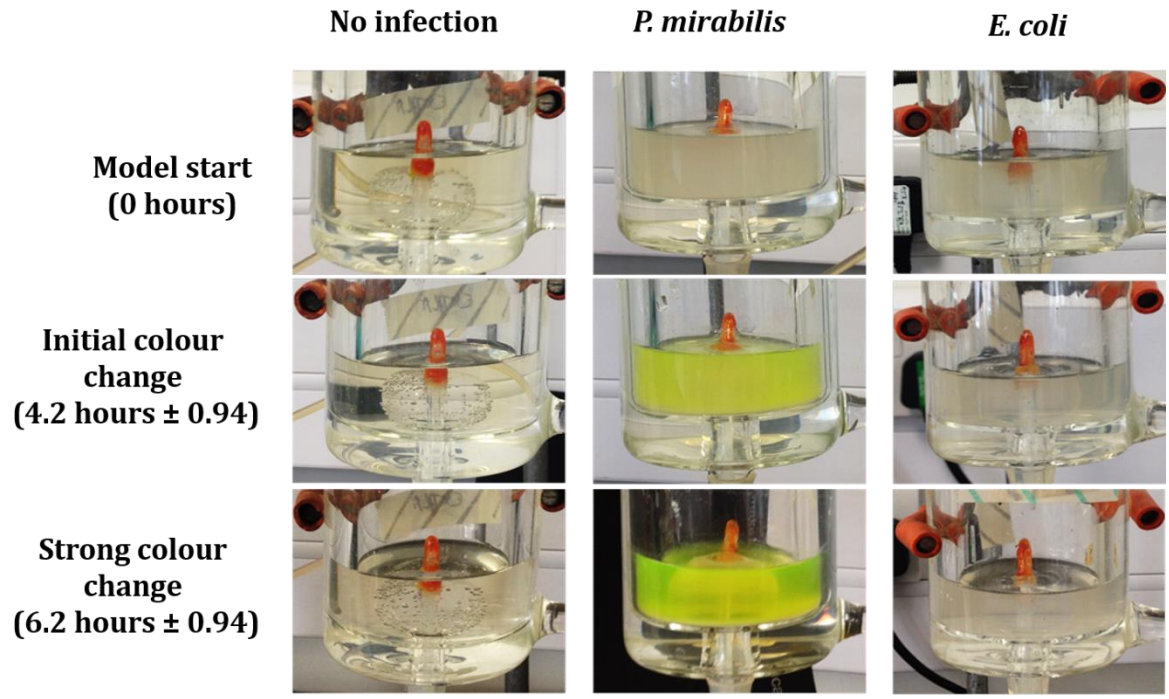

Figure 2.16: Representative images showing coating activation during the course of prototype testing in an *in vitro* bladder model system. Columns show models infected with urease-positive *P. mirabilis*, or urease-negative *E. coli* species, or control models devoid of bacteria. Rows show bladder models at key time points related to observed coating activation. For initial and strong colour change, values in parentheses indicate the average time after model start at which the colour change was observed ± SEM.

Average catheter blockage time of models inoculated with *P. mirabilis* was 16 hours. The intensity of urine colouration was slightly reduced over the course of the experiment, although remained visible within the drainage bag for the duration. Removal of Foley catheters from the control and *P. mirabilis* models 24 hours after the experimental start (8 hours post-blockage) confimed that whilst encapsulated dye had been released in response to the urease-positive species, the coating in the control models had remained intact, despite constant contact with a continuously flowing liquid culture.

Dye release and urinary color change observed visually were correlated with changes in pH of residual bladder urine (Figure 2.18a). A rise in urine pH of 1.2 pH units (from 6.1 to 7.3) was recorded at the point of initial colour change (4.2 hours). This further increased to a maximum of pH 8.6 at time of blockage.

The measured fluorescence of bladder urine (Figure 2.18b) within *P. mirabilis* models also corresponded with the observed response. A significant increase in fluorescence (ca. 20-fold) at the point of initial colour change (4.2 hours), which increased 5-fold at the point of maximum visual response. The reduction in visual fluorescence at the time of blockage is primarily owing to dilution effects of the continuous urine flow, and the exhaustion of the dye reservoir within the catheter coating.

Figure 2.17: Visual colour change within urine collection bag in response to uninoculated standard catheter control (A), and *P. miraiblis*-infected coated catheter. Images are representative of triplicate repeats at 6.2 hours after model start.

Overall, when considered in the context of catheter blockage, the infection-responsive coating gives a urinary colour change approximately 10-12 hours in advance of blockage, which is sufficient to permit intervention before the onset of any serious clinical complications. In comparison to the bromothymol blue sensor previously described (Section 2.1.2), the performace of the catheter coatings compares well to the sensor in early-scale laboratory trials. Moreover, the incorporation of pH-sensing functionality into a catheter surface coating has numerous advantages over systems that require fabrication and use of additional components. The use of an additive system component introduces additional cost and complexity for patients and carers, as well as adding junctures at which the sterility of the system may be compromised. Such issues were highlighted in pilot-scale clinical trials of the bromothymol blue-based sensor, where some patients reported issues with leakage, ease of use, and the ability to conceal the catheter drainage system.[12]

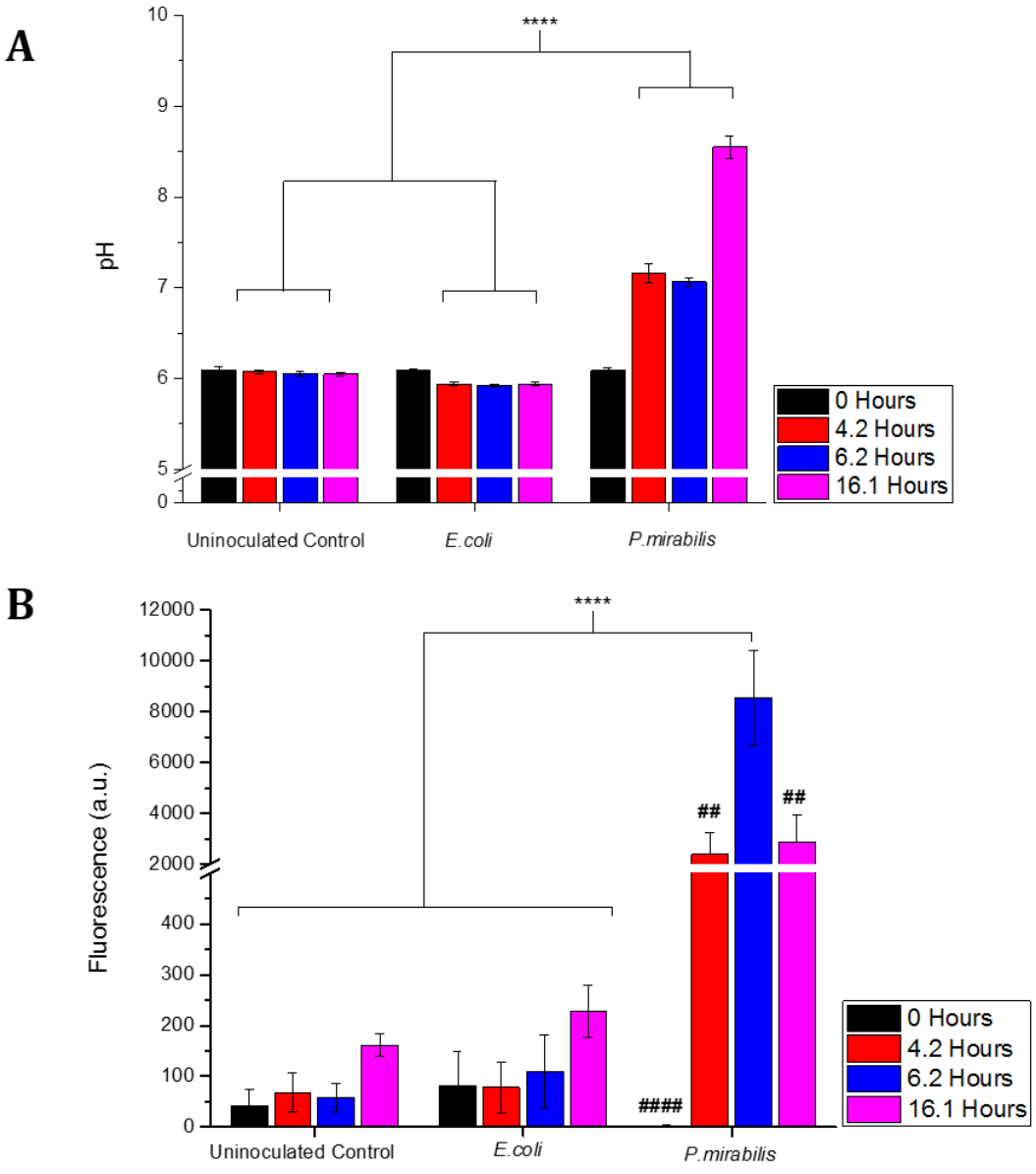

Figure 2.18: Analysis of *in vitro* bladder model conditions. (A) pH of residual urine within the bladder model at model start (0 hours), initial colour change (average 4.2 hours), maximum colour change (average 6.2 hours), and catheter blockage (average 16.1 hours). (B) Measured fluorescence of bladder model urine at previously mentioned time points. **** $p < 0.0001$. Data shown are the mean of triplicate repeats. Error bars represent SEM. For (B) only, ## $p < 0.01$; #### $p < 0.0001$ *P. mirabilis* at 0 hours vs. *P. mirabilis* at 6.2 hours.

2.5. Conclusion

The research presented in this chapter describes the design and optimisation of an infection-responsive surface coating for urinary catheters, able to provide a clear and unambiguous colour change in response to elevated urinary pH following infection by *P. mirabilis*. The fluorescent signal observed, following triggered release of the self-quenching dye 5(6)-carboxyfluroescein from the coating system, provides early warning of catheter blockage, permitting clinical intervention prior to the onset of serious clinical consequences. Performance was evaluated within a clinically relevant *in vitro* bladder model system, where a urinary colour change was detected approximately 10-12 hours in advance of catheter occlusion. Performance was comparable to previously described sensor systems, although the implementation of this approach holds considerable manufacturing and practical advantages, since the design is compatible with the existing Foley catheter design. Coatings were able to successfully discriminate ureolytic pathogens from non-urease producers. Generally, urease activity in species other than *P. mirabilis* is insufficient to raise urinary pH beyond the nucleation point (pH ~7.4). Indeed, among these species, only *Providencia rettgeri*, *Morganella morganii* and *Proteus vulgaris* have been reported to elevate urinary pH above 7, thus causing catheter encrustation.[65] However, as the coating is designed to respond to an elevation in urinary pH (rather than direct detection of urease activity or species-specific factors), the coating should, in principle, be able to detect impending blockage by any urease-positive species.

Perhaps the principal advantage of the surface coating approach described in this work is the potential to add further functionality to the system via the incorporation of additional active cargos into the hydrogel reservoir. Overall, this dual-layered coating system provides sound proof-of-concept for the formulation of a therapeutic coating, which will include agents to actively delay catheter blockage, thus extending the lifetime of the catheter and providing a significant positive impact on patient welfare via the reduction in blockage-associated complications. The potential to release antimicrobial species directly into the bladder allows targeted treatment , both in terms of release location and treatment time. The employment of location-specific triggered release may bypass complications traditionally associated with systemic drug administration, such as unfavourable pharmacokinetic or pharmacodynamic effects.

The limitations of this system lie within the regulatory differences between classes of medical device, and *in vitro* diagnostic devices. Since the catheter coating described in this chapter has been designed to function within the body, it would likely be subject to more stringent

regulatory testing in later clinical trials. By contrast, *in vitro* diagnostic devices function outside the body. Thus, the risk associated is purely regarding the information they reveal (i.e. the occurance of false positive/negative results), rather than a direct effect of the device with the patient.[66] If this system can be modified such that it does not come into direct contact with the patient, yet is still able to deliver the same information within a similar time frame, the regulatory issues surrounding this medical device will be significantly eased. Futhermore, the relocation of the diagnostic system described to an *ex vivo* diagnostic , may allow the perceptible fluorescence response to have greater visual strength and longevity, since the release of carboxyfluorescein will be external to the bladder and will not rely on elusion to enable visualisation. The externalisation of the diagnostic system may also allow the distal tip of the catheter to remain free for a pH-responsive coating containing a therapeutic agent, thus allowing the potential construction of a theranostic system within the catheterised urinary tract.

2.6. References

1. T. R. Kozel and A. R. Burnham-Marusich, *Journal of Clinical Microbiology*, 2017, **55**, 2313–2320.

2. I. Jones, M. Diver, N. Gertler, J. Rex, K. Spencer, T. Jinks and R. Seabrook, in *Wellcome Trust Executive Summary*, 2015, pp. 1–26.

3. R. Finch and P. A. Hunter, in *Journal of Antimicrobial Chemotherapy*, 2006, pp. 3–22.

4. P. A. Tambyah, in *International Journal of Antimicrobial Agents*, 2004.

5. T. M. Hooton, S. F. Bradley, D. D. Cardenas, R. Colgan, S. E. Geerlings, J. C. Rice, S. Saint, A. J. Schaeffer, P. A. Tambyah, P. Tenke and L. E. Nicolle, *Clinical Infectious Diseases*, 2010, **50**, 625–663.

6. Royal United Hospital Bath, 'My Catheter Passport', http://www.ruh.nhs.uk/patients/Urology/documents/patient_leaflets/RUH_Catheter_Passport_MALE_SAMPLE.pdf, (accessed 5 October 2018).

7. R. Eliot, *Infection Prevention and Control Improvement Plan. Royal United Hospitals, Bath*, 2017.

8. D. K. Newman, M. Fader and D. Z. Bliss, *Nursing research*, 2004, **53**, 42–48.

9. D. J. Stickler, S. M. Jones, G. O. Adusei and M. G. Waters, *Journal of Clinical Microbiology*, 2006, **44**, 1540–1542.

10. WO 2006/000764 A1, 2006.

11. D. J. Stickler, S. M. Jones, G. O. Adusei, M. G. Waters, J. Cloete, S. Mathur and R. C. L. Feneley, *BJU International*, 2006, **98**, 1244–1249.

12. A. Long, J. Edwards, R. Thompson, D. A. Lewis and A. G. Timoney, *BJU International*, 2014, **114**, 278–285.

13. M. Hidaka, A. Gotoh, T. Shimizu, K. Minamisawa, H. Imamura and T. Uchida, *Journal of Biological Chemistry*, 2016, **291**, 2260–2269.

14. WO2018058077, 2018.

15. EP2148713A1, 2007.

16. S. Massou, R. Albigot and M. Prats, *Biochemical Education*, 2000, **28**, 171–173.

17. L. Li, Y. Zhao, R. Yu, T. Chen and X. Chu, *Analytical Letters*, 2018, **51**, 998–1012.

18. M. V Kvach, D. A. Tysbulsky, A. V Ustinov, I. A. Stepanova, S. L. Bondarev, S. V Gontarev, V. A. Korshun and V. V Shmanai, *Bioconjugate Chemistry*, 2007, **18**, 1691–1696.

19. W.-H. Zhang, X.-X. Hu and X.-B. Zhang, *Nanomaterials*, 2016, **6**, 81.

20. R. F. Chen and J. R. Knutson, *Analytical Biochemistry*, 1988, **172**, 61–77.

21. D. Setiawan, A. Kazaryan, M. A. Martoprawiro and M. Filatov, *Physical Chemistry*

Chemical Physics, 2010, **12**, 11238–11244.

22. A. Muñoz-Losa, C. Curutchet, B. P. Krueger, L. R. Hartsell and B. Mennucci, *Biophysical Journal*, 2009, **96**, 4779–4788.

23. M. N. Holme, I. A. Fedotenko, D. Abegg, J. Althaus, L. Babel, F. Favarger, R. Reiter, R. Tanasescu, P. L. Zaffalon, A. Ziegler, B. Müller, T. Saxer and A. Zumbuehl, *Nature Nanotechnology*, 2012, **7**, 536–543.

24. G. Cevc, *Critical Reviews in Therapeutic Drug Carrier Systems*, 1996, **13**, 257–388.

25. E. Touitou, N. Dayan, L. Bergelson, B. Godin and M. Eliaz, *Journal of Controlled Release*, 2000, **65**, 403–418.

26. V. Z. Prokopovic, A. S. Vikulina, D. Sustr, E. M. Shchukina, D. G. Shchukin and D. V Colodkin, *ACS Applied Materials and Interfaces*, 2017, **9**, 38908–38918.

27. V. De Leo, M. Mattioli-Belmonte, M. T. Cimmarusti, A. Panniello, M. Dicarlo, F. Milano, A. Agostiano, E. De Giglio and L. Catucci, *Colloids and Surfaces B: Biointerfaces*, 2017, **158**, 387–396.

28. J. Han and K. Burgess, *Chemical Reviews*, 2010, **110**, 2709–2728.

29. N. T. Thet, D. R. Alves, J. E. Bean, S. Booth, J. Nzakizwanayo, a. E. R. Young, B. V. Jones and a. T. a. Jenkins, *ACS Applied Materials & Interfaces*, 2015, 151022154036007.

30. J. Zhou, T. N. Tun, S. ha Hong, J. D. Mercer-Chalmers, M. Laabei, A. E. R. Young and A. T. A. Jenkins, *Biosensors and Bioelectronics*, 2011, **30**, 67–72.

31. H. Priya James, R. John and A. Alex, *Acta Pharmaceutica Sinica B*, 2014, **4**, 120–127.

32. H. Lambers, S. Piessens, A. Bloem, H. Pronk and P. Finkel, *International Journal of Cosmetic Science*, 2006, **28**, 359–370.

33. J. Liu, Y. Huang, A. Kumar, A. Tan, S. Jin, A. Mozhi and X. J. Liang, *Biotechnology Advances*, 2014, **32**, 693–710.

34. S. L. Percival, S. McCarty, J. A. Hunt and E. J. Woods, *Wound repair and regeneration : official publication of the Wound Healing Society [and] the European Tissue Repair Society*, 2014, **22**, 174–186.

35. E. K. Rofstad, B. Mathiesen, K. Kindem and K. Galappathi, *Cancer Research*, 2006, **66**, 6699–6707.

36. N. J. Irwin, C. P. McCoy, D. S. Jones and S. P. Gorman, *Pharmaceutical Research*, 2013, **30**, 857–865.

37. S. Babic, A. J. M. Horvat, D. Mutavdzic Pavlovic and M. Kastelan-Macan, *TrAC - Trends in Analytical Chemistry*, 2007, **26**, 1043–1061.

38. W. Moore, G. Portmann, H. Stander and F. McChesney, *Journal of Pharmaceutical Sciences*, 1965, **54**, 36–41.

39. Evonik, Eudragit S100 Technical Information, http://eudragit.evonik.com/product/eudragit/en/products-services/eudragit-

products/enteric-formulations/s-100/Pages/default.aspx, (accessed 8 October 2018).

40. R. Coco, L. Plapied, V. Pourcelle, C. Jerome, D. Brayden, Y.-J. Schneider and V. Preat, *International Journal of Pharmaceutics*, 2013, **440**, 3–12.

41. A. El-Kamel, M. Sokar, S. Gamal and V. Naggar, *International Journal of Pharmaceutics2*.

42. P. Pawar, P. Sharma, A. Chawla and R. Mehta, *Journal of Advanced Pharmaceutical Technology & Research*, 2013, **4**, 31–41.

43. G. K. Vinner, G. T. Vladisavljević, M. R. J. Clokie and D. J. Malik, *PLoS ONE*, 2017, **12**, 1–27.

44. G. R. Agrawal, P. Wakte and S. Shelke, *Progress in Biomaterials*, 2017, **6**, 125–136.

45. S. Sharma, K. Jyoti, R. Sinha, A. Katyal, U. K. Jain and J. Madan, *Materials Science and Engineering C*, 2016, **67**, 378–385.

46. D. Jain, A. K. Panda and D. K. Majumdar, *AAPS PharmSciTech*, 2005, **6**, 100–107.

47. Z. a. Gencer, S. Odabas, H. T. Sasmazel and E. Piskin, *Journal of Bioactive and Compatible Polymers*, 2012, **27**, 419–428.

48. D. Stickler, N. Morris and C. Winters, *Methods in Enzymology*, 1999, **310**, 498–501.

49. H. Pan, J. N. Marsh, E. T. Christenson, N. R. Soman, O. Ivashyna, G. M. Lanza, P. H. Schlesinger and S. A. Wickline, *Methods in Enzymology*, 2012, **508**, 17–39.

50. E. Kiss, G. Gyulai, E. Pari, K. Horvati and S. Bosze, *Amino Acids*, 2018, **50**, 1557–1571.

51. A. S. Hoffman, *Advanced Drug Delivery Reviews*, 2012, **64**, 18–23.

52. C. M. Hassan and N. A. Peppas, *Macromolecules*, 2000, **33**, 2472–2479.

53. R. Ricciardi, F. Auriemma, C. Gaillet, C. De Rosa and F. Laupretre, *Macromolecules*, 2004, **37**, 9510–9516.

54. D. Bodas and C. Khan-Malek, *Sensors and Actuators, B: Chemical*, 2007, **123**, 368–373.

55. Y. J. Chuah, S. Kuddannaya, M. H. A. Lee, Y. Zhang and Y. Kang, *Biomaterials Science*, 2015, **3**, 383–390.

56. Y. Yuan and T. R. Lee, in *Surface Science Techniques*, Springer, Berlin, Heidelberg, 51st edn., 2013, pp. 3–34.

57. C. Rose, A. Parker, B. Jefferson and E. Cartmell, *Critical Reviews in Environmental Science and Technology*, 2015, **45**, 1827–1879.

58. S. Mathur, M. T. E. Suller, D. J. Stickler and R. C. L. Feneley, *British Journal of Urology*, 2005, **97**, 121–128.

59. D. R. Alves, University of Bath, 2015.

60. S. L. Kinniment, J. W. T. Wimpenny, D. Adams and P. D. Marsh, *Microbiology*, 1996, **142**, 631–638.

61. S. W. Lee and J. H. Kim, *Neurourology and Urodynamics*, 2008, **27**, 772–774.

62. N. Holling, D. Lednor, S. Tsang, A. Bissell, L. Campbell, J. Nzakizwanayo, C. Dedi, J. A. Hawthorne, G. Hanlon, L. A. Ogilvie, J. P. Salvage, B. A. Patel, L. M. Barnes and B. V. Jones, *Infection and Immunity*, 2014, **82**, 1616–1626.

63. N. Holling, C. Dedi, C. E. Jones, J. A. Hawthorne, G. W. Hanlon, J. P. Salvage, B. A. Patel, L. M. Barnes and B. V. Jones, *FEMS Microbiology Letters*, 2014, **355**, 20–27.

64. J. Denstedt and A. Atala, *Biomaterials and Tissue Engineering in Urology*, Woodhead Publishing Ltd, Cambridge, UK, 1st edn., 2009.

65. R. J. Broomfield, S. D. Morgan, A. Khan and D. J. Stickler, *Journal of Medical Microbiology*, 2009, **58**, 1367–1375.

66. R. A. Grifa and G. Pozzoli, *Microchemical Journal*, 2018, **136**, 279–282.

Chapter 3: Development of an *Ex-Vivo* 'Lozenge' Sensor for the Early Detection of Urinary Catheter Blockage

3.1. Abstract

This research is presented as an extension of the previous study reported in Chapter 2; the exploitation of pH as a proxy indicator of infection by *P. mirabilis*. In this case, the pH-responsive sensor is a dual-layered polymeric 'lozenge', able to release a fluorescent dye directly into the catheter drainage bag in response to alkaline urine (generated by the expression of bacterial urease). The system comprises a cylindrical hydrogel reservoir (PVA), containing the dye (5(6)-carboxyfluorescein), completely capped and sealed by the pH-sensitive polymer Eudragit S100. The sensors are placed directly into the urine drainage bag, thereby allowing a greater concentration of dye to be released into the visual portion of the catheterised urinary tract, providing an explicit urinary colour change signalling imminent catheter blockage (Figure 3.1).

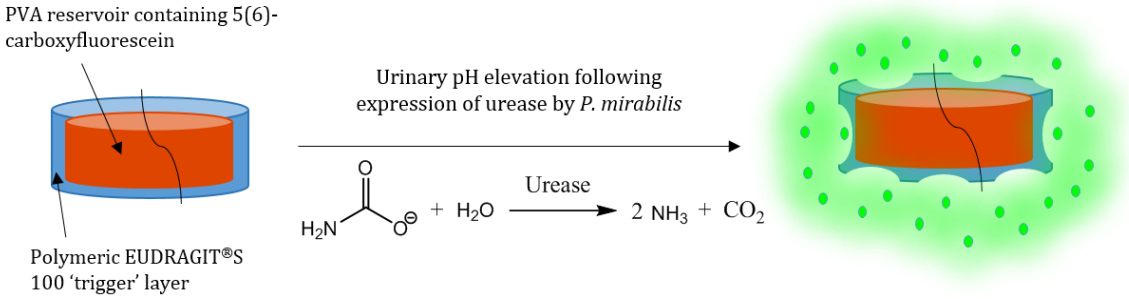

Figure 3.1: Schematic representation of the dual-layered polymeric lozenge sensor. Generation of an *in situ* fluorescent signal provides 'early warning'of catheter blockage following degradation of the sensor and release of 5(6)-carboxyfluorescein. Sensor activation is triggered in response to alkalinsation of urine upon infection by *P. mirabilis*.

Unlike the previously reported system, the lozenge sensor design avoids potential adverse *in vivo* effects such as urethral inflammation or promotion of microbial adhesion via deposition of a conditioning film on the luminal and external catheter surfaces. Furthermore, localised dye release within the catheter drainage bag enables the technology to bypass many of the stringent regulations surrounding indwelling medical devices, and leaves the distal tip of the catheter available for the incoportation of a therapeutic coating (Chapter 4). Since many patients suffering from recurrent catheter blockage are in community care, the system described here provides a means of alerting the patient themselves to catheter blockage, without the need for acquisition and analysis of urine samples.

3.2. Introduction

3.2.1. Medical Technology: Innovation to Commercialisation

As medical devices play an ever-growing role in the diagnosis and management of disease, the global medical device industry has surpassed US $350 billion in annual revenue. The UK is the third largest market for medical technology in Europe, consisting of 3,000 companies with a combined turnover of £15 billion, employing in the region of 115,000 highly-skilled personell.[1]

Whilst innovation lies in the heart of academia, commercial translation of intellectual property is often poor, particularly within the healthcare sector. Conversion of research from lab to clinic traditionally lacks success and efficiency. Only half of recommended healthcare practices are implemented, and the process of translation often takes upwards of 15 years to effectuate.[2] The barriers to translation are various and interrelated, and include inadequate research program design, insufficient marketing, or regulatory issues arising from the inherent differences between the academic and clinical setting.[3] In healthcare technology, the NHS have identified a need for the encouragement of universities to commercialise research. The National Institute for Health Research (NIHR) was established in 2006 to improve patient and service outcomes via creating and nurturing relationships between universities and industry. The NIHR also have the ability to fund collaborative research projects, whereby the migratory pathway to success is significantly increased. One such example is the Invention for Innovation (i4i) programme, which has been successfully applied to research and development of medical, active implantable, and *in vitro* diagnostic (IVD) devices.[4]

Medical device regulation (MDR) and *in vitro* diagnostic regulation (IVDR) are independently vast and rapidly growing fields, that are often complicated by legal technicalities. The design of novel medical devices that conform to regulations such that they may proceed through pre-market surveillance without hinderance is rare in academia. Hence, any potentially commercialisable product developed within a university setting may benefit from undergoing subsequent design iterations which prepare it for the long and arduous journey to market. In particular, the ability to identify the class of the device (i.e. as medial device or IVD, as well as the subclass of these fields) at the conceptual stage may aid the design in undergoing a defined route to market.[2]

3.2.1.1. Medical Devices

The European MDR (Article 2(1))[5] defines the term 'medical device' as any instrument, apparatus, appliance, implant, reagent, software, material or similar article, intended to be used, alone or in combination, for human beings for one or more of the following medical purposes:[6]

- Diagnosis, prevention, monitoring, treatment or alleviation of disease, disability or injury;
- Investigation, replacement, modification or support of the anatomy or of an anatomical, physiological or pathological process;
- Supporting or sustaining life;
- Control of conception ;
- Disinfection of medical devices;
- Providing information for medical purposes by means of *in vitro* examination of specimens derived from the human body.

Manufacturers of medical devices are required to determine the classification of their product, in order to determine the route to compliance. The four classes of medical device are shown in in Figure 3.2.

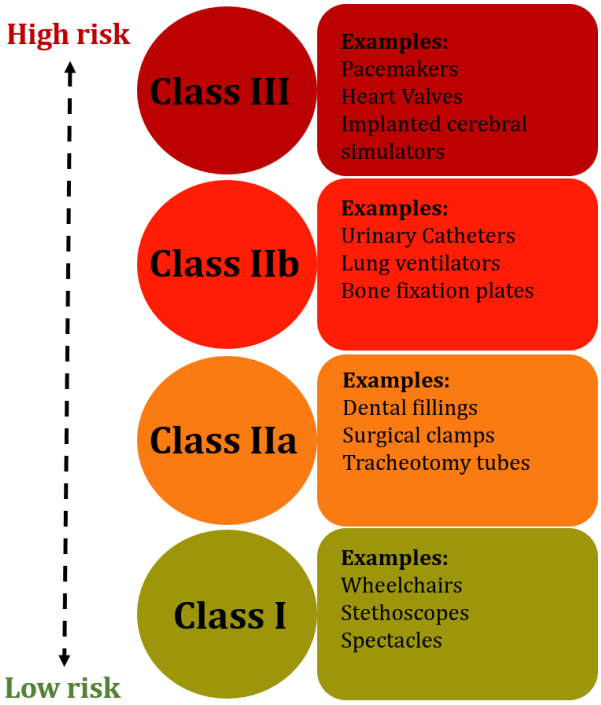

Figure 3.2: The four classes of medical device. Device manufacturers may use the classification rules in annex VIII of the MDR to accurately categorise novel products.

Devices which incorporate or administer a drug (e.g. medicated urinary catheters) often fall within a 'grey area' between medical device and medicinal product. Specifically, devices incorporating a medicinal product which may act upon the body with action ancillary to that of the device, are not only subject to MDR, but also must be verified with regards to the safety, quality and usefulness of the proprietary medical substance. Such a device would fall into Class III of the medical device directive, owing to the increased complexity and risk of the secondary function.[7]

3.2.1.2. *In Vitro* Diagnostic Devices

An IVD device is defined within the IVDR (Article 2(2))[8] as any reagent, product, control material, kit, instrument, apparatus, software or system, intended to be used for the *in vitro* examination of specimens derived from the human body, for the purpose of providing information on one or more of the following:

- A physiological or pathological process or state;
- A congenital physical or mental impairment;
- Predisposition to a medical condition or disease;
- Determination of safety and compatibility with potential recipients;
- Prediction of treatment response or reaction;
- Monitoring of therapeutic measures.

The original IVD Directive,[9] created in 1993, was generated for a fledgling industry, without broad scope or scalability. Changes in the regulatory landscape were thus introduced in 2017 to account for its inevitable evolution. The new legistalation requires up to 90% of IVDs to be approved by notified bodies, compared to the old IVD Directive, in which 90% of the industry could self-certify. In addition to increased pre-market scrutiny, a new rule-based classification system is to come into effect, superceeding the current list-based approach.[10]

IVDs are catergorised in order of increasing perceived risk according to Figure 3.3. If devices are intended to be used in combination, classification rules apply separately to each device.

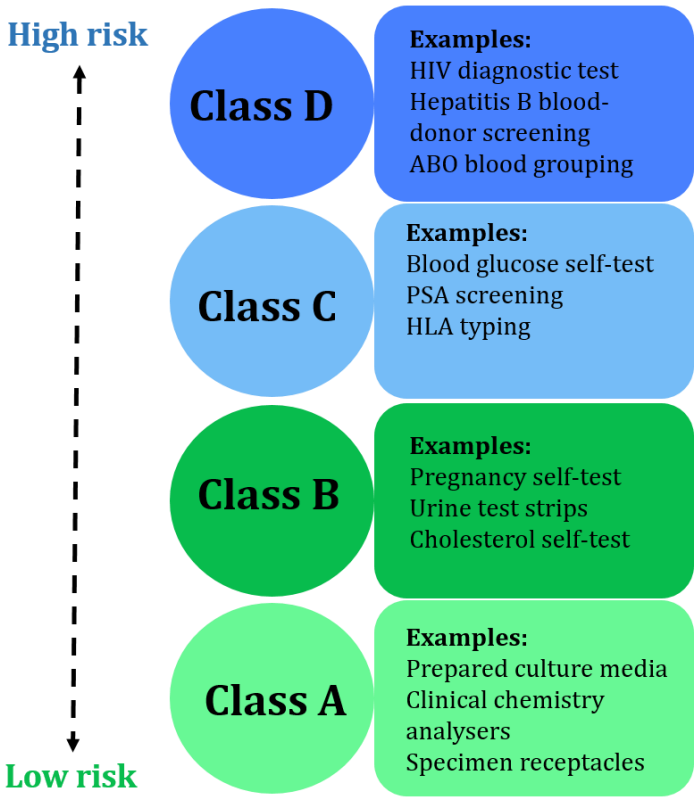

Figure 3.3: Classes of *in vitro* diagnostic device. Device manufacturers may use the classification rules in annex VII of the IVDR to accurately categorise novel products.

Innovation in diagnostics has become a major focal point of the NHS and NHIR within recent years. Approximately three quarters of all clinical decisions are made based on the results of standard diagnostic tests, many of which were previously only available in laboratory or hospital settings, but are now readily available as bedside POC or self-tests. Hence, recent regulatory changes aim to improve clarity regarding approval ,adoption and reimbursement of novel IVDs.[11]

3.2.1.3. CE Certification

A medical device may not be marketed or sold in Europe without a Conformité Européene (CE) mark, which is affixed by the manufacturer and indicates that the device meets the essential requirements of, and is compliant with, all relevant EU legislation. In order to apply for a CE mark, a conformity assessment procedure must be undertaken, the level of which reflects the perceived risk associated with the device (depending on its classification). For class I/A devices, the declaration of conformity is made by the manufacturer themselves. For higher classifications, conformity must be assessed by a notified body.

Recent changes in the legislational landscape are also reflected in the Clinical Trial Regulation (CTR),[12] which, after implementation in 2019, will replace the exisiting EU Clinical Trial Directive (EC) No. 2001/20/EC,[13] thus altering the way that clinical trials are conducted and recorded. The regulation harmonises the assessment and supervision processes for clinical trials throughout the EU, to both avoid unnecessary duplication of successful trials, or repetition of unsuccessful trials.

3.2.1.4. The Future of Medical Technology

In 2017, changes to MDR were made in response to concerns that medical devices and *in vitro* diagnostics, especially those that pose a high risk to the human body (e.g. breast implants), are not currently subject to sufficiently rigorous pre-clinical testing. To combat this, recently introduced legislational changes aim to strengthen regulation surrounding clinical investigation, promote control and monitoring of European medical device manufacturing and marketing, and encourage greater transparency and traceability throughout the product marketing process. Though these changes are likely to have a major impact on the medical technology industry, affected companies have only until 2020 (MDR) or 2022 (IVDR) to fully implement these changes, many of which are transformative.

Since EU directives are currently transitioning to a new MDR and IVDR, the withdrawal of the UK from the EU, universally referred to as 'Brexit', is causing a double transitional headache for the medical device industry in the UK, as the pathway to regulatory change remains uncertain. Previously, many low-risk medical devices that could formerly be marketed within the EU by obtaining CE Certification via self auditing (aided by notified bodies), will now be subject for far more stringent enforcement. New regulation expands the requirement for clinical trials to include low-risk IVD tests, which have never previously undergone clinical testing in Europe. Indeed, the German notified body Technischer Überwachungsverein (TUV) estimates that over 500,000 medical devices will require recertification in 2019 in order to comply with regulations.

3.2.1.5. Emerging Technologies for CAUTI

The current clinical need for efficient diagnosis of CAUTI and subsequent catheter blockage is considerable. The ability to initiate evidence-based treatment or preventative measures, following rapid profiling of bacterial pathogens may significantly improve patient care and stem the emergence of multi-drug resistant uropathogens.

Current screening assays for bacteriuria include dipstick tests for detecting nitrites, microscopic urinalysis, and urine Gram staining. Urine dipticks, whilst readily available and simple to use, are inadequately sensitive.[14] A meta-analysis of 34 studies assessing the accuracy of the nitrite dipstick test in a variety of clinical settings found a mean sensitivity of 48% for the detection of clinically significant bacteriuria (>10^5 CFU/mL).[15]

Recent developments in the POC detection of CAUTI generally revolves around rapid microbiological quantification and antibiotic susceptibility testing, as a development from traditional culturing methods (which are both time consuming and lacking in clinical accuracy). Novel diagnostic platforms, such as nucleic acid tests,[16] mass spectrometry,[17] electrochemical biosensors,[18,19] microfluidics[20] and lab-on-a-chip technology[21] have largely been approved for clinical use and thus improved the speed and accuracy of pathogen identification from primary cultures.[22] So called 'electronic noses' have been developed as a screening tool for bacteriuria, able to minic the olfactory system to detect a specific signature of volatile organic compounds (VOCs) produced by bacteria. The eNose (Specific Technologies) utilises ion mobility spectrometry to assess a VOC profile in just 15 minutes. Cultured uropathogens isolated from patient samples were detected with 95% sensitivity and 97% specificity,[23] although testing with unaltered urine sampes may cause inaccurate results owing to the variability of VOCs in urine. Nevertheless, the simplicity of VOC-based label-free biosensing renders it a promising approach for low-resource settings.[22]

The majority of developments in this field have been targeted towards decreasing turnaround time and enhancing throughput for batch processing. Thus far, very few attempts have been made to diagnose relevant clinical outcomes of CAUTI (e.g. catheter blockage) specifically, often resulting in common recurring catheter blockage and subsequent patient ill-health.[24,25] Despite substantial improvements in sensitivity and specificity in CAUTI biosensors in recent years, the commercialisation of such products is still in its infancy. Translation from lab to clinic appears to present significant challenges, owing to the differences between *in vitro* and *in vivo* samples. Whilst most biosensors appear to perform well with pristine samples in early stage testing (e.g. pure bacterial cultures, supernatants and artificial simulation fluids), unprocessed sampes, particularly urine, can be highly varied. Differences in salt concentration, pH and viscosity can interefere with analyte detection and may cause a high proportion of false positive/negative results in the clinical setting.[22]

3.3. Materials and Methods

3.3.1. Materials

Materials for the development and *in vitro* analysis of polymeric lozenge sensors were purchased according to Chapter 2.

3.3.2. Methods

3.3.2.1. Microbiological Methods

Bacterial culture and quantification protocols were followed according to Chapter 2.

I. Preparation of Bacterial Supernatants

Bacterial overnight cultures (grown from a single bacterial colony), were centrifuged (4,000 rpm, 20 minutes) to pellet whole cells. The liquid phase of each sample was collected, sterilised by filtration (0.22 μm pore size) to remove any residual cells, and used immediately. Sedimented cells were discarded.

II. Preparation of Bacterial Subcultures

Bacterial overnight culture (10 μL in LB media) was added to artificial urine media (10 mL). 1:1000 subcultures were grown at 37 °C with agitation to assess sensor response.

III. Correlation of Viable Cell Count with Urinary pH

The point at which sensor 'switch on' was achieved was evaluated using 1:1000 subcultures of *P. mirabilis* B4 and *E. coli* NSM59. Cultures were grown into the exponential phase over 3 hours. Samples (100 μL) were removed at 10 minute intervals for analysis of bacterial bioburden (via serial dilution and plating on NSLB agar). Plates were incubated overnight and viable cell numbers quantified via colony counting. Measurements of subculture pH and fluorescence were also recorded at 10 minute intervals using an electronic pH meter (Jenway 3540), and microplate reader, respectively.

3.3.2.2. Materials Preparation

Solutions of 5(6)-carboxyfluorescein, phosphate buffer (pH 6, 7 and 8), PVA and Eudragit S100 were prepared according to Chapter 2.

I. Dip Coating Optimisation

Lozenge sensors were prepared according to Section 3.2.2.2.II, and dip coated with 30, 40 or 50 coats of Eudragit S100 solution to assess dye retention with varying coating thickness. Release was assessed via overnight incubation at room temperature in phosphate buffer (10 mL) at pH 6 and 8. Fluorescence output was monitored using a microplate reader according to Chapter 2.

II. Preparation of pH-Sensitive Lozenge Sensors

To carboxyfluorescein solution (250 mM, adjusted to pH 6) was added PVA (14,000-18,000 g/mol, 15% w/v) and heated to 97 °C with constant stirring to facilitate diffusion. The resultant hydrogel (1 mL) was cast into a 24-well microplate containg a 2 cm length of sterilised cotton thread (Figure 3.4), and stored at -20 °C overnight to promote cryogenic crosslinking.

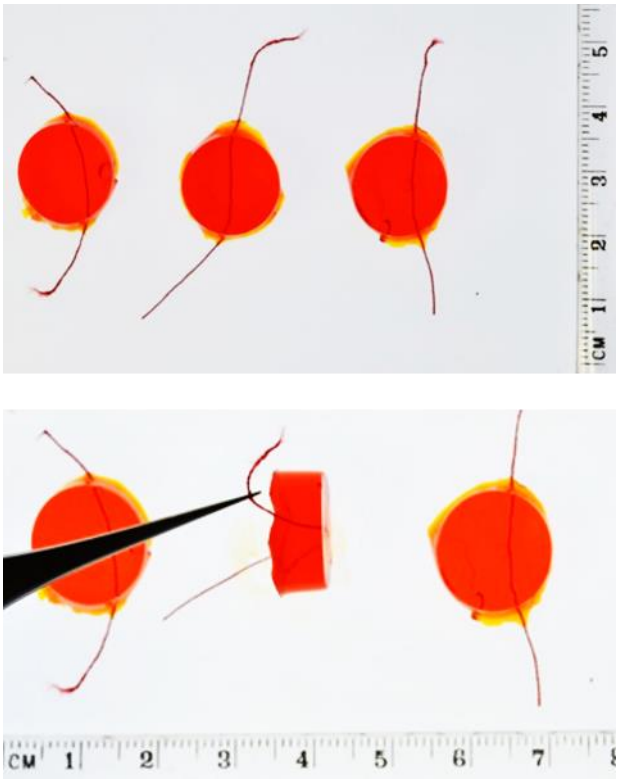

Figure 3.4: Dimensions of the pH-responsive polymeric lozenge sensors (containing self-quenched 5(6)-carboxyfluorescein), showing the positioning of the sterile thread.

Sensors were thawed at room temperature (4 hours) before dip coating with Eudragit S100 trigger layer via suspension from the thread. Sensors were manually dip-coated 50 times, with a 5 minute solvent evaporation period at room temperature between each coating. Coated sensors were stored at 4 °C until required.

3.3.2.3. Evaluation of Sensor Performance

I. Bacterial Subcultures

Protoype sensors were evaluated for species selectivity using live cultures of *P. mirabilis* B4 and *E. coli* NSM59 clinical isolates (~10^5 CFU/mL). Lozenge sensors were added to 1:1000 bacterial subcultures in artificial urine, and changes in pH and fluorescence response as a function of dye release were measured via sequential sampling.

II. Physiological Representation

Evaluation of prototype sensors under physiologically representive conditions was performed in order to assess duration of 'early warning' provided. *In vitro* bladder models were assembled and run according to Chapter 2. Models simulating late-stage infection were inoculated with *P. mirabilis* or *E. coli* (10^8 CFU/ml) and supplied with artificial urine media at a flow rate of 0.75 mL/min. Individual lozenge sensors were added aseptically to each drainage bag, and changes in visual urine color change were correlated with measured fluorescence output. Quantitative assessment of fluorescence response was undertaken using a microplate reader as above.

III. Kinetics of Carboxyfluorescein Release

To evaluate the quantity of, and rate at which the carboxyfluorescein dye is released from the sensors, the kinetics of dye release was analysed at pH 6, 7 and 8 (37 °C, phosphate buffer). Dye release from the lozenge sensors was monitored at regular time intervals, and subsequent graphs of initial release (first 15 minutes) were created. Standard curves of fluorescence intensity as a function of carboxyfluorescein concentration were also produced at pH 6, 7 and 8 (linear portion only). Values of dye concentration were calculated from the standard curves in order to achieve graphs of carboxyfluorescein concentration vs. time from the original sensor release. Kinetic evaluation was not completed for pH 6, as release of dye was negligible. The gradient of the resultant graphs at pH 7 and 8 shows the rate (mol dm^{-3} min^{-1}) of carboxyfluorescein release within the first 15 minutes of contact.

3.4. Results and Discussion

The optimisation of an infection-detecting polymeric lozenge for the early warning of catheter blockage, offers numerous advantages over the catheter coating concept described in Chapter 2. Primarily, the design discussed in this chapter transforms the aforementioned technology from a Class IIb medical device, to a Class B *in vitro* diagnostic device. Hence, the regulatory pathway to CE marking and subsequent use within a clinical setting is significantly less onerous, owing to the lower level of perceived risk associated with such a device.

3.4.1. Eudragit S100 Dip Coating Optimisation

Since the lozenge sensor design incorporates a significantly larger volume of PVA reservoir than the original catheter coating, it was predicted that a considerably thicker film of the Eudragit S100 trigger layer would be required to provide sufficient entrapment efficiency of the dye within the hydrogel. Encapsulation of 5(6)-carboxyfluorescein was investigated in solutions of phosphate buffer at pH 6 and 8 to simulate healthy and infected urine, respectively. Film thickness (30, 40 or 50 dip coats) was deemed sufficient when a visible fluorescence output was obtained at pH 8, but not at pH 6.

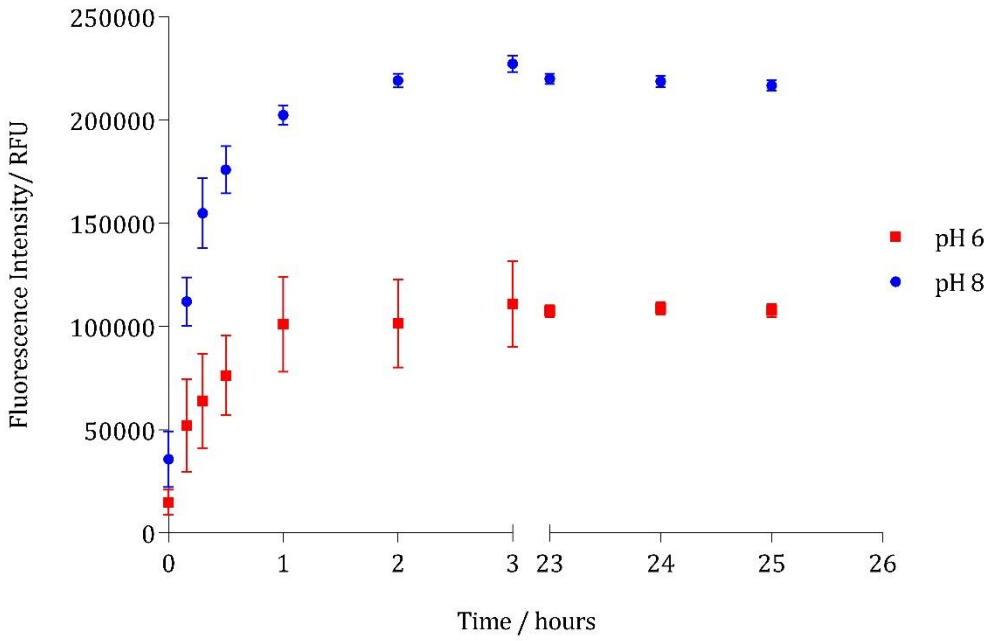

Figure 3.5: Encapsulation efficiency of 30 coats of Eudragit S100 at pH 6 and 8. Leaching of the fluorescent dye was observed upon room-temperature incubation of the lozenge sensor within phosphate buffer simulating healthy urine pH.

Dye retention within the hydrogel reservoir was insufficient after 30 coats of the polymeric trigger (Figure 3.5). Significant dye release was observed within the first hour of incubation in buffer solution mimicking healthy urine pH. When the film thickness was increased to 40 coats, carboxyfluorescein dye was more successfully retained within the central hydrogel region of the lozenge sensor (Figure 3.6).

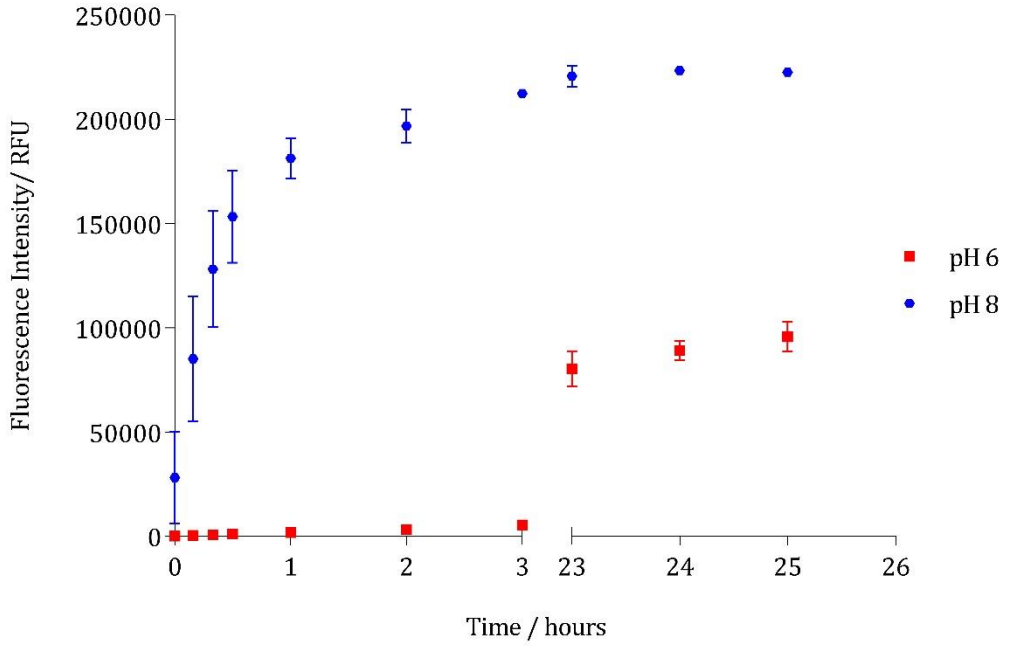

Figure 3.6: Encapsulation efficiency of 40 coats of Eudragit S100. Visual dye release was observed after 23 hours incubation in phosphate buffer at pH 6 and 8.

Lozenge sensors appeared stable at pH 6 after 3 hours incubation, as dye release and subsequent fluorescence 'switch on' was insufficient to cause a visual response. However, after overnight incubation, the structural integrity of the Eudragit shell was compromised, resulting in leaching of the loaded dye into the bulk solution. Dye release at pH 6 was less efficient than pH 8, yet sufficient to cause a visual colour change within the recipient medium.

Analysis of dye retention within lozenge sensors coated with 50 dip coats of Eudragit S100 showed effective encapsulation for the duration of the assay (Figure 3.7). Loaded dye was effectively maintained within the hydrogel reservoir in the presence of buffer mimicking healthy urine pH, but underwent a rapid and visually unambiguous fluorescence 'switch on' at pH representing urine infected with urease-positive species. As with the coating optimisation observed in Chapter 2, the rate of dye release appeared slower with increasing coating thickness, although still resulted in visual fluorescence within the first hour of incubation.

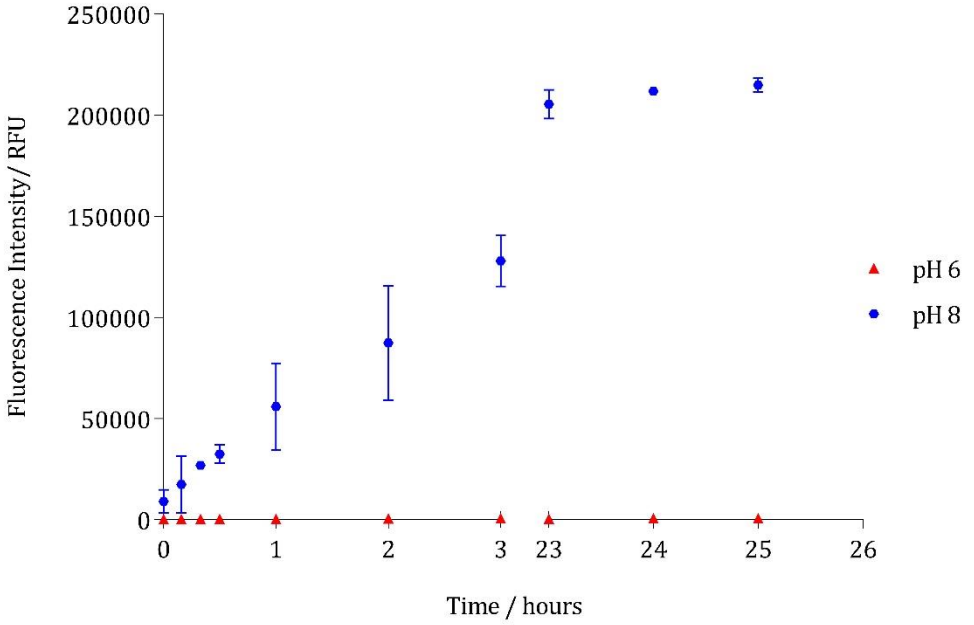

Figure 3.7: Encapsulation efficiency of 50 coats of Eudragit S100 at pH 6 and 8. Coatings remained stable for the duration of the 24 hours incubation at healthy urine pH. Rate of dye release into the recipient medium

Overall, analysis of carboxyfluorescein retention showed that dye encapsulation within the hydrogel matrix is dependent on Eudragit film thickness. Protoype production will henceforth be completed with 50 coats of Eudragit polymer, as this provides the optimum compromise between sensor stability and production time.

3.4.2. Kinetics of 5(6)-Carboxyfluorescein Release

The rate at which loaded dye was released from the lozenge sensors was evaluated at pH 6 (healthy urine pH), pH 7 (Eudragit dissolution threshold), and pH 8 (infected urine pH) (Figure 3.8). Fluorescence response from sensors was monitored over a 2 hour period, until the release at pH 8 had reached a steady state (Figure 3.8A). Initial rate was estimated within the first 15 minutes of exposure of lozenge sensors to phosphate buffer at relevant pHs, as this was the region in which a visual response was obtained (Figure 3.8B). Values of carboxyfluorescein concentration were read from a standard curve at the appropriate pH (Figure 3.8C/D) in order to obtain graphs detailing increasing carboxyfluorescein as a function of time (Figure 3.8 E/F). The gradient of the resultant graph is equal to the initial rate of dye release in units of mol dm^{-3} min^{-1}. Cumulative release from the polymer matrix at pH 6 was negligible, hence calculation of release rate was not possible with this method.

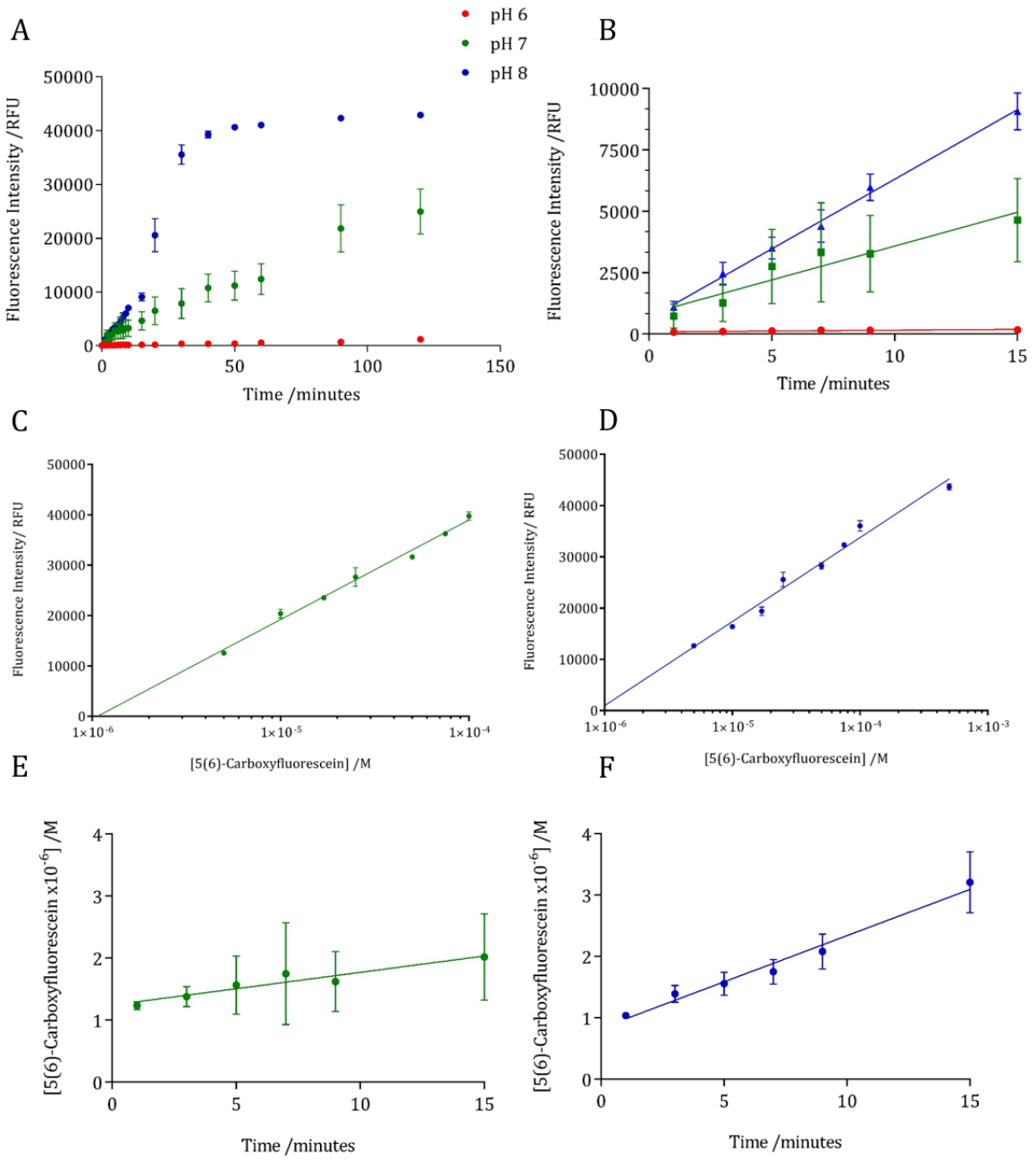

Figure 3.8: Determination of 5(6)-carboxyfluorescien release from pH-sensitive lozenge sensors at pH 7 and 8. Empirical dye release was monitored over the course of 120 minutes at physiological pHs (pH 6, 7 and 8) (A). Initial release was defined as the first 15 minutes of release, within which the fluorescence output was linear (B). Standard curves of fluorescence intensity as a function of [carboxyfluorescein] at pH 7 (C) and pH 8 (D) were used to evaluate the kinetic release of dye from the sensors at each pH (E, F for pH 7 and 8 respectively). Rate of release could not be analysed at pH 6, owing to negligible dye release. Data shown are the mean of triplicate repeats. Error bars represent SEM.

Rate of initial release of carboxyfluorescein at pH 7 and 8 are shown in Table 3.1. Observed release was seen to vary with pH as predicted, with the greater rate of release observed for the more highly alkaline buffer pH.

Table 3.1: Initial release of 5(6)-carboxyfluorescein from lozenge sensors at pHs representing healthy (pH 6) and infected (pH 8) urine

	pH 7 (±SEM)	**pH 8 (±SEM)**
Initial release (mol dm^{-3} min^{-1})	$5.3x10^{-8} \pm 8.4 x10^{-9}$	$1.5x10^{-7} \pm 1.9 x10^{-8}$

Maximum release of carboxyfluorescein was estimated to be 3.5 mM after 2 hours exposure to phosphate buffer at pH 8. Thus, despite only approximately 14% of the total encapsulated dye being released from the PVA reservoir, the resultant fluorescence output lies within the most strongly luminescent region of the fluorescent chromophore, according to Chapter 2.3.1. (Figure 7). In effect, the conservation of the majority of the dye within the hydrogel reservoir may serve to retain signal strength over longer time periods.

Kinetic release of a dye or other model drug from a multicomponent material system (i.e. integration of multiple materials with differing physicochemical properties) is known to be complex, and highly dependent on parameters such as delivery device size and shape. Such systems cannot be described using a single mathetmatical model, as release is driven by multiple factors (often working simultaneously to facilitate transport into the release matrix).[26] Thus, the rate of dye release described in this work is primarily aimed to give a simple, semi-empirical estimate of relative dye release from the lozenge sensor. A simple model to describe the kinetics of drug/dye release from polymeric matrices can be described using the Korsmeyer-Peppas model as follows (Equation 1).[27]

$$\frac{M_t}{M_\infty} = kt^n \qquad (1)$$

Where M_t and M_∞ denote cumulative release at time *t* and at infinite time, respectively. *k* is the release rate constant and *n* is the release index, indicative of the release mechanism. For a slab structure, when $n = 0.5$, Fickian diffusion is observed, whilst $0.5 < n < 1.0$ indicates non-Fickian diffusion ($n > 1.0$ for mass-transfer following a non-Fickian model).[28] In the case of a cylinder such as the lozenge sensor, $n = 0.45$ instead of 0.5, and 0.89 instead of 1.0.[29] Evaluation of

carboxyfluorescein release kinetics using the Korsmeyer Peppas model was fitted according to Equation 2. The resultant graph is shown in Figure 3.9.

$$\frac{M_t}{M_\infty} = kt^n \rightarrow \ln\left(\frac{M_t}{M_\infty}\right) = \ln(k) + n\ln(t) \quad (2)$$

Where ln(k) is the intercept and n is the slope of the fitted straight line $\ln(M_t/M_\infty)$ vs ln(time).

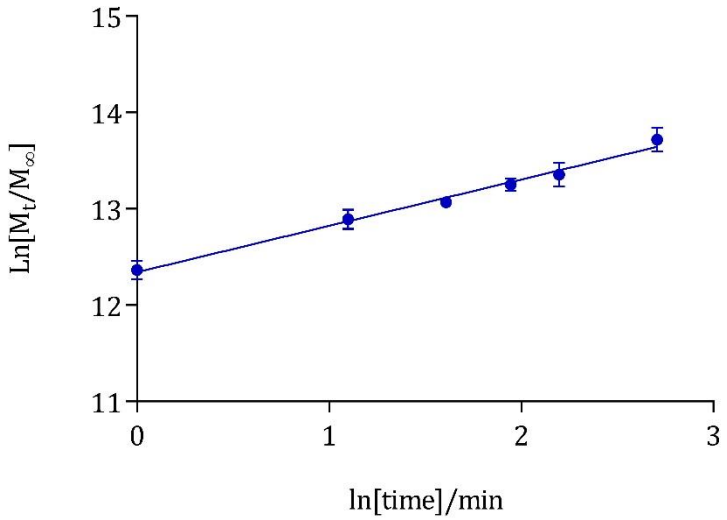

Figure 3.9: Korsmeyer-Peppas release plot for kinetic evaluation of 5(6)-carboxyfluorescein release at pH 8 (r^2 = 0.99).

The exponent *n* was calculated to be 0.48 ± 0.025, confirming that dye release is governed by Fickian diffusion. The process of diffusion-controlled drug release via an aqueous stimulus has distinct advantages in terms of the timing and control of the system's response. For example, the rate at which water may swell the matrix of a crosslinked system is greater for diffusive systems than those governed by degradation or dissolution. In the lozenge reservoir system, the swelling effect is seen as a nonuniform volume expansion, whereupon swelling of the barrier coating results in rapid aqueous diffusion from the internal components of the system.

3.4.3. Evaluation of Sensor Performance: Artificial Urine Supernatant

The ability of the sensors to release their fluorescent cargo in response to elevated artificial urine pH was evaluated using supernatant solutions of *P. mirabilis* B4 (average pH = 8.98) and *E. coli* NSM59 (average pH = 6.10). Sensor stability in sterile artificial urine was also evaluated, to ensure that no fluorescence output was obtained as a result of interactions between the

Eudragit S100 'shell', and the high ionic-strength artificial urine. Measured fluorescence intensity of artificial urine supernatants is shown in Figure 3.10.

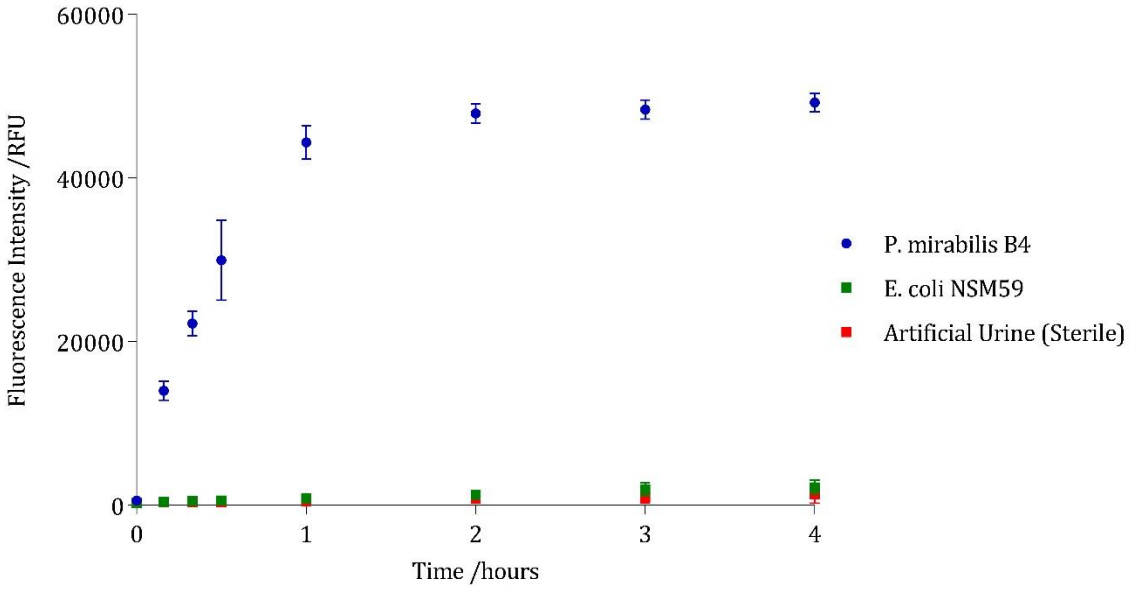

Figure 3.10: Analysis of sensor performance in artificial urine supernatants of *P. mirabilis* and *E. coli* species. Average pH of supernatants was 8.98 for urease-positive and 6.10 for urease–negative species, thus mimicking the urine of infected and healthy patients, respectively.

Since *E. coli* species are unable to express urease, the pH of the supernatant remained equivalent to that of the uninoculated artificial urine. Visual dye release was only observed for the urease-positive *P. mirabilis* supernatant, where the average urinary pH surpassed that of the Eudragit S100 swelling threshold.

3.4.4. Evaluation of Sensor Performance: Artificial Urine Subcultures

3.4.4.1. Correlation of Bacterial Bioburden with Urinary pH

The point at which sensor 'switch on' was achieved was evaluated using 1:1000 subcultures of *P. mirabilis* in artificial urine media. Urinary pH elevation to to pH 8 was achieved in 150 minutes of incubation, owing to the expression of urease and subsequent urea hydrolysis within the media. The threshold pH at which the Eudragit 'trigger' layer undergoes swelling as a consequence of repulsion (pH 7) was achieved at approximately 135 minutes. This corresponded to the transition period of bacterial replication from lag phase to exponential

growth phase (Figure 3.11). Approximate bacterial concentration at this point was 7.45 x10^6 CFU/mL.

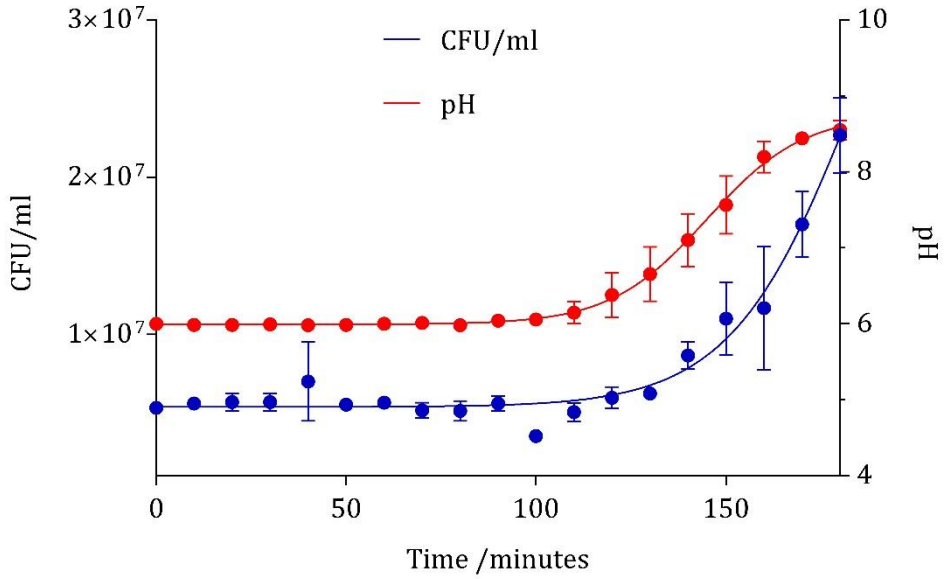

Figure 3.11: Evaluation of sensor 'switch on' using 1:1000 subculture of *P. mirabilis* in artificial urine. Urinary pH elevation owing to urease-mediated urea hydrolysis, and corresponding increase in bacterial bioburden during transition from lag phase to exponential growth.

These findings agree with previous observations made by Dattelbaum *et al*,[30] who reported that expression of urease with cultures of *P. mirabilis* was greatest at the mid-exponential phase. Moreover, since a substantial increase in urease production is associated with swarmer cell differentiation and expression of virulence factors, it is likely that *P. mirabilis* undergoes a coordinated virulence 'switch on' upon entering the exponential phase of growth.[31] Indeed, previous investigation into the effects of the known anti-swarming agent *p*-nitrophenylglycerol (PNPG) revealed that the expression of virulence factors such as protease, urease, haemolysin and flagellin were inhibited in addition to the transformation to hyperflaggerlate swarmer cell structure, upon incubation with PNPG.[32]

3.4.4.2. Species Selectivity

Elevation in urinary pH was found to correspond to a rapid and observable increase in fluorescence response as function of carboxyfluorescein release from lozenge sensors (Figure 3.12).

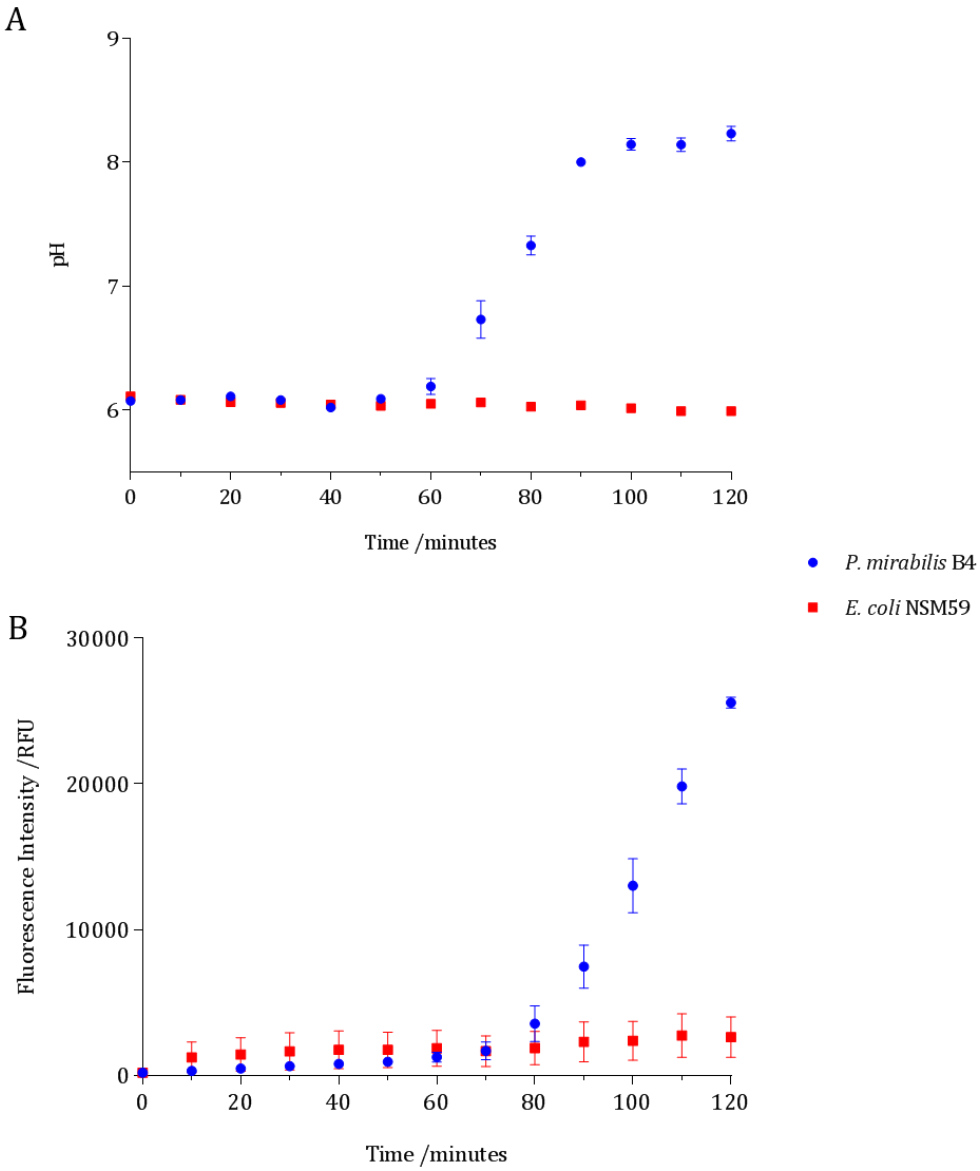

Figure 3.12: Analysis of sensor performance in artificial urine subcultures, modelling the onset of CAUTI. A) pH-elevation of *P. mirabilis* (urease-positive) and *E. coli* (urease-negative) cultures. B) Corresponding fluorescence emission of prototype sensors upon release of carboxyfluorescein.

Fluorescence emission was observed only in the presence of *P. mirabilis*, owing to expression of urease and subsequent accumulation of NH_3 within the artificial urine medium. *E. coli* was used as a control species, since it is unable to elevate urinary pH to alkaline values.

Limitations of this model, however, prevent speculation as to the performance of sensors *in vivo*. The absence of a continuously replenishing culture renders the cells nutrient-limited after a finite time period, thus such a system is not indicative of the catheterised bladder. Furthermore, the volume limitations (10 mL) imposed on such cultures limit the information gained on the strength of the visual colour change obtained within a full-sized catheter drainage bag (2 L capacity). Overall, this model proved the species-specific capabilities of the lozenge sensors in the presence of live bacterial cultures, but gave no information on the nature of the colour change or duration of early warning in a clinically relevant setting.

3.4.5. Evaluation of Sensor Performance: *In Vitro* Bladder Models

Capability of the lozenge sensor prototypes to provide advance warning of impending catheter blockage was evaluated in a clinically relevant *in vitro* model of the catheterised urinary tract. This model replicates the closed drainage system in its entirety, thus providing an accurate represenatation of conditions within the catheter drainage bag. Sensor 'switch on' was defined as the point at which a visual color change was observed in residual urine within the collection bag. Fluorescence output was judged by eye under ambient lighting, in order to mimic conditions in which a patient may undergo self-evaluation of their proximity to catheter blockage.

Observation of visual dye release prompted quantitative anaylsis of urinary fluorescence (Figure 3.13), so that the concentration of carboxyfluorescein in residual urine may be estimated at different time points. The response of lozenge sensors to *E. coli* was also assessed to determine the selectivity of the sensors towards urease-positive species under physiological conditions. Inoculation of infected bladders with large bacterial bioburdens (10^8 CFU/mL) endevours to replicate conditions within the catheterised urinary tract of patients suffering form recurring blockage, where the blocked catheter is removed and immediately replaced, directly into the existing cultures of *P. mirabilis* (where residual urine may already exist at highly alkaline pHs, and contain aggregates of microcrystalline material).[33] This situation occurs in up to 50% of long-term catheterised patients,[34] who may experience recurring

blockage as soon as 2 days post catheter reinsertion. Thus, the conditions used within the *in vitro* model aim to test sensor performance under 'worst case scenario' circumstances.

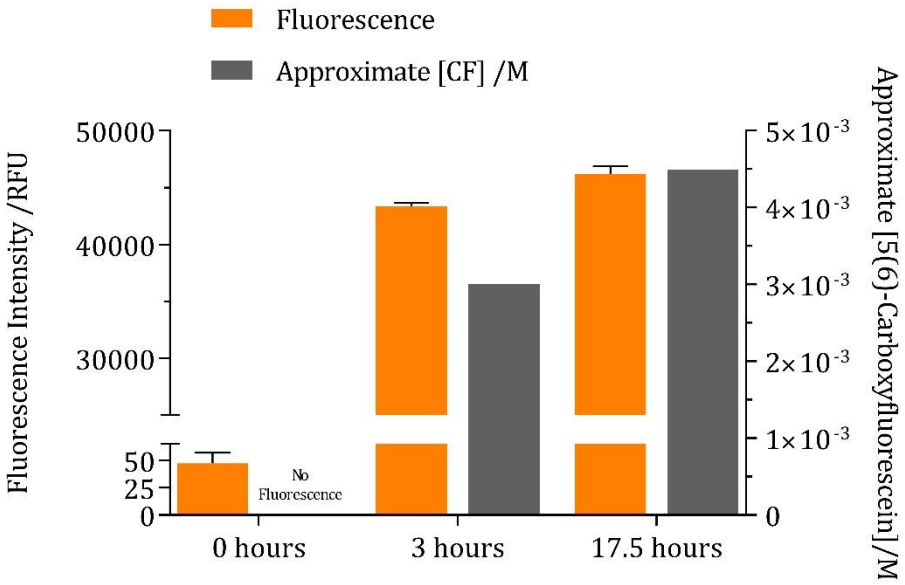

Figure 3.13: Quantitative analysis of 5(6)-carboxyfluorescein release into residual artificial urine of *P. mirabilis*-infected models. Samples were removed from the drainage bag in response to subjective visual prompts. Time points represent average time of consequential events throughout the course of the experiment: model start (0 hours), point of visual colour change (3 hours), and catheter blockage (17.5 hours).

Dye release and consequent visual colour change within the drainage bag was observed approximately 3 hours after model start. This corresponded to an average urinary pH of 7.2, and an approximate carboxyfluorescein concentration of 2 mM within the drainage bag. Average blockage time of models inoculated with *P. mirabilis* occurred at 17.5 hours, corresponding to a urinary pH of 8.6. Hence, the bag sensors acheived an average early warning of blockage of 14.5 hours, with a range of 12.5-18 hours. The duration of warning was deemed sufficient to allow clinical intervention before the manifestation of serious clinical consequences.

The appearance and progression of sensor activation within the bladder infection model is shown in Figure 3.14. Control bladders inoculated with *E. coli* exhibited negligible fluorescence emission throughout the duration (23 hours) of the experiment.

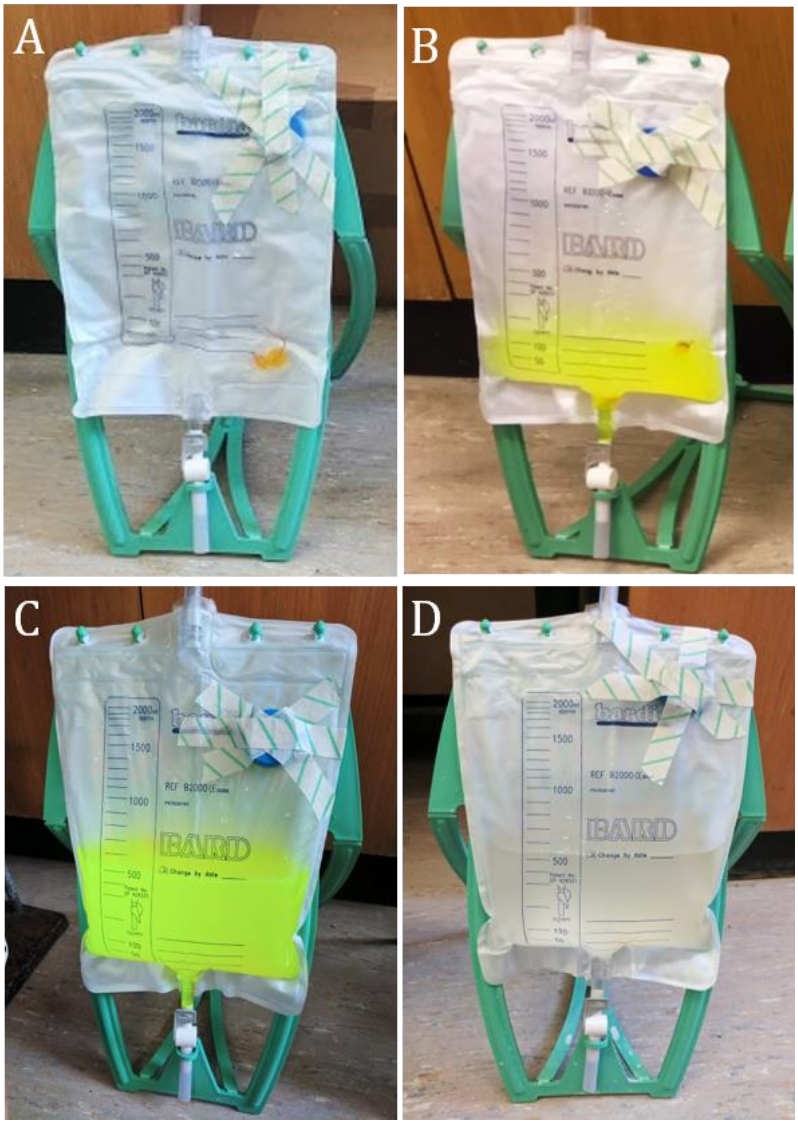

Figure 3.14: Progression of lozenge sensor activation within an *in vitro* model of the catheterised urinary tract. A) Appearance of drainage bag at experiment start (0 hours). B) Point of visual colour change (3 hours) within model inoculated with *P. mirabilis*. C, D) Colour change of residual drainage bag urine at point of catheter blockage (17.5 hours): C) in bladder model inoculated with *P. mirabilis* (urease-positive), and D) in models infected with *E. coli* (urease-negative) species. Images are representative of triplicate repeats.

Since many patients undergoing long-term indwelling catheterisation are within the community care setting, the collection and analysis of urine samples may prove both complex and time-consuming. Using the lozenge sensor system, a clear and unambiguous visual color change is observed within the catheter drainage bag approximately 14 hours in advance of blockage following infection by *P. mirabilis*. Thus, the patient or carer may be informed of imminent catheter complications, facilitating timely intervention.

Sensor performance was comparable to other reported sensors,[24,25,35,36] although the implementation of this approach provides significant advantages. The specific dissolution threshold of Eudragit S100 at pH 7 allows this system to be more sensitive to catheters progressing towards encrustation and blockage specifically, rather than asymptomatic bacteriuria. By comparison, the previously described bromothymol blue sensor responded to an increasing urinary pH over a broad range (pH 6-8),[24] making it highly susceptible to false positive results as a consenquence of activation by healthy, uninfected urine.

However, whilst the bladder infection model described provides an accurate *in vitro* depiction of the catheterised urinary tract, it is not fully representative of the catheterised bladder *in vivo*. Futher clinical studies are thus required to analyse the sensor performance in light of the full complexity and variation of these conditions. Progression to pilot-stage clinical trials will likely be expedited by the substantial advantages of this sensor design in terms of medical technology classification. Since the sensor is not intented for use within the body, and gives an easily-interpretable signal at the POC, it would likely be classified as a Class B *in vitro* diagnostic, rather than the Class III medical device coating described in Chapter 2. Consequently, this system would be subject to less stringent regulatory approval, potentially including self-certification by the device manufacturer.

3.5. Conclusion

Development of simple and accurate tests for highly specific clinical outcomes would represent a major milestone in the field of CAUTI. As scientific knowledge of host-pathogen interactions increases, the next generation of POC diagnostics may be refined to analyse speficic infection-responsive biomarkers. Providing an early, yet refined course of treatment might not only benefit the patient, but also result in improved antibiotic stewardship.

The design constraints of the Foley catheter system, and the medical technology classification of the sensor were important considerations in the design of the lozenge system described. Since the currently used Foley catheter design has remained unchanged for decades, any technological advances involving redesign of the current system, or fabrication of additional components have thus far been rejected by the clinical community, owing to the additional cost and complexity. Indeed, some of these issues were emphasised in the pilot scale clinical trials of the bromothymol blue sensor,[36] where some patients were unable or unwilling to accept an additional accessory to the existing layout. In constrast, the sensor system described here may be incoporated into all existing drainage bag designs, without altering patient experience. However, the insertion of the sensor into the bag must be taken into consideration. This process must take place at the point of manufacture, such that the sterility of the system is not compromised at the point-of-care.

Perhaps the most valuable aspect of the lozenge sensor system described is the potential to incorporate antimicrobial coatings to the catheter tip (using the infection-responsive coating approach described in Chapter 2). The relocation of the diagnostic system to an external location within the catheter drainage bag enables the internal portion of the catheter (namely the distal tip) to remain available for introduction of antimicrobial species, such as small-molecule antimicrobials or bacteriophage. Ultimately, this permits the eventual formulation of a theranostic catheter system, whereby the onset of blockage is delayed by the therapeutic coating, and subsequent elution/failure of the antimicrobial agent is signalled by the diagnostic sensor located within the drainage bag.

3.6. References

1. UK Government, UK Medical Technology: at a glance, https://invest.great.gov.uk/industries/health-and-life/medical-technology/, (accessed 17 October 2018).

2. M. Sanami, T. Flood, R. Hall, F. Kingscott, D. Jayne and P. Culmer, *Advances in Mechanical Engineering*, 2017, **9**, 1–9.

3. A. A. DiSessa and P. Cobb, *Journal of the Learning Sciences*, 2004, **13**, 77–103.

4. National Institiute for Health Research, Invention for Innovation, https://www.nihr.ac.uk/funding-and-support/funding-for-research-studies/funding-programmes/invention-for-innovation/, (accessed 18 October 2018).

5. European Commission, *Medical Device Regulatory Framework*, 2017.

6. World Health Organisation: Global Harmonisation Task Force, 2012, 4–6.

7. Medicines & Healthcare Products Regulatory Agency, *Borderlines between medical devices and medicinal products: Guidance on Legislation*, 2016.

8. European Commission, *In Vitro Diagnostic Medical Device Regulatory Framework*, 2017.

9. European Commission, *In Vitro Diangostic medical Devices Directive 98/79/EC*, 1993.

10. European Commission, The New Regulations on Medical Devices, https://ec.europa.eu/growth/sectors/medical-devices/regulatory-framework_en#new_regulations, (accessed 18 October 2018).

11. M. Thompson, C. Price, A. Van den Bruel, C. Heneghan, P. Wilson, N. Crabb, D. Williams, J. Deeks and P. Bossuyt, *Innovation in Diagnostics and Healthcare: Improving bench to bedside processes for testing*, 2011.

12. European Commission, *Regulation (EU) No 536/2014 of the European Parliament and of the Council*, 2014.

13. European Commission, *Clinical Trials - Directive 2001/20/EC*, 2001.

14. R. L. Lammers, S. Gibson, D. Kovacs, W. Sears and G. Strachan, *Annals of Emergency Medicine*, 2001, **38**, 505–512.

15. W. L. J. M. Devillé, J. C. Yzermans, N. P. Van Duijn, P. D. Bezemer, D. A. W. M. Van Der Windt and L. M. Bouter, *BMC Urology*, 2004, **4**, 4.

16. A. Niemz, T. M. Ferguson and D. S. Boyle, *Trends in Biotechnology*, 2011, **29**, 240–250.

17. A. Burillo, B. Rodríguez-Sánchez, A. Ramiro, E. Cercenado, M. Rodríguez-Créixems and E. Bouza, *PloS one*, 2014, **9**, 1–7.

18. E. Altobelli, R. Mohan, K. E. Mach, M. L. Y. Sin, V. Anikst, M. Buscarini, P. K. Wong, V. Gau, N. Banaei and J. C. Liao, *European Urology Focus*, 2017, **3**, 293–299.

19. C. Halford, R. Gonzalez, S. Campuzano, B. Hu, J. T. Babbitt, J. Liu, J. Wang, B. M. Churchill and D. A. Haakea, *Antimicrobial Agents and Chemotherapy*, 2013, **57**, 936–943.

20. Y. Lu, J. Gao, D. D. Zhang, V. Gau, J. C. Liao and P. K. Wong, *Analytical Chemistry*, 2013, **85**, 3971–3976.

21. N. J. Cira, J. Y. Ho, M. E. Dueck and D. B. Weibel, *Lab on a Chip*, 2012, **12**, 1052–1059.

22. M. Davenport, K. E. Mach, L. M. D. Shortliffe, N. Banaei, T. H. Wang and J. C. Liao, *Nature Reviews Urology*, 2017, 14, 298–310.

23. A. Roine, T. Saviauk, P. Kumpulainen, M. Karjalainen, A. Tuokko, J. Aittoniemi, R. Vuento, J. Lekkala, T. Lehtimäki, T. L. Tammela and N. K. J. Oksala, *PLoS ONE*, 2014, **9**, 1–11.

24. S. Malic, M. G. J. Waters, L. Basil, D. J. Stickler and D. W. Williams, *Journal of Biomedical Materials Research - Part B Applied Biomaterials*, 2012, **100 B**, 133–137.

25. S. Milo, N. T. Thet, D. Liu, J. Nzakizwanayo, B. V. Jones and A. T. A. Jenkins, *Biosensors and Bioelectronics*, 2016, **81**, 166–172.

26. Y. Fu and W. J. Kao, *Expert Opinion on Drug Delivery*, 2010, **7**, 429–444.

27. N. A. Peppas, *Pharmaceutica Acta Helvetiae*, 1985, **60**, 110–111.

28. S. Wang, *Microporous and Mesoporous Materials*, 2009, **117**, 1–9.

29. P. Costa and J. M. Sousa Lobo, *European Journal of Pharmaceutical Sciences*, 2001, **13**, 123–133.

30. J. D. Dattelbaum, C. V. Lockatell, D. E. Johnson and H. L. T. Mobley, *Infection and Immunity*, 2003, **71**, 1026–1030.

31. B. V. Jones, E. Mahenthiralingam, N. A. Sabbuba and D. J. Stickler, *Journal of Medical Microbiology*, 2005, **54**, 807–813.

32. S. J. Liaw, H. C. Lai, S. W. Ho, K. T. Luh and W. B. Wang, *Journal of medical microbiology*, 2000, **49**, 725–731.

33. D. J. Stickler and R. C. L. Feneley, *Spinal Cord*, 2010, **48**, 784–790.

34. D. J. Stickler, *Journal of Internal Medicine*, 2014, **276**, 120–129.

35. D. J. Stickler, S. M. Jones, G. O. Adusei, M. G. Waters, J. Cloete, S. Mathur and R. C. L. Feneley, *BJU International*, 2006, **98**, 1244–1249.

36. A. Long, J. Edwards, R. Thompson, D. A. Lewis and A. G. Timoney, *BJU International*, 2014, **114**, 278–285.

Therapeutic Approaches

Chapter 4: Prevention of Encrustation and Blockage of Urinary Catheters via pH-Responsive Release of Bacteriophage

4.1. Abstract

As medical procedures become ever-more reliant upon implanted devices for diagnosis and treatment of infectious disease, further emphasis is placed on safeguarding antibiotic therapy as the panacea of modern medicine. Therefore, recent research has focused on alternative antimicrobials, for example bacteriophage, in the battle against multi drug-resistant uropathogens. The research presented in this chapter describes the development and *in vitro* assessment of an infection-responsive therapeutic coating for urinary catheters, which endeavours to delay catheter encrustation and blockage following infection by *P. mirabilis*. The coating employs the dual-layered polymeric system described in Chapter 2, consisting of a lower PVA hydrogel reservoir layer, capped and sealed by the pH-sensitive polymer Eudragit S100. Morphological changes induced within the Eudragit 'trigger layer' in response to elevated urinary pH, induce the release of bacteriophage into the catheterised bladder (Figure 4.1).

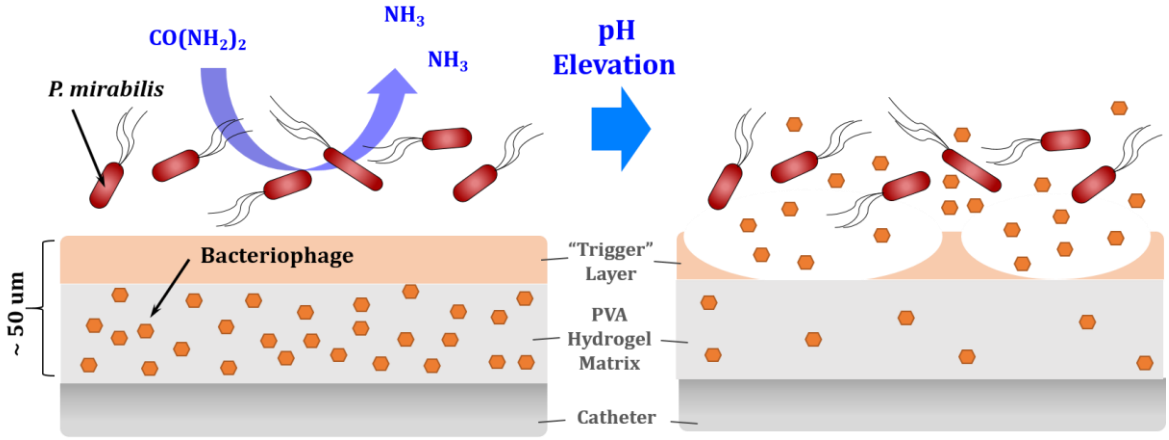

Figure 4.1: Schematic representation of the dual-layered polymeric architecture for the triggered release of bacteriophage from an infection-responsive urinary catheter coating.

The use of lytic bacteriophage was employed in order to evaluate the efficacy of a biological antimicrobial in inhibiting catheter blockage. The potential for bacteriophage to constitute an effective countermeasure for urinary catheter encrustation has a potentially wide-reaching impact, not only for improving patient welfare, but also in extending catheter lifetime, thus reducing associated healthcare costs. Protoype coatings were evaluated under conditions of established infection, prompting analysis of crystalline biofilm reduction in response to a 'burst-release' of bacteriophage within the physiological infection model.

4.2. Introduction

4.2.1. Antibiotic Resistance

At the turn of the twentieth century, infectious disease was the leading cause of death in humans.[1] The subsequent discovery and development of antibiotics within the last 100 years has revolutionalised modern medicine, forming the basis of contemporary infection control, both within the clinical and ambulatory care setting. The serendipitous discovery of penicillin in 1929[2] propelled the initiation of the 'golden era' of antibiotics, in which natural scaffolds and analogues of pioneering drugs were harvested, yielding revolutionary results. Invasive surgeries became routine, immunocompromising chemotherapy became a viable treatment option for cancer, organ transplantation extended lifespan, and the radical replacement of deteriorating joints, diseased corneas and burnt skin improved quality of life for millions of patients worldwide. Indeed, antibiotics have proved pivotal in the increase in life expectancy in the USA from 47 years in 1900, to 74 years for males and over 80 years for females in the year 2000.[3] Antibiotics remain one of the most commonly prescribed classes of drug, with the number of defined daily doses (DDDs) rising by 65% between 2000-2015, from 21.1 to 34.8 billion DDDs.[4]

Despite their initial success and consequent global impact, widesperead and indiscriminate use of antibiotics has induced and accelerated the evolution of biological countermeasures, whereby bacterial cells may resist destruction as a result of antibiotic exposure. Antimicrobial resistance (AMR) poses a serious global threat, estimated to cause 10 million annual deaths by 2050 if the progression of AMR is not impeded.[5] Factors including excessive use of antibiotics in commercial farming, over-the-counter sales, increased international travel, and the release of nonmetabolised antibiotic residues into the environment via manure spreading/poor sanitation programs have all contributed to the development of the global AMR crisis. In particular, the global consumption of antibiotics in livestock provides a significant risk, owing to extensive anthropogenic interaction and largely unregulated use of antibiotics at sub-lethal dosages.[6] In the USA alone, livestock receive over 13 million kilograms (approximately 80%) of antiobiotics annually,[7] the majority of which is administered in the form of continuous subtherapeutic quantitities to promote growth and prevent disease. Unsurprisingly, antibiotics used in this context have become associated with a high frequency of reistant bacteria in the gut flora of chickens, swine, and other food-producing animals. Without appropriate regulation, it is thought that such use will induce a large, diverse reservoir of resistance genes, which may facilitate the emergence of bacterial pathogens within the human population.[8]

4.2.1.1. Common Mechanisms of Antibiotic Resistance

The microbial population has possessed the molecular tools to drive resistance for many years before human interference. Surveys for microorganisms in samples of ancient permafrost revealed that the antibiotic resistome (the global collection of antimicrobial resistance genes) is genetically diverse,[9] widespread across all environmental niches,[10] and pre-dates modern antimicrobial resistance by millennia.[11] Antibiotic targets are generally conserved across the bacterial domain, and are absent or sufficiently different in eukaryotic cells. The current antibiotic arsenal generally attacks either the bacterial ribosome, thereby inhibiting protein synthesis (e.g. aminoglycosides); cell wall synthesis and lipid integrity, thus compromising membrane integrity or lysing cells (e.g. β-lactams); single-carbon metabolic pathways, inducing metabolic disruption (e.g. sulphonamides), or DNA maintanence, thus interfering with bacterial replication and genomic integrity (e.g. quinolones).[12–14]

Typical strategies employed by bacteria to resist antbiotic action often involve one of a few common pathways of modificiation.[15] One such mechanism involes the inactivation of the antibiotic via enzymatic degradation or modification of the chemical scaffold, thus rendering it ineffective. Examples of this mechanism include chloramphenicol acetyltransferases,[16] and, most notably, the widespread β-lactamases.[12,17] Alternatively, the protection, alteration or overexpression of the antibiotic target is employed by bacteria, for example vancomycin-resistant enterococci (which enzymatically modify peptidoglycan),[18] and methicillin-resistant *S. aureus* (MRSA), which expresses a redundant insensitive variation of the native penicillin-binding protein.[19] Two addtional mechanisms rely on externalising the antibiotic, either via efflux activity[20] or alteration of membrane permeability.[21] Increasingly, bacteria will utilise several complimentary mechanisms to achieve high levels of resistance. For example, high-level carbapenem resistance within clinical isolates of *Enterobacter cloacae* lacking in any known carbapenemase is achieved via a combination of porin mutations (that decrease drug uptake), and increased expression of a chromosomal β-lactamase.[22] Common antibiotic action and resistance mechanisms are shown in Figure 4.2.

Resistance can develop via two distinct pathways: vertical evolution, whereby mutations that enhance antibiotic tolerance are selected for and transmitted to progeny; or horizontal evolution, whereby antibiotic resistance genes are acquired from other bacteria via conjugation, transduction or transformation, and subsequently transmitted to progeny.[23] The resultant acquisition and spread of AMR renders many major classes of antibiotics obsolete,

making it increasingly difficult to establish and maintain even an ephemeral lead over bacteria in the AMR 'arms race'.

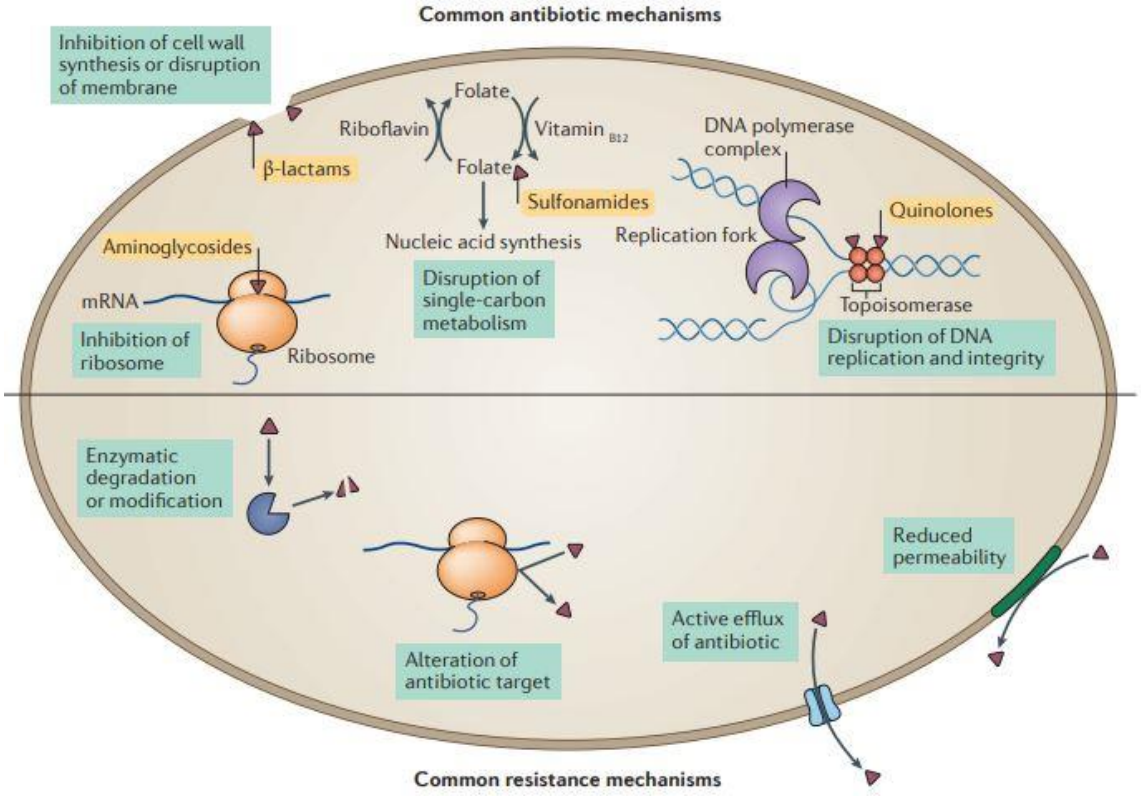

Figure 4.2: (Top) Overview of common classes of antibiotics and their mechanisms of action. (Bottom) Resistance mechanisms frequently employed by bacterial cells to counteract antibiotic therapy. Mutations may then be passed to bacterial progeny via vertical or horizontal evolution. Reprinted with permission from Crofts *et al*.[6] © Springer Nature 2017.

4.2.1.2. The Future of Antibiotic Discovery

The majority of antibiotic classes used clinically today were discovered and introduced to market by the end of the 1960s. Today, only 5 out of 5,000-10,000 antibiotic candidates will reach Phase I studies, with only 1 of those 5 ultimately receiving FDA approval.[24] Indeed, in the past 30 years, the approval of novel antibiotic drugs by the FDA has declined by 90%.[25] If the decline in discovery of novel classes of drug, combined with the increase in widespread AMR continues on its current trajectory, infectious disease-mortality will surpass that of cancer, and could cost up to $100 trillion worldwide.[26]

Barriers to antibiotic development, including scientific, regulatory and economic hurdles have proven antibiotic discovery and development to be less attractive to companies than more lucrative therapeutic areas. The developmental phase of a drug is a substantial investment; recent research suggests that a conservative estimate of bringing a single drug to market can be in excess of $2.5 billion. For antibitoics, the average cost of Phase III development alone can range from $30-50 million for acute bacterial skin structure infections, and $100-150 million for hospital-acquired and ventilator-associated bacterial pneumonia.[27] Furthermore, infectious disease trials involve a long turnaround time and low percentage yield of bacterial culture, thus studying a specific resistance phenotype/pathogen requires large patient populations, thereby further prolonging and increasing the cost of development.[28] Upon market entry, antibiotics capture a staggeringly low share of market value, accounting for only $1.87 billion of the total hospital expenditure ($419.4 billion) in the USA. Consequently, no single antibiotic drug features in the top 15 drug expenditure.[29]

The stagnation of the antibiotic pipeline is driving an urgent incentive for the establishment of global initiatives, aimed at reviving the research and development of antibiotics. Organisations such as the US Centres for Disease Control and Prevention (CDC),[1] the European Centre for Disease Prevention and Control (ECDC),[30] and the World Health Organisation (WHO)[31] are considering infections caused by multi-drug resistant bacteria as an emergent global disease and major public health issue. Such initiatives outline that effectively combatting AMR requires a multifaceted approach that facilitates sustainable and equitable use of antimicrobials, thwarts the spread of infectious disease, preserves existing antimicrobial therapies and fosters innovation of novel therapies and diagnostic tools. In the UK, research councils are responsible for several key antibiotic research and development initiatives including the Cross Research Council Initiative, the Global Challenge Fund and and the Newton Fund. AMR has been named as one of the key priorities for the NIHR, to direct funding and coordinate translational research programmes to benefit the NHS. NIHR biomedical research centres, which normally marry universities and Public Health England, have allocated approximately £8 million (2014-2019) to AMR research, and set out an AMR-themed call in 2014 allocating approximately £20 million to 18 focused projects.[32]

In 2017, the WHO published a list of antibiotic-resistant 'priority pathogens'- a catalogue of 12 bacterial families that pose the greatest threat to human health. The list was drawn up in a bid to guide and promote research and development of novel antibiotics, highlighting in particular the threat of Gram-negative species (displaying high-level resistance with potential for horizontal transfer of resistance gene cassettes). Pathogens were stratified into three priority tiers: critical, high and medium. Those classified as critical were deemed to pose a significant

threat in hospitals, nursing homes and among patients undergoing treatment using implantable medical devices, and include carbapenem-resistant *Acinetobacter baumannii* and *P. aeruginosa*, and carbapenem and 3rd generation cephalosporin-resistant Enterobacteriaceae (including *Klebsiella pneumonia*, *E. coli*, *Enterobacter* spp., *Serratia* spp., *Providencia* spp., *Morganella* spp., and *Proteus* spp.).[33] Until recently, the polypeptide colistin has been used as a last-line antibiotic for the treatment of multi-drig resistant Gram-negative bacterial infection (particularly in the event of carbapenem resistance). However, the emergence of the transferable, plasmid-mediated resistance gene mcr-1, which causes resistance to colistin, is now being reported from several countries including China, the UK, USA, Denmark and Germany, where it has been detected in the intestinal flora of farm animals, and more recently, in humans (including residents of long-term care facilities).[34]

4.2.2. Alternatives to Antibiotics

The global community is now in recognition of the seriousness and growing threat of AMR. The current set of R&D incentive programmes are laudable and contribute to making antibiotic development an economically viable business model once again. However, recent efforts are also aimed at the development of novel, alternative treatment options to be used as single or ancillary therapies, in order to broaden the arsenal of antimicrobial agents available to human medicine. Addressing the antibiotic resistance crisis requires a multidimensional approach, including improved stewardship of existing antibiotics, alongside the development of novel compounds and preventative strategies such as vaccines and immunotherapeutic measures.[35]

4.2.2.1. Drug-Based Strategies

Recent drug-based advances focused on the 'antivirulence paradigm' endeavour to disarm pathogenic bacteria by neutralising their virulence factors. Such strategies offer the potential to reduce, eliminate or even reverse the selective pressures that are characteristic of traditional antibiotics, whilst leaving commensal bacteria unaffected. Perhaps the most important advantage of antivirulence strategies is the large number of putative virulent targets which, whilst overlooked in traditional phenotypic assays conventionally used to discover antibiotics, may provide a library of novel targets for exisiting chemical archives. Furthermore, secreted or surface-exposed virulence factors are amenable targets for cell-impenetrable biologics such as natural and engineered antibodies.[36] However, the use of antivirulence drugs as alternatives to antibiotics may require combination therapy to account for multiple, redundant or strain-variable virulence factors. Furthermore, as such drugs are currently in

preclinical stages, many alleged advantages of antivirulence strategies have yet to verified clinically. Indeed, many potential virulence targets, which may have proved dispensible *in vitro*, may contribute to bacterial survival *in vivo*. Moreover, predicting the propensity of bacteria to develop resistance poses additional challenges owing to complex bacterial transmission and colonisation dynamics.[35]

Nevertheless, strategies such as quorum sensing inhibitors (QSIs) have proved promising in initial testing.[37] Recent investigation by Younis *et al*.[38] has assessed the QSI ability of secondary metabolites of the halophiles marine streptomyces to inhibit biofilm formation of uropathogenic *P. mirabilis* isolates. Sub–inhibitory concentrations of crude extracts displayed good biofilm inhibition on urinary catheter surfaces, and were also found to attenuate quorum sensing-dependent factors such as haemolysin activity, urease activity, and motility. However, the question of whether QSIs impact selective pressures favouring drug resistance remains controversial.[39] QSI-resistant mutants have been derived *in vitro* and identified in clinical isolates, although these may be selected for by nonspecific, antibiotic-like effects that incidentally confer resistance to QSIs.[40]

Antimicrobial peptides (AMPs) have proved a promising alternative treatment to conventional antibiotics in recent years. AMPs are chains of 5-50 amino acids displaying amphiphatic or cationic structures, and can be considered 'natural antibiotics', generally displaying a broad-spectrum of action against Gram-positive and –negative bacterial species, fungi, viruses and protozoa. Whilst mutants of *P. mirabilis* have been identified with increased sensitivity to AMPs,[41] the 54 kDa metalloprotease ZapA, expressed by *P. mirabilis* has been found to degrade a large spectrum of AMPs, as well as many proteins found within the urinary tract. Indeed, ZapA was the first reported bacterial protease capable of cleaving human β-defensin (a component of the human renal tubule innate immune response).[42]

Other strategies involve the disarming of known resistance mechanisms, such as cellular antibiotic expulsion, via the repurposing of drugs already used in human medicine such as efflux pump inhibitors (EPIs). Such drugs have been shown to be capable of restoring antibiotic potency in both Gram-positive and –negative species,[43] including uropathogenic *E. coli* strains.[44] The existing EPI drugs fluoxetine and thioridazine have recently been found to inhibit efflux in *P. mirabilis*, and control crystalline biofilm formation, swimming and swarming motilities via strong interaction with the *Bcr/CflA* efflux system. Both EPIs were able to increase time to catheter blockage within an *in vitro* model of the catheterised urinary tract, thus proving that licensed drugs exhibiting EPI activity provide a promising strategy for controlling biofilm formation and subsequent urinary catheter blockage.[45]

4.2.2.2. Biological Strategies

Nature provides an infinitely complex and inexhaustible source of bioactive molecules, which may be used to a competitive advantage in the AMR arms race. One such solution is to use natural predatory bacteria, which constitute an unconventional yet promising alternative to chemical antibiotics. Of the abundant predatory species found in nature, *Bdellovibrio* spp. and *Micavibrio* spp. are among the better studied for potential treatment of Gram-negative infection. *Bdellovibrio bacteriovorus* (*B. bacteriovorus)* is the Gram-negative Deltaproteobacterium that expresses a single polar flagellum, rendering it one of the fastest moving organisms in nature.[46] Upon encountering a prospective prey cell, *B. bacteriovorus is* believed to use a type IV pilus to attach itself to the outer membrane, where it modifies the prey's peptidoglycan membrane in order to create a two-cell complex known as a bdelloplast. Hydrolytic enzymes are expressed to break down the host cell molecules, which allow the complex to grow filmanetously. Once the nutrient source is exhausted, *B. bacteriovorus* undergoes separation, lysis of the bdelloplast and subsequent release of bacterial progeny. The process is both quick and efficient, as it takes just 2-3 hours for a prey cell to be completely digested.[47] Multiple studies have demonstrated the ability of predatory bacteria to prey on a broad range of Gram-negative species *in vitro*, including key human pathogens such as *Acinetobacter, Enterobacter, Escherichia, Klebsiella,* and *Pseudomonas* spp.[48,49]

Within bacteria and archaea, the prokaryotic immune system able to confer resistance to foreign genetic elements consists of clustered regularly interspaced short palindromic repeats (CRISPR), paired with Cas9, an RNA-guided endonuclease that uses CRISPR DNA sequences in order to edit specific genes within invasive organisms via double-strand DNA breaks.[50] One key feature of CRISPR-Cas is its highly sequence-specific targeting capability, allowing it to easily distinguish between pathogenic or commensal bacterial species. Thus, the CRISPR-Cas machinery may be repurposed to attack, rather than defend, invasive pathogenic species. Induction of double-strand DNA breaks generally results in bacterial fatality if chromosomally targeted, thereby resulting in the potential to selectively remove individual species within a complex bacterial population.[51]

4.2.3. Bacteriophage

Bacteriophage (phage) are the predatory viruses of bacteria, known to be most abundant organisms in nature. There are an estimated 10^{31} phage particles on the planet,[52] which translates to approximately one trillion phage for every grain of sand. The prokaryotic virosphere is remarkably diverse, resulting a wide range of virion size, shape and complexity.

Furthermore, phage genomes are highly mosaic and represent the largest reservoir of unexplored genes anywhere in the biosphere.[53] Given their ubiquity and diversity, is is unsurprising that phage play a pivotal role in a variety of biological and environmental processes . It is estimated that between 15-40% of the ocean's bacterial flora is lysed by phage every day, thereby influencing the ratio of particulate to dissolved carbon, rates of phytoplankton productivity and oxygen output. Moreover, phage are significant drivers of bacterial evolution, both owing to the avoidance of killing via lysis, and the prominence of horizontal gene transfer by lysogenic phage. Globally it is believed that phage-mediated gene transfer events occur up to 20 million billion times per second. [54]

In 1896, Ernest Hanbury Hankin, a British bacteriologist to the government of the Central Provinces of India, demonstrated that waters from the Ganga and Yamuna rivers contained a biological principle that destroyed cultures of cholera-inducing bacteria. Published in French in the *Annals of the Pasteur Institute*,[55] he detailed that the substance could pass through Millipore filters known to be able to retain larger organisms such as bacteria. Following this observation, phage were then independently discovered by Frederick Twort (1915)[56] and Felix d'Hérelle (1917)[57]. D'Hérelle in particular used phage suspensions to treat infections such as dysentery, which at the time had no other consistently effective treatment. The success of this treatment led to a period of widespread enthusiasm for phage therapy in humans, although this became rapidly eclipsed in western medicine upon the advent of antibiotics. Nevertheless, the use of phage to treat human disease has persisted in various regions of the world, including the former countries of the Soviet Union (most notably in Georgia, where phage are often used as the standard of care for bacterial infection).[58]

4.2.3.1. Bacteriophage Classification

Virus taxonomy is currently the responsibility of the International Committee on the Taxonomy of Viruses, whose classification scheme emcompasses 1 order, 13 families and 34 genera of phage. The families are distinguished by categorising the type of nucleic acid and virion morphology.[59] A full description of bacteriophage classification and characterisation is described elsewhere.[60] As well of being of greatest relevance to this thesis, tailed bacteriophage of the *Caudovirales* order are the most numerous and widely distributed group of bacterial viruses. The *Caudovirales* order consists of 3 distinct families: *Myoviridae, Siphoviridae* and *Podoviridae*, based on tail morphology (Figure 4.3). Virions of order *Caudovirales* contain

double stranded, linear DNA but vary in the contractile nature of the tail and adhesion structures.[61]

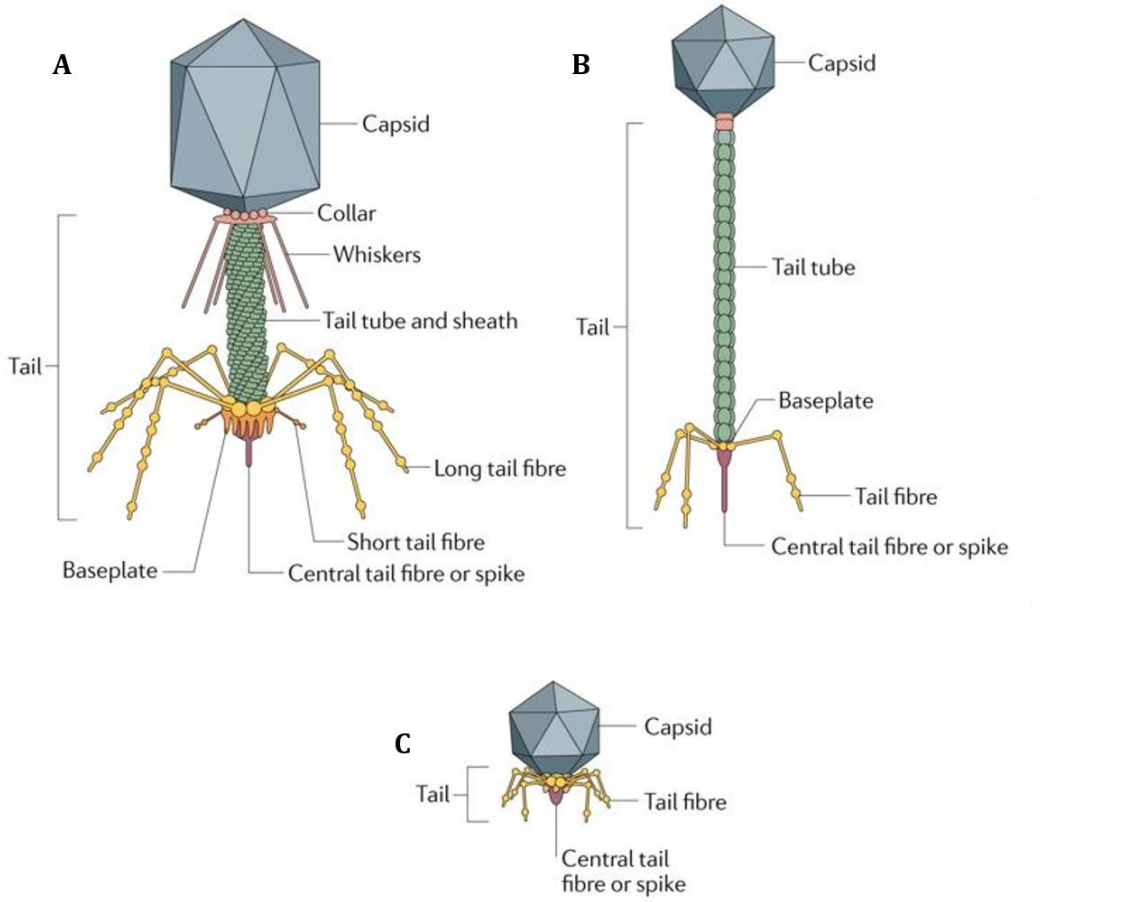

Figure 4.3: Representative structures of tailed phage of the order *Caudovirales*, classified as *Myoviridae* (A), *Siphoviridae* (B), or *Podoviridae* (C) based on tail morphology. *Myoviridae* tails consist of a neck, contractile sheath and a central tube. Myoviruses tend to be larger than other families and include some of the most highly-evolved tailed phage species. *Siphoviridae* tailes are simple, noncontractile tubular structures. Siphoviruses are the most numerous of all the tailed phage. *Podoviridae* tails are short and noncontractile. Phage belonging to both *Myoviridae* and *Siphoviridae* families have a baseplate at the distal end of the tail to which receptor binding proteins (RBPs) are attached. Since members of the *Podoviridae* family have no baseplate, RBPs attach directly to the tail. *Myoviridae* and *Siphoviridae* families additionally have a central tail fibre that protrudes from the distal end of the tail or baseplate. Adapted with permission from Nobrega *et al*.[61] © Springer Nature 2018.

4.2.3.2. Bacteriophage Life Cycles

Since phage lack the machinery required to express their own genes, and replicate their own genomes, they are therefore reliant upon host bacterial cells to fulfil their biological requirements. Much like other, eukaryotic viruses, phage have two distinct life cycles: the lytic cycle (a productive process leading to the synthesis of new phage particles), and the lysogenic cycle (a 'silent' stage whereby the phage genome is integrated with the host chromosome). Following contact with a bacterial cell encoding a receptor complimentary to the phage anti-receptor, the phage may inject its DNA via penetration of the cell membrane, before entering either the biosynthetic or quiescent pathways,[62] as detailed in Figure 4.4.

In conditions where susceptible hosts are abundant and actively growing, populations of lytic phage dominate. Upon injection of virulent phage DNA into the cell, major physiological changes are induced within the host cell. A cascade of finely-tuned sequential events take place, driven towards the production of phage progeny. The majority of host cellular process are interrupted, with the exception of those required for biosynthesis. Phage-encoded genes are orderly transcribed and translated into the regulatory and structural proteins. Thereafter, the structural consitituents are irreversibly assembled into precursor polymers and gradually processed into mature virions. The host cell wall is then disrupted by the dual action, phage-encoded holin and endolysin system, thereby releasing phage progeny capable of subsequent infective cycles.[63,64]

In contrast, lysogenic phage are capable of maintaining a stable relationship with the host. Upon infection and DNA translocation into the host cytoplasm, the phage genome becomes incorporated with the host chromosome. The genetic code of the integrated phage (also referred to as 'prophage') is replicated in tandem with the bacterial chromosome, and transmitted to daughter cells with every binary cell division. Prophages of this quiescent nature are highly stable and may be maintained indefinitely. However, stress-induced physiological changes of the host (such as starvation, heat-shock, and UV-induced DNA damage) may induce the triggering of the lytic cycle via regulatory proteins that modulate the expression of specific genes required to establish lysogenic or lytic cycles.[64]

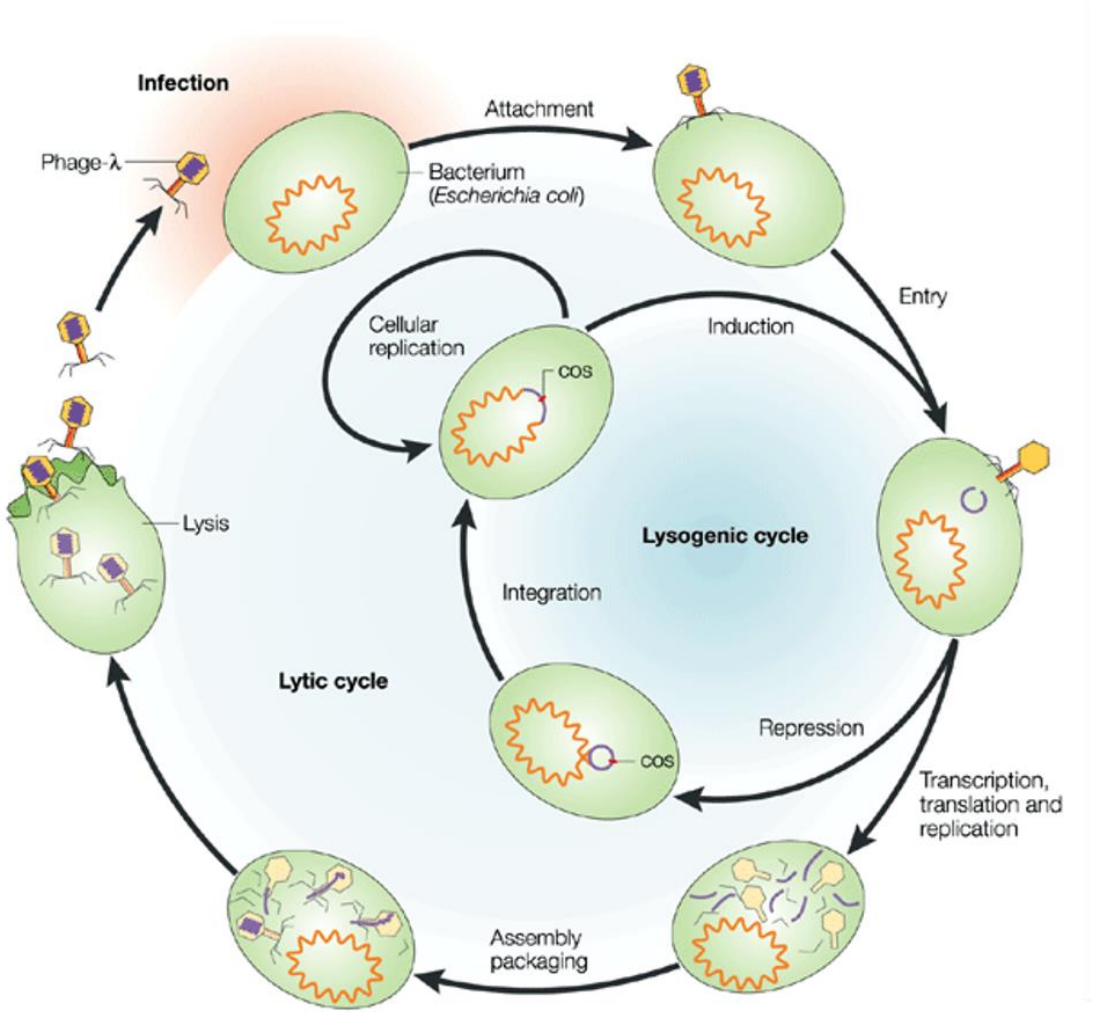

Figure 4.4: Viral replication cycles of bacteriophage. Following the insertion of the phage genetic material into the host bacterial cell, one of two life cycles may be followed: lytic (virulent) or lysogenic (temperate). Lytic replication involves hijacking the host's biosynthetic machinery to make new phage components. Lysis of the cell releases phage progeny which may then go on to perform further infection. Lysogenic phage incorporate their nucleic acid into the chromosome of the host cell and replicate quiescently without causing host destruction. In such cases, the closure of the newly-formed circular DNA and corresponding cohesive site is denoted 'cos'. Reprinted with permission Campbell *et al.*[62] © Springer Nature 2003.

Transduction is a mechanism of great importance in the selection of phage for therapeutic purposes. Transducing phage may insert a segment of the bacterial genome into a newly formed viral particle which may then be transferred to other bacterial hosts. Two mechanisms of transduction have been described, namely generalised and specialised transduction. During generalised transduction, random sections of the bacterial genomes may be packaged into viral

particles owing to chromosomal and plasmid DNA degradation during infection. Upon subsequent infection, bacterial genes are injected into a new bacterium and may recombine (by homologous recombination) with the host's genome. In this process, any single or cluster of bacterial genes may be transferred among genetically similar bacteria at equal frequency. Specialised transduction is a process restricted to lysogenic phage. Excision of the prophage DNA may be imprecise, resulting in the bacterial region neighbouring the insertion site to be packaged into viral particles and transferred between bacteria.[65] Even under optimal laboratory conditions, transduction is a relatively rare event (occurring once every approximately 10^8 phage particles).[54] However, considering the abundant nature of phage, transduction can be considered a major mechanism of lateral gene transfer within bacterial populations.

From a biosafety point of view, the introduction and transfer of new genetic material into the bacterial gene pool may have significant negative impacts on the therapeutic potential of phage.[65] Notoriously, the lysogenic conversion of non-toxigenic bacterial strains into deadly toxigenic pathogens via the expression of phage-encoded toxins is known to have occurred previously, for example Shiga toxins in *E. coli* O157:H7,[66] and the botulinum toxin in *Clostridium botulinum*.[67]

In light of the potential of transduction to improve the fitness and survival of bacteria, it is therefore essential that lysogenic, transducing phage are eliminated from any potential therapeutic formulations. Whilst the mechanism of transduction is known to occur in both lytic and lysogenic cycles, extensive degradation of the host genome during virulent infection renders this process largely inconsequential in lytic preparations.[68]

4.2.3.3. Bacteriophage Therapy

Advantages of phage therapy over the use of chemical antibiotics can be framed in terms of phage properties. Factors that contribute substantially to the utility of phage therapy in humans include:[69]

- '**Auto' dosing and single dose potential.** The pharmacokinetic profile of phage is such that the initial dose increases exponentially as the virus multiplies within the bacterial host. *In vivo* amplification of the phage population may potentially reduce costs associated with repeated treatments;
- **Minimal disruption of host flora**. Owing to narrow host specificity, phage typically recognise single or limited ranges of host bacterial strains. This reduces damage to the

commensal microbial community of the human host, unlike many chemical antibiotics, whose broad activity spectrums often induce superinfections (such as antibiotic-associated *Clostridium difficile* colitis, or *Candida albicans* yeast infections;

- **Narrower propensity for induction of host resistance**, as well as the absence of cross-resistance to antibiotics (making phage an effective 'last resort' solution for multidrug-resistant infection). The narrow host range of phage limits the number of related bacterial species which may select for specific resistance, whilst mutations to evade phage adhesion or infection may negatively impact bacterial fitness and cell function;
- **Low environmental impact.** Phage are inherently biocompatible, since they are predominantly composed of nucleic acids and proteins. Owing to their narrow host range, discarded phage are unable to significantly impact the natural microbiome. Phage not adapted to degradative conditions such as UV or temperature extremes will be rapidly inactivated;
- **Rapid discovery.** Whilst large-scale production of phage is more technically demanding than conventional antibiotics, they are easily discovered and isolated from sewage and other highly bacterial-dense waste materials. Accumulation of specific resistance to existing phage is offset by the tandem evolution of such virions with bacteria in nature;
- **Formulation and application versatility.** Phage are versatile in terms of formulation development, and may be combined with chemical antibiotics to achieve synergistic or additive effects on bacterial killing. Application design may include liquids, hydrogels, creams and solids. Groups of phage strains may be combined into 'cocktails', typically broadening the antibacterial spectrum of activity in situations where multispecies infections are prevalent.

One of the current challenges of progressing phage therapy into the clinic is the lack of validated and adequately controlled clinical trials. Whilst clinical trial design for phage therapy will inevitably share many parallels with standard drug trials, there are several factors that are unique to phage therapy (including pharmacological considerations such as dosage).[70] Nevertheless, recent developments in clinical trials for phage therapy have proved promising, and in agreement with observational human studies. The British company Biocontrol (now Ampliphi; VA, USA) has performed what is to date the only Phase II clinical trial with a phage product (clinical trial indentifier: NCT03395769). Following promising results in dogs,[71] a human trial for otitis was performed under the auspices of the Medicines and Healthcare Products Regulatory Agency in the UK. 24 patients with

chronic otitis, who had not responded to antibiotic therapy were recruited for a randomised, double-blind trial consisting of a single dose of 6 x10^5 virions. Differences in test and control groups (including complete resolution in 3 patients) were such that the trial was ended early so that the control group may receive treatment.[72] Phagoburn, a Phase I/II clinical trial (clinical trial indentifier: NCT02116010) launched in July 2015 aimed to assess the efficacy of phage cocktail treatment on wound infections due to *E. coli* or *P. aeruginosa* in burn patients. This trial has paved the trail for the re-implementation of phage therapy into the human therapeutic arsenal, including the first Good Manufacturing Practice (GMP)-like production of phage drug products, and thorough assessment of shelf-life and side effects.[73]

4.2.3.4. Bacteriophage Therapy: Regulatory Hurdles

Whilst phage therapy formulations have become embedded into the healthcare systems in Georgia, in other parts of the world, medical applications of phage present a unique regulatory agenda. Questions regarding the biological status of phage include determining whether or not they are regarded as living, which highlights the need for defined phage-specific terms of policy within regulatory structures. As it currently stands, phage therapy may in many cases represent the epitome of 'personalised medicine', as the process of treatment involves formulating tailor-made phage combinations specific for an individual infection. This presents difficulties in the regulatory pipeline, although such deviations from regulatory convention have already been achieved in areas such as cancer therapy.[74] The FDA has recently provided an opportunity for the new Center for Innovatve Phage Applications and Therapeutics (IPATH) to utilise pahge therapy via the Emergency Investigational Drug scheme. Such initiatives are lilely to improve clinical understanding and acceptance, as well as supporting evidence for the creation of dedicated regulatory guidelines.[75]

4.2.3.5. Bacteriophage Therapy for CAUTI

Recently, a number of studies have investigated the use of lytic bacteriophage in the treatment and prevention of biolfilms of bacterial species commonly associated with infections of indwelling urological devices and CAUTI.[76] Carson *et al*.[77] revealed that lytic phage provide effective prevention of biofilm growth of uropathogenic *P. mirabilis* and *E. coli* on urinary catheter surfaces. Visual examination via confocal imaging of catheter sections treated with phage showed a marked reduction in biofilm formation on the surface of Bard Lubri-Sil™ Foley catheters after 24 hours, compared with untreated controls (Figure 4.5). Furthermore, the

same study showed the potential of phage not only in the prophylactic prevention of biofilm formation (via pretreatment of the catheter surface), but also in the destruction/eradication of established biofilms. Established biofilm populations of *P. mirabilis* and *E. coli* were reduced by 3-4 log cycles (99.9-99.99% removal) upon treatment with lytic bacteriophage.

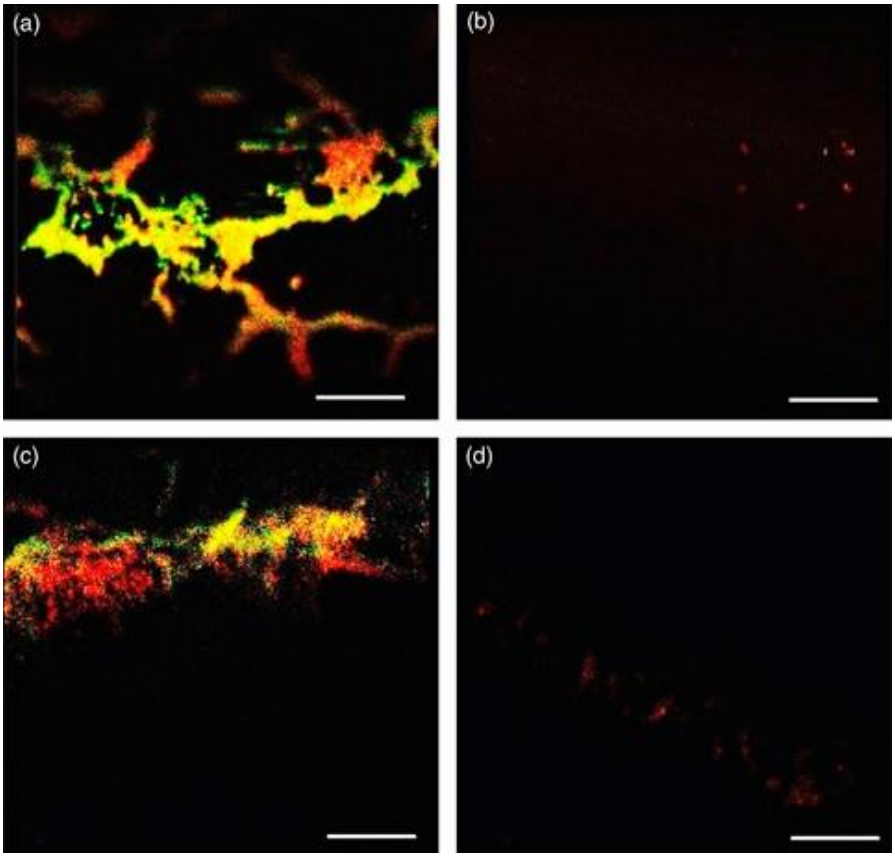

Figure 4.5: Confocal scanning laser microscopy images of biofilms on the surface of Bard Lubri-Sil™ Foley catheters, stained with Live/Dead BacLight™. Left-hand images depict biofilm growth of uropathogenic clinical isolates on the surface of untreated catheters. Right-hand images shows a marked reduction in biofilm biomass on the surface of bacteriophage-treated catheter surfaces. *E. coli* (A, B) and *P. miraiblis* (C, D) Scale bars = 30 μm. Reprinted with permission Carson *et al*.[76] © Oxford University Press 2010.

Bacteriophage cocktails for treatment and prevention of CAUTI have been recently investigated by Nzakizwanayo *et al*.[78] Models representing either an established infection or early colonisation of the catheterised urinary tract were treated with a single dose of a 3-phage cocktail. The impact on time to blockage and the formation of crystalline material was monitored. Established infection models (10^{10} CFU/mL initial inoculum) showed an approximately 3-fold increase in time to blockage, compared to untreated controls. Under conditions of early-stage infection (10^{3} CFU/mL initial inoculum), however, phage treatment

eradicated blockage entirely. Models drained freely for >8 days, until medium reserves were exhausted.

Evaluation of commercially available phage formulations registered in Georgia or from the bacteriophage collection of the George Eliava Institute of Bacteriophage, Microbiology and Virology have been investigated as potential treatment options for uropathogenic strains of *E. coli* and *Klebsiella pneumoniae* (*K. pneumoniae*). The lytic activity of commercial cocktails on 41 strains of *E. coli* varied between 66-93%. Furthermore, one phage of the Eliava collection was found to lyse all 9 tested *K. pneumoniae* strains.[79] Such studies utilising commercially-availabe phage cocktails prove the potential of standard formulations to impact common illnesses. Moreover, they support the notion that phage should not be treated as chemical drugs in the face of regulatory legistalation, but rather like the components of the influenza vaccine, which is re-evaluated yearly without separate clinical trial data.[80]

Numerical simulations of phage-bacterium population dynamics undertaken by Malik *et al*.[81] have highlighted the need for phage encapsulation to ensure that the phage titre remains stable and viable during storage . Thus, recent investigations into the encapsulation of phage into a hydrogel catheter coating have proven an important step towards the viral treatment of CAUTI *in situ*. A recent patent focuses on the controlled covalent attachment of bioactive phage to a hydrogel coating material for regulation of biofilm development with examples focusing on biofilm reduction on urinary catheters.[82] Bacteriophage have been shown to remain stable and viable in a variety of hydrogel formulations,[83] and, of particular relevance to this thesis, have been successfully released in response to a biochemical or physical stimulus as a direct consequence of infection (e.g. temperature[84] or secreted bacterial enzymes[85]).

4.3. Materials and Methods

4.3.1. Materials

Materials for the formulation of pH-responsive catheter coatings were purchased according to Chapter 2. Vegetable peptone no. 1 and tris-hydrochloride (pH 7.5) were purchased from Sigma-Aldrich (Poole, Dorset, UK).

4.3.2. Methods

4.3.2.1. Microbiological Methods

General bacterial culture and quantification protocols were followed according to Chapter 2.

I. *P. mirabilis* Biofilm Formation

For quantitative analysis, *P. mirabilis* B4 subculture (1:1000 in LB, 1 mL) was added to each well of a 12-well microplate, achieving a starting inoculum of 10^3 CFU/mL. Microplates were incubated statically for 24 hours (37 °C) to promote cell attachment.

For imaging, polycarbonate membranes (GVS Poretics) were positioned on NSLB agar plates, and UV-sterilised (10 minutes treatment time). Bacterial growth fluid (fetal calf serum mixed 1:1 with NaCl (0.85% w/v) and peptone (0.1% w/v) was aliquoted onto the surface of the membranes (20 µL). Membranes were inoculated with 1:1000 bacterial subculture (30 µL), and incubated statically for 24 hours (37 °C) to form confluent biofilms.

II. Crystal Violet Biofilm Staining

After incubation, biofilms were washed x3 with deionised water to remove planktonic cells. Adhered cells were stained with crystal violet solution (0.1% w/v, 500 µL),and incubated statically for 15 minutes (room temperature). The stain was removed via 3 exhaustive washes with deionised water, and dried at room temperature (30 minutes). To quantify adhered cells, decolourising solution (33% v/v acetic acid, 500 µL) was added to each well, and the absorbance measured at 595 nm to indicate the presence of a mature biofilm.

III. SEM Imaging of *P. mirabilis* Biofilms

The hexamethyldisilazane (HMDS) drying treatment[86] was used on membrane-bound biofilms of *P. mirabilis* as an alternative to conventional critical-point drying, to prevent sample distortion and achieve preservation of surface details. Biofilms were cross-sectioned using a razor blade prior to fixation. Film fixation was performed using glutaraldehyde (1.5%), and paraformaldehyde (3%) in phosphate buffer (pH 7.3) for 12 hours at 4 °C. Samples were dehydrated in an ethanol/water mixture at concentrations of 50%, 70%, 80%, 90%, 95% and 100% for 10 minutes each. Dehydrated samples were then submerged completely in HMDS for 2 x 30 seconds, then air-dried (10 minutes). Samples were sputter-coated with gold (Edwards S150B) and images obtained using a JEOL SEM6480LV SEM operating at 10 kV for electron imaging.

4.3.2.2. Bacteriophage Methods

I. SM Buffer Preparation

Aqueous SM phage suspension buffer was prepared according to Table 4.1. Compounds were dissolved in deionised water (200 mL) and sterilised via autoclaving prior to use.

Table 4.1: Components of SM phage suspension buffer

Compound	Mass (g)	Concentration (mM)
Sodium chloride	1.17	100
Magnesium chloride hexahydrate	0.42	8.5
Tris-hydrochloride (pH 7.5)	1.58	50

The solution was supplemented with gelatine (0.01% w/v, 20 mg) to aid the stability of phage during storage.

II. Bacteriophage Isolation and Single Plaque Purification

P. mirabilis phage were isolated from crude sewage. Bacterial enrichments with clinical isolates were performed to enhance phage populations. Actively growing cells from overnight liquid culture (5 mL) were added to LB liquid media supplemented with $MgSO_4$ (1 mM) and $CaCl_2$ (1 mM), and incubated overnight (37 °C, 200 rpm) with crude sewage solution (150 mL). An aliquot (10 mL) was removed from the enrichment post-incubation, to which was added NaCl

(1 mM) and chloroform (1% v/v). The culture was centrifuged (30 minutes, 30,000 x g) and the supernatant filter sterilised (0.45 μm pore size). The presence of lytic phage was confirmed using the double agar overlay metod (see below). From each plate, isolated single plaques were picked using a sterile pipette tip. If present, different plaque phenotypes were picked and resuspended in SM buffer (300 μL). Serial dilutions (SM buffer, 10^{-3}-10^{-7}) and plating were undertaken to allow purification and isolation of a single phage. To ensure clonality of phage types, single plaque purification was repeated a further 5 times until homogenous plaque purification was observed. Finally, an individual plaque was picked and resuspended in SM buffer for use in subsequent methods. Purified phage were stored in glycerol (50% v/v) in LB at -80 °C for long-term use. Short-term stock preparations were maintained at 4 °C in SM buffer.

III. Bacteriophage Propagation and Extraction

Non-swarming LB-derivative soft top agar (LBDTA) was prepared according to Table 4.2.

Table 4.2: Composition of LBDTA agar

Compound	Mass (g)
Yeast extract	5.00
Vegetable peptone	10.00
Bacteriological agar	5.75

Components were dissolved in deionised water (1 L), sterilised by autoclaving and stored at 50 °C. Plates displaying confluent lysis were obtained by performing a double agar overlay using LBDTA, to facilitate diffusion of phage through solid media. (Figure 4.6).

Phage lysate solution (100 μL), and host bacterial culture (100 μL) were added to molten LBDTA (3 mL). The resultant agar solution was poured onto an NSLB agar plate, and set at room temperature for 10 minutes. Plates were incubated overnight (37 °C) to result in confluent lysis.

To extract phage ,the flood infected plates method was employed. SM buffer (3 mL), containing chloroform (2% v/v) was added to individual plates, which were incubated at room temperature for 4 hours with gentle rocking (30 rpm, Suart gyratory rocker SSM4). High titre phage lysate was removed from the plates, centrifuged to remove bacterial cell debris (4,000

rpm, 10 minutes), and filter sterilised (0.22 µm pore size). Lysate was stored at 4 °C until required.

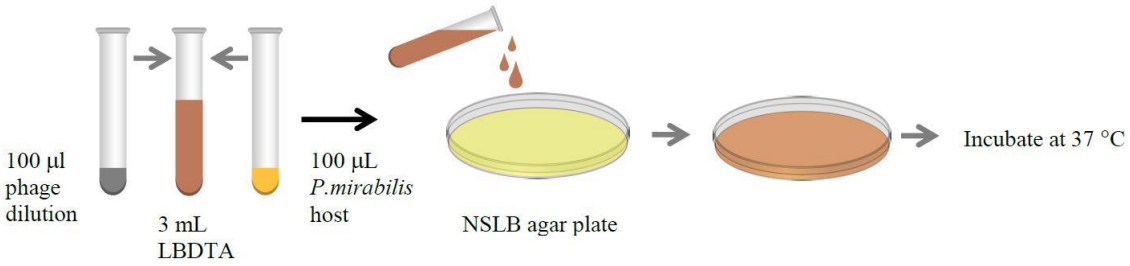

Figure 4.6: Schematic representation of the double agar overlay, to achieve confluent bacterial lysis.

IV. Bacteriophage Enumeration

To determine phage titre, the double agar overlay method (outlined above) was employed, following serial dilution of viruses (10-fold dilutions in SM buffer). Zones of inhibited growth (plaques) were counted, and the phage titre calculated according to Equation 1. Plates displaying 30-300 plaques were used to quantify plaque-forming units per unit mililitre (PFU/ mL).

$$\text{PFU/ mL} = \frac{\text{Average number of plaques}}{\text{d} \times \text{V}} \quad (1)$$

Where d is the dilution factor (from original culture), and V is the volume of inoculum (mL).

V. Bacteriophage Imaging

Bacteriophage morphology was assessed using transmission electron microscopy (TEM). Carbon-coated glow discharge grids were firstly exposed to ozone (5 minutes) to increase surface hydrophilicity. Each grid was then soaked in high-titre phage lysate, rinsed with deionised water and soaked in uranyl acetate stain (1%). Grids were dried for 4 hours (room temperature), and images acquired using a JEOL JEM1200EXII with Gatan Dualvision camera.

VI. Bacteriophage Minimum Inhibitory Concentration

Mininmum inhibitory concentration (MIC) of lytic pahge were determined using the microbroth dilution method. *P. mirabilis* B4 (~10^8 CFU/ mL) was distributed in a 96-well microplate (100 µL, LB). Phage preparations were diluted to represent a range of concentrations (10^{10} PFU/mL – 10^2 PFU/mL), and added to wells containing bacterial cells (100 µL). Corresponding cell controls, phage controls and media controls were performed.

Microtiter plates were incubated overnight (37 °C) in a microplate reader. Optical density (600 nm) was continuously monitored. The lowest concentration of phage at which no turbidity was observed was defined as the MIC.

VII. Bacteriophage Eradication of Established Biofilms

Biofilms were grown in 12-well microplates as above, and washed 3x with deionised water to remove unbound cells. Phage lysate (in LB media) at 10^{10} and 10^{8} PFU/mL (1 mL) were added to each well in triplicate after 24 hours initial biofilm growth. Plates were incubated statically (37 °C), and removed at 0, 6, 24 and 48 hour time points for crystal violet staining (according to Section 4.2.2.1.II). The absorbance of the decolourising solution was measured at 595 nm to quantify biofilm destruction by *P. mirabilis* phage.

VIII. Catheter Bridge Swarming Assays

The swarming of *P. mirabilis* bacteria over sections of all-silicone Foley catheter was assessed. The protocol was adapted from Sabbuba *et al*.[87] in order to evaluate the efficacy of phage in hindering the *P. mirabilis* swarming motiliy. Catheter segments (1 cm length) were silanised according to Chapter 2, and coated in PVA hydrogel (100 µL, 10% w/v) containing 10^{10} PFU/mL phage lysate. The 'bridges' were placed into the cut-out channels of an LB agar plate to permit swarming. The first channel was cut down the centre of the plate (1 cm width), to accommodate the catheter section. Two further channels (0.5 cm width) were cut perpendicular to the central channel to achieve adequate separation between experimental repeats (Figure 4.7). The exposed ends of the balloon-inflation line and catheter lumen were sealed with sterile plastic to prevent internal bacterial motility.

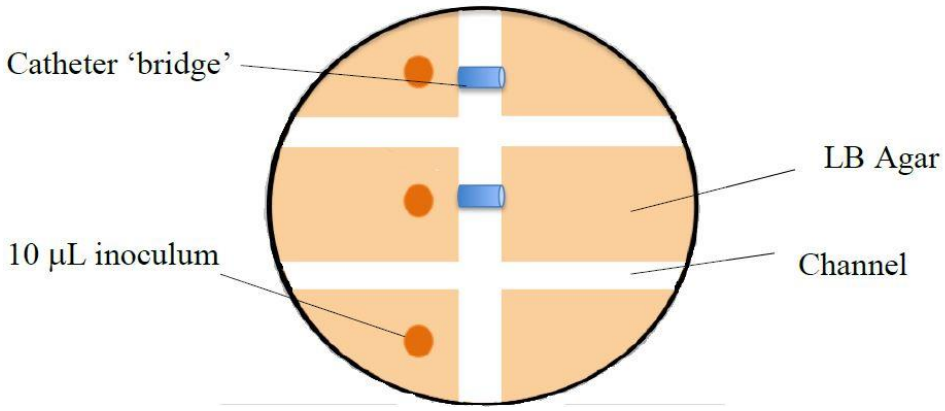

Figure 4.7: Schematic representation of the catheter 'bridge' swarming assay experimental setup.

Aliquots of 1:1000 bacterial subculture (10 μL) was used to inoculate the agar on one side of the catheter 'bridge', and the plates incubated statically for 24 hours (37 °C) before undergoing visual assessment. When growth of *P. mirabilis* appeared on the uninoculated side of the plate, adjacent to the bridge, it was concluded that the test strain had migrated across the catheter section via engagement of the swarming motility.

4.3.2.3. Materials Preparation

Solutions of PVA and Eudragit S100 were prepared according to Chapter 2.

I. Coating of Foley Catheters

To cooled PVA solution (20% w/v, 14,600-18,600 $gmol^{-1}$) was added high titre phage lysate (10^{10} PFU/mL), at a 1:1 ratio, to achieve a final PVA concentration of 10% w/v. All-silicone Foley catheters were coated with the hydrogel/phage solution (100 μL) between the retention balloon and the tip, and stored overnight at -20 °C to promote cryogenic gelation. Catheters were thawed at room temperature (2 hours), before coating with the pH-sensitive trigger layer (20 dip coats, with a 5 minute solvent evaporation period between each coating). Coated catheters were stored at 4 °C until required.

4.3.2.4. Prototype Evaluation

I. *In Vitro* Bladder Models

Evaluation of prototype coatings under physiologically relevant conditions was performed in order to assess the degree to which phage release would increase catheter lifespan. *In vitro* bladder models were assembled and run according to Chapter 2. Models simulating late-stage infection were incoluated with *P. mirabilis* B4 or *E. coli* NSM59 (10^8 CFU/mL), and supplied with artificial urine media at a constant flow rate of 0.75 mL/min. Numbers of viable bacterial cells, as well as bacteriophage concentration were enumerated at periodic intervals throughout the experiments, along with pH readings of resudial urine media. Experimental controls were undertaken in order to assess:

- Time to blockage in the absence of a bacteriophage-impregnated catheter coating;
- Bacterial health in the presence of an uncoated catheter;
- Coating stability in the presence of a urease-negative species (*E. coli*);
- Sterility of the closed-drainage system in the absence of infection.

II. Microbiological Quantification

Quantitative analysis of viable bacterial cells and phage populations were performed from culture removed directly from the *in vitro* bladder models (10 mL aliquot). For bacterial enumeration, serial dilutions of the original culture were performed (10^{-1}-10^{-8}), plated in triplicate on NSLB agar, and incubated overnight (37 °C). Colony counting was performed as previously described to estimate cell numbers. For phage, the original bladder culture was filter sterilised (0.22 μm pore size) to remove bacteria, then serial diluted (10^{-1}-10^{-8} in SM buffer) and plated in double agar overlay. Phage enumeration was performed to estimate populations of phage released from catheter coatings.

III. Atomic Absorption Spectroscopy

Biofilm biomass was quantified at the conclusion of each *in vitro* bladder model experiment via analysis of calcium concentration within the crystalline biofilms using atomic absorption spectroscopy (AAS). Catheters were removed from bladder models at the time of uncoated control blockage (13 hours after model start), and cut into sections (1 cm length). Catheter sections were soaked in nitric acid (4% v/v) for 24 hours, following sonication (44 kHz, 5 minutes), to facilitate diffusion of crystals embedded within the catheter biofilm. The resulting solution was assayed for calcium using a Perkin Elmer AAnalyst 100 spectrometer (nitrous oxide/acetylene flame, 422.7 nm), using a combined calcium and magnesium hollow cathode lamp (S&J Juniper & Co). Where necessary, samples were diluted further (4% v/v HNO_3) to ensure that the measured concentration lay within the experimental range (1-5 ppm). Linear calibration of the instrument was performed via dilution of standard Ca^{2+} solutions (BDH Prolabo), with 2000 ppm potassium (as KCl) as ionisation surpressant.

IV. SEM Imaging of Catheter Cross-Sections

Catheters were removed from bladder models at time of uncoated control blockage, and cross-sectioned both at the eyeholes, and 1 cm below the retention balloon. Cylindrical sections were mounted lengthways into a split mount vice holder, and grounded to the aluminium stage using carbon conductive tape. Mounted catheter sections were sputter coated with gold following dehydration under vacuum (12 hours). Imaging of catheter cross-sections was performed using a scanning electron microscope (JEOL JSM6480LV) operated at 10 kV. Secondary electron imaging was utilised for inspection of the sample topography.

4.4. Results and Discussion

Bacteriophage therapy offers an urgently required alternative to chemical antibiotics. However, the route to common clinical practice for phage is still frought with complication, as the current functional and practical legal framework does not offer the flexibility required to exploit and further explore the specificity of such viruses. The infection-responsive coating described in this chapter attempts to provide an effective countermeasure for the encrustation and blockage of urinary catheters.

4.4.1. Bacteriophage Morphology

Amongst the isolated phage, *P. mirabilis* B4 bacteriophage SM648 was selected as the model phage strain for this system, as it showed enhanced lytic activity against *P. mirabilis* B4. Bacterial strain B4 was deemed to be a suitable model *P. mirabilis* strain as it is widely known to display strong swarming and swimming characteristics, as well as high urease and flagella production in both motilities.[88] Phage SM648 was subjected to morphological evaluation using TEM (Figure 4.8).

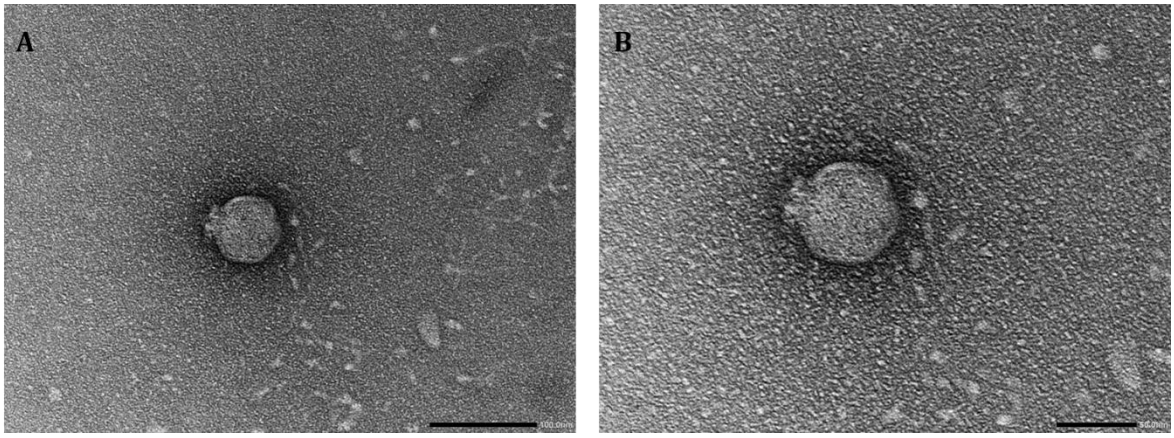

Figure 4.8: Transmission electron micrographs of *P. mirabilis* B4 bacteriophage SM648. Scale bars represent A) 100 nm, B) 50 nm.

TEM images suggest that the *P. mirabilis* phage are of the classifcation *Podoviridae*, owing to the observed capsid morphology. Observation of short, noncontractile tails with an icosahedral head group of diameter ~50 nm is in agreement with results observed previously,[76,89] including 6 of the 10 complete genomes of phage specific for *Proteus spp.* available in Gen Bank.[90]

4.4.2. Bacteriophage Minimum Inhibitory Concentration

The ability of phage to inhibit the growth of *P. mirabilis* B4 was assessed using optical density (OD) measurements, in order to determine the lowest concentration which, under strictly defined test conditions, will inhibit bacterial growth *in vitro*. Overnight growth curves of *P. mirabilis* B4, incubated with varying phage concentrations are shown in Figure 4.9.

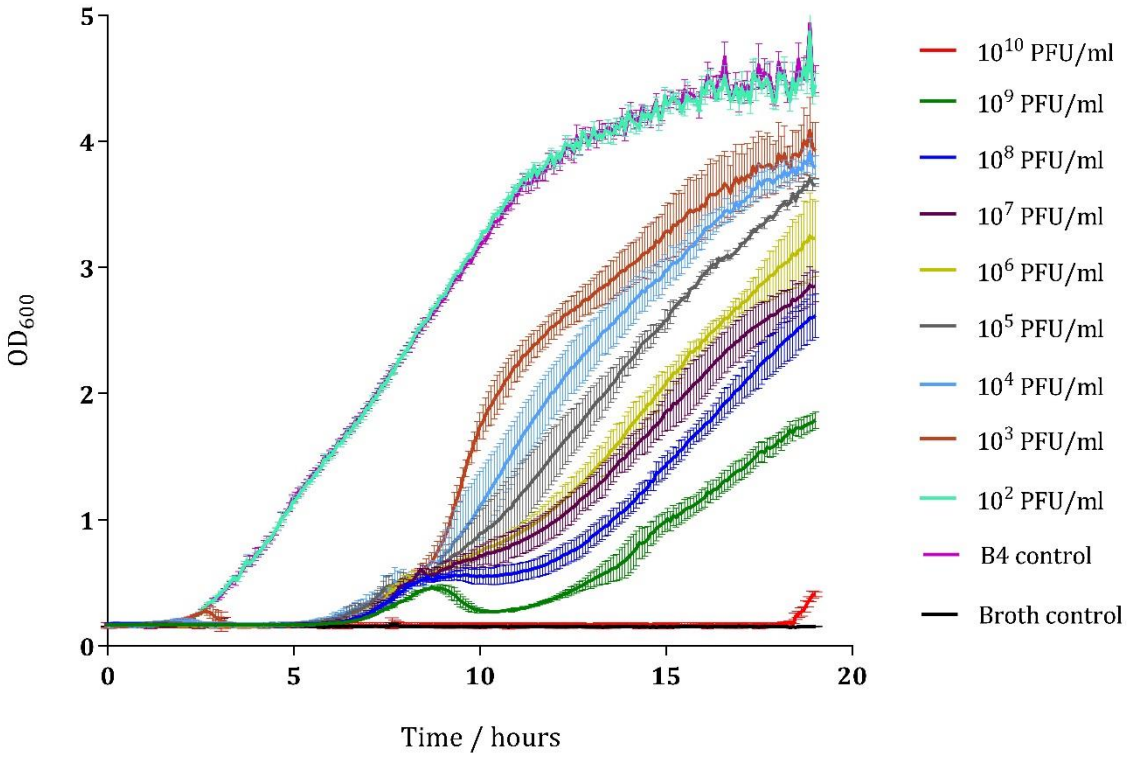

Figure 4.9: Overnight growth curves of *P. mirabilis* B4, incubated with varying concentrations of bacteriophage SM648. Each data point represents the mean of three individual repeats. Error bars represent SEM.

For therapeutic purposes, it is crucial to establish that bacterial lysis occurs in a phage dose-dependent matter. Characteristic dilution-dependent killing was observed upon incubation with phage, although a high multiplicity of infection (MOI) was required for high killing efficiency. Adequate sensivity for therapeutic purposes was only observed when bacterial cells were challenged with 10^{10} PFU/mL, which corresponds to an approximate MOI of 100. Thus, the maximum dosage of phage was also deemed to be the MIC in this case. Whilst this dose appears high in comparison to therapeutic concentrations of phage described for other Gram-negative species,[91] for *P. mirabilis*, doses in the region of 3 x10^{10} PFU/mL have been deemed necessary for the treatment of uropathogenic species *in vitro*.[78] Furthermore, the infective nature of phages still renders this concentration viable for therapeutic purposes. Slight

reinitiation in bacterial growth was observed for the highest phage concentration (10^{10} PFU/mL) after 18 hours incubation, although this was considered negligible in comparison to the untreated control.

An increase in bacterial population was observed for the lower phage dilutions after 10 hours incubation, initiating regrowth of bacteria in all phage dilutions where the MOI <100. Bacteria can resist phage infection via a number of different mechanisms, including spontaneous mutation, restriction modification systems, and adaptive immunity via the CRISPR-Cas system. Spontaneous mutations are the most commonly employed mechanisms driving both phage resistance and phage-bacteria coevolution. Such mutations may confer phage resistance by modifying the structure of the bacterial surface components that act as phage receptors (thus determining specificity). These include lipopolysaccharides, outer-membrane proteins, cell wall teichoic acids, capsules, and other bacterial appendices such as flagella, which may contribute to virulence. However, phage resistance may come at a price to the defending bacterium. In the case of mutations to surface virulence factors, evolution of phage resistance may coincide with a substantial decrease in virulence or fitness, owing to generalist adaptive mutations.[92]

To counteract phage resistance, the synergy of lytic phage with chemical antibiotics has been investigated and extensively reviewed elsewhere. Recently, a considerable synergistic effect was observed when *P. mirabilis* was treated with phage in combination with ampicillin, showing significant biofilm clearance *in vitro*.[93] In some cases, selection of phage-resistance may also restore antibiotic susceptibility.[94]

4.4.3. Clearance of Established Biofilms

The ability of *P. mirabilis* phage to eradicate a mature biofilm was investigated, in order to more accurately mimic the burst release of phage in response to established infection. Concentration of bacteriophage deemed to be effective for planktonic cultures (10^{10} PFU/mL, MOI = 100), as well as a lower dose (10^{8} PFU/mL, MOI = 1) to assess infectivity, were added to established biofilms in a simple *in vitro* model. Destruction of mature biofilms at time points following addition of phage is shown in Figure 4.10.

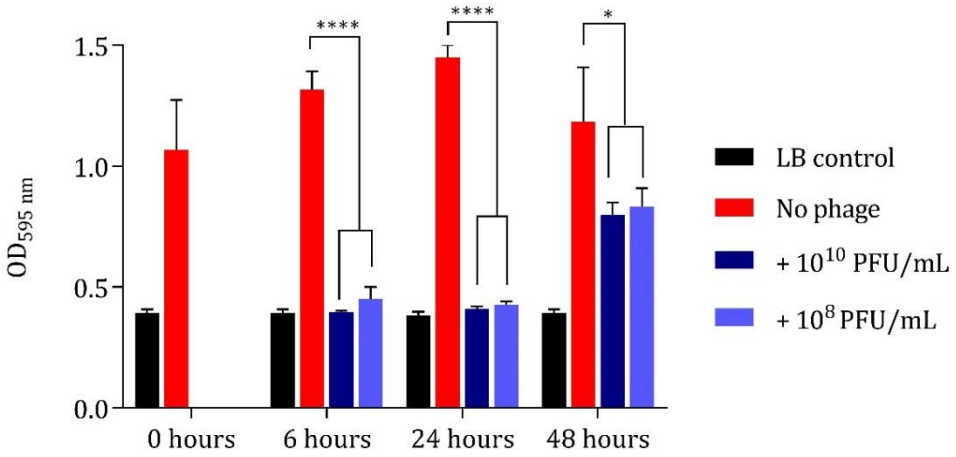

Figure 4.10: Evaluation of the ability of phage SM648 to eradicate mature single-species biofilms. Reduction in biofilm biomass was quantified using crystal violet biofilm staining at various time points post-phage addition (>0 hours), showing absorbance at 595 nm. Mean and SEM were calculated for three individual replicates. 10^{10} PFU/mL and 10^{8} PFU/mL corresponds to an MOI of 100 and 1, respectively.

At MOI of 100 and 1, the phage eradicated 97% (p<0.0001), and 96% (p<0.0001) of biofilm biomass after 24 hours, when compared to the untreated control. However, at 48 hours, these values became 49% and 44%, respectively. A reduction in untreated biofilm biomass was observed at 48 hours owing to biofilm-limiting factors such as nutrient limitations and accumulation of metabolic byproducts.

With regards to phage concentration, the applied dosage required to eradicate mature biofilms did not appear to be higher than that required to kill cells in planktonic culture. Whilst it is widely accepted that phage can replicated inside biofilms, the titre required to cause significant cell death is expected to be greater, owing to the diffusion limitations imposed by the extracellular matrix.[95] A possible explaination for this observation is the presence of polysaccharide depolymerases (specific hydrolytic enzymes which exploit polysaccharides or derivatives of as substrates). Expression of such enzymes confers the phage an important advantage, since it enhances the process of invasion and dispersion through a biofilm. Numerous studies have shown that polysaccharide depolymerase activity is related to tail-spike proteins, commonly associated with phage of the classification *Podoviridae*.[96] This particular advantage associated with phage treatment of biofilms provides a significant advantage over antibiotic therapy; the ability to express such enzymes and thus retain the concentration required to cause bacterial cell death when applied to biofilms is unique. When considering antibiotic treatement, the concentration required to successfully inhibit biofilm formation can be expected to increase up to 1000-fold relative to planktonic culture.[97]

4.4.4. Inhibition of *P. mirabilis* Swarming

Clinical studies indicate that *P. mirabilis* may initiate CAUTI by migration from the urethral meatus-catheter junction, along the luminal catheter sufaces into the bladder. The swarming phenomenon (discussed in Chapter 1), is known to be cyclic, multicellular behaviour, following the differentiation of *P. mirabilis* swimmer cells (1-2 μm in length), to elongated, hyperflagellated swarmer cells (up to 80 μm in length), which exhibit increased expression of related virulence factors (Figure 4.11).

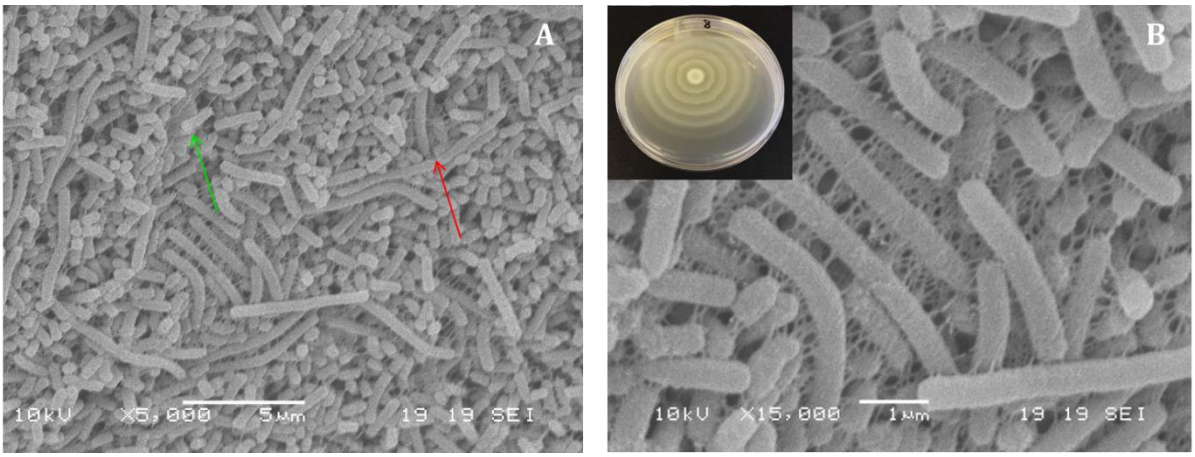

Figure 4.11: SEM observations of *P. mirabilis* B4 biofilm formation. A) Differentiation of bacterial cells from sparsely-flagellated swimmer cells (green arrow) into elongated, highly-flagellated swarmer cells (red arrow) upon contact with a solid substrate. B) Entanglement of flagella in differentiated swarmer cells, forming a multicellular raft. Inset) Characteristic 'bullseye' swarming structure of *P. mirabilis*, induced by multicellular cyclic swarming behaviour. Scale bars represent A) 5 μm, and B) 1 μm.

Swarmer cell differentiation in *P. mirabilis* is known to be accompanied by a substantial increase in the production of urease.[88,98] Initiation of this motility within the catheterised bladder may therefore expedite the generation of alkaline urine conditions that result in the deposition of crystalline material on the catheter surface. Furthermore, swarmer cells have been shown to move rapidly over all types of catheter surface, with accelerated swarming rates demonstrated on silicone catheters, particularly hydrogel-coated variations.[87]

The ability of phage to impede swarming via inducing cell lysis from a hydrogel coating was investigated. Whilst hydrogel coatings are known to provide specific advantages to patients undergoing long-term indwelling catheterisation (e.g. increased patient comfort), it is crucial that additive coatings do not accelerate the pathogenesis of infection by facilitating the differention of *P. mirabilis* cells to the swarming motility. The capability of uropathogenic *P.*

mirabilis to swarm over catheter sections, coated in PVA hydrogel containing 10^{10} PFU/mL phage SM648 is shown in Figure 4.12.

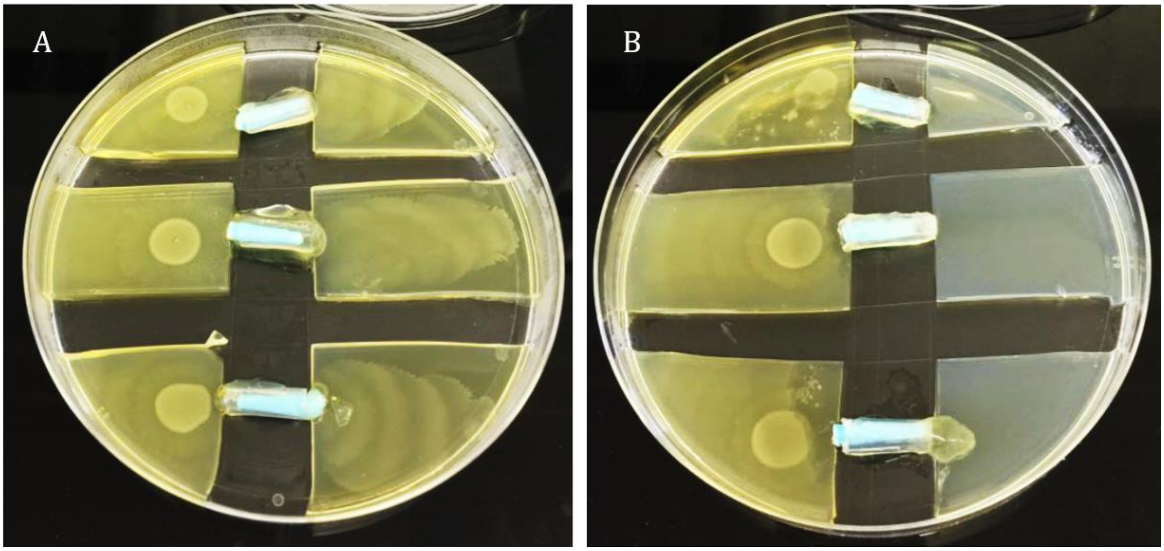

Figure 4.12: Migration of *P. mirabilis* B4 over 1 cm sections of all silicone catheters coated in 10% w/v PVA hydrogel, containing A) no phage, B) 10^{10} PFU/mL phage SM648. Successful translocational swarming was determined via the appearance of characteristic concentric swarming rings on the uninoculated side of the catheter 'bridge'. A significant reduction in the initiation of the swarming motility was observed upon incubation with the phage-containing hydrogel.

Control hydrogel coatings (without phage) were found to permit rapid swarming of *P. miraiblis* across the catheter 'bridges'. Characteristic concentric swarming rings were clearly visible on the uninoculated agar within 24 hours incubation. Hydrogel coating containing high titre phage lysates were able to effectively inhibit migration of bacterial cells across the catheter surface. Colonisation of *P. mirabilis* was limited to the sections of agar provided with the initial inoculum, whilst the impregnated phage successfully induced cell lysis of motile cells attempting to exapand the surface area of the established colony. Control plates that were not provided with a catheter bridge were also plated, to ensure that the catheter segment was the only pathway by which the bacterial cells migrate from one side to the other.

These results demonstrate that phage-impregnated hydrogel coatings show significant promise as an anti-biofilm strategy for indwelling Foley catheters, by preventing activation of the swarming motility and subsequent expression of associated virulence factors (e.g. urease). Phage of the order *Podoviridae* have been suggested to be particularly suited to this application, as their short, noncontractile tails and smaller surface area allow for higher titre formualtions to be incorporated into catheter coatings with less chance of virion damage.[76]

4.4.5. Evaluation of Prototype Coatings: *In Vitro* Bladder Models

4.4.5.1. Activation of Catheter Coating: Effect on Catheter Blockage

Experiments assessing the stability and efficacy of prototype phage coatings employed the *in vitro* bladder model system, mimicking late stage infection (initial inoculum of 10^8 CFU/mL). The simulation of established infection allowed for the evaluation of coatings under 'worst case scenario' conditions. Bladder model inoculums were left to establish for 1 hour before urinary flow was restored, allowing the initial biofilm conditioning layer to be deposited prior to model start. Hence, conditions were deemed to be more representative of the catheterised urinary tract during long-term indwelling catheterisation, particularly within patients suffering from recurrent blockage, where sterile catheters may be placed into an existing *P. mirabilis* culture.

The blockage of the catheters and subsequent cessation of urine flow was defined as the experimental end point. Parallel experiments evaluating the response of coatings to infection by *E. coli* were also undertaken, in order to determine the ability of the system to distinguish between urease positive (*P. mirabilis*) and negative (*E. coli*) species. Since *E. coli* species are the most commonly encountered pathogens in the urinary tract (including CAB),[99] differential switch-on of the phage-release coating system is essential, in order for the released phage to be of sufficient concentration during the later-stage colonisation of *P. mirabilis*. Further controls evaluating the effect of the polymeric coating (not containing phage) were also performed. No significant effect on urinary pH, bacterial population, or time to blockage was observed in the presence of the coating control in comparison to uncoated control catheters.

Inoculation with *P. mirabilis* and subsequent urease expression caused a significant increase in residual urine pH within the two hours of the experiment start. Following the accumulation of ammonia within the urine, the formation of the carboxylate anion within the Eudragit trigger layer results in swelling of the crosslinked network, thereby exposing the PVA reservoir containing phage. Released phage may then diffuse out from the coating into the surrounding medium, where they coincide with and infect cells of *P. miraiblis* encased within the crystalline catheter biofilm (Figure 4.13).

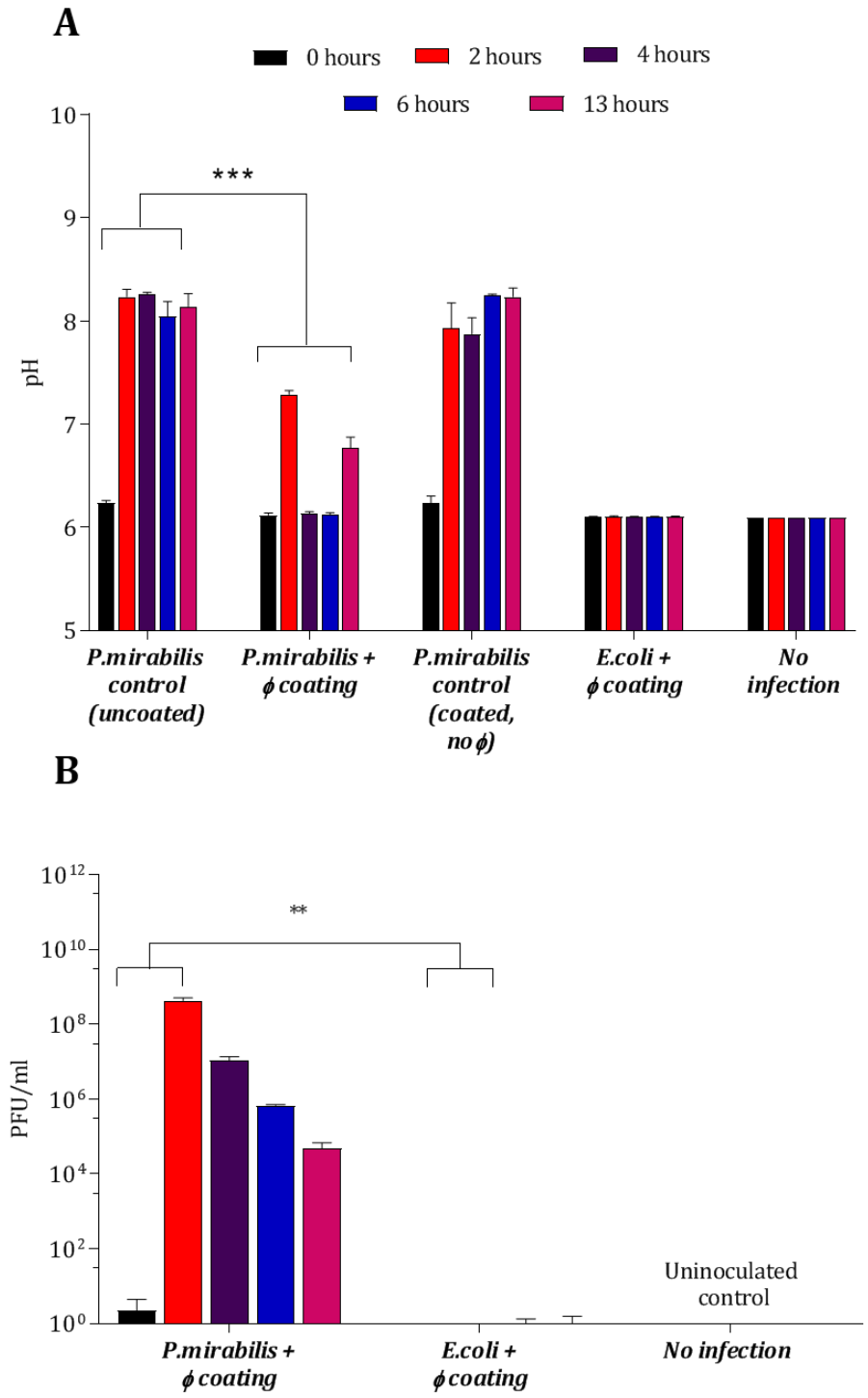

Figure 4.13: Analysis of *in vitro* bladder model conditions at 0, 2, 4, 6 hours after model start, and at time of uncoated control blockage (13 hours). A) Measured pH of residual bladder urine. B) Release of bacteriophage (ϕ) from the catheter coating. Data shown are the mean of triplicate biological repeats. Error bars represent SEM. *** $p < 0.001$, ** $p < 0.005$.

Since the threshold for Eudragit swelling occurs at pH 7, elevation of urinary pH above this value results in a burst release of phage from the coating (p = 0.0008). The concentration of phage release after 2 hours (4.3 x10^8 PFU/mL) (p = 0.0048) is sufficient to cause significant eradication of an established *P. mirabilis* biofilm, according to previous results. Such response was found to correspond to an increase in urinary pH from the healthy region (pH 6.24) to the infected region (pH 8.24) within the two hour period.

A reduction of urinary pH to the healthy region (~pH 6) was observed after release in the phage-coated catheter. In contrast, elevated urinary pH was maintained within the uncoated control model throughout the duration of the experiment, leading to eventual catheter blockage at 13 hours. Gradual decrease of the phage population within the bladder model, and hence the failure of the catheter coating to completely inhibit blockage was primarily a consequence of elution of virions form the bladder post-release. No significant phage release was observed in models devoid of *P. mirabilis* indicating the stability of the coatings for the duration of the experiment, despite exposure to a continuously flowing culture system.

As a direct consequence of phage release from catheter coatings, a significant reduction in bacterial biomass was observed within populations of *P. mirabilis* (p = 0.0016) (Figure 4.14). Decline in cell numbers was directly correlated to the release profile of phage. Contrarily, bladders containing uncoated catheters sustained cell populations in the region of 10^8 CFU/mL, leading to eventual blockage of the *P. mirabilis* models via formation of crystalline biofilms. Notably, no significant reduction in cell numbers was observed in the presence of the dual-layered coating not containing phage, indicating that any observed cell death was as a direct result of phage infection.

Phage remained stable and viable within the hydrogel coating throughout the entire experimental procedure, including the process of encapsulation, coating, storage and exposure to bladder model conditions (including both acidic, neutral and alkaline pHs, as well as the high ionic strength of the urine media). Phage stability within clinical formulations is considered a barrier to potential therapeutic applications, yet has received little attention in phage therapy literature.[81,100] Therefore, the proof of stability within a hydrogel matrix, as well as the maintenance of infectivity in the face of challenging physiological conditions represents a step forward in this field.

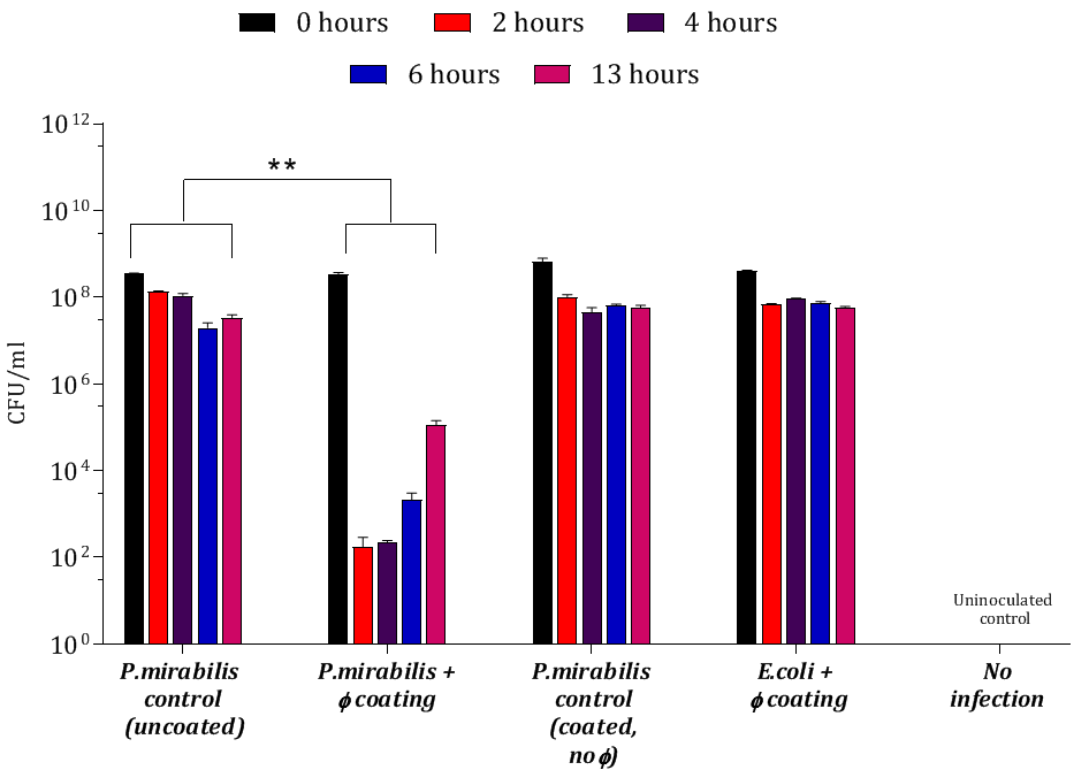

Figure 4.14: Analysis of *P. mirabilis* population within the *in vitro* bladder models, containing phage (ϕ)-coated and uncoated control catheters. Measurement of bacterial biomass at regular intervals (0, 2, 4, and 6 hours) after model start, as well as at time of control blockage (13 hours) was undertaken via direct sampling of residual bladder urine. Data shown are the mean of triplicate biological repeats. Error bars represent SEM. ** $p < 0.005$.

Despite an approximately 6-log reduction in *P. mirabilis* concentration within 2 hours of coating activation, triggered release of phage was only successful in delaying catheter blockage, rather than preventing it completely. Restoration of bacterial populations within phage-treated models beteen 4-13 hours after the experimental start point was expected, owing to the proportional elution of phage from the bladders. However, it is likely that this observation was multifactorial, aided by the development of reistance upon exposure of *P. miraiblis* to the released phage. Although comparable resistance has been observed within *in vitro* infection models in a similar time-frame,[101] the fact that this proof-of-concept study utilises a single bacteria/phage combination is worth noting. The issue of resistance may be eased via the use of phage 'cocktails'; two or more species of phage used simultaneously to target bacterial infection for clinical applications. Treatment of uropathogenic isolates with phage cocktails has shown recent success *in vitro*,[78] although formulation of an effective cocktail requires detailed study into host-range profiles, and binding between virus and host under relevant physiological conditions. In terms of stability, phage cocktails necessitate careful consideration

of formulation conditions, as each contributing strain may require individually tailored formulations to ensure phage viability and stability during storage.

In this study, burst release of phage from dual-layered coatings, and subsequent reduction in viable *P. mirabilis* population successfully doubled the time to blockage in models containing coated catheters, compared to the uncoated control ($p = 0.0199$) (Figure 4.15).

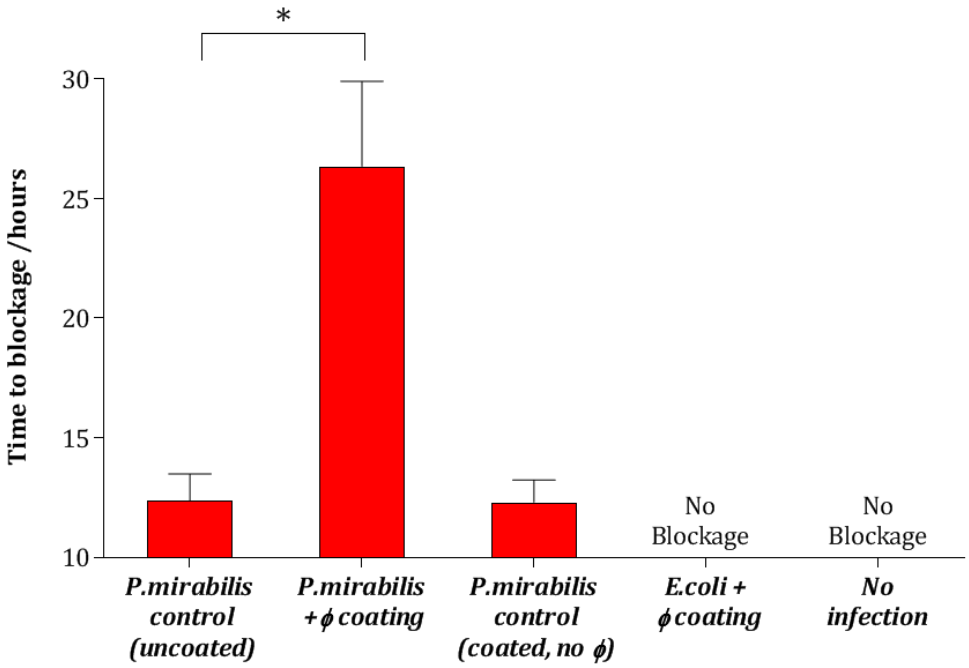

Figure 4.15: Effect of bacteriophage 'burst reslease' on catheter blockage. Elevated urinary pH within *in vitro* bladder models induces phage (ϕ) release from dual-layered, infection-responsive catheter coatings. The point at which urine flow through the catheters ceased was defined as the experimental end point. Data represents the mean of 3 independent biological replicates. Error bars represent SEM. *$p < 0.05$.

These findings are in agreement with previous studies, which have assessed the ability of lytic phage to reduce biofilms caused by common uropathogens, including *E. coli* and *P. aeruginosa*.[102,103] Recent investigation into the effect of phage on *P. miraiblis*-induced CAUTI has shown a delay in catheter blockage of more than 8 days, when infection was modelled in its infancy (starting inoculum of 10^3 CFU/mL). Hence, the delay in catheter blockage presented here may translate to days, rather than hours, when assessed using an early stage infection model. Achieving such delay of catheter blockage has the potential to improve the health and welfare of millions of patients worldwide, as well as relieving some of the substantial financial demands that this issue places on the resources of the health service.

4.4.5.2. Activation of Catheter Coating: Effect on Crystalline Biofilm Formation

Visual examination of crystalline biofilm formation on the luminal surfaces of the catheter showed a significant reduction in biomass within phage coated catheters, compared to uncoated controls. Models containing both coated and uncoated catheters were halted after 13 hours (time of control blockage), and catheters from varying luminal locations were imaged using SEM (Figure 4.16).

At the time of blockage of the uncoated control catheters, which showed significant encrustation, the phage-coated catheters can be seen to be devoid of prominent encrustations. The average urinary pH within the coated catheter models 13 hours after the experiment start point was 6.77, which is below the nucleation pH of urine and thus insufficient to cause crystalline precipitation. Within the control model, the majority of crystalline material can be seen to have accumulated in the eyehole region of the uncoated catheter, owing to surface irregularitites formed by the extrusion production techniques used in catheter manufacture. Such surface striations are particularly prominent in the catheter eyeholes, clearly observable in Figure 16F. Experiments in laboratory models showed that *P. mirabilis* cells may be detected in the surface crevices of urinary catheters within 2 hours of incubation. After 4 hours, microcolony development was detected from pioneer cells, and, by 6 hours, corresponding to the rising urinary pH, crystalline deposits began to form in the developing biofilm, leaing to eventual blockage of the eyehole or central lumen.[104] Since the release of phage from the triggered-release coating prevented the elevation of urinary pH via facilitating bacterial cell lysis, eyehole and luminal surfaces of catheters in these models can be seen to be devoid of microcrystal aggregates at the time of control blockage.

The ability of phage to mitigate the growth of uropathogenic biofilms has been explored previously, although has shown more efficacy in speacies of *E. coli* (3-4 log reduction) and *P. aeruginosa* (4 log reduction) than *P. mirabilis* (1-2 log reduction).[77,105] The 6-log reduction observed in this study is likely owing to the initiation of a burst response from the polymeric coating, resulting in exposure of viable phage to exponential-phase bacterial cells and subsequent rapid and substantial decline in cell numbers. Such triggered release systems achieve delivery of a therapeutic agent to the relevant physiological location in an adequate dosage, at the point of critical colonisation, thus providing a more significant therapeutic impact than passive release systems, whose therapeutic reservoirs may be severely depleted at more advanced stages of infection.

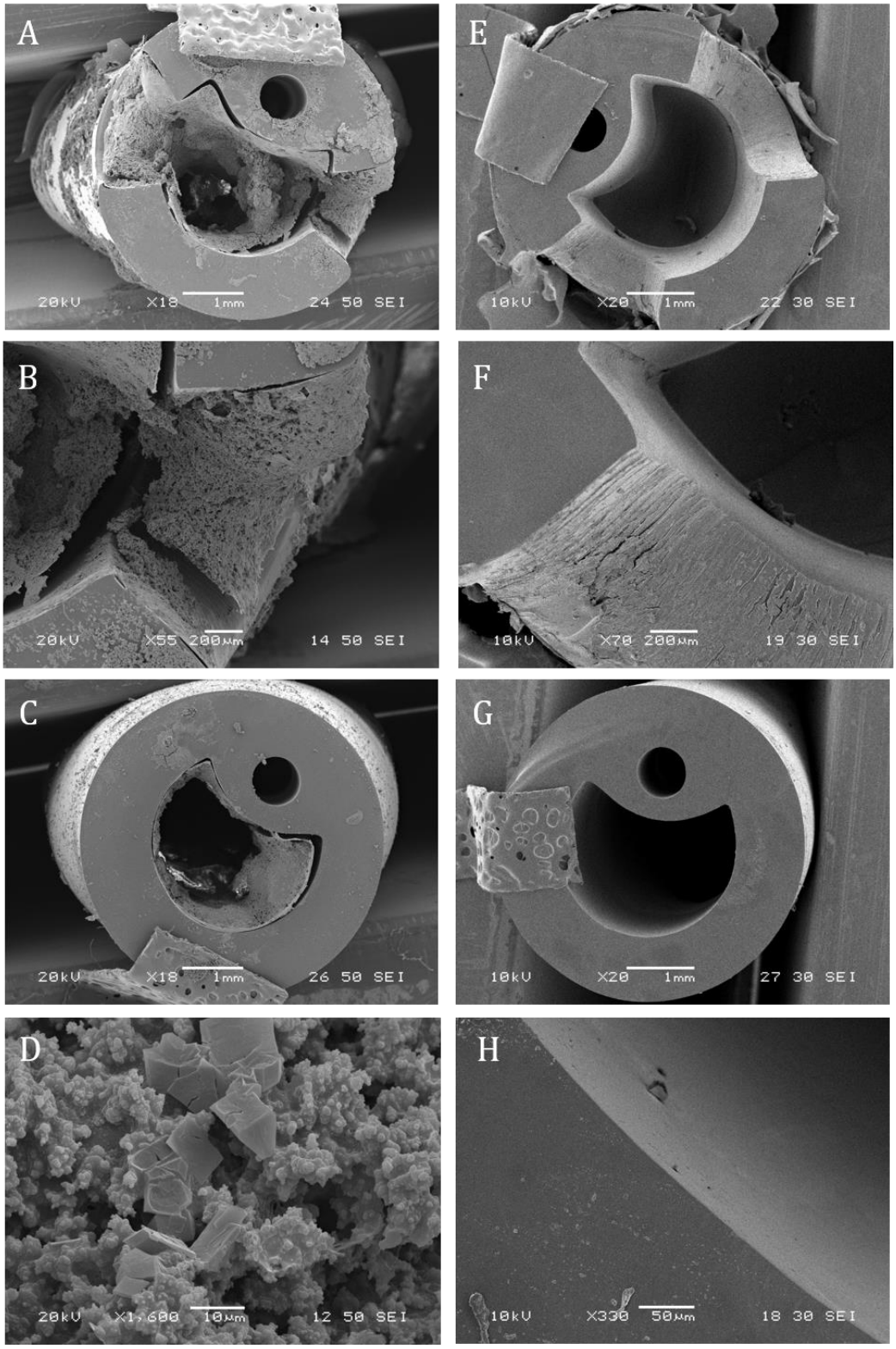

Figure 4.16: Representative SEM images of catheter cross sections, comparing levels of encrustation and blockage by the crystalline biofilms of *P. mirabilis*. (A-D) Uncoated control. (E-H) With bacteriophage coating. All catheters were removed from *in vitro* bladder models 13 hours after model start. (A,B,E,F) Cross sections of catheter eyehole region. (C,D,G,H) Cross sections of catheter lumen 1 cm below retention balloon.

Quantification of crystalline biofilm formation at the same time point was performed using AAS measurements (Figure 4.17). These results revealed low levels of calcium apatite in the biofilms of the phage-treated catheter. This is likely due to the distinct stages of complex crystalline biofilm formation by *P. mirabilis* , whereby the accumulation of loose crystalline material gathers within the bladder before defined crystals precipitate into the biofilm matrix.[106]

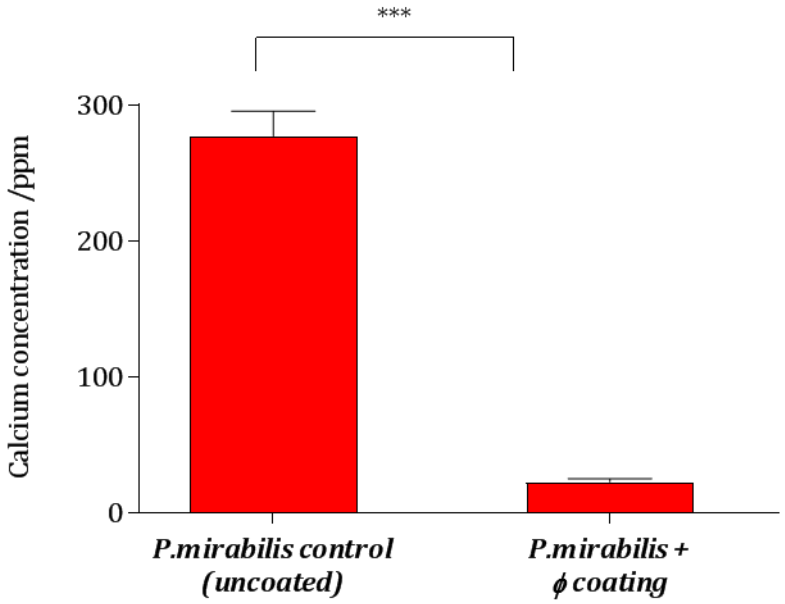

Figure 4.17: Quantitative analysis of crystalline biofilm biomass on catheter surfaces by atomic absorption spectroscopy. Comparison of phage(ϕ)-coated and uncoated catheters 13 hours post-incoluation of *in vitro* bladder models with *P. mirabilis*. Data shown are the mean of triplicate repeats. Error bars represent SEM. *** $p < 0.001$.

Limitations of this proof-of-concept model of phage delivery into the catheterised urinary tract include the use of a single phage strain on a single species biofilm of *P. mirabilis*. It is widely acknowledged that *P. mirabilis* is commonly found in mixed communities with other urinary tract pathogens. Thus this model does not take in to consideration the potential impact of other species on the biofilm structure, phage treatment kinetics and, ultimately, the time taken to reach catheter blockage. Indeed, the co-habitaiton of *Enterococcus cloacae*, *Morganella morganii*, *P. aeruginosa* and *E. coli* within catheter biofilms has shown to significantly increase the time to blockage within *in vitro* models of the catheterised urinary tract, owing to active exclusion and a degree of antagonism between *P. mirabilis* and other organisms.[107]

Furthermore, the use of only a single phage strain, whilst providing sound proof-of-concept of the stability and release capacity in this setting, has a potentially limited therapeutic impact on eliminating *P. mirabilis* crystalline biofilms, and subsequently extending catheter lifetime.

Whilst it is logical to assume that the use of a phage cocktail may successfully increase time to blockage, in reality, increasing phage productivity requires careful consideration of a number of potential limiting factors. Phage therapy with cocktails results in complex pharmacology, potentially resulting in reduced infection robustness or interference by one or more of the participating phage types.[108] Moreover, treatment via phage cocktail may not effectively prevent the development of phage-resistant mutant populations. Such populations may not be present in sufficiently high concentration to support phage amplification to control population growth, resulting in cocktail populations ultimately equivalent to primary treatment. Successful secondary treatment via administration of phage cocktails may only be possible if phage types are supplied in sequential doses or as a continuous, high titre formulations.[58]

4.5. Conclusion

There is no doubt that phage therapy is an attractive solution for combatting the escalating antibiotic crisis. Numerous studies have highlighted the *in vitro* and *in vivo* potential of lytic phage, resulting in a number of clinical trials over the last decade . Nevertheless, there remains obvious challenges ahead for phage therapy, particularly in terms of regulatory policy. Fuelled by the ever-increasing need for antibiotic alternatives, regulatory processes must be refined and approached from a novel phage-based perspective, based on knowledge of phage applications for specific implementation.

This study demonstrates the potential of phage therapy for the control of CAUTI, in particular the delay of encrustation and blockage following infection and device colonisation by *P. mirabilis*. Local delivery of lytic phage was achieved via the employment of a dual-layered polymeric architecture, and manifested in an approximately 6-log reduction in viable bacterial cells within an *in vitro* model of the catheterised urinary tract. Reduction in bacterial population and consequent prevention of crystal aggregation was successful in doubling the time to catheter blockage, thus extending catheter lifetime and potentially reducing the likelihood of serious symptomatic episodes associated with catheter occlusion. Phage release was achieved *in situ,* in direct response to elevation of urinary pH and without external interference or treatment administration. Phage were found to remain stable and viable throughout production and degradation of the polymeric coating, representing a novel encapsulation and delivery mechanism for lytic bacteriophage within the body.

Further development of the proof-of-concept system described here involves the formulation of a multiphage 'cocktail', to improve the broad-spectrum capabiltiies and therapeutic potential of phage. However, an in-depth understanding of phage kinetics, interference, competition and synergy is required to optimise the compatibility of contributing strains. Furthermore *in vitro* evaluation of this system on multispecies biofilms would provide a more accurate representation of the pathogenic spectrum *in vivo*.

Whilst phage has undoubtedly shown potential for the prevention and treatment of CAUTI, fulfilment of the potential of phage within the clinical setting requires a paradigm shift throughout human medicine. Additionally, the issue of phage resistance remains problematic in the design of generalised medical products such as phage-impregnated urinary catheters. Ultimately, the success of phage therapy will reply upon the acquisition of detailed information on the properties and behaviour of the specific-bacterial system, both *in vitro* and *in vivo*.

4.6. References

1. E. Martens and A. L. Demain, *Journal of Antibiotics*, 2017, **70**, 520–526.
2. A. Fleming, *British Journal of Experimental Pathology*, 1929, **10**, 226–236.
3. J. Lederberg, *Science*, 2000, **288**, 287–293.
4. E. Y. Klein, T. P. Van Boeckel, E. M. Martinez, S. Pant, S. Gundra, S. A. Levin, H. Goossens and R. Laxminarayan, *Proceedings of the National Academy of Sciences*, 2018, **115**, E3463–E3470.
5. *The Review on Antimicrobial Resistance, Antimicrobial Resistance: Tackling a crisis for the health and wealth of nations,* 2014.
6. T. S. Crofts, A. J. Gasparrini and G. Dantas, *Nature Reviews Microbiology*, 2017, **15**, 422–434.
7. A. Hollis and Z. Ahmed, *New England Journal of Medicine*, 2013, **369**, 2474–2476.
8. Q. Chang, W. Wang, G. Regev-Yochay, M. Lipsitch and W. P. Hanage, *Evolutionary Applications*, 2015, **8**, 240–247.
9. J. A. Perry, E. L. Westman and G. D. Wright, *Current Opinion in Microbiology*, 2014, **21**, 45–50.
10. K. J. Forsberg, S. Patel, M. K. Gibson, C. L. Lauber, R. Knight, N. Fierer and G. Dantas, *Nature*, 2014, **509**, 612–616.
11. V. M. Dcosta, C. E. King, L. Kalan, M. Morar, W. W. L. Sung, C. Schwarz, D. Froese, G. Zazula, F. Calmels, R. Debruyne, G. B. Golding, H. N. Poinar and G. D. Wright, *Nature*, 2011, **477**, 457–461.
12. H. C. Neu, *Applied microbiology*, 1969, **17**, 783–786.
13. R. I. Aminov, M. Otto and A. Sommer, *Frontiers in Microbiology*, 2010, **1**, 1–7.
14. K. Lewis, *Nature Reviews Drug Discovery*, 2013, **12**, 371–387.
15. C. Walsh, *Nature*, 2000, **406**, 775–781.
16. W. V. Shaw, L. C. Packman, B. D. Burleigh, A. Dell, H. R. Morris and B. S. Hartley, *Nature*, 1979, **282**, 870–872.
17. K. Bush, *Critical Care*, 2010, **14**, 224.
18. P. Courvalin, *Clinical Infectious Diseases*, 2006, **42**, S25–S34.
19. Y. Katayama, T. Ito and K. Hiramatsu, *Antimicrobial Agents and Chemotherapy*, 2000, **44**, 1549–1555.
20. P. Ruggerone, S. Murakami, K. M. Pos and A. Vargiu, *Current Topics in Medicinal Chemistry*, 2013, **13**, 3079–3100.
21. A. Poulou, E. Voulgari, G. Vrioni, V. Koumaki, G. Xidopoulos, V. Chatzipantazi, F. Markou and A. Tsakris, *Journal of Clinical Microbiology*, 2013, **51**, 3176–3182.

22. B. B. Flury, M. J. Ellington, K. L. Hopkins, J. F. Turton, M. Doumith, R. Loy, P. Staves, V. Hinic, R. Frei and N. Woodford, *Antimicrobial Agents and Chemotherapy*, 2016, **60**, 2383–2390.
23. M. O. A. Sommer, C. Munck, R. V. Toft-Kehler and D. I. Andersson, *Nature Reviews Microbiology*, 2017, **15**, 689–696.
24. K. H. Luepke and J. F. Mohr, *Expert Review of Anti-Infective Therapy*, 2017, **15**, 425–433.
25. B. Spellberg, *Critical Care*, 2014, **18**, 288.
26. J. O'Neil, *Securing New Drugs for Future Generations: The Pipeline of Antibiotics*, 2015.
27. A. Sertkaya, J. Eyraud, A. Birkenbach, C. Franz, N. Ackerley, V. Overton and E. R. Group, *ERG*, 2014, **14–25**, 1–107.
28. K. H. Luepke, K. J. Suda, H. Boucher, R. L. Russo, M. W. Bonney, T. D. Hunt and J. F. Mohr, *Pharmacotherapy*, 2017, **37**, 71–84.
29. G. T. Schumock, J. A. Stubbings, M. D. Wiest, E. C. Li, K. J. Suda, L. M. Matusiak, R. J. Hunkler and L. C. Vermeulen, *American Journal of Health-System Pharmacy*, 2018, **73**, 1058–1075.
30. ECDC, *ECDC Country Visit to Belgium to Discuss Antimicrobial Resistance Issues*, 2018.
31. World Health Organisation, *Global Action Plan on Antimicrobial Resistance*, 2015.
32. V. L. Simpkin, M. J. Renwick, R. Kelly and E. Mossialos, *Journal of Antibiotics*, 2017, **70**, 1087–1096.
33. World Health Organisation, *Global Priority List of Antibiotic-Resistant Bacteria to Guide Research, Discovery and Development of New Antibiotics*, 2017.
34. J. A. Al-Tawfiq, R. Laxminarayan and M. Mendelson, *International Journal of Infectious Diseases*, 2017, **54**, 77–84.
35. S. W. Dickey, G. Y. C. Cheung and M. Otto, *Nature Reviews Drug Discovery*, 2017, **16**, 457–471.
36. A. DiGiandomenico and B. R. Sellmna, *Current Opinion in Microbiology*, 2015, **27**, 78–85.
37. S. Yu, X. Zhu, J. Zhou and Z. Cai, *Royal Society Open Science*, , DOI:10.1098/rsos.170702.
38. K. M. Younis, G. Usup and A. Ahmad, *Environmental Science and Pollution Research*, 2016, **23**, 4756–4767.
39. R. C. Allen, R. Popat, S. P. Diggle and S. P. Brown, *Nature Reviews Microbiology*, 2014, **12**, 300–308.
40. T. Maeda, R. García-Contreras, M. Pu, L. Sheng, L. R. Garcia, M. Tomás and T. K. Wood, *ISME Journal*, 2012, **6**, 493–501.
41. A. J. McCoy, H. Liu, T. J. Falla and J. S. Gunn, *Antimicrobial Agents and Chemotherapy*, 2001, **45**, 2030–2037.
42. R. Belas, J. Manos and R. Suvanasuthi, *Infection and Immunity*, 2004, **72**, 5159–5167.

43. Y. Wang, H. Venter and S. Ma, *Current drug targets*, 2016, **17**, 702–719.
44. A. Pantel, C. Dunyach-Remy, C. N. Essebe, J. Mesureur, A. Sotto, J. M. Pagès, M. H. Nicolas-Chanoine and J. P. Lavigne, *Antimicrobial Agents and Chemotherapy*, 2016, **60**, 2901–2911.
45. J. Nzakizwanayo, P. Scavone, S. Jamshidi, J. A. Hawthorne, H. Pelling, C. Dedi, J. P. Salvage, C. K. Hind, F. M. Guppy, L. M. Barnes, B. A. Patel, K. M. Rahman, M. J. Sutton and B. V. Jones, *Scientific Reports*, , DOI:10.1038/s41598-017-12445-w.
46. H. Stolp and M. P. Starr, *Antonie van Leeuwenhoek*, 1963, **29**, 217–248.
47. R. E. Sockett, *Annual Review of Microbiology*, 2009, **63**, 523–539.
48. R. M. Q. Shanks, V. R. Davra, E. G. Romanowski, K. M. Brothers, N. A. Stella, D. Godboley and D. E. Kadouri, *PLoS ONE*, 2013, **8**, e66723.
49. K. Harini, V. Ajila and S. Hegde, *Journal of Indian Society of Periodontology*, 2013, **17**, 823–825.
50. A. C. Greene, *Trends in Biotechnology*, 2017, **36**, 127.
51. A. A. Gomaa, H. E. Klumpe, M. L. Luo, K. Selle, R. Barrangou and C. L. Beisel, *mBio*, 2014, **5**, e00928-13.
52. A. M. Comeau, G. F. Hatfull, H. M. Krisch, D. Lindell, N. H. Mann and D. Prangishvili, *Research in Microbiology*, 2008, **159**, 306–313.
53. E. C. Keen, *BioEssays*, 2015, **37**, 6–9.
54. S. Chibani-Chennoufi, A. Bruttin, M. L. Dillmann and H. Brüssow, *Journal of Bacteriology*, 2004, **186**, 3677–3686.
55. E. H. Hankin, *Annales De l'Institut Pasteur*, 1896, **10**, 511–523.
56. F. Twort, *Lancet*, 1915, **186**, 1241–1243.
57. F. D'Herelle, *L'academie des Sciences Paris*, 1917, **165**, 373–375.
58. B. K. Chan, S. T. Abedon and C. Loc-Carrillo, *Future microbiology*, 2013, **8**, 769–83.
59. G. F. Hatfull and R. W. Hendrix, *Current Opinion in Virology*, 2011, **4**, 298–303.
60. H. W. Ackermann, in *Bacteriophages. Methods in Molecular Biology*, eds. M. R. J. Clokie and A. M. Kropinski, Humana Press, 501st edn., 2009, pp. 127–141.
61. F. L. Nobrega, M. Vlot, P. A. de Jonge, L. L. Dreesens, H. J. E. Beaumont, R. Lavigne, B. E. Dutilh and S. J. J. Brouns, *Nature Reviews Microbiology*, , DOI:10.1038/s41579-018-0070-8.
62. A. Campbell, *Nature Reviews Genetics*, 2003, **4**, 471–477.
63. S. Gandon, *Trends in Microbiology*, 2016, **24**, 356–365.
64. E. Emond and S. Moineau, in *Bacteriophage: Genetics and Molecular Biology*, eds. S. McGrath and D. van Sinderen, Caister Academic Press, Norfolk, UK, 2007, pp. 93–125.
65. C. Verheust, K. Pauwels, J. Mahillon, D. R. Helinski and P. Herman, *Applied Biosafety*,

2010, **15**, 32–44.

66. T. Hayashi, K. Makino, M. Ohnishi, K. Kurokawa, K. Ishii, K. Yokoyama, C. G. Han, E. Ohtsubo, K. Nakayama, T. Murata, M. Tanaka, T. Tobe, T. Iida, H. Takami, T. Honda, C. Sasakawa, N. Ogasawara, T. Yasunaga, S. Kuhara, T. Shiba, M. Hattori and H. Shinagawa, *DNA Research*, 2001, **8**, 11–12.
67. M. W. Eklund, F. T. Poysky and S. M. Reed, *Nature New Biology*, 1972, **172**, 480–482.
68. O. Sekulovic and L.-C. Fortier, in *Clostridium difficile: Methods and Protocols, Methods in Molecular Biology*, eds. A. P. Roberts and P. Mullany, Springer, 2106, pp. 143–145.
69. C. Loc-Carrillo and S. T. Abedon, *Bacteriophage*, 2011, **1**, 111–114.
70. J. R. Clark, *Future Virology*, 2015, **10**, 449–461.
71. C. Hawkins, D. Harper, D. Burch, E. Änggård and J. Soothill, *Veterinary Microbiology*, 2010, **146**, 309–313.
72. A. Wright, C. H. Hawkins, E. E. Änggård and D. R. Harper, *Clinical Otolaryngology*, 2009, **34**, 349–357.
73. P. Jault, T. Leclerc, S. Jennes, J. P. Pirnay, Y.-A. Que, G. Resch, A. F. Rousseau, F. Ravat, H. Carsin, R. Le Floch, J. V. Schaal, C. Soler, C. Fevre, I. Arnaud, L. Bretaudeau and J. Gabard, *The Lancet Infectious Diseases*, , DOI:10.1016/S1473-3099(18)30482-1.
74. A. K. Daly, *Current Opinion in Drug Discovery and Development*, 2007, **10**, 29–36.
75. L. F. Furfaro, M. S. Payne and B. J. Chang, *Frontiers in Cellular Infection and Microbiology*, 2018, **8**, 1–7.
76. L. D. R. Melo, P. Veiga, N. Cerca, A. M. Kropinski, C. Almeida, J. Azeredo and S. Sillankorva, *Frontiers in Microbiology*, 2016, **7**, 1–12.
77. L. Carson, S. P. Gorman and B. F. Gilmore, *FEMS Immunology and Medical Microbiology*, 2010, **59**, 447–455.
78. J. Nzakizwanayo, A. Hanin, D. R. Alves, B. McCutcheon, C. Dedi, J. Salvage, K. Knox, B. Stewart, A. Metcalfe, J. Clark, B. F. Gilmore, C. G. M. Gahan, A. T. A. Jenkins and B. V. Jones, *Antimicrobial Agents and Chemotherapy*, 2016, **60**, 1530–1536.
79. W. Sybesma, R. Zbinden, N. Chanishvili, M. Kutateladze, A. Chkhotua, A. Ujmajuridze, U. Mehnert and T. M. Kessler, *Frontiers in Microbiology*, 2016, **7**, 1–9.
80. J. P. Pirnay, D. De Vos, G. Verbeken, M. Merabishvili, N. Chanishvili, M. Vaneechoutte, M. Zizi, G. Laire, R. Lavigne, I. Huys, G. Van Den Mooter, A. Buckling, L. Debarbieux, F. Pouillot, J. Azeredo, E. Kutter, A. Dublanchet, A. Górski and R. Adamia, *Pharmaceutical Research*, 2011, **28**, 934–937.
81. D. J. Malik, I. J. Sokolov, G. K. Vinner, F. Mancuso, S. Cinquerrui, G. T. Vladisavljevic, M. R. J. Clokie, N. J. Garton, A. G. F. Stapley and A. Kirpichnikova, *Advances in Colloid and Interface Science*, 2017, **249**, 100–133.

82. US9457132B2, 2016.
83. A. M. Brown, Iowa State University, 2014.
84. H. Hathaway, D. R. Alves, J. Bean, P. P. Esteban, K. Ouadi, J. Mark Sutton and A. T. A. Jenkins, *European Journal of Pharmaceutics and Biopharmaceutics*, 2015, **96**, 437–441.
85. J. E. Bean, D. R. Alves, M. Laabei, P. P. Esteban, N. T. Thet, M. C. Enright and A. T. A. Jenkins, *Chemistry of Materials*, 2014, **26**, 7201–7208.
86. D. Bray, J. Bagu and P. Koegler, *Microscopy Research and Technique*, 1993, **6**, 489–495.
87. N. Sabbuba, G. Hughes and D. J. Stickler, *BJU International*, 2002, **89**, 55–60.
88. B. V. Jones, E. Mahenthiralingam, N. A. Sabbuba and D. J. Stickler, *Journal of Medical Microbiology*, 2005, **54**, 807–813.
89. V. Morozova, Y. Kozlova, E. Shedko, I. Babkin, A. Kurilshikov, O. Bokovaya, A. Bardashova, A. Yunusova, A. Tikunov, A. Tupikin, E. Ryabchikova and N. Tikunova, *Archives of Virology*, 2018, **163**, 2189–2197.
90. GenBank, *National Center for Biotechnology Information*, Nucleotide, EST, and GSS Databases.
91. P. Manohar, R. Nachimuthu and B. S. Lopes, *BMC Microbiology*, 2018, **18**, 1–11.
92. F. Oechslin, *Viruses*, 2018, **10**, 1–23.
93. M. Yazdi, M. Bouzari and E. A. Ghaemi, *Journal of Molecular Microbiology and Biotechnology*, 2018, **28**, 37–46.
94. B. K. Chan, M. Sistrom, J. E. Wertz, K. E. Kortright, D. Narayan and P. E. Turner, *Scientific Reports*, , DOI:10.1038/srep26717.
95. S. González, L. Fernández, A. B. Campelo, D. Gutiérrez, B. Martínez, A. Rodríguez and P. García, *Applied and Environmental Microbiology*, 2017, **83**, e1-16.
96. D. Gutiérrez, L. Rodríguez-Rubio, B. Martínez, A. Rodríguez and P. García, *Frontiers in Microbiology*, 2016, **7**, 1–15.
97. S. M. Jacobsen, D. J. Stickler, H. L. T. Mobley and M. E. Shirtliff, *Clinical Microbiology Reviews*, 2008, **21**, 26–59.
98. C. Ariison, H. Lai and C. Hughes, *Molecular Microbiology*, 1992, **6**, 1583–1591.
99. S. M. Jacobsen, D. J. Stickler, H. L. T. Mobley and M. E. Shirtliff, *Clinical Microbiology Reviews*, 2008, **21**, 26–59.
100. H. Hathaway, S. Milo, J. M. Sutton and T. A. Jenkins, *Therapeutic Delivery*, 2017, **8**, 543–556.
101. W. Fu, T. Forster, O. Mayer, J. J. Curtin, S. Lehman and R. M. Donlan, *Antimicrobial Agents and Chemotherapy*, 2010, **54**, 397–404.
102. A. Chibeu, E. Lingohr, L. Masson, A. Manges, J. Harel, H. W. Ackermann, A. Kropinski and P. Boerlin, *Viruses*, 2012, **4**, 471–487.

103. K. S. Liao, S. M. Lehman, D. J. Tweardy, R. M. Donlan and B. W. Trautner, *Journal of applied microbiology*, 2012, **1131530**-, 1530–1539.
104. D. Stickler, R. Young, G. Jones, N. Sabbuba and N. Morris, *Urological Research*, 2003, **31**, 306–311.
105. S. M. Lehman and R. M. Donlan, *Antimicrobial Agents and Chemotherapy*, 2015, **59**, 1127–1137.
106. S. a. Wilks, M. J. Fader and C. W. Keevil, *PLoS ONE*, 2015, **10**, 1–13.
107. S. M. Macleod and D. J. Stickler, *Journal of Medical Microbiology*, 2007, **56**, 1549–1557.
108. A. S. Nilsson, *Upsala Journal of Medical Sciences*, 2014, **119**, 192–198.

Chapter 5: Development of a Novel Small-Molecule Urease Inhibitor for the Control of Urinary Catheter Encrustation

5.1. Abstract

With the looming prospect of the diminishing efficacy of current chemical antibiotics, the world's population faces the dawn of the 'post-antibiotic era', owing to the widespread and indiscriminate use of antibiotics in both the healthcare and agricultural setttings. Enzymes, particularly those vital for pathogenesis, are considered to be effective and promising targets for small molecule intervention in human bacterial infection.

Urease is a nickel-dependent metalloenzyme known to play a crucial role in the pathogenesis and virulence of catheter-associated *P. mirabilis* infection. Targeting urease as a novel therapeutic candidate facilitates the disarming of bacterial virulence without effecting bacterial fitness, therefore limiting the selective pressure placed on the invading population. Small molecule enzyme inhibitors based on the molecular structure of the native substrate have proved promising in rational drug design, including those with antiureolytic inhibitory effects on urease.

The research presented in this chapter decribes the design, synthesis, and *in vitro* evaluation of a novel small molecule enzyme inhibitor, able to prevent encrustation and blockage of urinary catheters in a physiologically representative *in vitro* model of the catheterised urinary tract. The synthesised organic thiol compound is a structural analogue of urea, showing promising competitive activity against urease from jack bean (*Canavalia ensiformis*) as well as cytoplasmic *P. mirabilis* urease (Figure 5.1).

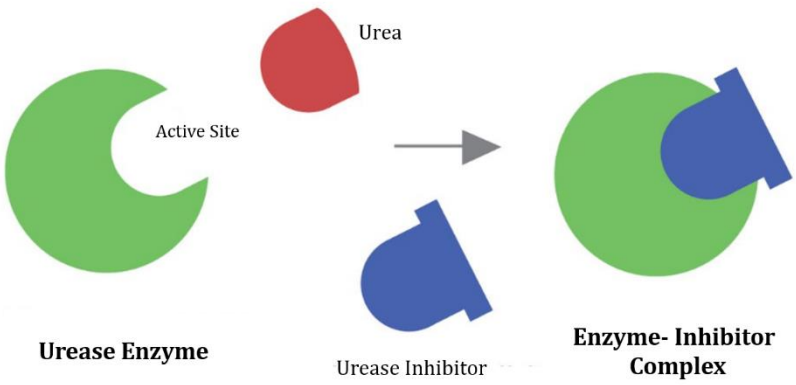

Figure 5.1: Schematic representation of antiureolytic effects of a competitive small molecule urease inhibitor.

5.2. Introduction

5.2.1. Enzymes

Biological processes depend on a well-orchestrated series of chemical reactions, many of which proceed too slowly on their own to sustain life. Enzymes are natural catalysts, which greatly accelerate the rates of such reactions, thus facilitating many biochemical processes within living cells. Like all catalysts, enzymes are characterised by two main properties. Firstly, they increase the rate of rection without themselves being consumed or permanently altered by the process. Secondly, they accelerate the reaction rate without altering the chemical equilibrium between reactants and products. The equilibrium of the reaction is determined by the final energy states of the substrate and product. In order for the reaction to proceed spontaneously, the substrate must first be converted into a higher energy transition state. The energy required to reach the transition state (known as the activation energy) constitutes a barrier to the progress of the reaction, thus limiting the rate of both the forward and backward reactions.[1] Enzymes facilitate a reduction in activation energy, thereby increasing the rate of reaction (Figure 5.2).

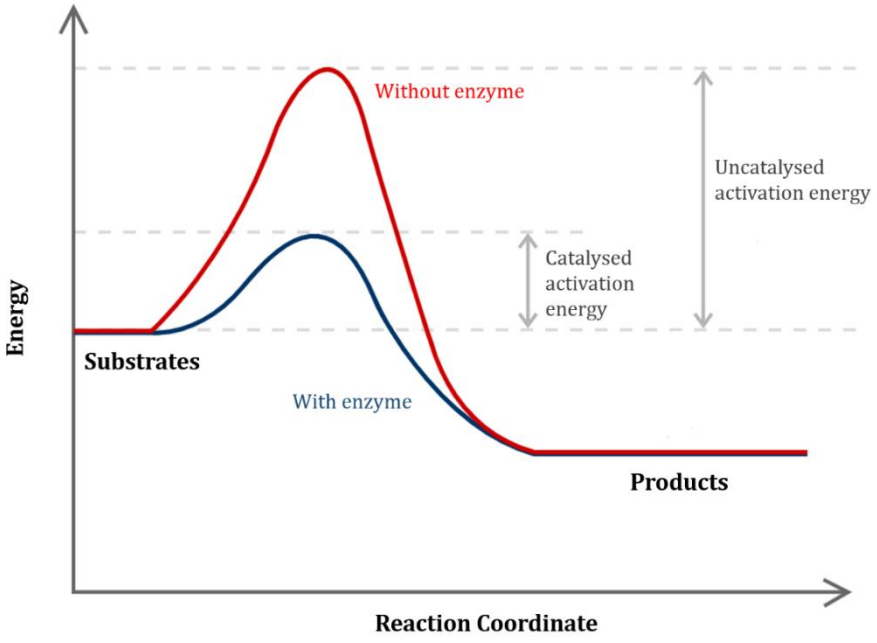

Figure 5.2: Energy diagram for enzyme-catalysed and uncatalysed biochemical reactions. Addition of a enzyme lowers the energy required to reach the transition state (activation energy), thus accelerating the overall rate of reaction.

Owing to their complex 3-dimensional proteinaceous structures, enzymes are capable of exhibiting remarkable specificity for their molecular substrates, including

chemo/stereoselectivity, enantiomeric and regioselectivity. To account for this speficity, a number of binding models have been proposed. The simplest 'lock-and-key' model assumes that the enzyme's active site is a rigid, static structure, to which only one complementary substrate structure may fit. However, this model has been proven to be largely oversimplified. Indeed, the majority of enzyme active sites actively undergo alteration in protein geometry upon substrate binding. In such cases, the conformation of the substrate is altered such that it more closely resembles the transition state. In this 'induced fit' model, the substrate distortion may facilitate its conversion to the transition state via the weakening of critical bonds, and stabilisation via tight-binding to the enzyme.[2]

5.2.2. Enzyme Kinetics

The study of enzyme kinetics concerns the rate of product formation over time as a function of enzyme and substrate concentration under specific, predefined conditions. Such investigations facilitate the calculation of key parameters related to product turnover, thus allowing quantifiable determination of enzyme activity.

5.2.2.1. The Michaelis Menten Model

The binding of an enzyme [E] to a substrate [S], forms a complex [ES], which in turn releases a product [P], regenerating the original enzyme. The generalised reaction scheme for enzyme-catalysed product formation may be expressed as:

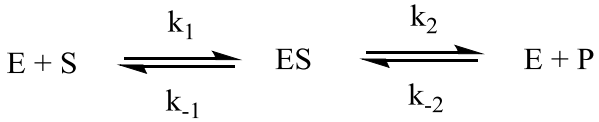

Scheme 1: General form of a single-substrate enzyme-catalysed reaction. Rate constants for each step are represented by k_1, k_{-1}, k_2, and k_{-2}.

In 1913, Leonor Michaelis and Maud Menten postulated that the formation of the enzyme-substrate complex was almost instantaneous, and the rate of reaction was proportional to the concentration of this complex.[3] Thus, the kinetic consideration can be restricted to the initial period of the reaction. Under these conditions, the reaction simplifies to:

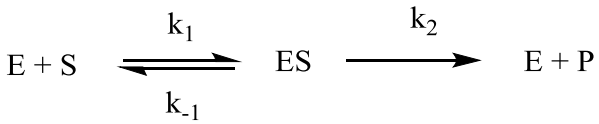

Scheme 2: Single-substrate enzyme-catalysed reaction under conditions considering initial rate. Since [P] = 0, k_{-2} is considered negligible.

The general expression for the rate (ν) of this reaction may be described as:

$$\nu = \frac{d[P]}{dt} = k_2[ES] \quad (1)$$

The overall rate of production of ES equates to the difference between the rates of the elementary reactions leading to its appearance and disappearance:

$$\frac{d[ES]}{dt} = k_1[E][S] - k_{-1}[ES] - k_2[ES] \quad (2)$$

Equation 2 cannot be explicitly integrated without two simplifying assumptions:

1. **Assumption of equilibrium.** Since $k_{-1} >> k_2$, the first step of the reaction may reach equilibrium:

$$K_s = \frac{k_{-1}}{k_1} = \frac{[E][S]}{[ES]} \quad (3)$$

Where K_s is the dissociation constant of the first step of the enzymatic reaction.

2. **Assumption of the steady state.** First proposed by Briggs and Haldane,[4] the so called 'steady state' assumption states that the concentration of [ES] remains constant, as the rate of formation of the complex is equal to its rate of breakdown:

$$\frac{d[ES]}{dt} = 0 \quad (4)$$

Kinetic expressions for overall reactions must be formulated in terms of experimentally measurable quantities. Whilst the quantities [ES] and [E] are not generally directly measurable (since [E] refers to active sites), the total enzyme concentration [E_0] is usually readily determined:

$$[E_0] = [E] + [ES] \quad (5)$$

The rate equation for the enzymatic reaction is then derived as follows. Combining (2) with the steady state assumption (4) and the conservation condition (5), yields:

$$k_1([E]_0 - [ES])[S] = (k_{-1} + k_2)[ES] \quad (6)$$

Which, on rearrangement becomes:

$$[ES](k_{-1} + k_2 + k_1[S]) = k_1[E]_0[S] \quad (7)$$

Dividing both sides by k_1 and solving for [ES]:

$$[ES] = \frac{[E]_0[S]}{K_M + [S]} \quad (8)$$

Where K_M is known as the Michaelis constant and is defined:

$$K_M = \frac{k_{-1} + k_2}{k_1} \quad (9)$$

The initial rate (Equation 1) may then be expressed in terms of the experimentally measurable quantities $[E]_0$ and [S]:

$$\nu_0 = \left(\frac{d[P]}{dt}\right) = k_2[ES] = \frac{k_2[E]_0[S]}{K_M + [S]} \quad (10)$$

The use of initial velocity (experimentally defined as the measured velocity before more than ~10% of the substrate is converted to product) minimizes complicating factors such as the effects of reversible reaction, inhibition of the enzyme by the product, and progressive inactivation of the enzyme.

The maximal velocity of a reaction (V_{max}), occurs at high substrate concentrations when the enzyme is saturated, thus existing purely in the form of ES:

$$V_{max} = k_2[E]_0 \quad (11)$$

Therefore, combining Equations (10) and (11) yields:

$$\nu_0 = \frac{V_{max}[S]}{K_M + [S]} \quad (12)$$

This expression, the Michaelis Menten equation, is considered the fundamental equation of enzyme kinetics.

5.2.2.2. The Significance of the Michaelis Menten Constants

The Michaelis Menten equation is applicable to most enzymes, and is of critical importance in the understanding of enzyme action in biological systems. The parameters K_M and V_{max} are determined by measuring reaction velocity at varying concentrations of substrate.

Whilst V_{max} is not an intrinsic property of the enzyme, it may be obtained via various extrapolation techniques, and demonstrates the maximal velocity of a given enzyme under predefined conditions. In contrast to V_{max}, the parameter K_M is an intrinsic property of the enzyme, and has a simple operational definition. K_M is the substrate concentration at which the reaction velocity is half-maximal (the magnitude of which is highly dependent on the nature of the enzyme and substrate, and behaves as a function of temperature and pH). Therefore, if an enzyme has a small value of K_M, it achieves maximal catalytic efficiency at low substrate concentrations. Provided that the assumption $k_2 < k_1$ remains true, K_M provides an inverse measure of the enzyme's affinity for its substrate- where a high K_M indicates a low affinity, and vice versa.[5]

5.2.2.3. Sigmoidal Kinetics

Sigmoidal kinetic profiles are the result of enzymes that demonstrate positive cooperative binding. The term cooperativity refers to the observation that the binding of the substrate at one site affects the affinity of other sites for their substrates. The resultant sigmoid saturation curve (unlike the rectangular hyperbola traced by the Michaelis Menten equation) is described by the Hill equation, and accounts for allosteric binding sites other than the active site:[6]

$$\nu = \frac{V_{max}[S]^h}{K + S^h} \tag{13}$$

Where *h* is the Hill coefficient, widely used as a measure of cooperativity. If an enzyme exhibits no cooperativity, *h* = 1. A value of *h* greater than 1 implies positive cooperativity, where initial binding facilitates subsequent binding . The constant K is analogous to K_M of the Michaelis Menten model, although only represents an approximation, since neither substrate can fully saturate the enzyme. Since the obtained values of K_M and V_{max} obtained in this matter are approximate, they are generally referred to as 'apparent' K_M and V_{max} values.[7]

5.2.3. Enzyme Inhibition

Substances that reduce the activity of an enzyme-catalysed reaction are known as inhibitors. Inhibitory action of such molecules may occur either by directly or indirectly influencing the catalytic properties of the active site. The design, synthesis, characterisation and exploration of the potency and spectrum of biologically active enzyme inhibitors has become an area of great interest in recent years, particularly in the fields of medicinal and pharmacological research.

The activity of an enzyme may be influenced by nonspecific factors (e.g. temperature and pH), owing to their inherent sensitivity. Alternatively, specific molecules may reduce or inhibit the catalytic activity of the enzyme via binding to the active site, blocking the entry of the substrate to the site, or inducing a conformational change within the enzyme structure that prevents the admission of the substrate to the active site.[8] Based on the mechanism of interaction with the enzyme, inhibitor binding may be classified as either reversible or irreversible (Figure 5.3).

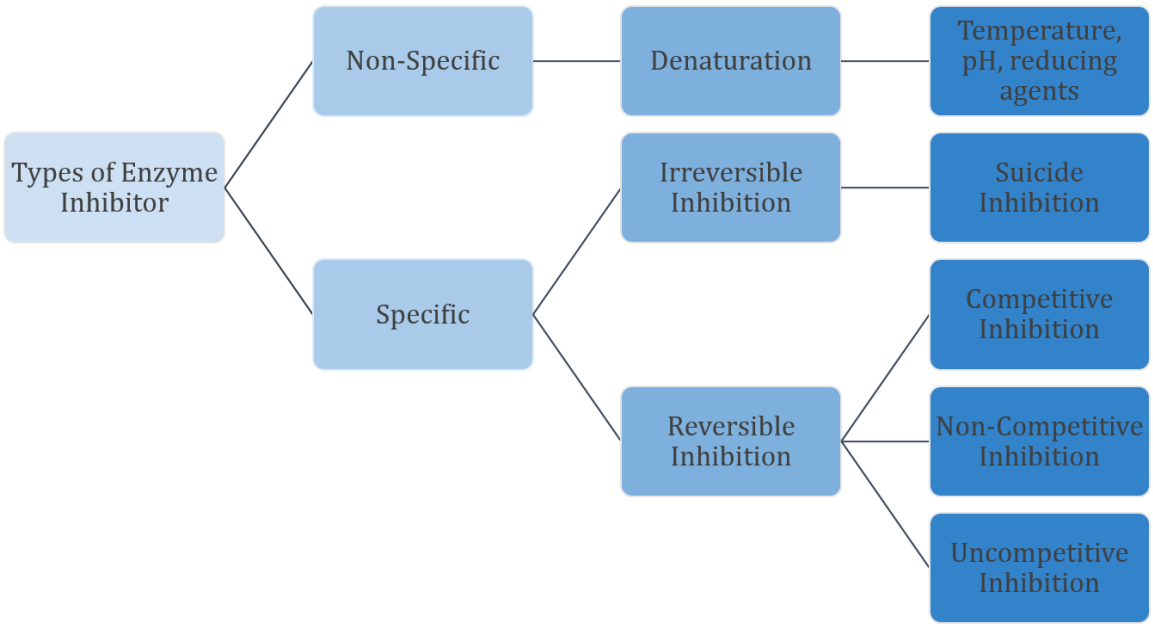

Figure 5.3: General classification of enzyme inhibitors.

Generally, reversible inhibitors form non-covalent interactions with various parts of the enzyme surface, which may be easily reversed by dilution or dialysis. In contrast, irreversible inhibitors covalently interact with surface functional groups, forming strong bonds that may persist even during complete protein degradation.[9]

5.2.3.1. Reversible Inhibitors

Reversible inhibitors may be classed as competitive, uncompetitive or non-competitive, employing non-covalent interactions such as hydrogen bonding, hydrophobic interactions and ionic bonding to disrupt enzyme activity. Different variations of reversible inhibition affect the Michaelis Menten constants differently and thus are distinguished by the relationship between the velocities of the inhibited and uninhibited reactions.[9] General forms of the three canonical modes on enzymatic inhibition are shown in Figure 5.4.

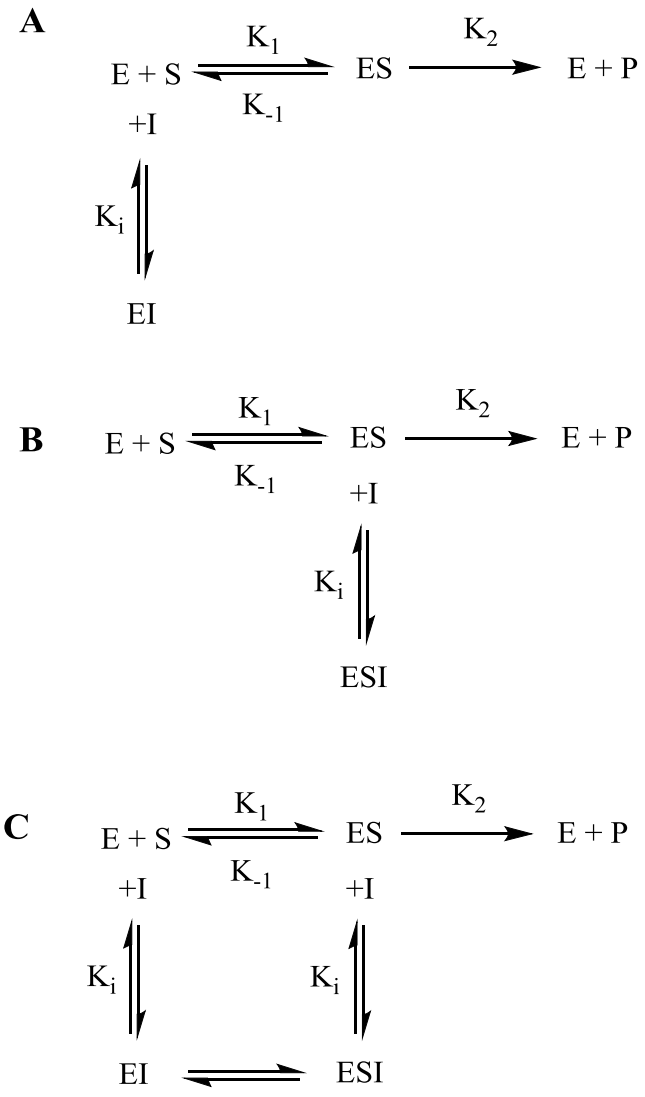

Figure 5.4: General forms of reversible enzyme inhibition. A) Competitive, B) uncompetitive , and C) non-competitive inhibition. The inhibition constant (K_i) governs transitions between the different binding states: free enzyme (E), enzyme-substrate complex (ES), enzyme-inhibitor complex (EI), and enzyme-substrate-inhibitor complex (ESI). The enzyme + product (E + P) state represents the end of the enzymatic turnover cycle.

The enzyme-inhibitor dissociation constant, K_i, is analogous to K_M for uninhibited reactions, and reflects the binding affinity of the inhibitor for a particular enzyme. Experimentally, the K_i may be defined as the inhibitor concentration at which half-maximal inhibition is observed.

I. Competitive Inhibition

Competitive inhibitors are structurally related to the substrate, and bind reversibly to the active site. Occupation of the active site by the inhibitor is mutually exclusive with the substrate, hence both inhibitor and substrate are in direct competition. Since the reaction rate is directly proportional to [ES], reduction in [ES] concentration to account for formation of [EI] lowers the catalytic efficiency. Consequently, rate reduction is directly proportional to inhibitor concentration; increasing substrate concentration towards saturation alleviates competitive inhibition.

Kinetically, formation of the catalytically inactive [EI] reduces the availability of free enzyme for substrate binding. Thus, the K_M of the reaction is increased, whilst the turnover number (V_{max}) remains unchanged. This may be shown mathematically by modifying the standard Michaelis Menten kinetics for competitive inhibition.[10]

From Michaelis Menten kinetics, the steady state assumptions states that:

$$\frac{d[ES]}{dt} = 0 \tag{14}$$

Therefore,

$$k_1[E][S] = (k_{-1} + k_2)[ES] \tag{15}$$

Substituting K_M:

$$[ES] = \frac{[E][S]}{K_M} \tag{16}$$

Similarly, the rate of formation of an enzyme-inhibitor complex will yield:

$$[EI] = \frac{[E][I]}{K_i} \tag{17}$$

The total enzyme concentration in the system is the sum of the concentration of the three forms in which the enzyme exists:

$$[E_0] = [E] + [ES] + [EI] \tag{18}$$

Substituting terms for [ES] (Equation 16) and [EI] (Equation 17):

$$[E_0] = [E]\left(1 + \frac{[S]}{K_M} + \frac{[I]}{K_i}\right) \tag{19}$$

Rearraging (19) for [E], and substituting into (16):

$$[ES] = \frac{[S]}{K_M}\left(\frac{[E_0]}{\left(1 + \frac{[S]}{K_M} + \frac{[I]}{K_i}\right)}\right) \tag{20}$$

Substituting (20) into the rate of product formation (Equation 1) yields the modified rate equation for competitive inhibition:

$$\frac{d[P]}{dt} = \nu_0 = k_2\frac{[S]}{K_M}\left(\frac{[E_0]}{\left(1 + \frac{[S]}{K_M} + \frac{[I]}{K_i}\right)}\right) \tag{21}$$

The apparent Michaelis constant for competitive inhibition is defined as:

$$K_M^{app} = 1 + \frac{[I]}{K_i} \tag{22}$$

Substituting (22) into (21) yields the final form of the rate equation:

$$\nu_0 = \frac{V_{max}[S]}{K_M^{app} + [S]} \tag{23}$$

Hence, the effect of a competitive inhibitor is to increase the apparent value of K_M by the factor $(1+[I]/K_i)$, to reduce that of V_{max}/K_M by the same factor, yet leave V_{max} unchanged.[11]

II. Uncompetitive Inhibition

Uncompetitive inhibition occurs when the inhibitor (which need not be structurally similar to the substrate) is unable to bind to the free enzyme, but instead binds to the pre-formed enzyme-substrate complex. Such action renders the ES complex catalytically inactive, via inducing structural distortion of the active and allosteric sites of the complexed enzyme. Increasing substrate concentration towards saturation is ineffective at reversing uncompetitive inhibition; reversal may only be achieved via dialysis.

Modification of Michaelis Menten kinetics for uncompetitive inhibition may be followed according to the derivation in Section 5.1.3.1.I. Briefly, the total enzyme concentration in the system may be described as the sum of the three forms in which the enzyme exists:

$$[\mathrm{E_0}] = [\mathrm{E}] + [\mathrm{ES}] + [\mathrm{ESI}] \tag{24}$$

Since the expression for the [ES] complex may be defined according to Equation 16, the inactive [ESI] complex may therefore be expressed:

$$[\mathrm{ESI}] = \frac{[\mathrm{ES}][\mathrm{I}]}{[K_i]} \tag{25}$$

$$[\mathrm{ESI}] = \frac{[\mathrm{E}][\mathrm{S}][\mathrm{I}]}{\mathrm{K_i K_M}} \tag{26}$$

The derivation may then be completed as follows:

$$[\mathrm{E_0}] = [\mathrm{E}]\left(1 + \frac{[\mathrm{S}]}{\mathrm{K_M}} + \frac{[\mathrm{I}][\mathrm{S}]}{\mathrm{K_i K_M}}\right) \tag{27}$$

$$[\mathrm{E}] = \left(\frac{[\mathrm{E_0}]}{1 + \frac{[\mathrm{S}]}{\mathrm{K_M}}\left(1 + \frac{[\mathrm{I}]}{\mathrm{K_i}}\right)}\right) \tag{28}$$

$$[\mathrm{ES}] = \frac{[\mathrm{S}]}{\mathrm{K_M}}\left(\frac{[\mathrm{E_0}]}{\left(1 + \frac{[\mathrm{S}]}{\mathrm{K_M}} + \frac{[\mathrm{I}]}{\mathrm{K_i}}\right)}\right) \tag{29}$$

$$\frac{\mathrm{d}[\mathrm{P}]}{\mathrm{dt}} = \nu_0 = \frac{\mathrm{k_2}[\mathrm{E_0}][\mathrm{S}]}{\mathrm{K_M} + [\mathrm{S}]\left(1 + \frac{[\mathrm{I}]}{\mathrm{K_i}}\right)} \tag{30}$$

The apparent maximal velocity for uncompetitive inhibition is defined as:

$$\mathrm{V_{max}^{app}} = \frac{\mathrm{k_2}[\mathrm{E_0}]}{\left(1 + \frac{[\mathrm{I}]}{\mathrm{K_i}}\right)} \tag{31}$$

The apparent Michaelis constant for competitive inhibition is defined according to Equation 22, yielding the overall rate equation for uncompetitive inhibition:

$$\nu_0 = \frac{V_{max}^{app}[S]}{K_M^{app} + [S]} \tag{32}$$

Thus, a decrease in the apparent values of both K_M and V_{max} is observed (V_{max}/K_M is unchanged since the effect is equal on both parameters). The seeming increase in affinity of the enzyme for its substrate (i.e. a decrease in K_M^{app}) is owing to unproductive substrate binding, resulting in a decrease in free enzyme concentration.[12]

III. Non-Competitive Inhibition

In situations of non-competitive inhibition, the binding of the inhibitor reduces enzyme activity, but does not affect the binding of the substrate. This is achieved via the binding of the inhibitor to sites other than the active site, known as allosteric sites. Hence, the degree of inhibition is dependent only on the concentration of the inhibitor, and the relative rates of substrate and inhibitor binding are independent of each other. Since binding occurs at an allosteric site, non-competitive inhibitors have identical affinities for both free [E] and [ES] complexes. The total enzyme concentration may now be expressed in as four individual contributing states:

$$[E_0] = [E] + [ES] + [ESI] + [EI] \tag{33}$$

Thus the derivation may be completed as follows:

$$[E_0] = [E]\left(1 + \frac{[S]}{K_M} + \frac{[I]}{K_i}\frac{[S]}{K_M} + \frac{[I]}{K_i}\right) \tag{34}$$

$$[E] = \left(\frac{[E_0]}{\left(1 + \frac{[S]}{K_M}\right)\left(1 + \frac{[I]}{K_I}\right)}\right) \tag{35}$$

$$\frac{d[P]}{dt} = \nu_0 = \frac{k_2[E_0][S]}{(K_M + [S])\left(1 + \frac{[I]}{K_i}\right)} \tag{36}$$

Yielding the overall rate law for non-competitive inhibition:

$$\nu_0 = \frac{V_{max}^{app}[S]}{K_M + [S]} \tag{37}$$

Thus, non-competitive inhibition reveals an unaltered K_M but a reduced V_{max}, since the enzyme is rendered enzymatically hindered, yet the binding affinity for the substrate is unaffected. [5,13]

5.2.3.2. Irreversible Inhibition

Compounds that interact with the enzyme in such a way to cause permanent loss of function are known as irreversible inhibitors. Formation of highly stable covalent bonds (generally with active site residues) are able to render the enzyme inactive even in trace concentrations. Thus, such inhibitors are often referred to as 'catalytic poisons'.[9]

Irreversible inhibitors are generally of limited use in human medicine, as many such compounds behave as potent toxins. For example, organophosphorus compounds including diisopropyl fluorophosphate (DFP) inhibit acetylcholinesterase activity via covalent interaction with a serine residue of the active site. The physiological manifestation of this inactivation is interference with the neurotransmitter activation at nerve synapses, resulting in the constant propagation of nerve impulses. DFP was originally evaluated by the British as a chemical warfare agent during World War Two, and modified versions of this compound have recently been widely exploited as organophosphate pesticides.[14]

A subset of irreversible inhibitors, known as 'suicide inhibitors' provide useful information on the binding location and composition of the active site. Suicide inhbitors become activated by the first intermediary steps of the biochemical transformation upon binding with the active site, in the same manner as the true substrate. However, the irreversible binding process prevents the release of product, thus inactivating the enzyme. Kinetically, the binding of suicide inhibitors reduces the possible concentration of [ES] complex, although the reimaining unbound molecules remain functional in terms of K_M and V_{max}.[15]

5.2.3.3. Enzyme Inhibition in Drug Discovery

In recent years, the increased knowledge of the function of enzymes in signalling pathways has lead to the identification and exploitation of enzymes as medicinal targets. With the improvement of global healthcare and an ageing population in the developed world, the demand and market for novel treatments targeting complex biological malfunctions (such as neurodegeneration, dementia and cancer) is ever-growing. As such, enzyme inhibitory drugs remain prominent throughout medicine, with 47% of all current drugs inhibiting enzymatic targets.[16] Recent multitarget-directed ligand approaches in medicinal chemistry have combined inhibitors of cholinesterases and monoamine oxidases to combat the loss of neurotransmitters in Alzheimer's disease,[17] or with properties such as antioxidant and metal complexation for Parkinson's disease.[18] For cancer treatment, compounds that combine kinase inhibitors, or include cyclooxygenase inhibition (to reduce inflammation) have been

suggested.[19] Structure-based drug design for a single enzyme target has been rendered possible via the use of crystal structures, which enable the computational searches of huge chemical databases to identify lead compounds for refinement. With such large-scale computational approaches readily available, combining suitable pharmacophores for novel enzyme combinations is entirely feasible via high-througput screening. Such compounds may then be synthesised and tested experimentally to confirm predicted inhibitory effects, before progressing to complex systems such as cell and *in vivo* models.[16,20]

Evaluation of novel enzyme inhibitory drugs to target bacterial virulence has been an area of increasing interest in recent years, since the impending antibiotic crisis has caused a resurgence of various alternative anti-infection approaches. Such antivirulence enzyme inhibitors, unlike classic antibiotics, are aimed at disarming pathogens rather than inhibiting growth. Since human pathogens rely on a plethora of enzymatic virulence factors, inactivation of specific aspects of this arsenal will attenuate pathogenicity, potentially rendering them less pestilential or more susceptible to host defences.[21]

Enzymes associated with virulence in *P. mirabilis* have been extensively researched and targeted as an alternative to antibiotic therapy, since systemic antibiotic prophylaxis is not recommended for long-term indwelling catheterisation.[22] Of particular importance to this thesis is the development of a library of *N*-alpha mercaptoamide dipeptide inhibitors, for the inhibiton of the *P. mirabilis* metalloprotease virulence factor ZapA. This 54-kDa secreted metalloprotease possesses a broad specificity and is capable of degrading a wide-range of host defensive proteins including immunoglobulin A (IgA) (one of the few microorganisms able to do so).[23] ZapA is specifically upregulated during swarmer-cell differentiation , thus is known to play a key role in pathogenesis. Carson *et al*.[24] described the synthesis and *in vitro* analysis of a number of inhibitor sequences which display inhibitory activity against ZapA (Figure 5.5).

Screening of the synthesised inhibitor library revealed a preference for large aromatic residues in the R_1 position, and aliphatic residues in the R_2 position. From the library, six compounds were found to exhibit micromolar values of K_i. Since ZapA is known to be critical for colonisation and establishment of infection by *P. mirabilis*, effective inactivation of this enzyme has potential to provide protection to the cognate substances *in vivo* and may represent a putative anti-infective/anti-virulence strategy.

Interestingly, these trends appeared to match those observed during the profiling of the same focused library on the *P. aeruginosa* metalloprotease, LasB. Since *P. aeruginosa* is also a known

uropathogen present during CAUTI, inhibitors of this nature may present an interesting strategy for broad spectrum CAUTI anti-virulence treatment.

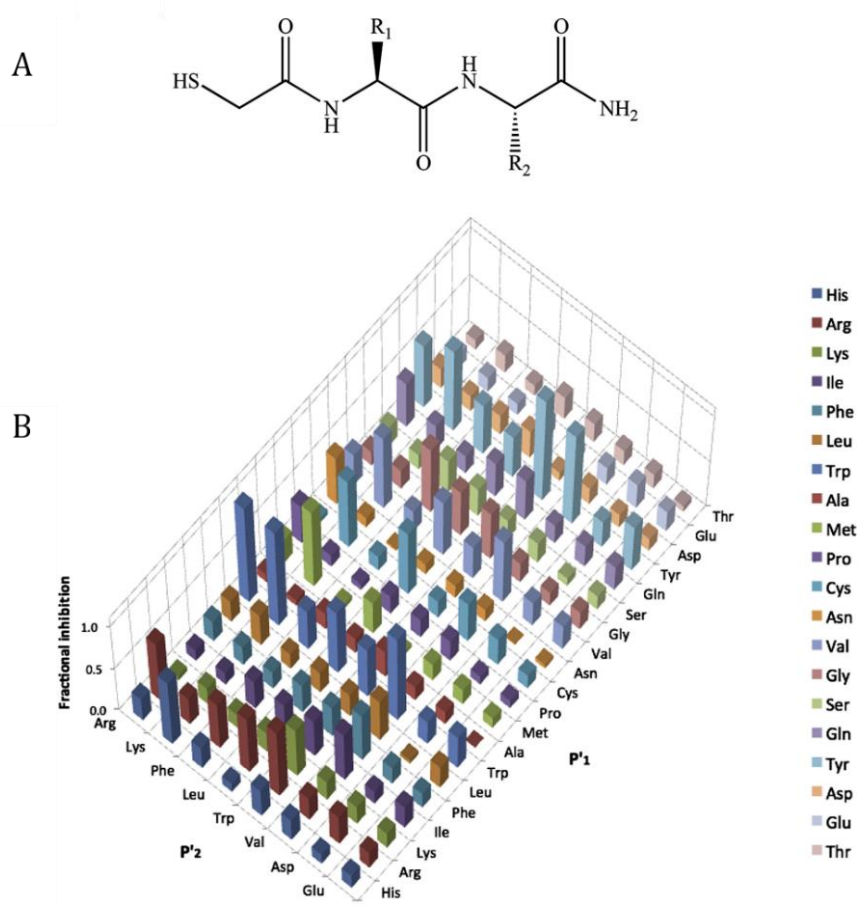

Figure 5.5: A) General structure of the *N*-alpha mercaptoamide dipeptide inhibitor library, according to the dipeptide amino acid sequences. B) Relative potency of indidivdual compounds, displayed as the fractional inhibition of ZapA activity at an inhibitor concentration of 25 μM. Reprinted with permission from Carson *et al*.[22] © 2011, with permission from Elsevier.

5.2.4. Urease

5.2.4.1. Biological Significance

Urease (urea aminohydrolase) is a 250 kDa nickel-dependent metalloenzyme of great biological significance. Found in a wide variety of organisms (including plants, algae, fungi and several prokaryotes), urease catalyses the rapid hydrolytic decomposition of urea, thus playing a vital role in the global nitrogen cycle. Since the hydrolytic processing of urea produces ammonia as a byproduct, expression of urease by human pathogens such as *Proteus,*

Helicobacter, Klebsiella, Pseudomonas and *Mycobacterium* spp. is known to have severe negative consequences on human health.[25]

Urease holds a significant place in twentieth-century science, having played a pivotal role in two fundamental landmarks of biochemistry. In 1926, James Sumner succeeded in isolating and crystallising the urease enzyme from *Canavalia ensiformis* (*C. ensiformis*, jack bean), thus demonstrating for the first time that enzymes are proteinaceous structures.[26] In 1975, the requirement for nickel in urease catalysis was established, providing the first example of the biological essentiality of this metal as an enzymatic cofactor.[27]

Urea is produced in large amounts by vertebrates as the catabolic byproduct of nitrogen-containing compounds. Indeed, humans produce and excrete ca. 10 kg urea per year.[25,28] Considering the long half-life for nonenzymatic urea hydrolysis (which has never been observed experimentally, but is estimated to be ca. 520 years), severe physiological and environmental imbalances would arise in the absence of an efficient enzymatic degradation process. In contrast, the catalysed process has a half-life of a few microseconds, with an efficiency that is 3 x10^{15} times higher than that of the uncatalysed reaction, making urease the most efficient hydrolase known.[29]

5.2.4.2. Structure and Mechanism

The reaction of urea hydrolysis catalysed by urease occurs in two steps: the first, strictly enzymatic step, consists of the hydrolysis of urea to yield ammonia and carbamate, followed by the spontaneous decomposition of carbamate to give a second molecule of ammonia and bicarbonate (Scheme 1, Chapter 1).[30] Urease exhibits typical Michaelis Menten behaviour (with observed values of K_M in the millimolar region), and displays maximal activity in the pH region of 5-9.[31]

The protein architecture for *C. ensiformis* urease is shown in Figure 5.6, which is known to be representative of the majority of bacterial ureases. The quaternary structure is composed of a trimer of trimers of the type $(\alpha\beta\gamma)_3$, where α, β, and γ represent different subunits. The active site is found in the *α* subunit, giving rise to three active sites per biological unit.[32] An important feature, conserved throughout all known ureases, is the conformation of a helix-turn-helix motif within the *α* subunit, flanking the active site cleft. This motif may be found in an open or closed conformation, and plays an important role in modulating the afflux of substrate and efflux of producs to and from the active site during catalysis.[30] The coordination environment of the Ni atoms within the active site consists of two Ni(II) ions, separated by 3.5-3.7 Å, bridged

by the oxygen atoms of a carbamylated lysine residue, and bound to two histidines. The coordination geometry is completed by a terminally bound water molecule, and a bridging hydroxide ion, stabilised by an extensive network of hydrogen bonds.[25,32]

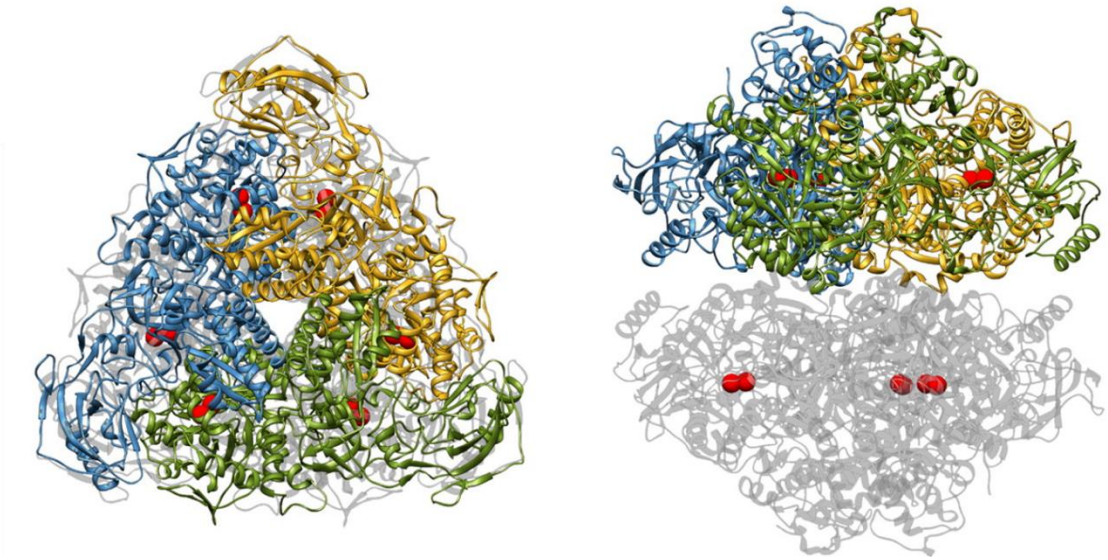

Figure 5.6: Ribbon scheme of the functional oligomer $(\alpha\beta\gamma)_3$ of *C. ensiformis* urease, through the ternary axis (left), and rotated by 90 ° along the horizontal axis (right). Reprinted with permission from Maroney *et al*.[25] © 2014, American Chemical Society.

The reaction mechanism for the enzymatic hydrolysis of urea is shown in Figure 5.7. Upon the entrance of urea into the active site channel (facilitated by the opening of the helix-turn-helix 'flap'), the hydrated state of the enzyme (Figure 5.7A) evolves towards an initial substrate-bound intermediate, where three water molecules bound to Ni(II) are displaced by urea. Urea initially binds the more electrophilic and coodinatively unsaturated metal atom (denoted Ni1) using the carbonyl oxygen of the urea (Figure 5.7B). Flap closure facilitates urea coordination to Ni2 via its amine group, stabilised by a hydrogen-bonding network which holds the substrate in a specific conformation, so that hydrolysis may occur (Figure 5.7C). The nucleophilic attack onto the bridging substrate profoundly modifies the electronic structure, thus increasing the pK_a of the distal urea N atom (not involved in Ni-binding). Thus, the Ni-bridging -OH group (Figure 5.7D) has a pK_a sufficiently low that it may transfer a proton to the distal urea amine group. The stabilisation of the resultant C-NH_3^+ by the catalytic histidine, causes the breakage of the distal C-N bond, subsequently releasing ammonia. The resulting carbamate spontaneously decomposes into ammonia and hydrogen carbonate, and the opening of the active site flap facilitates product release, thus allowing bulk water to rehydrate the active site (Figure 5.7A), regenerating the resting state of the enzyme.[25,30,33,34]

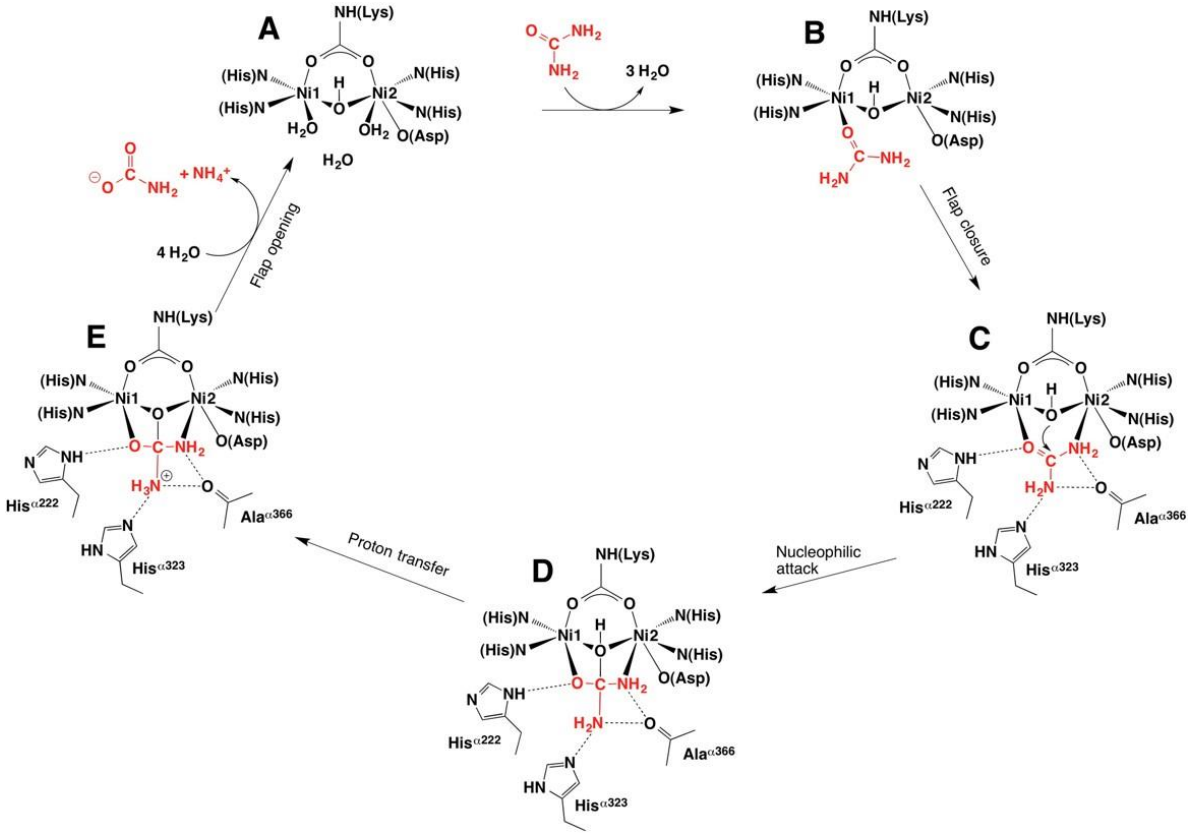

Figure 5.7: Mechanism of the enzymatic hydrolysis of urea. Reprinted with permission from Maroney *et al.*[25] © 2014, American Chemical Society.

5.2.4.3. Role of Urease in CAUTI Pathogenesis

The *P. miraiblis* gene cluster consists of *ureABC*, which encode the apoenzyme structural subunits, and *ureDEFG*, which encode proteins that facilitate insertion of the nickel atoms in to the active site.[35] Positive upregulation of urease is moderated by the polypeptide transcriptional regulator *UreR*, and repressed by the nucleoid-associated protein H-NS. Both *UreR* and H-NS compete for the same regulatory region of upstream of *ureD*, resulting in tight control of urease expression. Successful transcriptional repression of the *ure* operon by H-NS occurs at room temperature, although a transition to physiological temperature and high concentrations of urea alleviate H-NS transcriptional repression, allowing *UreR* to activate urease expression.[36]

During the course of infection, the production of ammonia by urease activity raises the pH within the local environment, thus facilitating the precipitation of the normally soluble polyvalent ions struvite [$MgNH_4PO_4{\cdot}6H_2O$] and carbonate apatite [$Ca_{10}(PO_4)_6CO_3$]. Deposition of these crystalline materials onto the luminal surfaces of the catheters may cause serious clinical consequences as a result of catheter blockage (as discussed in Chapter 1). Furthermore,

ammonia liberated by urease may contribute to urothelial damage, potentially exposing niches for adherence or providing nutrients for bacterial replication.[37]

Assessment of the contribution of urease to *P. mirabilis* virulence in a mouse model of ascending urinary tract infection using a urease-negative mutant (containing a mutation in the *ureC* structural subunit gene), showed that expression of urease is critical for bacterial colonisation within the urinary tract. Transurethral challenge yielded recovery rates from the urine, bladder and kidneys that were significantly lower for the urease-negative strain compared to the wild-type strain.[38] Further evaluation using the same model revealed that the ability of the urease-negative strain to colonise the urinary tract is approximately 100-fold less than the parent strain.[37] Use of the urease mutants in the mouse model of ascending infection unambiguously places urease as a critical virulence factor in *P. mirabilis* infection. Indeed, further studies have revealed that within the catheterised urinary tract, urease is expressed constitutively and plays a continuously active role in pathogenesis and virulence.[39]

5.2.4.4. Urease Inhibitors

Owing to the tremendous medical importance of urease, urease inhibitors with improved stability and low toxicity may be an effective therapy against diseases caused by urease-dependent pathogenic microorganisms. Several classes of molecules have thus far been tested for urease inhibition in medicine and agriculture. In CAUTI, the development of systemic drugs displaying antiureolytic activity may provide a promising prophylactic treatment, without placing a significant selective pressure on colonies of pathogenic *P. mirabilis*.

I. Thiols

Thiols, particularly β-mercaptoethanol, are of historic importance as urease inhibitors, since they helped to reveal crucial information about the active site of *C. ensiformis* urease in 1980.[30] Thiols inhibit urease with a competitive mechanism in their thiolate anion form RS-, which bridges the two Ni(II) atoms in the urease active site and chelates the metal centre with the alcoholic group interacting with Ni1 (further stabilised by a hydrogen bond with the carbonyl oxygen of the conserved αGly280). Additionally, a second molecule of β-mercaptoethanol forms a disulphide bond with the conserved αCys322 residue, belonging to the mobile flap. The subsequent formation of hydrogen bonds decreases the flexibility of the flap, preventing access to the active site via steric hinderance.[33] This chelating mode of competitive inhibiton may be inferred for all cases involving thiol-containing small molecule inhibitors.[25] Recent synthesis of a range of substituted thiourea derivatives by Khan *et al.*[40] support the chelating ability of

the inhibitor within the urease active site, displaying half-maximal inhibiton values of 5.53 ± 0.02 – 91.50 ± 0.08 μM.

II. Hydroxamic Acids

Hydroxamic acids have been well characterised for their urease-inhibitory activity since 1962.[41] Acetohydroxamic acid (AHA) (Figure 5.8), the most studied derivative of this group, is well known to act as a slow-binding inhibitor of plant, bacterial and fungal ureases.

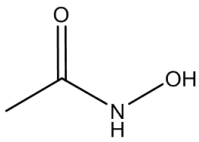

Figure 5.8: Structure of acetohydroxamic acid (AHA).

X-ray crystal structures of AHA with urease from *Sporosarcina pasteurii* have detailed that AHA interacts with the two Ni atoms in the active site. The hydroxamate oxygen atom bridges the two Ni(II) ions, whilst the carbonyl oxygen of the AHA chelates with Ni1. Two hydrogen bonds, between the carbonyl of the AHA and an αHis222 residue, and between the AHA-NH and the αAsp363, stabilise the interaction (Figure 5.9).

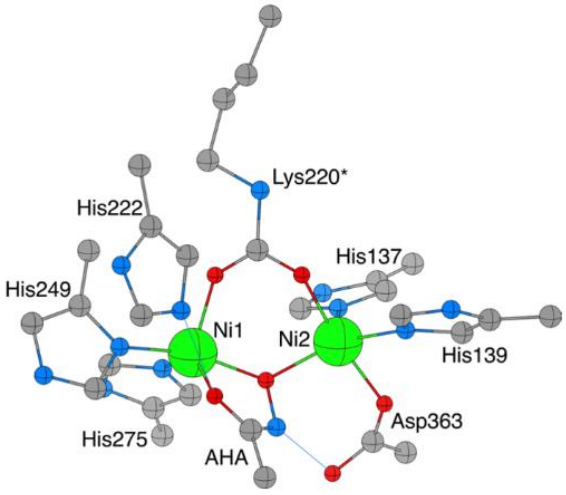

Figure 5.9: Crystallographic structural model of the *Sporosarcina pasturii* urease active site (showing only selected resiudes) in complex with AHA. The nickel atoms are represented in green, nitrogen in blue and oxygen in red. Thin blue lines represent hydrogen bonds. Adapted with permission from Maroney *et al*.[23] © 2014, American Chemical Society.

AHA is thus far the only urease inhibitor to be commercially available for antiureolytic therapy. Having gained FDA approval in 1983 (marketed under the trade name Lithostat in the USA, and

Uronefrex in Europe),[42] it has been extensively used to treat hyperammonemia in cirrhosis of patients infected with the urease-positive bacteria *Helicobacter Pylori*, as well as chronic urea splitting and recurrent urinary tract infection by *P. miraiblis*. However, this compound is known to induce severe side effects, including teratogenesis and haemolytic anaemia, as well as psychoneurological and muscular symptoms.[43] Awareness of such severe mutagenic side effects has made AHA an undesirable therapeutic in recent years, inducing a surge of research into alternative urease inhibitors with less severe toxicological profiles.

Extensive research into alternative groups of potential urease inhibitors, including quinones, polyphenols, heterocyclic compounds, boronic acids, organophosphorus compounds and heavy metals has also been undertaken, and extensively reviewed elsewhere.[25,30,44–46] It is evident from such reviews that the formulation and development of a novel drug to replace AHA as the 'gold-standard' in treating urease-mediated infection will require a balance to be struck between inhibition efficiency and toxicity. Whilst many potential candidates are selected purely on inhibitory performance *in vitro*, the pharmacokinetics and *in vivo* cytotoxicity of the compound must be taken into consideration in the early stages of drug design. Thus, achieving a compromise between systemic biocompatibility and activity may indeed require the progression of less potent candidates over their highly active, yet highly toxic counterparts.

5.3. Materials and Methods

5.3.1. Materials

Methyl thioglycolate, Stuart's Broth (SB), urea, dipotassium hydrogen phosphate, potassium dihydrogen phosphate, phenol red, Triton™ X-100, Dulbecco's Modified Eagle Medium (DMEM), trypsin, foetal calf serum, EDTA, penicillin, streptomycin, T75 culture flasks and urease from *C. ensiformis* (Type III powder, 15,000-50,000 units/g), were purchased from Sigma-Aldrich (Poole, Dorset, UK). CyQUANT™ XTT cell viability assay, methanol and ammonia solution (7 M in methanol) were purchased from Fisher Scientific (Loughborough, UK).

5.3.2. Methods

5.3.2.1. Inhibitor Synthesis

2-Mercaptoacetamide (2-MA) was prepared according to Latli *et al*.[47] Briefly, methyl thioglycolate (3.6 g, 34 mmol) was added to a solution of ammonia in methanol (7.0 M, 45 mL) and stirred at room temperature for 14 hours under a nitrogen atmosphere. The solution was concentrated under reduced pressure to give 3.1 g of a white solid in quantitative yield. Presence of 2-MA was confirmed using spectroscopic methods (^{1}H and ^{13}C nuclear magnetic resonance (NMR), and electrospray ionisation mass spectrometry (ESI-MS)).

5.3.2.2. Enzyme Assays

I. Colourimetric Urease Quantification

The high throughput colourimetric assay for rapid urease quantification was employed for initial enzymatic assays, originally described by Okyay *et al*.[48] The colour change of SB from yellow (absorbance at 430 nm) to pink (absorbance at 560 nm) may be observed in the presence of urease, owing to the presence of urea (20 mg/mL standard) in the broth composition. Absorbance output (560 nm) was observed on a microplate reader (BMG Labtech), using the inbuilt injector system to analyse intial rate of colour change. Uninoculated media was employed as a negative control. All measurements were repeated in triplicate.

II. Enzyme Kinetic Assays

Enzyme kinetic parameters V_{max} and K_M were obtained via the measurement of initial reaction velocities at varying urea concentrations. Since SB contains fixed urea concentration (20 mg/mL), the colourimetric broth was prepared manually according to Table 5.1.

Table 5.1: General components of SB

Compound	Mass (g)
Dipotassium hydrogen phosphate	4.75
Potassium dihydrogen phosphate	4.55
Yeast extract	0.05
Phenol red	5×10^{-3}

Compounds were dissolved in deionised water (500 mL) and sterilised via syringe filtration (pore size 0.22 μm). Urea was manually added to aliquots (20 mL) of the above solution to result in a range of substrate concentrations (1 mM-3 M). Urease concentration was fixed (9 mg/ml in PBS, pH 7.4). Enzyme solution (100 μL) and SB (100 μL) were added in triplicate to a 96-well microplate. SB containing a predefined concentration of urea was added to the injector system, and each triplicate was measured (560 nm) individually to achieve a cycle time of 6 seconds. Each well was measured for a total of 10 cycles (60 seconds), before replacing the SB with a different substrate concentration. The injection needle and associated tubing were rinsed with ethanol (70% in deionised water) between each concentration to avoid substrate accumulation or dilution. To determine kinetic parameters in the presence of inhibitor, the enzyme solution was supplemented with a predefined concentration (10 mM) of 2-MA solution (100 μL dissolved in SB), in place of the standard SB as previously described.

Kinetic curves were also analysed as Dixon plots, to support kinetic models and analyse the 2-MA inhibition mechanism. Dixon plot analysis was performed at 3 different concentrations of urea (1, 5 and 10 mg/mL) and at 5 different concentrations of 2-MA (1, 2.5, 5, 7.5 and 10 mg/mL). The reciprocal of the initial reaction rate was plotted against varying inhibitor concentration to yield information on K_i and inhibition type.

III. Statistical Analysis

Curve-fitting and statistical analyses were performed using GraphPad Prism (version 7, GraphPad Software Inc., San Diego, CA). Kinetic constants were obtained by fitting

experimental data to kinetic models using the nonlinear regression function. The fit of the data for each model was assessed from the SEM, 95% confidence intervals and R^2 values. Both Michaelis Menten and Hill equations were employed as nonlinear fitting models, and resultant kinetic constants were reported as the mean ± SEM of triplicate experiments.

IV. Enzymatic IC_{50} Assays

To calculate the concentration of 2-MA and AHA required to cause half maximal inhibition of urease, standard time-dependent IC_{50} protocols were employed, according to Burt *et al*.[49] Both urea (20 mg/mL, standard SB) and urease (9 mg/mL in PBS) concentrations were kept constant, whilst inhibitor concentrations were varied (0-900 mM in PBS) to assess the degree of yellow-pink colour change upon incubation for a predetermined time period (10 minutes). Inhibitor solution (100 μL) was added to urease solution (100 μL) in a 96-well microplate, before the addition of SB (100 μL) using the plate reader injector system. Inhibiton of enzyme activity was monitored (560 nm) for 1 hour (60 second cycle time for 60 cycles). Enzyme response in the absence of inhibitor was defined as the 0% inhibition (MAX), and SB in the absence of enzyme was defined as the maximum inhibition (MIN). Thus, % inhibition of each inhibitor concentration (X) was calculated according to Equation 38.

$$\% \text{ Inhibition} = 100 \times \left[\frac{1 - (\text{X} - \text{MIN})}{(\text{MAX} - \text{MIN})}\right] \tag{38}$$

The calculation of % inhibition at the 10 minute time point was selected to give optimum distribution of data points both above and below the IC_{50}. The data were fit to sigmoidal dose-response curves, and values of IC_{50} extracted using nonlinear regression.

5.3.2.3. Biological Evaluation

General bacterial culture and quantification protocols were followed according to Chapter 2.

I. Urease Quantification in Bacterial Culture

The concentration of cytoplasmic urease within bacterial cultures was estimated via the measurement of the rate of colour change of SB upon incubation with actively growing cells of *P. mirabilis* B4 and *E. coli* NSM59.

A standard curve of rate of SB colour change with varying urease concentration was produced in order to quatify the rate of colour change in the live bacterial culture. Standard urease solutions were prepared via serial dilution from stock (20 mg/mL in PBS), to give a range of concentrations from 3-12 mg/mL. The plate reader injector system was used to add SB (100 μL) to enzyme solution (100 μL), and the colourimetric response measured at 560 nm (cycle time 16 seconds, 450 cycles). Each urease concentration was reproduced in triplicate.

Overnight cultures of *P. mirabilis* B4 and *E. coli* NSM59 were centrifuged (4,000 rpm, 15 minutes) and the supernatants discarded. Pellets were resuspended in SB (5 mL) and incubated (37 °C) with agitation (200 rpm) throughout the course of the experiment. The rate of colour change of SB was recorded every minute for 20 mintues. For each measurement, test culture aliquots (500 μL) were syringe filtered (0.22 μm pore size) to remove bacterial cells, and the absorbance measured at 560 nm in triplicate. Cultures of *E. coli* were employed as urease-negative controls.

II. Determination of *In Vitro* Susceptibility

In vitro susceptibility of inhibitors 2-MA and AHA were determined using the microbroth dilution method. Stock solutions of the inhibitor to be evaluated were made up to twice the starting concentration required (200 mM), to account for for plate dilutions. Overnight bacterial cultures were subcultured (1:1000 in LB). To a 96-well microplate, LB (100 μL) was added to columns 2-12, and inhibitor stock solution to columns 1 and 2. Inhibitor solution was serial diluted (100 μL each time) across the plate to column 10, to create a gradient of inhibitor concentrations from 10-100 mM. Columns 11 and 12 were revserved for controls in the absence of inhibitor and bacteria, respectively. To each well (except column 12) was added bacterial subculture (100 μL), and the plate incubated overnight (37 °C). Affect on bacterial growth was assessed as a function of OD at 600 nm.

III. Whole-Cell Evaluation

To evaluate the ability of inhibitors to cross the bacterial cell membrane and inhibito urease *in vivo*, without altering the viability of cells, changes in culture pH and viable cell count were monitored in the presence of 2-MA and AHA. Overnight cultures of *P. miraiblis* B4 and *E. coli* NSM59 were prepared according to 5.2.2.3.I and assessed at the start (0 minutes) and end (90 minutes) of the experiment for media pH and CFU/mL.

IV. *In Vitro* Bladder Models

The ability of 2-MA to extend catheter lifespan via *in vivo* inhibition of *P. mirabilis* urease was evaluated within a physiologically representative model of the catheterised urinary tract. Bladder models were assembled and operated according to Chapter 2. Inhibitory drugs were dissolved in urine reservoirs (2 x 5 L, 10 mM per reservoir) to replicate drug excretion following oral administration. Models simulating late-stage infection were inoculated with *P. miraiblis* B4 and *E. coli* NSM59 (10^8 CFU/mL), and supplied with artificial urine media containing drug at a constant flow rate of 0.75 mL/min. Quantification of CFU/mL and residual urine pH was performed at periodic intervals throughout the experiments. Time to blockage of inoculated catheters treated with 2-MA was compared to those treated with AHA, and those without treatment as a positive blockage control.

V. Crystal Violet Biofilm Analysis

Biofilm inhibitory activity of 2-MA and AHA was assessed using crystal violet biofilm staining, as described in Chapter 4. Briefly, biofilms of *P. mirabilis* B4 were incubated statically for 24 hours with various concentrations of inhibitor (1, 2.5, 5, 7.5, 10 and 15 mM) to assess the inhibition of biofilm growth *in vitro*. Stained biofilms were assessed for biofilm formation via measurement of optical density at 595 nm. Positive and negative controls were performed, in the absence of inhibitor and bacteria, respectively.

VI. Mammalian Cell Culture Conditions

Spotaneously transformed aneuploid immortal keratinocytes (HaCaTs) were resuscitated from frozen stocks (liquid N_2) in DMEM supplemented with foetal calf serum (10%) and antibiotics (1% penicillin-streptomycin), and cultured in a controlled atmosphere (5% CO_2, 37 °C). The adherent cells were routinely passaged in T75 culture flasks every 2-3 days, or when cells reached 70-80% confluency (low passage number cell lines were used for experimental analysis). HaCaT cells were detached via pre-washing with PBS containing EDTA (1 mM, 10 mL, incubated for 12 mintues in order to chelate divalent cations), followed by trypsinisation (0.25%, 3-4 minutes). Cells were resuspended in fresh medium, counted using a haemocytometer/ inverted microscope, and the cell solution diluted appropriately (DMEM) to acheieve ~5 $x10^3$ cells per well. Cells were seeded in triplicate into a 96-well microplate (200 µL) and incubated overnight to form sub-confluent monolayers.

VII. XTT Cell Viability Assay

After 24 hours incubation, cells were treated with increasing concentrations of inhibitor drug solutions. Half of the incubated media (100 µL) was removed and replaced with filter sterilised drug solution (100 µL in PBS) at concentrations 80, 40, 20, 10, 5, 2.5, 1.25, and 0.625 mM to assess concentration-dependent cytotoxicity. After overnight incubation with the drug, cells were washed (3x PBS, 200 µL) to remove residual drug, and cell proliferation was assessed using a standard 2,3-*bis*[2-methoxy-4-nitro-5-sulphophenyl]-*2H*-tetrazolium-5-carboxanilide inner salt (XTT) assay kit (CyQUANT™). This test is based on the cleavage of the yellow XTT salt by ubiquitous dehydrogenases, leading to the formation of an orange formazan dye. The intensity of the observed dye is commensurate to the number of metabolically active cells in the sample. XTT reagent was freshly prepared according to manufacturer's instructions: XTT-labelling reagent and electron coupling reagent were mixed in a ratio of 50:1, and added to each well of the 96-well plate (50 µL), with fresh DMEM media (not containing phenol red, 100 µL). Plates were incubated for 4 hours (37 °C, 5% CO_2 in a humidified atmosphere), and assessed after incubation. Quantification of cell cytotoxicity was performed in a microplate reader (450 nm). The cytotoxic effect of treatment was expressed as the % viability compared to untreated cells, according to Equation 39.

$$\% \text{ Cell Viability} = \frac{\text{Corrected absorbance of sample cells}}{\text{Corrected absorbance of untreated cells}} \times 100 \qquad (39)$$

Where background correction was undertaken according to the blank (media only) value. Cells treated with Triton X-100 (20% v/v) were used as a positive control for cytotoxic effects. All tested concentrations and controls were reproduced in triplicate.

VIII. *Ex Vivo* Haemolysis Assay

Whole blood (25 mL) was obtained from an anonymous human donor, drawn directly into lithium heparin-coated Vacutainer tubes to prevent coagulation. Blood was centrifuged (2,000 rpm, 10 minutes), and levels of haematocrit (red, lower layer), and plasma (yellow, upper layer) were marked on the tube. The plasma layer was carefully aspirated and discarded, whilst the haematocrit tube was filled to the marked line with sterile saline solution (150 mM NaCl, autoclaved to sterilise). Blood cells were washed a total of 3 times (centrifugation, aspiration of supernatant and replacement with fresh saline solution). The pellet containing red blood cells was resuspended in sterile PBS (pH 7.4) and divided into Eppendorf tubes (500 µL). Aliquots were centrifuged (2,000 rpm, 10 minutes), and the supernatant replaced with filter

sterilised drug solution (pore size 0.22 μm) at varying concentrations (500 μL, 40, 20, 10, 5, 2.5, 1.25, 0.625 mM, made up to double the required concentration to account for dilution in the erythrocyte solution). Cells were incubated with inhibitor drugs for 30 minutes (37 °C, with agitation) before being centrifuged (2,000 rpm, 10 mintues), and the supernatant removed to measure the absorbance of liberated haemoglobin at 410 nm. Total lysis of the erythrocyte suspension was obtained via treatment of cells with Triton X-100 (20% v/v). Degree of haemolysis was expressed as % haemolysis, relative to the spontaneous lysis controls (Equation 40).

$$\% \text{ Haemolysis} = \frac{\text{Corrected absorbance of sample cells}}{\text{Corrected absorbance of lysed cells}} \times 100 \qquad (40)$$

Values were background corrected according to the average blank (PBS only) value. Results from each concentration of tested drug were reproduced in triplicate.

5.4. Results and Discussion

Conventional and alternative antimicrobial therapies which kill or impair the growth of bacteria exert strong selective pressure for the development and maintenance of resistance. By contrast, a drug that inhibits microbial virulence without inhibiting growth generates minimal selective pressure, whilst significantly easing the risk of virulence-based morbidity. Bacterial enzymes offer a potential target for the suppression of virulence, since they play a key role in pathogenicity and biochemical fitness. The research presented in this chapter describes the formulation and *in vitro* analysis of a novel small-molecule drug, capable of inhibiting urease expressed by uropathogenic *P. mirabilis*, thus preventing encrustation and blockage of urinary catheters.

5.4.1. Inhibitor Design

Urease as a potential target for antimicrobial drugs has received considerable attention, given its versatile role in microbial infection, particularly CAUTI. However, development of effective urease inhibitors has proved a significant challenge owing to the deeply buried active site and highly specific substrate preference of bacterial urease.[50]

Design of the small-molecule inhibitor described in this chapter was developed following the *N*-alpha mercaptoamide dipeptide inhibitor library described in Section 5.1.3.3 by Carson *et al*.[24], which showed *in vitro* success in inhibiting the extracellular *P. mirabilis* protease ZapA. Inhibitors containing Gly-Gly and Gly-Val in the R_1 and R_2 positions, respectively, showed negligible activity against urease (unpublished observations; data not shown), likely owing to the narrow and prohibitively inaccessible nature of the urease active site.[51,52] Thus, a design was proposed whereby the bulky, peptide-containing regions of the inhibitor were eliminated, leaving only the thiol-containing amide 'warhead' of the molecule (Figure 5.10). The conserved thiol moiety of the inhibitor shows structural potential for the inhibiton of bacterial urease as it represents a structural analogue of urea. Since urease displays high substrate specificity, the active site is only capable of binding molecules that are chemically analogous to urea with binding mode that resembles that of the native enzyme-substrate complex.

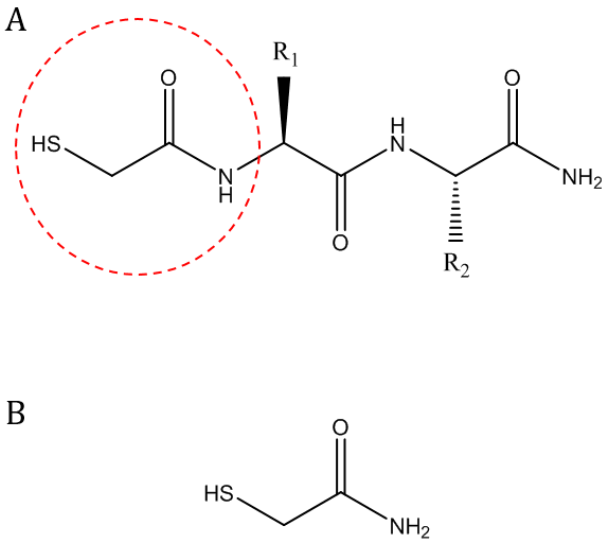

Figure 5.10: General molecular structure of the original *N*-alpha mercaptoamide dipeptide inhibitor (A), designed to inhibit the extracellular metalloprotease ZapA, excreted by *P. mirabilis*. The thiol-containing 'warhead' of this molecule (red circle) was isolated as a potential inhibitor for the urease enzyme. The molecular structure of the resultant 2-mercaptoacetamide (2-MA) inhibitor (B), shows structural similarities to the native substrate of the enzyme, as well as containing an enzymatically active thiol group.

Furthermore, the proposed 2-MA inhibitor contains a thiol (SH) group, which are known to display active inhibition of the urease enzyme (as discussed in Section 5.1.4.4.I). Indeed, the compound diallyl thiosulphate (commonly known as allicin, the main biologically active component of garlic), has been shown to act as a powerful natural inhibitor of urease from both *C. ensiformis* and *P. mirabilis*.[53,54] Inactivation of urease by allicin takes place in the active site of the enzyme, as a result of SH-group modification (analogous to other thiol-containing compounds). Modification of the active site structure interferes with flap-closure, thus significantly reducing the activity of the enzyme.[53]

Synthesis of 2-MA yielded a highly water-soluble white powder in a quantitative yield. Details of synthesis and characterisation of 2-MA are shown in Appendix 1.

5.4.2. Quantification of Urease Activity

The research presented in this chapter utilises a high throughput, quantitative, colourimetric assay to determine the activity and inhibition of urease from both *C. ensiformis* and *P. mirabilis*.[48] This method utilises Stuart's broth (SB), since it is commonly used to distinguish urease-positive from urease-negative bacteria via a clear and unambiguous colour change. SB contains the pH-sensitive indicator phenol red, thus the alkalinisation of residual media following urea hydrolysis induces a colour change from yellow to pink in the presence of urease. Figure 5.11 presents a visual and graphical representation of the urease-induced colour change of SB. Upon incubation with exponential-phase *P. mirabilis* B4, the pink colour of the phenol red indicator is clearly visible. By contrast, equivalent incubation with the urease-negative uropathogenic strain *E. coli* NSM59 does not yield a colour change, since the pH of the media remains within the acidic/neutral region (pH 6.8 ± 0.2 at 25 °C).

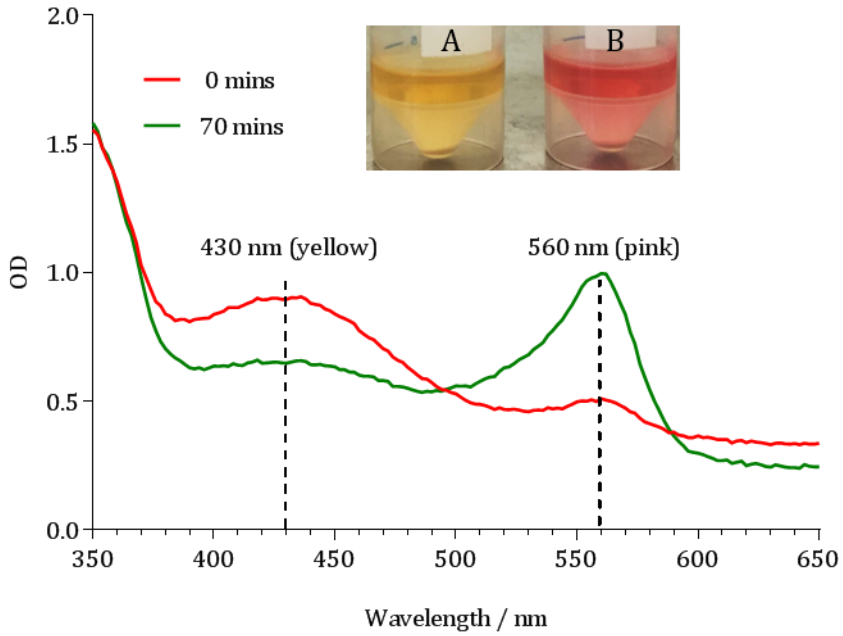

Figure 5.11: Spectral scan of Stuart's Broth (SB) during incubation with *P. mirabilis* B4. At time 0 (red line), the absence of urease activity manifests as a yellow colour, absorbing at 430 nm. After incubation for 70 minutes (green line), the increase pH of residual SB as a consequence of urea hydrolysis causes a pink colour change, with the corresponsing absorbance peak at 560 nm. Inset: Distinction of urease-positive and –negative uropathogenic species by SB. A) *E. coli* NSM59 (urease-negative). B) *P. mirabilis* B4 (urease-positive).

At time 0, a peak at OD_{430} was apparent, owing to the yellow colour of the broth (corresponding to no urease activity). During incubation, the peak at 430 nm decreased as the peak at 560 nm

(corresponding to urea hydrolysis by urease) appeared for the urease-positive organism. Quantification of urease activity is facilitated by monitoring the appearance of the absorbance peak at 560 nm, the rate of which corresponds directly to the concentration of active enzyme.

Owing to the intracellular, cytoplasmic location of bacterial ureases, the isolation and purification of these enzymes is highly technical, time-consuming, and largely unproductive. Therefore, plant ureases (such as urease from *C. ensiformis*) are frequently used as a proof-of-concept model for novel inhibitor compounds before assessment in pathogenic bacteria. Since ureases from both *C. ensiformis* and *P. mirabilis* has been found to display significant amino acid similarities (suggesting an evolutionary relationship),[55] urease from *C. ensiformis* was used to evaluate initial inhibition by 2-MA, as well well estimation of enzyme kinetic parameters.

5.4.3. Quantification of *P. mirabilis* Urease

Calculation of urease concentration in live cultures of *P. mirabilis* B4 was undertaken, in order to estimate the concentration of urease to be used in initial kinetic *C. ensiformis* assays. This estimate will define the standard enzyme concentration to be used in subsequent Michaelis Menten and initial 2-MA inhibition studies.

A standard curve was produced to quantify the initial rate of SB colour change in response to urea hydrolysis by *C. ensiformis* urease (Figure 5.12).

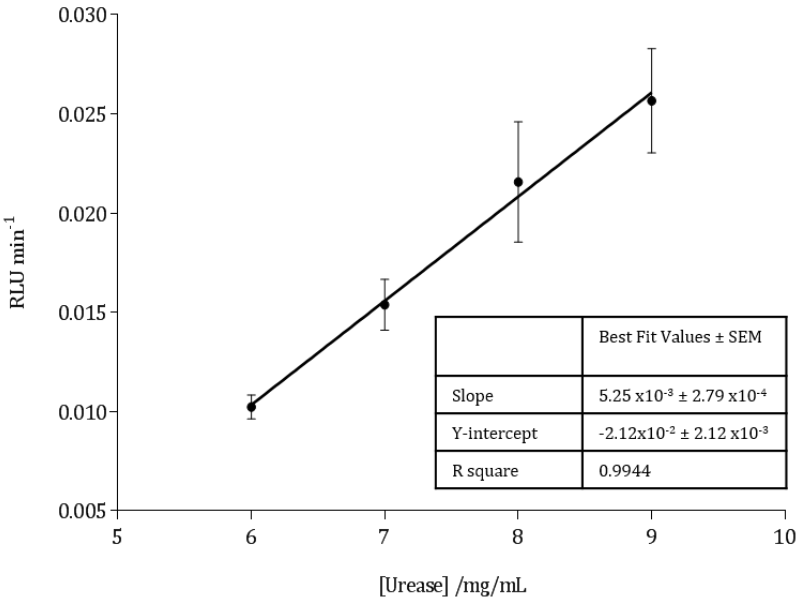

Figure 5.12: Standard curve showing rate (relative light units (RLU)/min^{-1}) of SB colour change with increasing *C. ensiformis* urease concentration. Rate of enzyme activity was monitored as a function of OD at 560 nm over a 5 minute period.

The standard curve demonstrated a linear correlation between change in absorbance at 560 nm, and urease concentration. From this graph, it was possible to estimate the concentration of bacterial urease within a *P. mirabilis* B4 subculture. The rate of SB colour change was

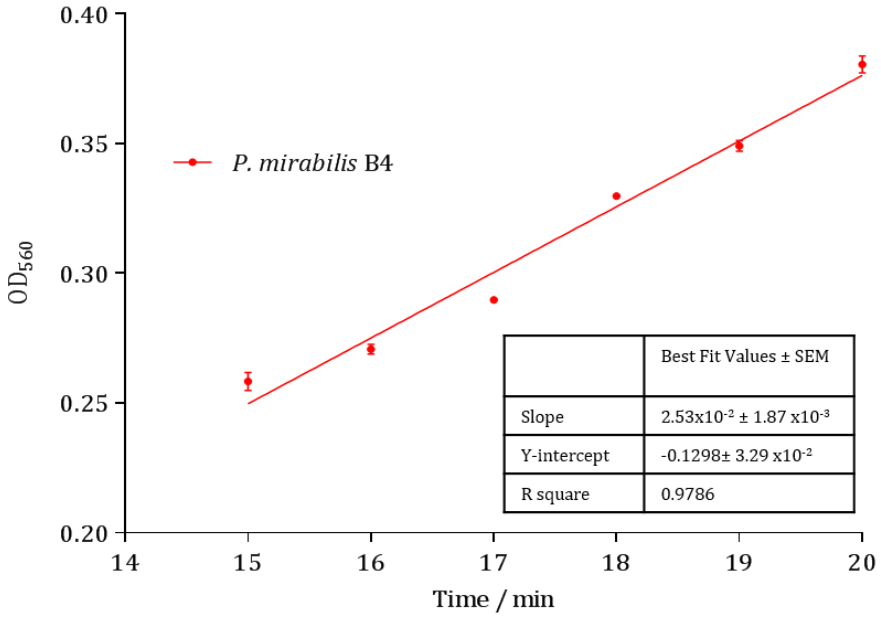

monitored throughout the incubation period, and the linear portion of the resultant graph (Figure 5.13) used to estimate bacterial urease concentration.

Figure 5.13: Colour change of SB in the presence of live *P. mirabilis* B4 overnight culture, at 15-20 minutes incubation. Development of the pink phenol red indicator following urease-mediated urea hydrolysis is followed via measurement of OD_{560}.

From the linear regression model fitted to the standard curve, the equation of the best-fitting line was found to be:

$$Y = 5.25 \times 10^{-3} \times X - 2.12 \times 10^{-3} \quad (41)$$

Substituting the value of the slope from Figure 13 into the standard curve eqution and solving for X:

$$X = \frac{2.53 \times 10^{-2} + 2.12 \times 10^{-2}}{5.25 \times 10^{-3}} \quad (42)$$

$$X = 8.86 \text{ mg/mL}$$

Thus, for subsequent proof-of-concept kinetic experiments involving *C. ensiformis* urease, the standard enzyme concentration was set to 9 mg/mL. Whilst this calculation serves only as an estimate of *P. mirabilis* urease concentration owing to inherent differences in structure, and locational restrictions within the bacterial cells, a general valuation of urease concentration in a live culture will assist in improving the accuracy of the initial *C. ensiformis* studies.

5.4.4. *C. ensiformis* Urease Kinetic Parameters

5.4.4.1. Michaelis Menten Kinetics

In order to assess the inhibition of *C. ensiformis* urease by 2-MA in terms of alteration of kinetic parameters, it was first necessary to determine the standard Michaelis Menten parameters V_{max} and K_M in the absence of inhibitor. The determination of such parameters was undertaken via measurement of the initial reaction rate at various substrate concentrations. Variation of substrate concentration should be within the range $K_M/10$ to 10 K_M where experimentally possible,[56] hence a wide range of concentrations of urea were evaluated for enzyme activity in terms of colour change of SB. Variation in rate of enzymatically catalysed urea hydrolysis by *C. ensiformis* urease at different substrate concentrations is shown in Figure 5.14.

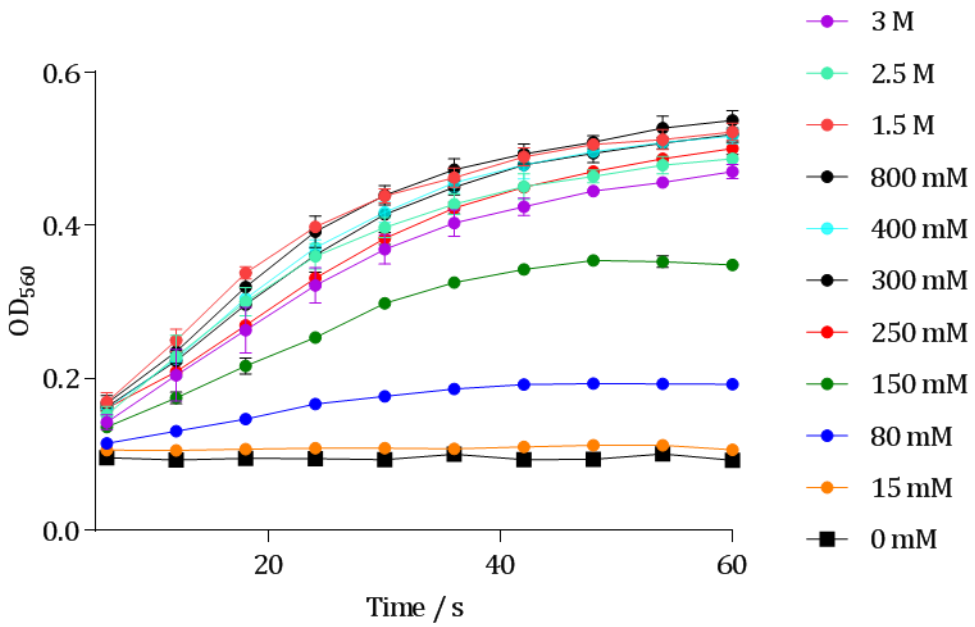

Figure 5.14: Absorbance (560 nm) plotted as a function of urea concentration over time. Rate of colour change of SB is characterised by a change in optical density (OD), representing the rate of the enzyme-catalysed reaction at varying substrate concentration. Data shown are the mean of three independent repeats. Error bars represent SEM.

The fundamental derivation of the Michaelis Menten equation is shown in Section 5.1.2.1. Equation 12 requires the determination of initial rates (so that $[S] = [S]_0$), to ensure that there is no effect of reaction reversibility or product inhibition which may affect the integral method. Thus, the initial rate of reaction from Figure 14 was defined as the first 6-24 seconds of the reaction. The rate of change of optical density within the defined initial rate period was calculated by means of tangents and plotted as a function of urea concentration (Figure 5.15).

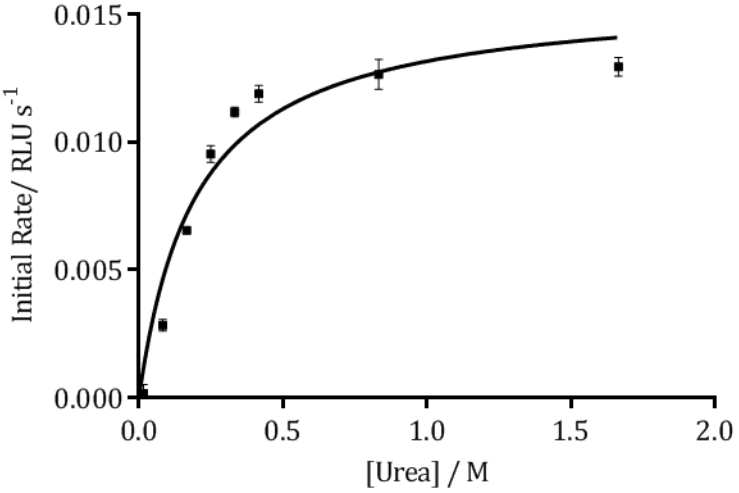

Figure 5.15: Michaelis Menten kinetics of *C. ensiformis* urease, describing the relationship between substrate (urea) concentration and maximum velocity of reaction. Determination of kinetic parameters was facilitated via the fitting of the Michaelis Menten non-linear regression (GraphPad Prism 7). Goodness of fit ($R^2 = 0.9537$).

Fitting of the Michaelis Menten nonlinear regression analysis to the initial rate of the enzymatic reaction yields the kinetic parameters V_{max} and K_M according to Table 5.2.

Table 5.2: Fitting values of the Michaelis Menten constants.

Parameter	Fitting Value	± SEM
V_{max}	1.58 x10^{-2} M	7.70 x10^{-4} M
K_M	0.20 M	2.99 x10^{-2} M

Previously described values for the kinetic parameters of *C. ensiformis* urease quote K_M to be in the region of 2.7-8.81 mM (according to BRENDA enzyme database).[57] Thus, the observed values are roughly 100-fold higher than those calculated under strict Michaelis Menten conditions. This is likely owing to the employment of a non-standard assay for the

measurement of reaction rate, leading to erroneous conditions and subsequent unrepresentative enzyme performance. For example, the optimum pH of urease from *C. ensiformis* is known to pH 7.4,[57] yet the experimental pH at which this assay is undertaken is defined by the pH of the SB medium (~pH 6.8). Slight variation from optimum conditions described for the determinsation of kinetic parameters may manifest as a substantial alteration of the value of K_M. Indeed, the conditions under which the Michaelis Menten equation accurately captures the steady-state kinetics of a simple enzyme-catalysed reaction is contrasted with the conditions under which the same equation can be used to estimate the parameters V_{max} and K_M from a progress data curve.[58] The validity of the underlying assumptions are necessary for the derivation of the equation, but not experimentally sufficient or realistic to guarantee accurate estimation of such parameters. Indeed, the treatment of V_{max} and K_M with respect to enzyme and substrate concentrations relies on simplifying assumptions relating to the quasi-steady state of the intermediate ES complex. Since this is often not the case in real systems, using values of V_{max} and K_M measured *in vitro* (particularly to predict the activity of an enzyme in a living organism) can prove unreliable.[59] Nevertheless, the measurement of kinetic constants in this case provides parameters that may be compared to those in the presence of inhibitor, giving a relative comparison of enzyme activity both in the presence and absence of inhibitory drugs.

5.4.4.2. The Hill Fit

An interesting observation from the determination of the Michaelis Menten parameters is the Goodness of fit (R^2) value of ~0.95 for the rectangular hyperbolic plot shown in Figure 15. At low values of substrate concentration, the data shows some exponential character, as opposed to the expected linear nature of the Michaelis Menten. This slightly sigmoidal nature of of the data is representative of a certain degree of cooperativity in a multisubstrate reaction, as described by the Hill equation (Section 5.1.2.3). Fitting of the initial rate tangents as a function of substrate concentration to the Hill equation yields an improved R^2 value, indicating some degree of bisubstrate binding within *C. ensiformis* urease (Figure 5.16).

The improved fit observed with the Hill slope (R^2 = 0.9959) is in agreement with previous observations for urease, where the urease active site binds both a molecule of urea, as well as a nucleophilic water molecule. This nucleophilic group participates in substrate modification during the catalytic mechanism (as described in Section 5.1.4.2).[57,60]

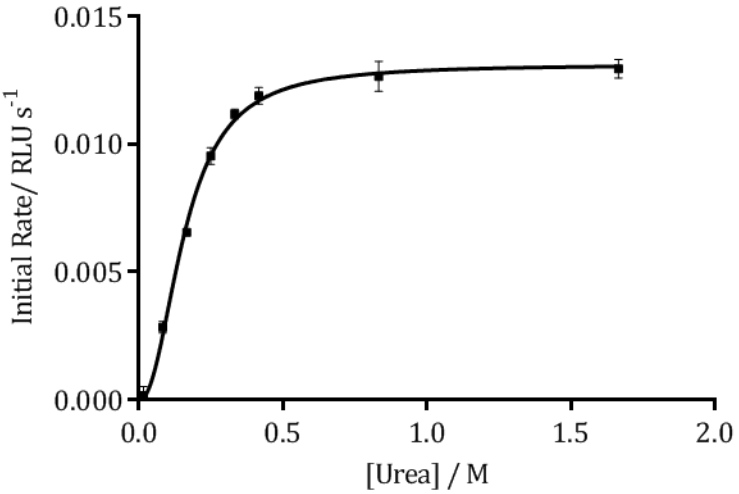

Figure 5.16: Sigmoidal kinetics displayed by *C. ensiformis* urease. Initial rate data were fitted to the Hill equation, to account for cooperativity in the bisubstrate binding model. Determination of kinetic parameters was facilitated via the fitting of the Hill slope. Goodness of fit (R^2 = 0.9959).

Fitting of the Hill fit nonlinear regression analysis to the initial rate of the enzymatic reaction yields the apparent kinetic parameters V_{max} and K_M according to Table 5.3.

Table 5.3: Fitting values of the Hill Equation. Apparent values of V_{max} and K_M are analogous to those obtained with the Michaelis Menten model. The Hill coefficient (*h*) represents a measure of cooperativity.

Parameter	**Fitting Value**	**± SEM**
Apparent V_{max}	1.31 x10^{-2} M	1.59 x10^{-4} M
Apparent K_M	0.16 M	3.71 x10^{-3} M
Hill Coefficient (*h*)	2.19	0.10

The calculated value of the Hill coefficient (*h)* represents positive cooperativity within the urease active site. This is in agreement with previously calculated values of *h* for bi-nickel binding (*h* = 2.0).[61] The apparent value of K_M obtained via fitting to the Hill equation is closer to the literature value, although still represents a significant overestimation. Whilst the Hill fit gives arguably more accurate values of the kinetic constants for *C. ensiformis* urease, subsequent experiments investigating the inhibition of urease will utilise standard Michaelis

Menten kinetics, to remain consistent with previous investigations undertaken in the literature.[11,53,62]

5.4.4.3. Urease Inhibition: Alteration of Kinetic Parameters K_M and V_{max}

Modification of Michaelis Menten constants upon addition of inhibitor yields insights into the mechanism of inhibition. As discussed in Section 5.1.3, different mechanisms of enzyme inhibition display varying effects on kinetic parameters K_M and/or V_{max}. Since the synthesised inhibitor 2-MA displays structural similarities to urea, it was predicted that competitive inhibiton would be observed. In this case, the inhibitor would compete directly with the substrate for access to the enzyme's active site, manifesting as an increased K_M value, reflecting the decrese in the affinity of the enzyme for the substrate (owing to the formation of the inactive EI complex). The observed V_{max} for competitive inhibiton remains unaltered since the binding velocity of the enzyme is unchanged. The effect of the addition of 2-MA to *C. ensiformis* urease in comparison to the uninhibited reaction is shown in Figure 5.17.

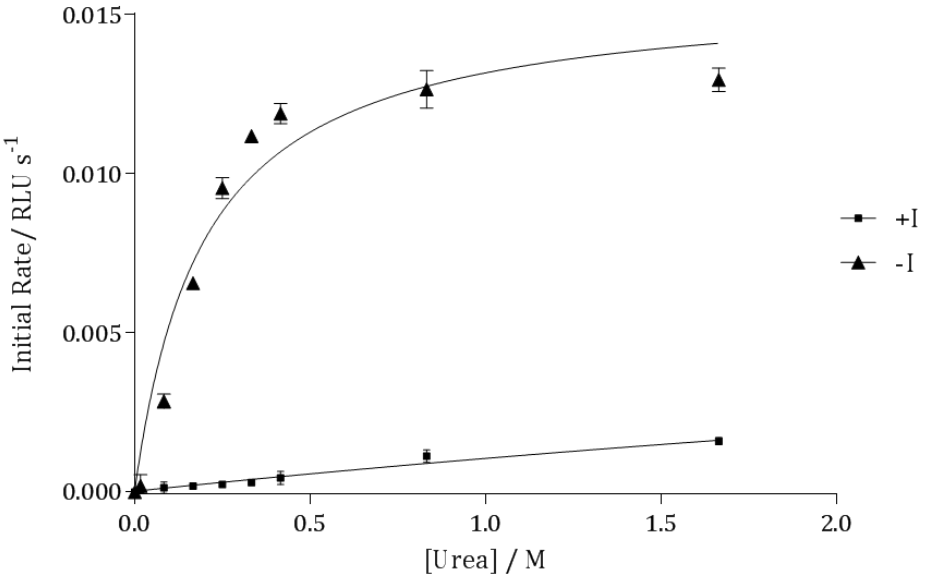

Figure 5.17: Michaelis Menten kinetics for competitive inhibition of *C. ensiformis* urease by 2-MA (+I) compared to the uninhibited reaction (-I). Determination of kinetic parameters was facilitated via the fitting of the Michaelis Menten non-linear regression. Goodness of fit (R^2) = 0.9537 for –I, and 0.9337 for +I.

Comparison of Michaelis Menten parameters both in the presence and absence of the 2-MA inhibitor provided further evidence of competitive inhibition (Table 5.4).

Table 5.4: Calculated kinetic parameters for Michaelis Menten kinetics in the presence (+I) and absence (-I) of inhibitor 2-MA.

	K_M ± SEM	**V_{max} ± SEM**
-I	0.2 ± 2.99 $x10^{-2}$ M	1.58 $x10^{-2}$ M ± 7.70 $x10^{-4}$ M
+I	8.27 ± 6.07	9.56 $x10^{-3}$ ± 6.03$x10^{-3}$

Calculated values of V_{max} for urease-catalysed urea hydrolysis remain unchanged within the calculated error. However, the values of K_M for the inhibited/uninhibited reaction do not overlap within the error. Thus, it is likely that 2-MA behaves as a reversible competitive inhibitor. This observation is in agreement with other structurally analogous inhibitors of urease, including thiol inhibitors such as β-mercaptoethanol.[63,64]

5.4.4.4. The Dixon Plot

The mechanism of enzyme inhibition by 2-MA, as well as the dissociation constant (K_i) were confirmed via the linear graphical method known as the Dixon plot. The effect on the enzymatic intitial rate (V_0) is determined at two or more substrate concentrations, over a range of inhibitor concentrations. For competitive inhibition, a plot of 1/ initial rate against inhibitor concentration will yield a series of straight lines that intersect above the x axis; the abscissa at which they converge represents the inhibitor constant, $-K_i$ (Figure 5.18).

The calculated K_i value from the Dixon plot is 2.97 mM. This value provides a quantitative measure of inhibitory potency that is independent of substrate concentration.[65] Thus, determination of K_I for a novel inhibitor allows for direct comparison with existing inhibitory compounds. Previous investigation of thiols as urease inhibitors has revealed a wide range of inhibitory potency for such structures, varying from 5.0 μM – 10 mM for mercaptamine and 3-mercaptopropionate, respectively.[63] Recently, Grela *et al*.[66] have evaluated a series of aminophosphinic urease inhibitors, active against pure urease isolated from *P. mirabilis* with extremely high inhibitory potency (K_i = 0.20-0.62 μM). However, such effectiveness comes at a significant cost to cell viability; for the most potent inhibitors, a 96-98% reduction in bacterial cell viability was observed, compared to the untreated control, thus placing a significant selection pressure on treated cultures of *P. mirabilis*. The inhibitory constant for AHA has been previously stated as 5.7 ± 0.4 μM and 0.053 mM for *P. mirabilis* and *C. ensiformis* urease, respectively.[66,67] Whilst the observed K_i value calculated for 2-MA appears approximately 100-fold lower than that observed for the 'gold-standard' AHA, the use of AHA in human medicine

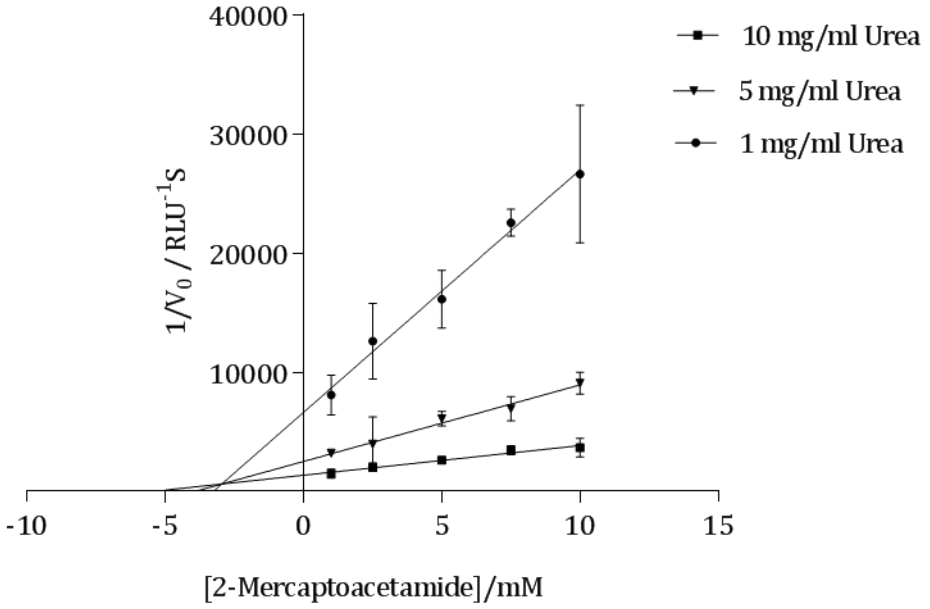

Figure 5.18: Dixon plot for the competitive inhibition of *C. ensiformis* urease by 2-MA. The abscissa of line intersection yields the dissociation constant ($-K_i$).

is known to be riddled with serious clinical side-effects (as previously discussed). Thus, a compromise must be struck between inhibitory potency and cyctotoxicity of novel inhibitory drugs, both for human and bacterial cells. Whilst a less potent drug may require higher dosages, or even be less effective at preventing urolithiasis *in vivo*, a more biocompatible drug will both reduce the onset of adverse reactions within the human patient, and the development of drug resistance within the bacterial population.

5.4.5. Inhibition of *C. ensiformis* Urease by 2-MA

The *in vitro* ability of 2-MA to inhibit urease activity was evaluated using *C. ensiformis* urease as a model system. All inhibitory studies were performed in direct comparison to AHA, so that drug performance may be directly comparable to the paradigmatic treatment for *in vivo* urolithiasis without being limited by variation in experimental conditions.

5.4.5.1. Determination of Inhibitor IC_{50}

The determination of the half-maximal inhibitory concentration (IC_{50}) of an inhibitory compound provides a further measure of the antagonistic potency, in a manner depenedent on defined experimental conditions (e.g. substrate concentration). Dose-response curves and subsequent determination of IC_{50} for 2-MA and AHA are shown in Figure 5.19.

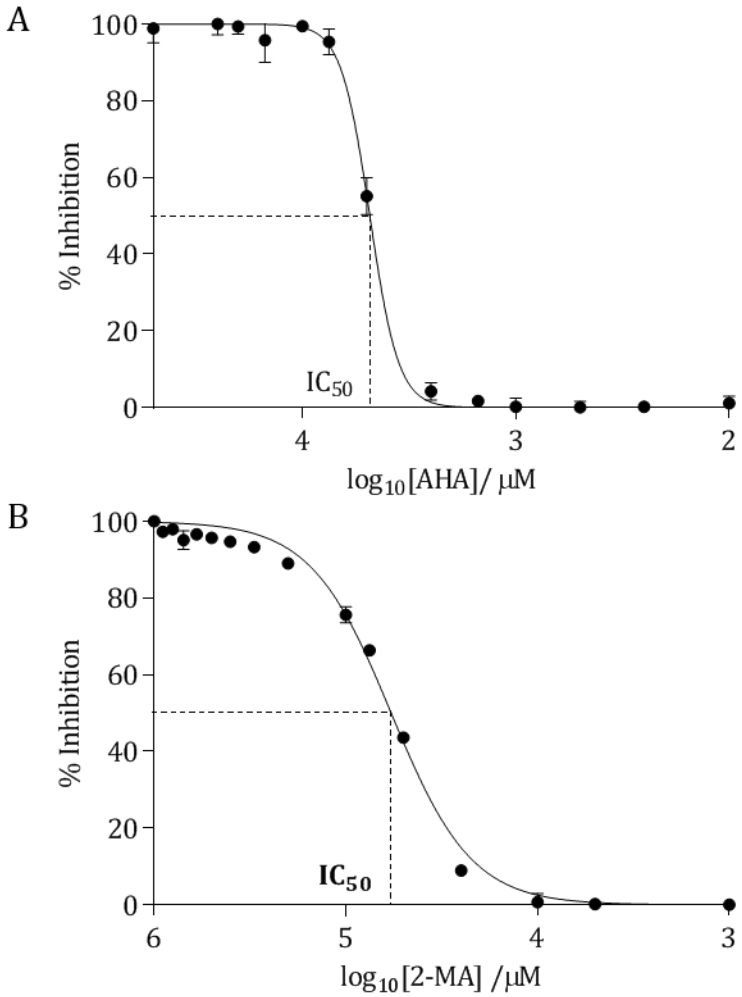

Figure 5.19: Determination of half-maximal inhibiton (IC_{50}) of (A) acetohydroxamic acid (AHA), and (B) 2-mercaptoacetamide (2-MA) against urease from *C. ensiformis*. The enzymatic inhibition was related to the activity in the absence of inhibitor (defined as 0% inhibition), and activity in the presence of 300 mM inhibitor (defined as 100% inhibition). Background measurements were obtained from the signal in the absence of enzyme. Inhibition dose-response curves of normalised, logarithm-transormed data were performed. Data shown are the mean of independent triplicate repeats. Error bars represent SEM.

Values of IC_{50} for both inhibitors were calulcated following the fitting of the data to a four-parameter logistic equation. The calculated parameters for both 2-MA and AHA are shown in Table 5.5.

Table 5.5: Comparison of IC_{50} values for AHA and 2-MA using urease from *C. ensiformis* as a model system.

		Best Fit Value	95% Confidence Interval
AHA	$Log_{10}IC_{50}$	3.684 μM	3.673 - 3.695 μM
	IC_{50}	4.835 mM	4.714 - 4.958 mM
	R^2	0.995	
2-MA	$Log_{10}IC_{50}$	4.763 μM	4.742 – 4.783 μM
	IC_{50}	57.902 mM	55.201 – 60.643 mM
	R^2	0.994	

Whilst the IC_{50} provides an arguably more accurate measurement of relatively potency between two drugs under the same assay conditions, the IC_{50} for 2-MA was approximately 10-fold greater than that for AHA, thus remaining in agreement with results determined by comparison of the inhibitor constant of 2-MA with the literature value for AHA. Nevertheless, since determination of IC_{50} yields no pharmakokinetic information on biocompatibility, cytotoxitiy, or indeed whether or not the novel drug is capable of inhibiting bacterial urease *in vivo*, further biological evaluation is required before true assessment of the drug's therapeutic potential can be made.

5.4.6. Inhibition of *P. mirabilis* Urease by 2-MA

Evaluation of the ability of 2-MA to inhibit intracellular *P. mirabilis* urease adds a crucial, clinically relevant dimension to the inhibitory analysis. Progression from the *C. ensiformis* urease model to cytoplasmic bacterial urease provides a significant challenge to the novel inhibitory compound, since its activity depends on first traversing the bacterial cell membrane to gain access to the enzyme. As previously discussed, all whole-cell 2-MA inhibition studies were undertaken in direct comparison to AHA, providing a point of reference for archetypal enzyme-inhibitory treatment of chronic urea-splitting infection.

5.4.6.1. *In Vitro* Antimicrobial Susceptibility

Prior to the assessment of 2-MA within *P. mirabilis* B4, it was first necessary to determine an appropriate dosage of drug with which to treat live bacterial cultures. *In vitro* susceptibility tests were performed via standard microbroth dilution methods for both 2-MA and AHA (Figure 5.20).

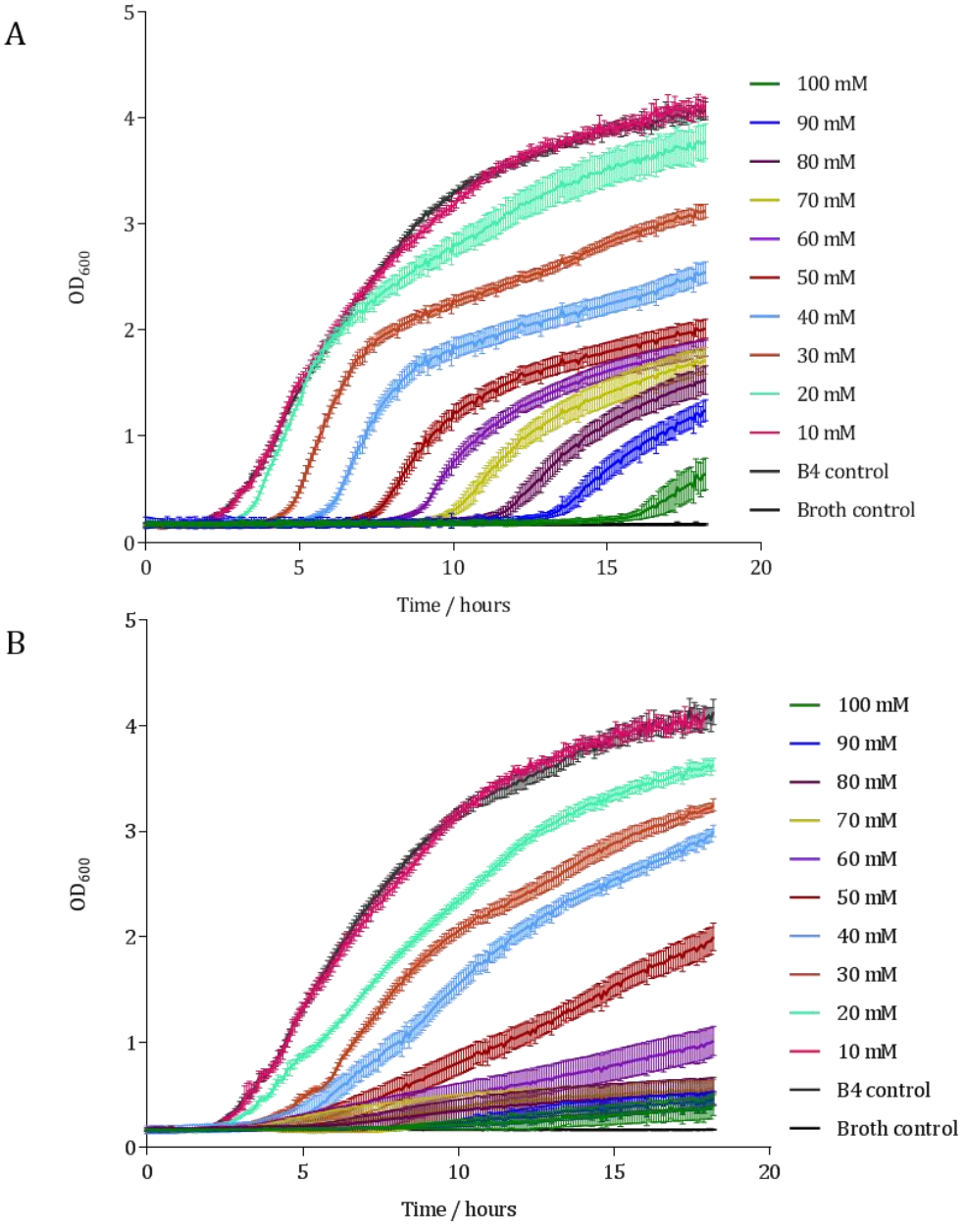

Figure 5.20: Susceptibility of *P. mirabilis* B4 to 2-MA (A) and AHA (B). Determination of the maximum inhibitory concentration for both drugs was achieved via standard microbroth dilution methods. Inhibition of bacterial growth was measured as a function of OD at 600 nm. Data shown are the mean of quadruplicate repeats on the same bacterial isolate. Error bars represent SEM.

The objective of 'maximum inhibitory concentration' determination for both 2-MA and AHA was to discover the concentration of drug at which the bacterial fitness remains unaffected. Since the pathogenicicty of *P. mirabilis* is characterised by instrinsic properties such as virulence factors (including urease), the ability to 'disarm' the population via reducing or eliminating urease activity provides a novel strategy of treatment for CAUTI. Dose selection requires a compromise between inhibitory efficacy and directing bacterial evolution, since it is well-known that the application of an antimicrobial drug may result not only in direct selection of the corresponding resistance, but also in the development of cross-resistance (resistance to several structurally-related antimicrobials) and coresistance (resistance to several structurally-unrelated antimicrobials) via specific mechanisms.[68]

Both 2-MA and AHA induced a decrease in observed cell viability at concentrations greater than 10 mM. At high concentrations (>50 mM), AHA appeared to induce a greater decrease in viable bacterial cells than 2-MA. For whole-cell urease evaluation, it was imperitive to employ a concentration of drug that will not affect the growth of bacterial populations, such that any reduction in urinary crystal formation may be attributed solely to urease inhibition. Thus, the selected dosage for futher biological evaluation was 10 mM for both 2-MA and AHA.

5.4.6.2. Whole-Cell Studies

The ability of 2-MA to inhibit cytoplasmic *P. mirabilis* urease was investigated, using urinary pH elevation as a proxy indicator of enzymatic activity. Permeation of the cell membrane provides a significant challenge in the design of small molecule drugs such as enzyme inhibitors, with many promising drug candidates failing to reach their cytosolic targets when tested in whole-cell screening assays.[69] The mechanism of membrane permeation is governed by parameters including molecule size and polarity. Small, uncharged, polar molecules are generally able to move across the lipid bilayer down the concentration gradient by means of simple diffusion. However, the majority of polar drug molecules may only penetrate the cell membrane in the presence of membrane-transport proteins (including channel and carrier proteins) via either passive or active transport.[70]

Cytosolic uptake is frequently confirmed via measurement of a biological effect generated only when the payload is successfully delivered to the cytoplasm. In this system, the macroscopic effect of urinary pH elevation was monitored before and after a short incubation period with both 2-MA and AHA (Figure 5.21A), in order to assess the ability of the drugs to access their intracellular target. Viable cell counts of bacterial cultures were also performed at the beginning and conclusion of each incubation period (Figure 5.21B), to ensure that any effect

on residual medium pH was not as a consequence of cell death. The effect of inhibitory drugs were also evaluated on a uropathogenic strain of *E. coli*, which acts as a ureae-negative control (Figure 5.21C and D)

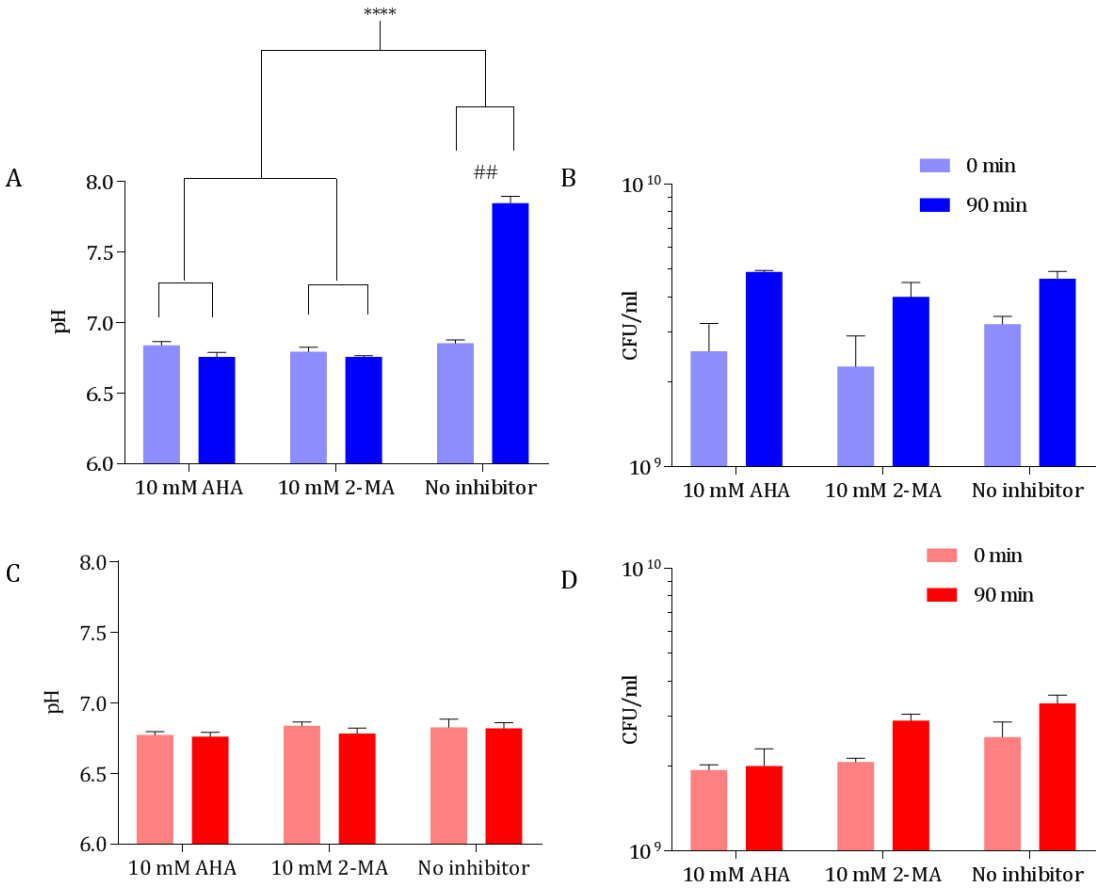

Figure 5.21: Whole cell evaluation of 2-MA and AHA. Ability to penetrate the bacterial cell membrane and inhibit intracellular urease activity was determined by elevation of urinary pH (A, C). Viable cell counts were performed to ensure the viability of cultures before (0 minutes) and after (90 minutes) treatement with inhibitory drugs (B, D). Evaluation was undertaken on both urease-positive (*P. mirabilis* B4) (A,B) and urease-negative (*E. coli* NSM59) (C,D) uropathogenic clinical isolates. Data shown are the mean of triplicate biological repeats. Error bars represent SEM. **** $p < 0.0001$, ## $p < 0.005$.

Treatment of *P. mirabilis* B4 cultures with 10 mM 2-MA successfully prevented urinary pH elevation via urease activity. Inhibition appeared to be comparable with that of 10 mM AHA; both drugs achieved significant enzyme inhibition in comparison to the untreated control ($p < 0.0001$). No alteration in urinary pH observed within cultures of *E. coli* owing to the lack of expressed urease, whilst the untreated *P. mirabilis* culture yielded a significant elevation of

urine pH even after the short incubation period (p = 0.0015). Furthermore, no statistically significant change in viable cell count was observed for either strain in the presence of 2-MA or AHA, compared to the untreated control. Thus, it was concluded that the observed alteration in residual urine pH was as a direct result of intracellular urease inhibition by 2-MA and AHA.

5.4.7. *In Vitro* Bladder Models

Efficacy of 2-MA in a clinically representative system was assessed using the *in vitro* bladder model mimicking late-stage infection (as previously described). In order to mimic oral administration of urease inhibitory drugs, 2-MA and AHA were dissolved directly into the urine reservoirs at 10 mM concentration.

The blockage of urinary catheters and subsequent termination of urine flow was defined as the experimental end point. Performance of 2-MA was compared directly to that of AHA within triplicate experiments, in order to reference the extension of catheter lifetime under the same experimental conditions. Periodic measurements of bladder conditions (pH and CFU/mL) were performed throughout the experiment, to monitor the urease activity as a function of residual urine pH, as well as the viability of colonising bacteria. Both inhibitors achieved significant extension of catheter lifetime compared to the untreated control (Figure 5.22).

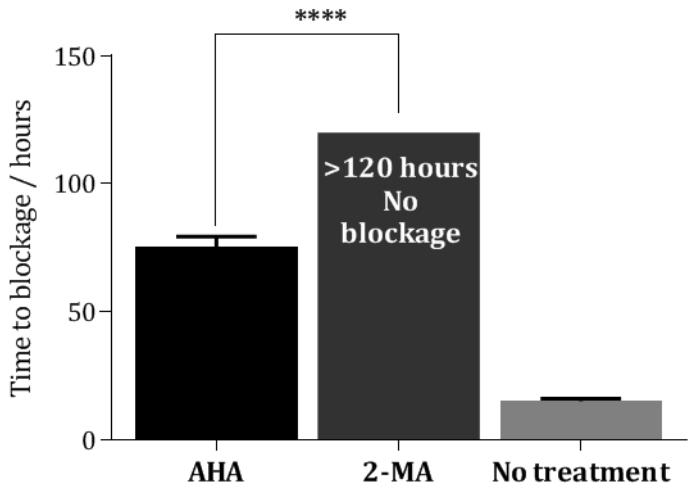

Figure 5.22: Extension of catheter lifetime upone treatment (10 mM dosage) with urease inhibitory drugs 2-MA and AHA. Average blockage times for the untreated and AHA treated models were 15 and 74.3 hours, respectively. No blockage was observed for the 2-MA treated models within the experimental time-frame. Models were run for 5 days (120 hours) until media reservoirs were exhausted. Data represents the mean of 3 biological repeats. Error bars represent SEM. **** $p < 0.0001$.

When urease activity was uninhibited, blockage of control models (initial inoculum 10^8 CFU/mL) occurred 15 hours after model start. Treatment with AHA extended average blockage time by 400%, to 74.3 hours ($p < 0.0001$). This result is in agreement with previous observations of catheter blockage prevention *in vivo*, where treatment of 5 catheterised patients with AHA decreased catheter encrustation by 81% and significantly reduced the need for frequent catheter changes.[71] Surprisingly, treatment of *P. mirabilis*-infected models with 2-MA further extended catheter lifetime within the *in vitro* model, such that blockage was not observed througout the 5-day duration of the experiment. Reservoirs of artificial urine media were exhausted 120 hours after model start, at which point catheters treated with 2-MA were still draining freely.

The outperformance of AHA by 2-MA in the bladder model system was an unexpected outcome, since early kinetic data suggested that AHA displayed more inhibitory potency in terms of kinetic parameters and early evaluation using the *C. ensiformis* model system. Periodic measurement of residual bladder conditions confimed the efficacy of 2-MA at preventing urinary pH elevation and catheter colonisation by *P. mirabilis* (Figure 5.23).

Within the untreated control models, the pH of artificial urine media within the bladder underwent rapid alkalinisation, owing the urease-mediated urea hydrolysis within the *P. mirabilis* population. Indeed, the pH of residual media was elevated to pH 8 within 5 hours of the experiment start (Figure 5.23A). This was accompanied by an increase in viable cells within the bladder, since urease expression was able to facilitate rapid colonisation and biofilm formation. Local supersaturation and precipitation of crystalline materials within the catheter lumen and eyehole region therefore elicited total occlusion of the catheter within 15 hours of the model start. In contrast, pH elevation within treated models was unable to surpass to nucleation point (~pH 7.4) until approximately 45 and 108 hours for AHA and 2-MA, respectively. Eventual elevation of urine to pH 8 in AHA-treated models was accompanied by catheter blockage via crystalline biofilm formation. In models treated with 2-MA, models were unable to reach pH 8 within the experimental term, thus the degree of crystalline biofilm formation was insufficient to result in catheter blockage.

Both the AHA and 2-MA-treated models underwent an approximately 1-log reduction in viable cell count within the first 24 hours of the experiment (Figure 5.23B). Since *P. mirabilis* virulence factors (particularly urease) are known to play an extensive role in bacterial pathogenesis and biofilm formation,[36] it is therefore unsurprising that inhibition of urease activity manifested as a decrease in bacterial colonisation. Since urease-negative mutants have previously been shown to colonise the urinary tract 100-fold less efficiently than the parent strain (Section

5.1.4.3), it is likely that the reduction in adherence resulted in direct elution of a large portion of the bacterial population from the bladder in the early stages of infection.

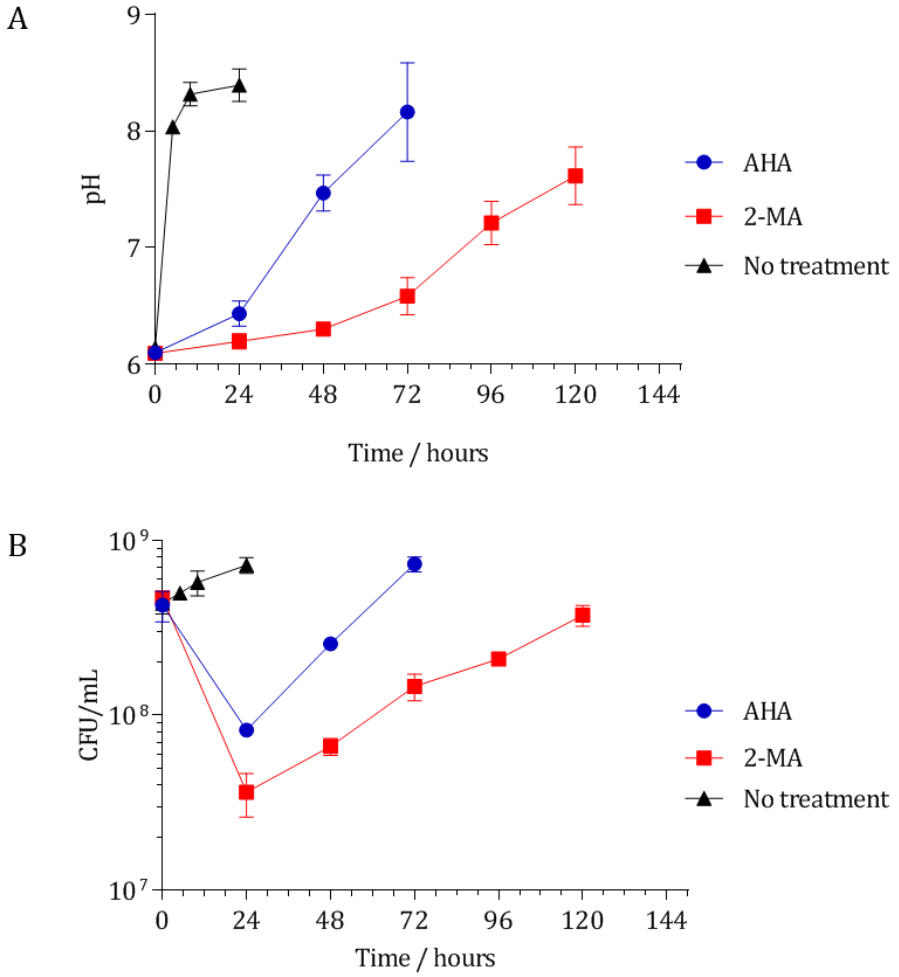

Figure 5.23: Analysis of *in vitro* bladder model conditions at periodic intervals after model start (0 hours) via direct sampling of bladder model urine. A) Residual urine pH. B) Bacterial biomass. Data shown are the mean of triplicate biological repeats. Error bars represent SEM.

Within the 2-MA-treated models, bacterial biomass was unable to recover and surpass the value of the intial inoculum at the point of pump activation (3.7 x10^8 CFU/mL at 120 hours vs 4.7 x10^8 at 0 hours) . Thus, whilst the measured conditions within the 2-MA-treated bladder suggest that blockage was forthcoming, it was not reached within the timecourse of this experiment.

Disparities in the degree of encrustation on catheter luminal surfaces at time of AHA-treated model blockage (~74 hours) and unblocked 2-MA-treated model (120 hours) were observed visually (Figure 5.24). Total occlusion of the eyehole and drainage lumen were observed in the

catheter removed from the blocked model. Significantly less crystalline material was observed within the catheter removed form the 2-MA-treated model.

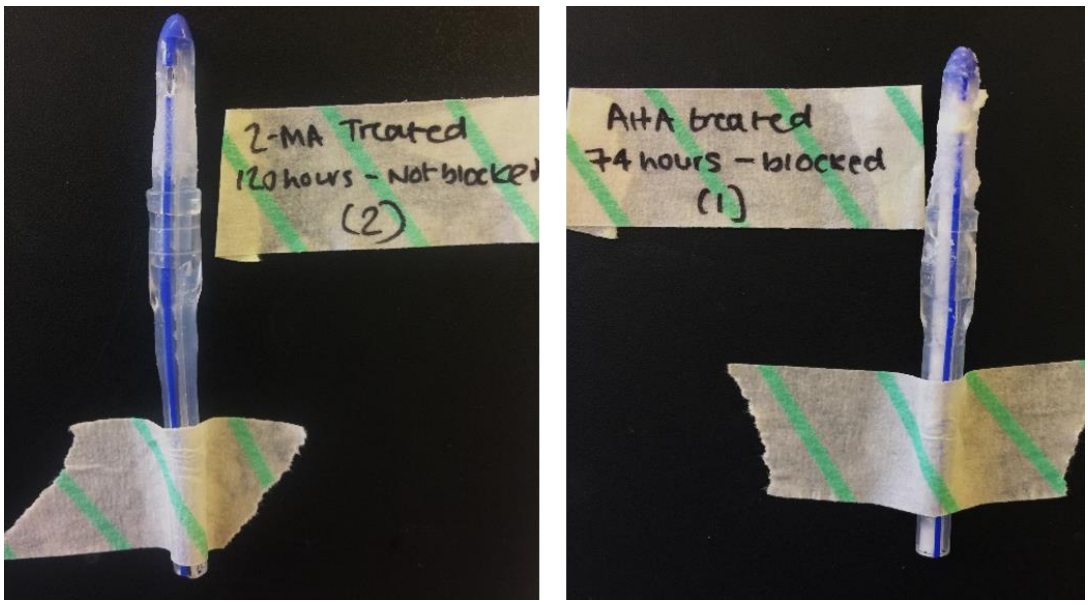

Figure 5.24: Distal regions of catheters removed from 2-MA-treated model (left) at experimental end point (120 hours), and AHA-treated model (right) at time of blockage (74.3 hours). Crystalline biofilm encrustation as a result of urease activity is observed in the eyehole and luminal surfaces of the AHA-treated catheter. Images are representative of three independent biological repeats.

Whilst the degree of encrustation for the 2-MA-treated catheter is significantly lesser than its AHA-treated counterpart, there is evidence of encrustation around the eyehole region at 120 hours post-inoculation. Thus, the visual results are in agreement with the measurement of residual pH/ CFU/mL in predicting the extrapolated blockage of this model. Nevertheless, the novel inhibitor 2-MA appears to outperform AHA in this model.

5.4.7.1. 2-MA Biofilm Inhibition

The ability of 2-MA to inhibit the formation of *P. mirabilis* biofilms was investigated using a simple *in vitro* crystal violet staining model. Since treatment of the *in vitro* catheterised bladder with 2-MA (10 mM, described previously) resulted in significant elution of planktonic cells from the bladder in the early stages of the experiment, it was hypothesised that this drug is preventing the early colonisation of a biofilm on the catheter's luminal surfaces. The ability of both enzyme inhibitory drugs to prevent biofilm formation of *P. mirabilis* is shown in Figure 5.25.

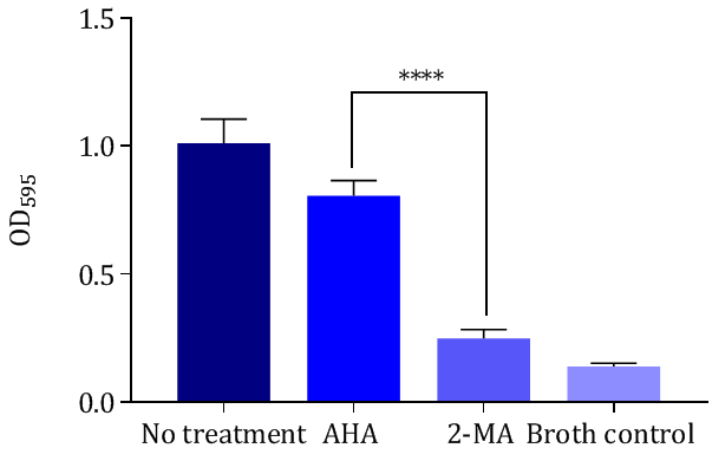

Figure 5.25 : Quantitative measurement of *P. mirabilis* B4 static biofilm inhibition by 10 mM 2-MA and AHA. Quantification was performed via crystal violet biofilm staining. Data shown are the mean of triplicate repeats. Error bars represent SEM. **** $p < 0.0001$.

At the therapeutic concentration of 10 mM, 2-MA showed significantly greater biofilm inhibitory activity than AHA ($p < 0.0001$), although it did not succeed in complete prevention of biofilm formation ($p = 0.0214$). Since previous investigation into the antimicrobial susceptibility of *P. mirabilis* to both 2-MA and AHA has confirmed that 10 mM concentrations are unable to induce bacterial cell death (Section 5.2.2.3.II), it appeared that the reduction in biofilm formation (and hence extension of catheter lifetime) is owing to the prevention of catheter colonisation and adherence to the catheter surface.

As the observed biofilm inhibitory activity cannot have occured as a result of bacterial cell death, it was thus hypothesised that 2-MA behaved as a quorum sensing antagonist, thus interfering with cell-cell signalling processes that mediate biofilm formation within the catheterised bladder. Whilst confirmation of this conjecture would require testing of specific *P. miraiblis* reporter systems, similar attenuation of biofilm formation has previously been observed on uropathogenic strains of *P. aeruginosa* using garlic extract as a phophylactic agent.[72] As discussed in Section 5.3.1, allicin, the biologically active component of garlic, is known to display potent urease inhibitory activity. Fresh garlic extract induced significant reduction in AHL production when compared to the untreated control, manifesting in lowered renal bacterial counts in a mouse kidney model.[73] Recent investigation in to the mechanism of urease inhibition by allicin has theorised it to be similar in nature to that of small-molecule thiol inhibitors,[54,74,75] thus supporting the argument for quorum sensing antagonism by 2-MA.

5.4.8. Cytotoxicity Testing

5.4.8.1. Mammalian Cells

In vitro cytotoxicity testing provides a crucial means of ranking compounds for consideration in drug discovery. For cell culture systems, a compound is considered cytotoxic if it interferes with cellular attachment, significantly alters morphology, adversely affects growth rate, or causes cell death.[76] The XTT assay, as described in Section 5.2.2.3.VII, measures cell proliferation based on the metabolic activity, and is frequently used in 2D culture conditions. The ability of metabolically active cells to reduce the tetrazolium salt XTT to a water-soluble formazan product provides a quantifiable measure of dose-related compound toxicity.

2-MA was evaluated for cytotoxicity using a HaCaT immortalised keratinocyte cell line. Metabolic activity of HaCaT cells in the presence of various concentrations was compared directly to those in the presence of the same concentrations of AHA. The results were expressed as a percentage viability compared to the untreated controls (Figure 5.26).

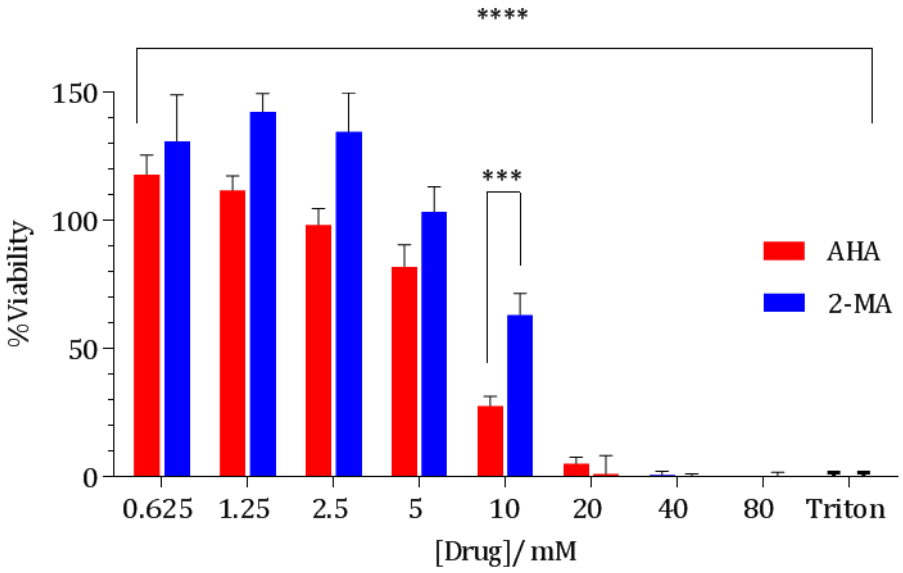

Figure 5.26: Viability of HaCaT keratinocytes in the presence of varying concentrations (0.625-80 mM) of 2-MA and AHA. Corrected values of absorbance at 450 nm are displayed as a percentage of untreated control, to yield % viability. **** $p < 0.0001$. *** $p < 0.001$.

Throughout the range of tested concentrations, 2-MA displayed significantly less cytotoxicity than AHA ($p < 0.0001$). Of particular interest is the comparison at 10 mM concentration, since this was the therapeutic dose employed in earlier studies ($p = 0.0002$). These results are in

agreement with previously observed toxicity studies for AHA, which is known to display significant cytotoxicity both *in vitro* and *in vivo*. Indeed, AHA has been shown to behave synergistically with bacterial virulence factors to increase toxicity to human cell lines. Evaluation of HeLa cell viability in the presence of *Helicobacter pylori* (*H. pylori)* (a known producer of potent bacterial urease), showed that a *H. pylori* cytotoxin caused damage to the cell membranes of HeLa cells, thus allowing AHA to accumulate intracellularly and exert cytotoxic effects.[77]

Enchanced cytotoxicity of AHA in comparison to 2-MA at the defined therapeutic concentration (10 mM) were observed qualitatively, to compare the degree of cell damage induced by drug exposure. For the AHA treated cells, the presence of cellular debris after overnight exposure indicated possible necrosis and apoptosis (Figure 5.27).

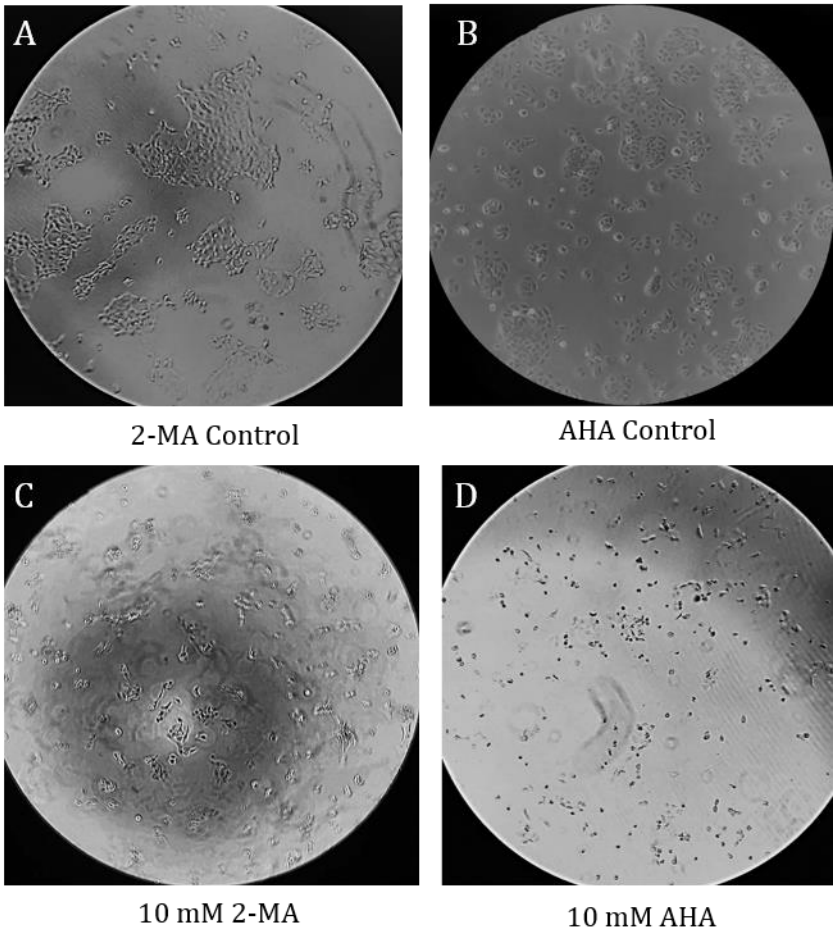

Figure 5.27: Visual examination of HaCaT cells both in the absence of inhibitor (A,B) and following (C,D) treatment with 2-MA (A,C) and AHA (B,D) (10 mM). Images are representative of three individual replicates. Exposure of cells to AHA appears to induce nectrotic and apoptotic effects.

The limitations of this assay lie in the reliability of *in vitro* assays as a model of human medication. Whilst drug screening in assays such as the XTT viability assay allow rapid and facile identification of promising compounds, favourable results do not mean an automatic green-light for *in vivo* application. Furthermore, the evaluation of 2-MA on a single immortalised cell line from an arguably unrelated organ may limit the scientific value of this study. Nevertheless, it has recently been noted within the literature that the significance of *in vitro* toxicity data may be improved by performing comparative studies between established and novel drugs, in preference to static IC_{50} values.[78]

5.4.9. Haemolytic Evaluation

In clinical practice, AHA is the only urease-inhibitory drug to have gained FDA-approval for the treatment of infections caused by urease-producing bacteria.[79] However, significant limitations associated with severe side effects (such as teratogenicity, psycho-neurological and musculo-integumentary symptoms) have resulted in limited use and clinical acceptance of this drug.[80] In particular, AHA is known to cause severe haemolytic anaemia within human patients, as well as direct damange to human erythrocytes as a result of toxic haemolysis. [81]

Within the healthy circulatory system, the rate of red blood cell (RBC) destruction is in a steady state with RBC production. Liberated iron (Fe^{3+}) from destroyed RBCs is bound by transferrin with high affinity, rendering it unable to react with reactive oxygen species and other substances *in vivo*. As a result of toxic haemolysis (as observed for AHA in concentrations greater that 1.25 mM) the rate of iron release into circulation may surpass the rate of uptake by transferrin, thus producing non-transferrin-bound iron (NTBI). A fraction of NTBI, known as labile plasma iron (LBI), may become loosely bound to proteinaceous structures and is known to be highly redox active, thus causing iron-mediated oxidative stress. Both NTBI and LBI can also enter a variety of cell types, including liver, pancreas, endrocrine glands and cardiomyocytes, where cell antioxidant defences may be overcome, compromising cell integrity and causing organ damage or failure.[82]

The degree of haemolytic anaemia induced by a drug may be evaluated *ex vivo* by assessing the dose-dependent liberation of haemoglobin from human RBCs via measurement of absorbance at 410 nm. Obtained values were corrected against media controls, and degree of haemolysis

expressed as a percetange of the positive lysis control (Triton-X 100). Percentage haemolysis for both 2-MA and AHA at varying concentration is shown in Figure 5.28.

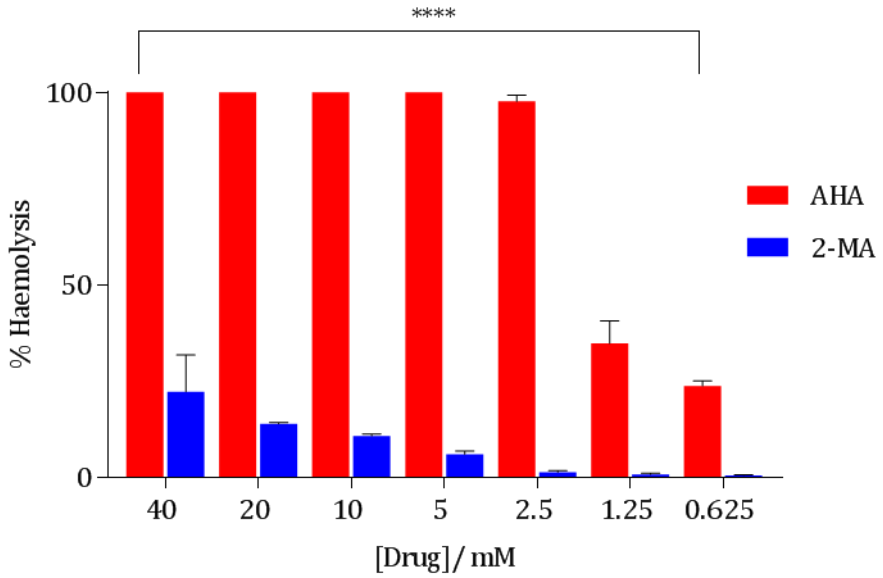

Figure 5.28: Percentage *ex vivo* haemolytic acitivity of dose-dependent 2-MA and AHA treatment on human erythrocytes. Drug concentration was varied from 0.625-40 mM. Corrected values of absorbance at 410 nm are displayed as a percentage of untreated control, to yield % viability. **** $p < 0.0001$.

Toxic haemolytic activity was significantly lower for 2-MA than AHA ($p < 0.0001$). Of particular relevance was the result at the defined therapeutic concentration (10 mM), where % haemolysis was observed to be 10.7 % ± 0.8 for 2-MA; an 89% reduction from the value observed for AHA at the equivalent concentration. Even at the highest evaluated concentration of 40 mM, observed haemolysis was still 78% lower following treatment with 2-MA in comparison to AHA ($p < 0.0001$ for all comparative concentrations).

Visual results reinforced quantitiative measurement of toxic haemolysis for the drug performance comparison. Liberated haemoglobin as a result of drug toxicity appears as a deep red colouration in the liquid media, thus displaying clear evidence of the lower toxicological value of 2-MA in this haematological assay (Figure 5.29).

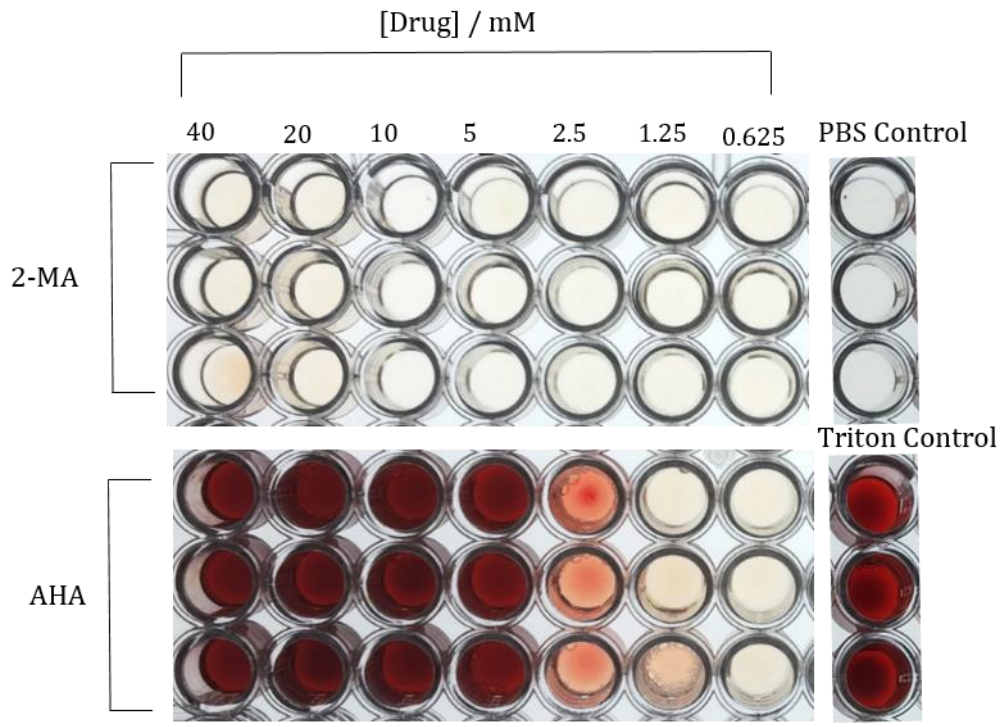

Figure 5.29: Haemolysis observation within a 96-well microplate. Visual assessment of toxic haemolysis was undertaken following incubation of various concentrations of 2-MA and AHA (0.625-40 mM) with human red blood cells. Liberated haemoglobin released in the supernatant of samples can be observed via the red colouration of the PBS media. Negative (PBS) and positive (Triton X-100) controls are shown for comparison.

Visual similarity of AHA-treated erythrocytes with the positive surfactant control suggest complete destruction of RBCs. Moderate toxicity is observed at a concentration of 2.5 mM, and low toxicity between 0.625-1.25 mM. Conversely, 2-MA does not appear to induce RBC damage at any of the tested concentrations, owing to its visual resemblance to the negative buffer control. Thus, from a purely toxicological point of view, 2-MA appears to be the most promising drug following comparison with AHA, as it lacks both RBC, keratinocyte, and bacterial toxicity at a therapeutic concentration.

5.5. Conclusion

Drugs that function as enzyme inhibitors constitute a significant portion of the orally bioavailable therapeutic agents that are in clinical use today. Consequently, many of the current drug discovery and developmental efforts are focused on the identification and optimisation of drug candidates that act via the inhibition of specific enzymatic targets. The attraction of enzymes as novel drug targets stems from the high levels of disease association (target validation) and target traceability that typically characterise this class of proteins. Furthermore, the 'disarming' of such potent bacterial virulence factors without placing a significant selective pressure on the cells themselves comprises a therapeutic approach of great clinical significance in light of the dawn of the post-antibiotic era.

Whilst 2-MA has shown significant promise *in vitro,* further work is required to determine the mechanism of bacterial membrane permeation. Caco-2 cells and renal MDCK cells (allowing passive permeation and transporter-mediated permeation, respectively) would provide valuable insight into the specific mechanism of action of this drug, and its pathway of entry into the cytoplasmic space of the cell. In terms of cytotoxicity cell culture studies, the use of primary cell lines from human tissue as opposed to previously described immortalised cell lines may provide a more representative *in vitro* model of the human bladder. Furthermore, *in silico* mechanistic and molecular docking studies would provide information as to the mechanism of urease inhibition and binding affinity to *P. miraiblis* urease. Such evaluation may direct the synthesis of further 2-MA-based inhibitor anlogues, resulting in a library of structurally related molecules from which to chose a lead compound. Following candidate selection, the pharmacokinetic profile may be evaluated via techniques such as 3D cell culture absorption models and prediction of *in vivo* drug metabolism.

Further development of 2-MA as a possible treatment for CAUTI will involve investigation into novel delivery methods of this drug into the catheterised bladder. The catheter coating concept described in Chapters 2 and 4 would provide the ideal platform from which to release this chemical cargo into the infected area at high local concentration. This would subsequently ease the pressure on achieving high systemic doses of drug via oral administration, as well as limiting any potential side effects as yet uncovered in the cytotoxic profile.

Overall, the clear outperformance of the 'gold standard' treatment for chronic urea-splitting infection in the comparison of the two described drugs highlights the urgent need for novel urease inhibitors that have a less extensive portfolio of side effects than AHA. Pharmaceutical development of such compounds evidently requires a compromise to be struck between

potency and toxicity. The results of the initial toxicity profiling of 2-MA in comparison to AHA, along with the performance within the *in vitro* catheterised bladder model clearly demonstrate that novel drugs with lower initial promise in terms of *in vitro* efficacy are perhaps overlooked in light of low dosage formulation, but at the cost of systemic patient health and inherent cytotoxicity.

5.6. References

1. G. M. Cooper, *The Cell: A Molecular Approach*, Sinauer Associates, Sunderland (MA), 2nd edn., 2000.
2. F. A. Bettelheim, W. H. Brown, M. K. Campbell and S. O. Farrell, *Introduction to Organic and Biochemistry*, Brooks/Cole, Belmont, CA, 7th edn., 2009.
3. L. Michaelis and M. L. Menten, *Biochemische Zeitschrift*, 1913, **49**, 333–369.
4. G. E. Briggs and J. B. S. Haldane, *Biochemical Journal*, 1925, **19**, 338–339.
5. P. K. Robinson, *Essays In Biochemistry*, 2015, **59**, 1–41.
6. A. V. Hill, *Journal of Physiology*, 1910, **40**, iii–vii.
7. N. S. Punekar, *Enzymes: Catalysis, Kinetics and Mechanisms*, Springer, Singapore, Online., 2018.
8. T. Robin, S. Reuveni and M. Urbakh, *Nature Communications*, 2018, **9**, 1–24.
9. J. H. Smith and C. Simons, *Enzymes and Their Inhibitors: Drug Development*, CRC Press, Boca Raton, FL, 2nd edn., 2004.
10. R. L. Stein, *Kinetics of Enzyme Action: Essential Principles for Drug Hunters*, John Wiley & Sons, New Jersey, 10th edn., 2011.
11. M. Vijayalakshmi, Michaelis Menten Kinetics-Enzyme Inhibition, https://nptel.ac.in/courses/102106035/Module 3/Lecture 3/Lecture 3.pdf, (accessed 21 November 2018).
12. A. . Marangoni, *Enzyme Kinetics:A Modern Approach*, John Wiley & Sons, New Jersey, 10th edn., 2011.
13. C. Mohan, K. Long and M. Mutneja, *An Introduction to Inhibitors and Their Biological Applications*, 2014.
14. M. Agrawal, D. F. Gallis, J. A. Greathous and D. S. Sholl, *The Journal of Physical Chemistry*, 2018, **122**, 26061–26069.
15. R. Sharma, Enzyme Inhibition: Mechanisms and Scope, http://cdn.intechopen.com/pdfs/36550/intech-enzyme_inhibition_mechanisms_and_scope.pdf, (accessed 21 November 2018).
16. R. R. Ramsay and K. F. Tipton, *Molecules*, 2017, **22**, 1–42.
17. D. Knez, M. Sova, U. Košak and S. Gobec, *Future Medicinal Chemistry*, 2017, **9**, Epub.
18. G. Pagano, G. Rengo, G. Pasqualetti, G. D. Femminella, F. Monzani, N. Ferrara and M. Tagliati, *Journal of Neurology, Neurosurgery and Psychiatry*, 2015, **7**, 767–773.
19. S. Consalvi, M. Biava and G. Poce, *Expert Opinion on Therapeutic Patents*, 2015, **25**, 1357–1371.
20. K. Nikolic, L. Mavridis, T. Djikic, J. Vucicevic, D. Agbaba, K. Yelekci and J. B. O. Mitchell,

Frontiers in Neuroscience, 2016, **10**, e265.

21. M. Totsika, *Future Medicinal Chemistry*, 2017, **9**, 267–269.
22. P. Tenke, M. Tunde, I. Bode and B. Koves, *European Urology Supplements*, 2017, **16**, 138–143.
23. L. M. Loomes, B. W. Senior and M. A. Kerr, *Infection and Immunity*, 1990, **58**, 1979–1985.
24. L. Carson, G. R. Cathcart, C. J. Scott, M. D. Hollenberg, B. Walker, H. Ceri and B. F. Gilmore, *Biochimie*, 2011, **93**, 1824–1827.
25. M. J. Maroney and S. Ciurli, *Chemical Reviews*, 2014, **114**, 4206–4228.
26. J. Sumner, *The Journal of Biological Chemistry*, 1926, **69**, 435.
27. N. E. Dixon, C. Gazzola, R. L. Blakeley and B. Zerner, *Journal of the American Chemical Society*, 1975, **97**, 4131–4133.
28. H. Krebs and K. Henseleit, *Hoppe-Seyler´s Zeitschrift für physiologische Chemie*, 1932, **210**, 33–66.
29. B. P. Callahan, Y. Yuan and R. Wolfenden, *Journal of the American Chemical Society*, 2005, **127**, 10828–10829.
30. L. Mazzei, F. Musiani and S. Ciurli, in *The Biological Chemistry of Nickel*, The Royal Society of Chemistry, 10th edn., 2017, pp. 60–97.
31. B. Krajewska and M. Brindell, *Journal of Enzyme Inhibition and Medicinal Chemistry*, 2011, **26**, 309–318.
32. S. Benini, W. R. Rypniewski, K. S. Wilson, S. Miletti, S. Ciurli and S. Mangani, *Structure*, 1999, **7**, 205–216.
33. M. J. Todd and R. P. Hausinger, *Journal of Biological Chemistry*, 1987, **262**, 5963–5967.
34. B. Zambelli, F. Musiani, S. Benini and S. Ciurli, *Accounts of Chemical Research*, 2011, **44**, 520–530.
35. J. D. Dattelbaum, C. V. Lockatell, D. E. Johnson and H. L. T. Mobley, *Infection and Immunity*, 2003, **71**, 1026–1030.
36. C. E. Armbruster and H. L. T. Mobley, *Nature Reviews Microbiology*, 2012, **10**, 743–754.
37. D. Johnson, R. Russell, V. Lockatell, J. Zulty, J. Warren and H. Mobley, *Infection and Immunity*, 1993, **61**, 2748–2754.
38. B. D. Jones, V. Lockatell, D. E. Johnson, J. W. Warren and H. L. T. Mobley, *Infection and Immunity*, 1990, **58**, 1120–1123.
39. C. Coker, C. A. Poore, X. Li and H. L. T. Mobley, *Microbes and Infection*, 2000, **2**, 1497–1505.
40. K. M. Khan, F. Naz, M. Taha, A. Khan, S. Perveen, M. I. Choudhary and W. Voelter, *European Journal of Medicinal Chemistry*, 2014, **74**, 314–323.
41. K. Kobashi, J. Hase and K. Uehara, *Biochimica et Biophysica Acta*, 1962, **64**, 380–383.

42. C. Marwick, *Journal of the American Medical Association*, 1983, **240**, 321–322.
43. K. Kappaun, A. R. Piovesan, C. R. Carlini and R. Ligabue-Braun, *Journal of Advanced Research2*, 18AD, **13**, 3–17.
44. P. Kosikowska and Ł. Berlicki, *Expert Opinion on Therapeutic Patents*, 2011, **21**, 945–957.
45. L. V. Modolo, A. X. de Souza, L. P. Horta, D. P. Araujo and Â. de Fátima, *Journal of Advanced Research*, 2015, **6**, 35–44.
46. S. Hassan and M. Šudomová, *Children*, 2017, **4**, 1–5.
47. B. Latli, M. Eriksson, M. Hrapchak, C. A. Busacca and C. H. Senanayake, *Journal of Labelled Compounds and Radiopharmaceuticals*, 2016, **59**, 300–304.
48. T. Onal Okyay and D. Frigi Rodrigues, *Journal of Microbiological Methods*, 2013, **95**, 324–326.
49. H. J. Burt, A. Galetin and J. B. Houston, *Xenobiotica*, 2010, **40**, 331–343.
50. X. Yang, M. Koohi-Moghadam, R. Wang, Y. Y. Chang, P. C. Y. Woo, J. Wang, H. Li and H. Sun, *PLoS Biology*, 2018, **16**, e2003887.
51. M. A. Farrugia, L. Macomber and R. P. Hausinger, *Journal of Biological Chemistry*, 2013, **288**, 13178–13185.
52. H. N. Dietrich and S. Silver, *Molecular Biology of Heavy Metals*, Springer, Berlin, Heidelberg, 5th edn., 2007.
53. A. Juszkiewicz, W. Zaborska, J. Sepioł, M. Góra and A. Zaborska, *Journal of Enzyme Inhibition and Medicinal Chemistry*, 2003, **18**, 419–424.
54. M. Ranjbar-Omid, M. Arzanlou, M. Amani, S. K. Shokri Al-Hashem, N. A. Mozafari and H. P. Doghaheh, *FEMS Microbiology Letters*, 2015, **362**, 1–9.
55. B. D. Jones and H. L. T. Mobley, *Journal of Bacteriology*, 1989, **171**, 6414–6422.
56. R. Huttl and N. Frank, *Enzymatic Kinetic Determinations*, John Wiley & Sons, Online., 2013.
57. BRENDA: Enzyme Database, https://www.brenda-enzymes.org/, (accessed 30 November 2018).
58. W. Stroberg and S. Schnell, *Biophysical Chemistry*, 2016, **219**, 17–27.
59. K. van Eunen and B. M. Bakker, *Perspectives in Science*, 2014, **1**, 126–130.
60. Z. Amtul, B. S. P. Atta-ur-Rahman, R. Siddiqui and M. Choudhary, *Current Medicinal Chemistry*, 2002, **9**, 1323–1348.
61. N. Mehta, J. W. Olson and R. J. Maier, *Journal of Bacteriology*, 2003, **185**, 726–734.
62. L. Tan, J. Su, D. Wu, X. Yu, Z. Su, J. He, X. Wu, S. Kong, X. Lai, J. Lin and Z. Su, *The Scientific World Journal*, 2013, **2013**, 1–9.
63. L. S. B. Upadhyay, *Indian Journal of Biotechnology*, 2012, **11**, 381–388.

64. Y. F. Rego, M. P. Queiroz, T. O. Brito, P. G. Carvalho, V. T. Queiroz, A. Fatima and F. Macedo, *Journal of Advanced Research*, 2018, **13**, 69–100.
65. H. Wapenaar, T. van den Bosch, N. G. J. Leus, P. E. van der Wouden, N. Eleftheriadis, J. Hermans, G. S. Hailu, D. Rotili, A. Mai, A. Dömling, R. Bischoff, H. J. Haisma and F. J. Dekker, *European Journal of Medicinal Chemistry*, 2017, **136**, 480–486.
66. E. Grela, A. Dziełak, K. Szydłowska, A. Mucha, P. Kafarski and A. M. Grabowiecka, *Journal of Medical Microbiology*, 2016, **65**, 1123–1129.
67. S. Kumar and A. M. Kayastha, *Medicinal Chemistry Research*, 2010, **19**, 113–114.
68. L. Zhang, K. Levy, G. Trueba, W. Cevallos, J. Trostle, B. Foxman, C. F. Marrs and J. N. S. Eisenberg, *Antimicrobial Agents and Chemotherapy*, 2015, **59**, 6733–6740.
69. N. J. Yang and M. J. Hinner, *Methods in Molecular Biology*, 2015, **1266**, 29–53.
70. B. Szachowicz-Petelska, Z. Figaszewski and W. Lewandowski, *International Journal of Pharmaceutics*, 2001, **222**, 169–182.
71. J. R. Burns and J. F. Gauther, *The Journal of Urology*, 1984, **132**, 455–456.
72. N. C. Cady, K. A. McKean, J. Behnke, R. Kubec, A. P. Mosier, S. H. Kasper, D. S. Burz and R. A. Musah, *PLoS ONE*, 2012, **7**, e38492.
73. K. Harjai, R. Kumar and S. Singh, *FEMS Immunology and Medical Microbiology*, 2010, **58**, 161–168.
74. D. Wallock-Richards, C. J. Doherty, L. Doherty, D. J. Clarke, M. Place, J. R. W. Govan and D. J. Campopiano, *PLoS ONE*, 2014, **9**, e112726.
75. R. Mathialagan, N. Mansor, B. Al-Khateeb, M. H. Mohamad and M. R. Shamsuddin, *Procedia Engineering*, 2017, **184**, 449–459.
76. A. L. Niles, R. A. Moravec and T. L. Riss, *Expert Opinion on Drug Discovery*, 2008, **3**, 655–669.
77. H. von Wufflen and T. Marquardt, *Journal of Clinical Pathology*, 1994, **47**, 188–189.
78. I. Bacskay, D. Nemes, F. Fenyvesi, J. Varadi, G. Vasvari, P. Feher, M. Vecsernyes and Z. Ujhelyi, in *Cytotoxicity*, ed. T. A. Celik, IntechOpen, 2018, pp. 70–90.
79. A. L. Flores-mireles, J. N. Walker, M. Caparon and S. J. Hultgren, *Nature Reviews Microbiology*, 2015, **13**, 269–284.
80. D. P. Griffith, M. J. Gleeson, H. Lee, R. Longuet, E. Deman and N. Earle, *European Urology*, 1991, **20**, 243–247.
81. Lithostat Full Prescribing Information, https://www.lithostat.com/sites/default/files/lth001_r0715_lit_pi_fnl.pdf, (accessed 7 December 2018).
82. F. Rapido, *Blood Transfusion*, 2017, **15**, 218–221.

5.7. Appendix 1

5.7.1. Synthesis of 2-Mercaptoacetamide

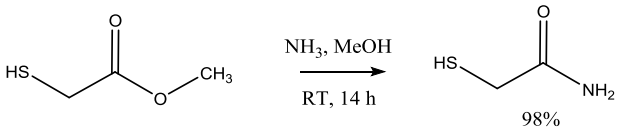

Scheme 5.3: Synthesis of 2-Mercaptoacetamide

The title compound was obtained as a white solid (Scheme 5.3) (3.1 g, 98%). ^{1}H NMR (400 MHz, DMSO-d_6) δ: 7.35 (brs, 1H), 3.47 (s, 2H), 1.51 (brs, 1H) (Figure 5.30A). ^{13}C NMR (DMSO-d_6) δ: 170.86, 34.68 (Figure 5.30B).

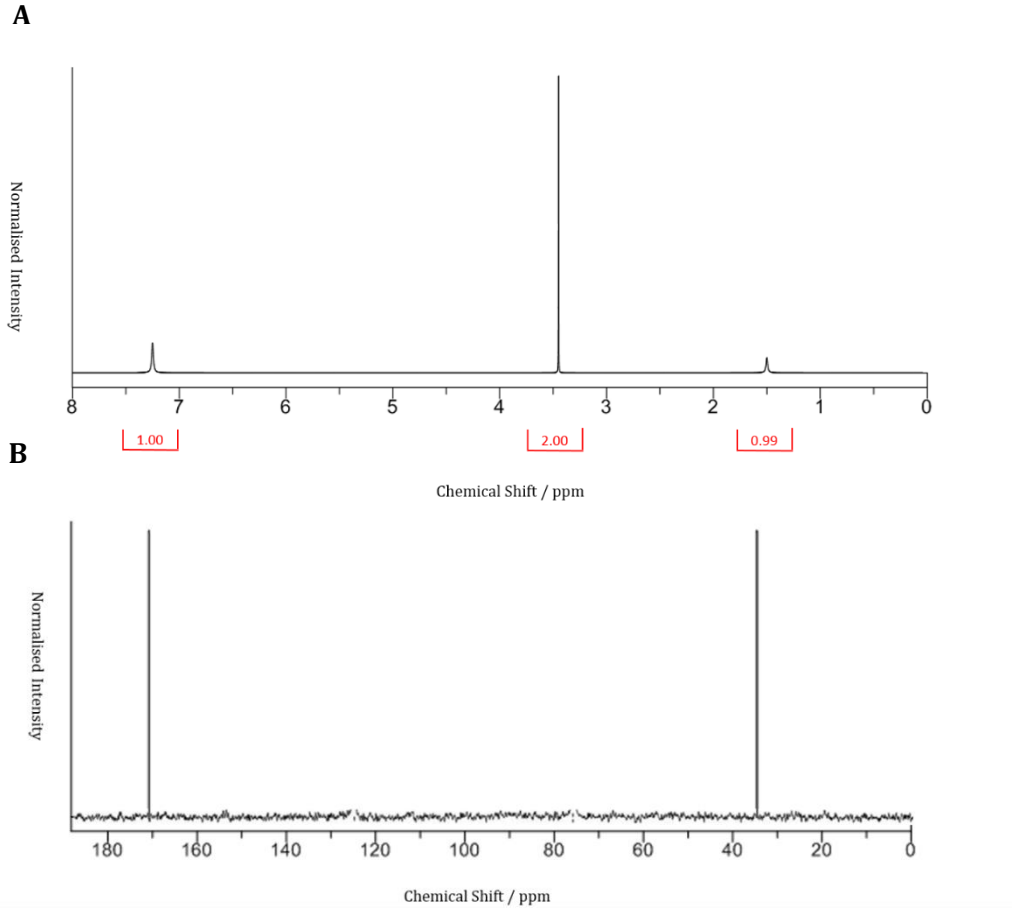

Figure 5.30: NMR spectra of 2-mercaptoacetamide. A) ^{1}H NMR. B) ^{13}C NMR.

Synthesis of 2-MA was confirmed by electrospray ionisation (ESI) mass spectrometry (MS) in positive ion mode m/z: [M+Na]+. Theoretical m/z 113.9984, measured m/z 113.9983 (sigma: 0.0326).

Concluding Remarks and Future Perspective

General Conclusion

The overall objectives of this research endeavoured to develop diagnostic and therapeutic strategies for the detection and prevention of urinary catheter encrustation, following infection by the Gram-negative bacterium *P. mirabilis*. Such research is unavoidably multidisciplinary, combining chemical, biological and engineering advances in tandem for the treatment and prevention of CAUTI. All described strategies aimed to evaluate the chemical and biological capabilities of the modified Foley catheter system, whilst remaining sympathetic to the limations of the clinical requirements and patient usage.

The diagnostic approaches described in Chapters 2 and 3 attempted to fulfill the proveb "*prevention is better than cure*", in order to counteract the onset of serious symptomatic episodes as a result of catheter blockage. The purely diagnostic standpoint of these methodologies represents an amelioration of the intention all of medical technology; to avoid therapeutic usage where possible, in order to preserve efficacy. The initial iteration of the catheter coating design descried in Chapter 2 provided sound proof-of-concept that species may not only be released directly into the catheterised urinary tract in response to elevated urinary pH, but also that an unambiguous urinary colour change may be achieved within residual urine in advance of catheter blockage. Nevertheless, the shortcomings of this design mainly included complications regarding regulatory pathways and toxicity issues concerning the release of chemical species directly into the human bladder. Thus, the second design iteration of this diagnostic system (described in Chapter 3) aimed to externalise this system, removing the pH-responsive release system from *in vivo* to *ex vivo* in its entirety. The resultant 'lozenge' sensor was placed directly into the catheter drainage bag, releasing the fluorescent dye 5(6)-carboxyfluorescein in response to an infection-induced increase in urinary pH. Early diagnosis of catheter blockage was achieved within a physiologically relevant model of the catheterised urinary tract approximately 14.5 hours in advance of urine occlusion, which was deemed sufficient to allow clinical intervention prior to vesicoureteral reflux. Limitations of this model include the lack of testing with pooled human urine in favour of artificial urine; an issue which will endeavour to be solved during an upcoming pilot clinical study of the sensors, in collaboration with the Royal United Hospital, Bath.

The therapeutic approaches described in Chapters 4 and 5 intended to increase the lifespan of the catheter whilst avoiding the use of conventional antibiotics, owing to the rapid initiation and accumulation of antimicrobial resistance within the acute and ambulatory care settings. Bacteriophage offer an elegant natural system for the control of bacterial populations that has

been arguably underexploited in recent years. Impregnation of the catheter coating (originally described in Chapter 2) with *P. mirabilis* bacteriophage proved promising in doubling the time to catheter blockage (13 hours to 26 hours), thus significantly extending catheter longevity and potentially improving patient quality of life. However, whilst phage therapy has proved encouraging in the treatment of CAUTI, the regulatory challenges surrounding this treatment pathway are extensive and likely prohibitive. Indeed, it is likely that phage therapy will not undergo a revival in western medicine until even the most potent chemical antibiotics are rendered ineffective. The current clinical framework for conventional antibiotic approval may prove unsuitable for phage, which as self-replicating biological entities, are unlikely to conform to classical drug analysis. Nevertheless, investigation of phage products (such as phage endolysins) may conform more successfully to current clinical assessment, thus allowing the benefits of phage therapy to appear within the clinic in the near future.

Finally, the development of a small-molecule enzyme inhibitor characterised an appealing approach for the incapacitation of uropathogenic bacteria. Chapter 5 described the rational design, synthesis and *in vitro* evaluation of such a drug, proving the potential of this approach in the field of CAUTI. Physiological models mimicking late-stage *P. mirabilis* infection were unable to reach blockage in the presence of 2-mercaptoacetamide (10 mM concentration), up to 120 hours post-inoculation. Drugs capable of inhibiting bacterial urease have significant potential in the treatment of *P. mirabilis* infection, since the subsequent prevention of urinary alkalinisation may prevent the cascade of events resulting in blockage, without placing a selective pressure on the bacterial cells themselves. Therefore, resistance to such drugs is expected to be hindered or impossible, as mutation for resistance to such a drug would likely result in a fatal decrease in bacterial fitness. Small molecule drugs such as that described in this chapter may also be substituted into the pH-responsive coating as a therapeutic cargo in order to delay catheter encrustation and blockage. Indeed, such therapeutic approaches may be used in tandem with the diagnostic lozenge sensor to provide a theranostic system capable of delaying catheter blockage and warning of its own impending failure. Limitations of this drug design may be overcome by the screening of a larger library of inhibitor analogues, as well as further investigation into the genetic response of *P. mirabilis*. Additional evaluation of drug cytotoxicity will also be necessary prior to clinical progression, including pharmacokinetic and pharmacodynamic evaluation *in vitro*.

Overall, the research agenda initially presented in Chapter 1 has been largely fulfilled. The design, synthesis, engineering and *in vitro* evaluation of novel diagnostic and preventative strategies within physiologically representative models of the catheterised urinary tract has allowed the development of four novel control measures for CAUTI. All of the described

approaches are compatible with the current design of the Foley catheter, such that the original design and operation of the closed drainage system will remain unchanged for care-givers and patients within the clinical setting. Future evaluation of all novel strategies described will involve the employment of more physiologically accurate evaluation, including the use of multispecies biofilms and pooled human urine. Nevertheless, the research presented has successfully achieved both the advanced diagnosis and prevention of catheter blockage, whilst taking into consideration the practical implications of such systems within the clinical setting,

Future Perspective: The Role of Biotechnology in the Treatment and Prevention of CAUTI

Many clinical challenges persist in the management and treatment of catheter-associated urinary tract infection. Whilst applied research within the engineering sciences has proven its potential to directly address challenges associated with the original, flawed design of the Foley catheter, there has undoubtedly been a paucity of of technological innovation compared with major advances in other areas of healthcare for conditions of similar prevalence. Despite potentially significant health and economic gains, the social stigma often associated with incontinence has proven detrimental to engagement by researchers in academic settings. Nevertheless, the need for the acceleration of innovation for CAUTI is being increasingly recongnised, not only for the development of new technology, but also for the improvement of existing systems.

For continence technologies, the research challenge emcompasses a wide-range of underpinning interdisciplinary knowledge. Addressing these challenges has the potential to bring forth incremental improvements in previously overlooked areas. In turn, this will deliver short- and long-term improvements to diagnosis, treatment, prevention and management of CAUTI to profoundly improve the lives of sufferers.

The marriage of broad and often tenuously-linked scientific disciplines must occur in order to overcome the complexity of catheter encrustation and blockage. Stimulation of interdisciplinary research among the scientific, engineering, industrial and clinical communities is necessary to develop novel technologies that are sympathetic to aspects of the original design. Indeed, the passive release of antimicrobial cargos should not be considered a panacea or universally effective strategy. Rather, they should be considered part of a concerted effort to control known risk factors of CAUTI, and form the basis of more microbiologically advanced methods, such as stimuli-resposnive release. Such ‘smart’ catheter coatings provide

the basis of a multifaceted solution, in which the properties and local concentration of released species are taken into consideration, whilst limiting systemic exposure. However, several key challenges remain in this field in order for stimuli-responsive approaches to become a truly valued tool in the CAUTI-preventative arsenal (including long-term stability, maintenance of catheter functionality, and ease of commercial manufacture).

Future challenges for the described technology involve progression towards clinical platforms in the face of a changing regulatory landscape. Translational success relies heavily upon objective evaluation and validation methods, such that clinical efficacy may be accurately extrapolated. Overcoming these challenges will require collaborative effort from those working in across a broad range of disciplines, though success will offer ample opportunity for innovation, as well as a long-overdue solution to a complex and ubiquitous clinical problem.